NUREG/CR-6012
RD, RM

Stiffness and Damping Properties of a Low Aspect Ratio Shear Wall Building Based on Recorded Earthquake Responses

Manuscript Completed: February 1993
Date Published: March 1993

Prepared by
P. S. Hashimoto, L. W. Tiong, L. K. Steele, J. J. Johnson, EQE Engineering Consultants
J. L. Beck, California Institute of Technology

EQE Engineering Consultants
18101 Von Karman Ave., Suite 400
Irvine, CA 92715

Subcontractor:
California Institute of Technology
Pasadena, CA 91125

Prepared for
Division of Engineering
Office of Nuclear Regulatory Research
U.S. Nuclear Regulatory Commission
Washington, DC 20555
NRC FIN D1730

ABSTRACT

An investigation into the structural properties and seismic responses of a low aspect ratio shear wall building, which has construction similarity to typical nuclear plant structures, has been performed using actual recorded earthquake motions. This effort used a combination of modal identification to obtain structure modal parameters directly from the recorded motions, and elastic structural analysis using methods and criteria frequently employed by the nuclear industry. Modal parameters determined by modal identification provide excellent fits to the building motions recorded during the 1984 Morgan Hill earthquake. Modal parameters identified for the 1989 Loma Prieta earthquake are more uncertain. Investigation of building stiffnesses generally confirms the adequacy of bounding estimates currently recommended for nuclear plant structure seismic analysis. Damping values identified for this building supplement the database being compiled to investigate current nuclear plant structure damping criteria.

TABLE OF CONTENTS

TABLE OF CONTENTS (CONTINUED)

LIST OF TABLES

LIST OF TABLES (CONTINUED)

LIST OF FIGURES

LIST OF FIGURES (CONTINUED)

LIST OF FIGURES (CONTINUED)

LIST OF FIGURES (CONTINUED)

LIST OF FIGURES (CONTINUED)

LIST OF FIGURES (CONTINUED)

LIST OF FIGURES (CONTINUED)

LIST OF FIGURES (CONTINUED)

LIST OF FIGURES (CONTINUED)

EXECUTIVE SUMMARY

The Watsonville telephone building is a low aspect ratio reinforced concrete shear wall building with similar construction to nuclear power plant structures. Strong motion records have been obtained from this building from the Loma Prieta earthquake of October 17, 1989 and the prior Morgan Hill earthquake of April 24, 1984. The building experienced significant seismic response during the Loma Prieta event, with peak accelerations as high as any recorded, roof peak acceleration of 1.24g. Seismic responses during the Morgan Hill earthquake were much less.

The recorded motions in the Watsonville telephone building provide a unique opportunity to investigate the behavior of a low aspect ratio shear wall structure subjected to earthquake ground motions of different intensity. The objectives of this study were:

- To support on-going USNRC seismic research programs by obtaining additional data on the damping and stiffness properties of an actual low aspect ratio shear wall building.

- To support the development of nuclear plant seismic analysis criteria and guidelines by investigating the ability of current structure modeling methods to duplicate the recorded seismic response of a low aspect ratio shear wall building.

The technical approach consisted of three tasks: Data collection, modal identification, and elastic analyses. Data collection entailed obtaining detailed information concerning the building (drawings, photographs, and walkdowns) and the recorded motions from the Morgan Hill and Loma Prieta earthquakes.

Modal identification was performed to estimate modal parameters of the structure including frequencies, mode shapes, damping values, and modal participation factors. A well-established modal identification procedure was applied. The method estimates modal parameters by a nonlinear least-squares matching of the calculated and recorded responses. Because sufficient strong motion instruments were installed at the base of the building, modal parameters for the structure itself, assuming its base to be rigid, were identified as one case. A second case, including the effects of soil-structure interaction (SSI) was also treated. The modal identification process was invaluable in understanding the behavior of the building. However, three aspects of the building's behavior made identification of the modal parameters extremely difficult. Soil-structure system properties so dominated the overall response that modal frequencies and damping for the structure by itself were not always identified with confidence. Second, the flexibility of the foundation was a significant factor in understanding the behavior of the structure. Although the modal identification process has the ability to account for this phenomenon, its application did not indicate the necessity to do so. Finally, nonlinear structure

behavior had a significant impact on the results. This phenomenon is not treated by the modal identification process.

The latter two items discussed above (flexibility of the base and nonlinear behavior) generally led to some difficulty in matching modal parameters and building response when using elastic structure analytical models. The Morgan Hill earthquake was matched better than the Loma Prieta earthquake. Several observations and conclusions concerning stiffness of shear wall structures and dynamic models were obtained.

Laboratory testing of low aspect ratio shear walls has generally obtained stiffnesses less than uncracked, theoretical values even at stress levels below which cracking might be expected. At stress levels for which representative nuclear plant structures are designed, estimates of effective stiffness obtained here support the range of stiffnesses obtained by laboratory testing. The estimated stiffnesses of the Watsonville telephone building are generally towards the lower end of ranges obtained by testing. This suggests that sources of greater flexibility, such as cracking due to shrinkage, temperature, settlement, etc. may be more significant to this building than laboratory specimens.

The building stiffness data generally confirm the adequacy of bounding stiffness estimates for nuclear plant structures seismic analysis recommended by the ASCE Dynamic Analysis Working Group on Stiffness of Concrete Shear Wall Structures. The Watsonville telephone building stiffness data are slightly below the lower bound stiffness recommendations.

The damping data obtained by modal identification are useful additions to the damping data base compiled for the USNRC's Structure Damping Research Program.

The structure capacity evaluation obtained estimates of demand to capacity ratios that significantly exceeded one for the Loma Prieta earthquake. Despite significant seismic demands, the building experienced only minor cracking in certain walls. These results and observations indicate that current acceptance criteria for nuclear plant structure design are appropriately conservative. Further, structure capacity evaluations for beyond design basis earthquakes should consider additional sources of structure capacity to obtain more realistic structure resistances against seismic loads.

Additional investigations are strongly recommended to complete the effort. In particular, structure models should be developed to include modeling the effects of the flexible base and nonlinear structure behavior.

PREFACE

The study described in this report was conducted by EQE Engineering Consultants under contract to the U.S. Nuclear Regulatory Commission as part of the Structure Damping Research Program. Other reports prepared for this program included NUREG/CR-6011, "Review of Structure Damping Values For Elastic Seismic Analysis of Nuclear Power Plants," and NUREG/CR-6013, "Methods Used For the Treatment of Non-Proportionally Damped Structural Systems".

EQE was responsible for overall administration of this effort, and data collection and seismic analysis efforts in particular. Professor James L. Beck of the California Institute of Technology, under subcontract to EQE, was responsible for modal identification activities and Section 3 of this report. Professor Beck also provided additional project support, including guidance for the seismic analyses and report review.

The USNRC project manager for this study was Dr. James F. Costello, whose support and guidance are greatly appreciated. The contributions of Pacific Bell, the building owner who provided building drawings and access, the California Division of Mines and Geology, Office of Strong Motion Studies, who provided the earthquake records, and Dr. Charles R. Farrar of Los Alamos National Laboratory, who provided data from the Seismic Category I Structures Program, are gratefully acknowledged.

1. INTRODUCTION

1.1 Background

Buildings housing essential equipment components at commercial nuclear power plants in the United States, aside from reactor containment structures, are typically constructed of low aspect ratio reinforced concrete shear walls. These buildings generally have overall height-to-length ratios less than or equal to 1. Loads induced by earthquake excitation are resisted primarily by concrete walls.

In the response analysis to obtain seismic loads for design of the structure and floor response spectra for design of attached equipment and piping, the building is typically represented by a mathematical model based on linear elastic behavior. Key parameters that are input to such a model include the structure stiffness and damping. To date, modeling of structure stiffness for design basis seismic analysis has generally been left to the analyst. U.S. Nuclear Regulatory Commission (USNRC) seismic analysis criteria contained in the Standard Review Plan [U.S. Nuclear Regulatory Commission, 1987] do not provide specific guidance on how the stiffness of concrete shear wall structures should be modeled. ASCE Standard 4-86 [American Society of Civil Engineers, 1986], which contains recommendations on nuclear plant seismic analysis, provides general, but not specific, guidance on stiffness modeling of nuclear plant concrete structures.

Current USNRC guidance on equivalent viscous damping values to be used in the elastic seismic design analysis of nuclear power plant structures is contained in Regulatory Guide 1.61. R.G. 1.61 was prepared in the early 1970's based on data and other information available at that time. Since the original issue of R.G. 1.61, significant amounts of additional damping data have been obtained.

The USNRC seismic analysis criteria described above are based upon structure response that is essentially elastic under design basis events. However, more recent developments, such as the Individual Plant Examination of External Events [Partlow, 1991; U.S. Nuclear Regulatory Commission, 1991], could result in the evaluation against earthquakes beyond the design basis. Such earthquakes could cause nuclear plant structures to respond in the inelastic range.

To provide guidance on nuclear plant structure properties to be used in response analysis for design basis and beyond design basis earthquakes, the USNRC is currently sponsoring the following two research programs:

- Structure Damping Research Program
- Seismic Category I Structures Program

Two of the major objectives of the Structure Damping Research Program are (1) to review the R.G. 1.61 structure damping values specified for elastic design analysis and recommend revisions as appropriate, and (2) to investigate damping values for inelastic analysis. In the course of

this effort, available damping data from nuclear, non-nuclear, and test structures have been collected, compiled, and statistically evaluated [Hashimoto, et al, 1991].

One observation obtained from the Structure Damping Research Program is that damping data from actual nuclear power plant structures and low aspect ratio reinforced concrete shear wall buildings are relatively limited. Most of the data from nuclear plant structures have been obtained primarily from low amplitude motions associated with vibration testing or earthquakes with peak ground acceleration levels of 0.1g or less. While greater quantities of damping data are available for non-nuclear buildings, the amount of data available from structures subjected to significant motions is also quite limited. Very little data have been obtained from low aspect ratio concrete shear wall buildings constructed similar to typical nuclear plant structures.

The overall objective of the Seismic Category I Structures Program, performed by Los Alamos National Laboratory (LANL) is to investigate the dynamic response of Seismic Category I reinforced concrete structures (excluding containments) that are subjected to seismic loads within and beyond their design basis [Kenneally and Burns, 1986]. Extensive testing of scale model nuclear plant structures and individual low aspect ratio shear wall specimens has been performed. Significant amounts of stiffness and damping data have been obtained from the test program.

Results from the testing of very small scale specimens performed at early stages of the program indicated that frequencies at low excitations were reduced by factors of two or more from values predicted by an uncracked cross-section strength-of-materials approach [Endebrock, et al, 1985; Dove, et al, 1987]. This suggests significant reduction in the structure stiffness below theoretical values at low stress levels. However, more recent testing has obtained good correlations between measured and theoretical stiffnesses prior to concrete cracking [Farrar and Bennett, 1989; Farrar, et al, 1991a; Farrar, et al, 1991b]. The closer agreement with theory in these more recent tests has been attributed to careful specimen construction and handling [Farrar, et al, 1991a].

Damping data have also been obtained from the test program [Farrar and Baker, 1991c]. These data constitute part of the population of damping data obtained from test structures considered in the Structure Damping Research Program. Farrar and Baker [1991c] conclude that the damping data obtained do not support the values recommended by R.G. 1.61.

A review of the two research programs described above suggests that additional data on the seismic response of low aspect ratio concrete shear wall buildings is needed for the following reasons:

- Very little damping data are available from nuclear or other low aspect ratio shear wall structures subjected to significant ground motion levels.

- Substantial data on stiffness and damping of low aspect ratio shear walls have been obtained from laboratory testing. However, the applicability of results obtained from laboratory testing of scale model structures to actual structures should be confirmed.

1.2 Study Objective

The Watsonville telephone building is a low aspect ratio reinforced concrete shear wall building with construction similarity to nuclear power plant structures. Strong motion records have been obtained from this building by the California Division of Mines and Geology (CDMG) from the Loma Prieta earthquake of October 17, 1989 [Huang, et al, 1990] and the prior Morgan Hill earthquake of April 24, 1984 [Huang, et al, 1985]. The building experienced significant seismic response during the Loma Prieta event, with peak accelerations as high as any ever recorded. Seismic responses during the Morgan Hill earthquake were much less.

The existence of motions recorded in the Watsonville telephone building provides a unique opportunity to investigate the behavior of a low aspect ratio shear wall structure subjected to earthquake ground motions of different intensity. The study described in this report has been performed with the overall objectives of providing additional data not currently available to on-going USNRC research programs and to support development of seismic criteria for industry application. Specific research objectives are as follows:

- To support on-going USNRC seismic research programs by obtaining additional data on the damping and stiffness properties from an actual low aspect ratio shear wall building.

- To support the development of nuclear plant seismic analysis criteria and guidelines by investigating the ability of current structure modeling methods to duplicate the recorded seismic response of a low aspect ratio shear wall building.

1.3 Technical Approach

The technical approach adopted in this research study consists of the following three tasks:

- Data Collection

- Modal Identification

- Elastic Analysis

Data collection was first performed to obtain detailed information that serves as input to the subsequent analyses. This information included drawings, ground motion recordings, walkdown data, etc.

Following the data collection, analytical activities were conducted in two separate tasks. Modal identification was first performed to obtain structure modal parameters, including frequencies, mode shapes, damping values, and participation factors. The methodology used is based on the assumptions of linearity and classical normal modes, and does not require a structure model. The modal parameters were obtained by nonlinear least-squares matching of the model and measured responses. Because sufficient strong motion instruments were installed at the base of the building, it was possible to identify the modal parameters for the fixed base structure (i.e., with rigid body response due to soil-structure interaction considered separately).

Two types of linear elastic analyses were performed. In the first, building seismic responses due to the recorded input motion were calculated using structure analytical models developed in accordance with current USNRC criteria and industry guidelines. The analytically calculated and actual recorded responses were compared. For the second analysis, the stiffness properties of the structure model were adjusted so that calculated structure frequencies match values obtained by modal identification. These stiffness properties were compared to values determined in accordance with the current criteria and guidelines. The comparisons of structure properties, modal parameters, and seismic responses generated in this task provide data on the adequacy of current methods used by the industry to predict seismic response of low aspect ratio shear wall structures.

Investigation of building response using recorded earthquake motions has been the object of many previous efforts. In several previous analyses, such as those presented in Murphy [1973], the stiffnesses and modal damping values of structure models have been iteratively adjusted to provide a match between recorded and analytically calculated seismic responses. However, the quality of the match, and thus accuracy of the inferred stiffnesses and damping values, is based upon the analyst's judgement, rather than a consistent quantitative criterion as implemented in the modal identification methodology. Iterative adjustment of the structure stiffness and damping properties does not always result in an optimal fit between the recorded and calculated responses, and can lead to significant errors in some cases, as illustrated by McVerry [1979} in the case of the KB Valley Center Building. In contrast, while structure modal parameters have been systematically obtained by previous modal identification efforts, these studies have not always extended their results to obtain inferences on modeling methods traditionally used by the industry.

The technical approach described here represents a departure from most previous investigations of building response using recorded earthquake motions and blends the most attractive features of modal identification and structure analysis in a unique manner. It takes advantage of the systematic method of modal parameter identification, and casts results into the context of current practice in the seismic analysis of nuclear plant structures.

1.4 Report Organization

Section 2 presents a description of the building and the equipment housed within, earthquake strong motion records, and earthquake effects. The results of the modal identification analyses are presented in Section 3. Section 4 describes the elastic analyses performed to current criteria and guidelines, while Section 5 describes the analyses performed in an attempt to match the recorded seismic responses. Observations obtained from a review of specific structure stiffness and damping data are the focus of Section 6. A summary of analyses performed, results and conclusions obtained, and recommendations for future research is presented in Section 7. Cited references are identified in Section 8. Appendices contain additional supporting information.

2. BUILDING AND SEISMIC RESPONSE DATA

2.1 Data Collection

Data collection was performed to obtain all information necessary as input to the subsequent analytical activities. The following data was obtained:

- Drawings
- Strong-motion records
- In-situ conditions

A complete set of structural, architectural, electrical, and mechanical drawings was provided by the building owner. These drawings provide a complete record of the building configuration from original construction, through several modifications, to its current state.

Processed strong-motion acceleration time-history records [Huang, et al, 1985; Huang, et al, 1990] were obtained from the State of California Division of Mines and Geology, Office of Strong Motion Studies. Recordings from a total of 13 channels for both the Loma Prieta and Morgan Hill earthquakes were received.

Two field walkdowns of the building were performed to obtain data on in-situ conditions. The first walkdown was conducted shortly after the Loma Prieta earthquake, primarily to obtain perishable data, such as any earthquake damage. The second, more detailed, walkdown was performed to obtain specific information on the building, including types and locations of equipment components, comparison of drawings to as-built conditions, locations of strong-motion instruments, interviews with facility personnel, etc. The walkdown data were documented in the form of field notes, sketches, and photographs.

Based on the data collected, the following descriptions of the building, strong-motion records, and earthquake effects have been prepared.

2.2 Building Description

The building is located at 340 Rodriguez Street in the city of Watsonville, California. Epicenters of the Loma Prieta and Morgan Hill earthquakes were approximately 18 km to the northwest and 45 km to the north, respectively. It houses equipment for telephone communications operations.

The building was originally constructed in 1948 with a total of three stories. Provision for future expansion to increase the building height and length was included in the design. The fourth story was added in 1955. No other significant structural modifications have been introduced since 1955. Drawings indicate that the original construction and the 1955 addition were seismically designed for a static coefficient

of 0.08 in accordance with the 1946 Uniform Building Code. The effective building weight in the seismic design was taken as the total dead load plus half of the design live load. The building has experienced changes in occupancy and functionality over the years, resulting in several architectural, electrical, mechanical, and heating and ventilating alterations.

The four-story building is approximately 70 feet by 74 feet in plan, and about 66 feet high. Plan views of the floors and roof which identify structural walls and columns are shown in Figures 2-1 to 2-5. Views of the north, south, east, and west elevations are shown in Figures 2-6 and 2-7. The first floor is a slab on grade. A cable vault is located below the first floor and extends along the entire west side of the building. The building is supported on soil by spread footings or partial base mats, located at depths varying from about eight to 18 feet below grade.

The concrete floor slabs of the original construction are five inches thick, and supported by structural steel beams and columns fully encased in concrete (Figure 2-8). A floor live load of 150 psf was typically included in the design. The roof added in 1955 consists of a seven inch thick concrete slab supported by concrete beams and columns. It was designed for a typical live load of 20 psf.

Lateral loads are resisted primarily by the reinforced concrete exterior and interior shear walls. As shown in Figures 2-6 and 2-7, the north, south, and west exterior walls are perforated by relatively small window openings or doors, while the east exterior wall is solid. These walls are typically ten inches thick, with slight variations at certain locations, and typically reinforced by 1/2 inch diameter bars spaced at twelve inches on center, at both faces and in both directions. Continuity of the reinforcement at embedded structural steel columns was maintained by passing the bars through holes in these members. The exterior faces are typically covered with plaster or terra cotta, while the interior faces are covered with plaster or lath and plaster over furring.

The south exterior wall is discontinued at the first story, and replaced with masonry in-fill panels (Figure 2-9). The masonry was grouted solid and doweled to the surrounding concrete, with horizontal joint reinforcement at every third course. Various other door and window openings in the exterior walls were also filled with masonry after original construction.

Interior concrete walls enclose the staircase, elevator shaft, and first floor HVAC equipment room. These walls are typically eight inches thick and reinforced with 1/2 inch diameter bars spaced at twelve inches on center, at both faces and in both directions. An exception is the central E-W interior wall, which is ten inches thick and reinforced with 5/8 inch diameter bars, at both faces and in both directions. The interior wall faces are typically plastered.

Concrete in the original construction was specified to have a minimum compressive strength of 2,750 psi at 28 days. For the 1955 addition, the concrete was specified to have a minimum compressive strength of 3,250 psi at 28 days. The structural drawings do not identify reinforcement specifications.

The building contains telephone switching equipment (Figure 2-10) and various other mechanical and electrical components. Most of the contained equipment is located in the lower two stories, with the upper two stories being nearly empty during the Loma Prieta earthquake. The equipment was typically well anchored, with taller components anchored to the floor and attached to an overhead steel framing system anchored into the overhead slab (Figure 2-11). The building contains equipment components also found in nuclear power plants, including batteries (Figure 2-12), electrical gear (Figure 2-13), air handling units (Figure 2-14), cable trays, HVAC ducting, etc. Only limited other non-structural features were contained within the building. These included a few room partitions, light office furniture, lighting, elevator hoist, etc.

As shown, this building has good similarity to typical nuclear power plant structures. It has an overall aspect (height-to-length) ratio less than 1. Resistance against seismic loads is provided by reinforced concrete shear walls. The wall thicknesses appear to be heavier than necessary to meet the original seismic design criteria, based on the current configuration. Even though some of the major walls are perforated by small window or door openings, the piers and spandrels are comparable in configuration to low aspect ratio walls, with their deformations primarily due to shear. The only non-structural elements of significance are the masonry panels, which are also found in nuclear structures. Extensive interior partitions and exterior curtain wall, that can influence the stiffness and damping characteristics, are not present. Structural steel framing encased in concrete has been used in nuclear plant construction, such as the Zion auxiliary building [Wesley and Hashimoto, 1981].

2.3 Recorded Motions

The building has been instrumented for a number of years by the CDMG. A total of thirteen accelerometers are located within the building. Seven of these instruments are provided at the ground floor, with one at each corner of the building to record vertical motion, and the remaining three recording horizontal motion (Figure 2-1). This instrumentation is sufficient to completely define the input motion to the structure for all six degrees of freedom of the nearly rigid base. The third floor and roof have three instruments each, two in the N-S direction and one in the E-W direction, to record horizontal and torsional responses (Figures 2-3 and 2-5).

The Kinemetrics FB1 instruments are typically mounted on the structure close to the intersections of walls and slabs, thus excluding potential amplifications associated with local structure response (Figure 2-15). The locations of all of these instruments were confirmed in the field

walkdown, with the exception of Channels 2 and 6 which were inaccessible. The instruments feed a Kinemetrics CR-1 central recording system located at the ground floor that ensures that the recordings are synchronized in time.

Recorded peak accelerations for the Loma Prieta and Morgan Hill earthquakes, respectively, are listed in Table 2-1 [Huang, et al, 1985; Huang, et al, 1990]. These values correspond to the instrument-corrected and band-pass filtered records processed by the CDMG.

In the Loma Prieta earthquake, peak horizontal accelerations at the ground floor of 0.26g (average of two channels) and 0.36g were measured in the N-S and E-W directions, respectively. At the roof, peak N-S accelerations of 0.42g and 0.79g were obtained at the northwest and northeast corners of the building, representing amplifications of about 1.6 and 3.0 above the ground floor acceleration. A peak E-W acceleration at the roof of 1.20g was recorded, corresponding to an amplification of about 3.3 above the ground floor acceleration. This is one of the highest accelerations recorded at any site in the Loma Prieta event. Peak vertical accelerations at the corners of the ground floor range from 0.50g to 0.66g.

Selected acceleration time histories recorded at the ground floor and roof in the N-S and E-W directions during the Loma Prieta earthquake are shown in Figures 2-16 to 2-19. The strongest motions were concentrated in the time window from about 3 seconds to 10 seconds after the instruments were triggered. Five percent damped response spectra from the channels at the ground floor are presented in Figures 2-20 to 2-22.

Peak horizontal accelerations recorded in the Morgan Hill earthquake were typically about one-fifth to one-third of those measured in the Loma Prieta earthquake (s

Table 2-1). In the N-S direction, peak accelerations of 0.06g and 0.14g were obtained at the ground floor and roof. In the E-W direction, peak accelerations at the ground floor and roof of 0.11g and 0.33g were measured. Peak vertical accelerations at the ground floor ranged from 0.05g to 0.08g. Selected acceleration time-histories are shown in Figures 2-23 to 2-26. Five percent damped response spectra from the channels at the ground floor are presented in Figures 2-27 to 2-29.

2.4 Earthquake Effects

Considering the high accelerations attained, earthquake effects associated with the Loma Prieta event were relatively minor. Light diagonal cracking of the central E-W interior wall at the first story was observed (Figure 2-30). Isolated cracks were observed in the plaster covering various other interior walls. Inspection of the exterior walls was limited by the furred interior surfaces through much of the building. Only isolated, minor cracks were observed at exposed concrete or plastered surfaces. These cracks may not necessarily have resulted from seismic response.

Relative slip between the masonry in-fill and the surrounding concrete was observed at the first story of the south exterior wall (Figure 2-31). Cracking of the plaster typically occurred at all joints. Damage to the mortar at the masonry-concrete joints was observed at certain locations (Figure 2-31).

Relative slip between HVAC ducting and their rod-hung, trapeze supports was noted in the upper story (Figure 2-32). Positive attachment of the ducting to their supports was lacking. One support failed, as shown in Figure 2-33, which was a consequence of an improperly set anchor into the concrete beam. However, duct damage resulting from support failure was not observed.

It appears that the peak Loma Prieta seismic responses, although intense, did not have sufficient energy content to cause significant structural damage. The peak in-structure accelerations appear to be sharp spikes within a relatively short window of significant motion. Lack of damage to equipment components is attributable to their robust anchorage.

Table 2-1

RECORDED PEAK ACCELERATIONS [HUANG, ET AL, 1985; HUANG, ET AL, 1990]

Channel	Floor	Direction	Loma Prieta	Morgan Hill
9	Ground	N-S	0.27	0.06
10	Ground	N-S	0.25	0.06
7	Third	N-S	0.33	0.10
8	Third	N-S	0.45	0.10
5	Roof	N-S	0.42	0.14
6	Roof	N-S	0.79	0.14
13	Ground	E-W	0.36	0.11
12	Third	E-W	0.60	0.22
11	Roof	E-W	1.20	0.33
1	Ground	Vertical	0.57	0.05
2	Ground	Vertical	0.50	0.06
3	Ground	Vertical	0.51	0.07
4	Ground	Vertical	0.66	0.08

Note: Accelerations listed in units of gravity, g

WATGF/ A1173/ 9/10/91

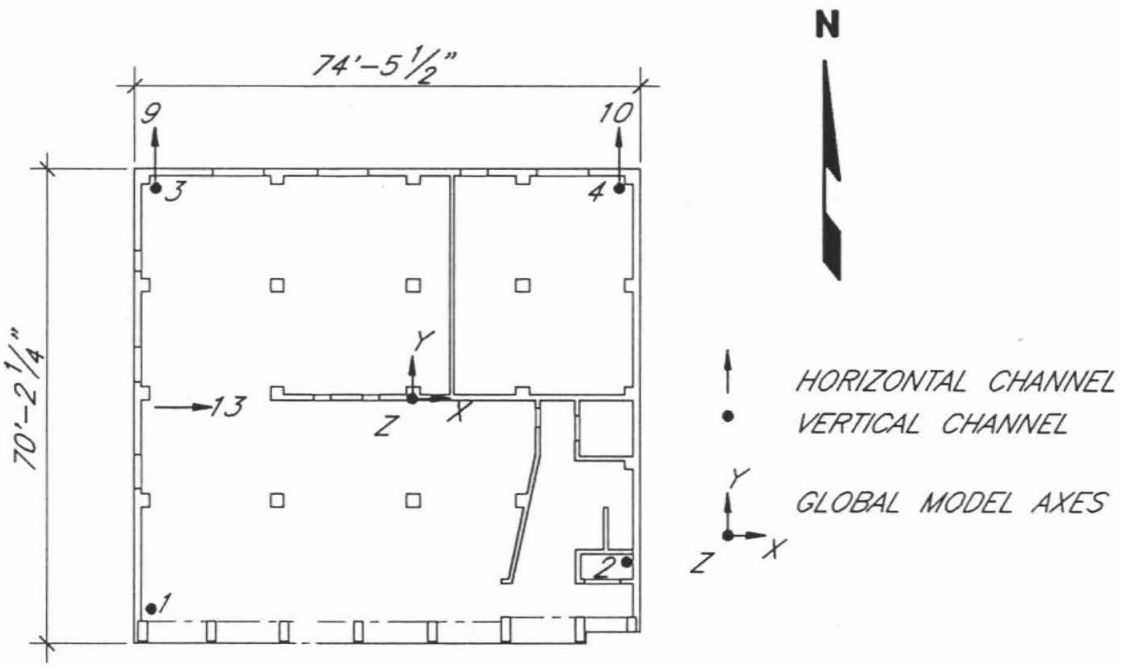

Figure 2-1: Plan View of Ground Floor, Elevation 0'-0"

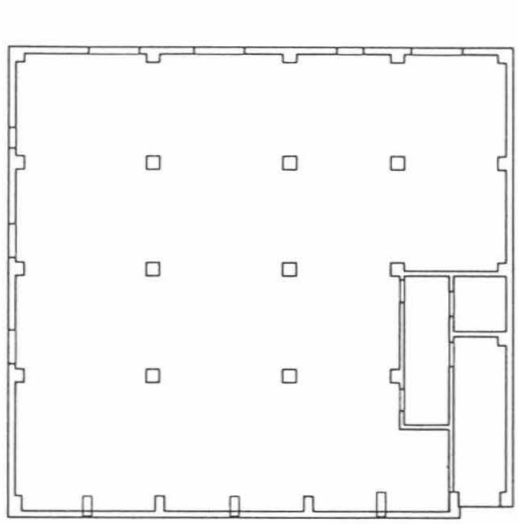

Figure 2-2: Plan View of Second Floor, Elevation 17'-10"

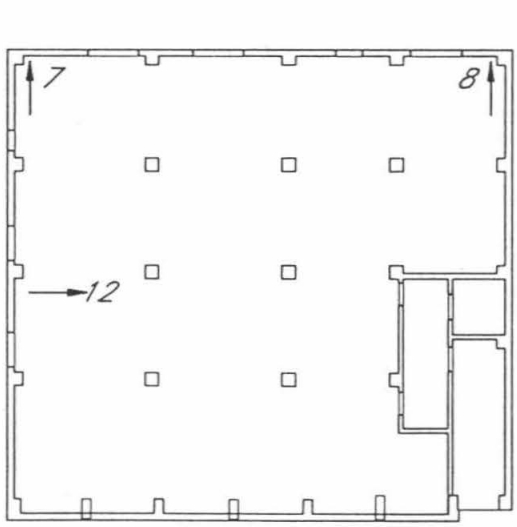

Figure 2-3: Plan View of Third Floor, Elevation 34'-4"

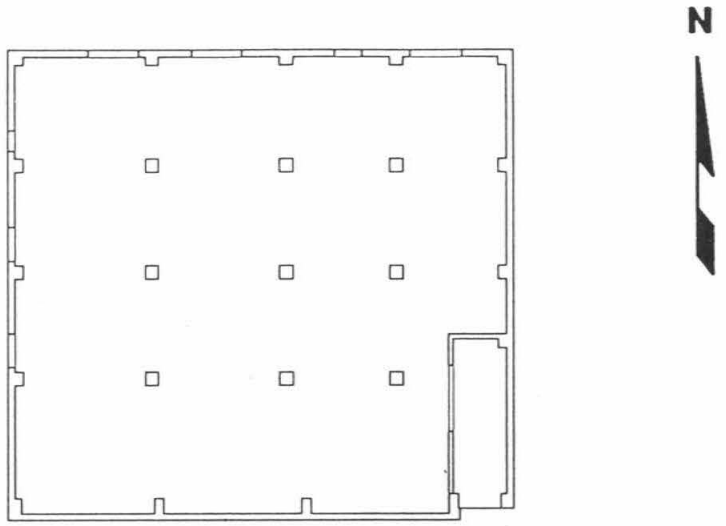

Figure 2-4: Plan View of Fourth Floor, Elevation 50′-10"

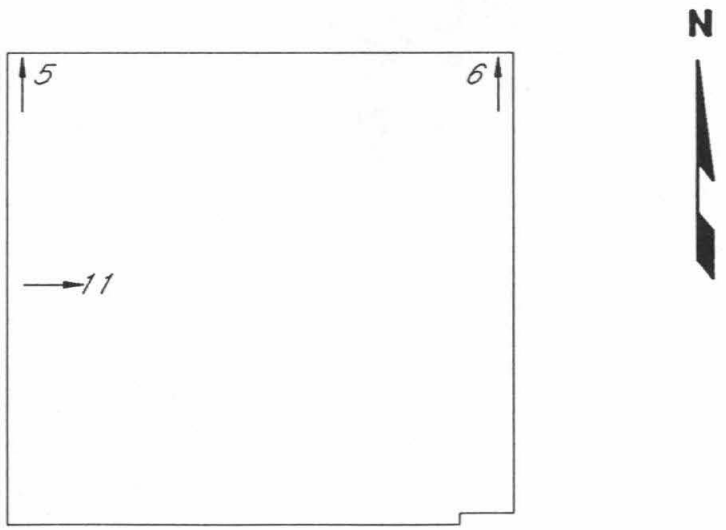

Figure 2-5: Plan View of Roof, Elevation 66′-4"

a. South Elevation (Front);

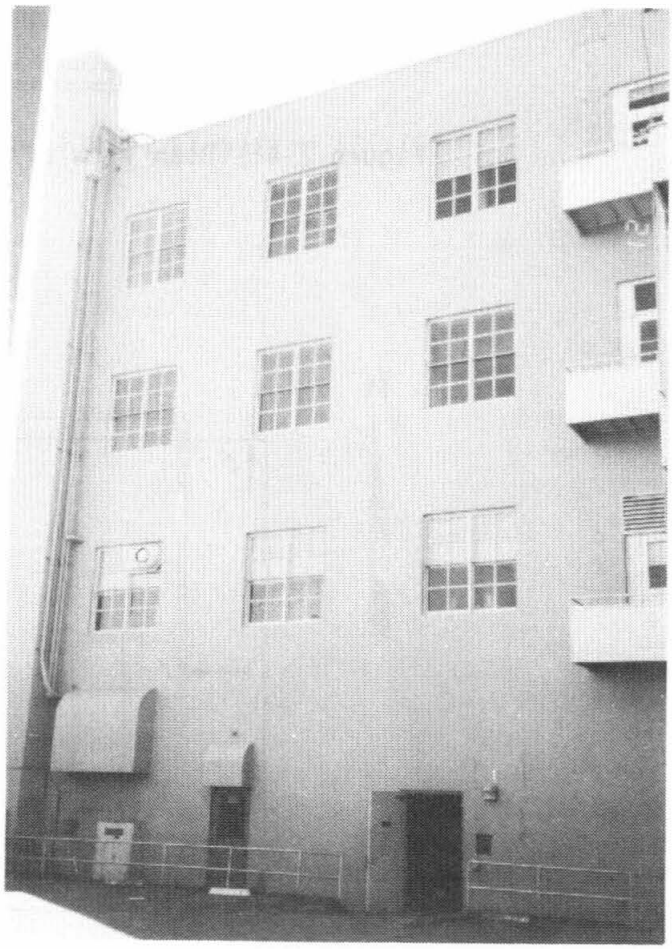

b. North Elevation (Back)

Figure 2-6: Views of North and South Elevations

a. West Elevation (Side);

b. East Elevation (Side)

Figure 2-7: View of East and West Elevations

Figure 2-8: Structural Steel Floor Beams Encased In Concrete

Figure 2-9: Masonry In-Fill At South Wall

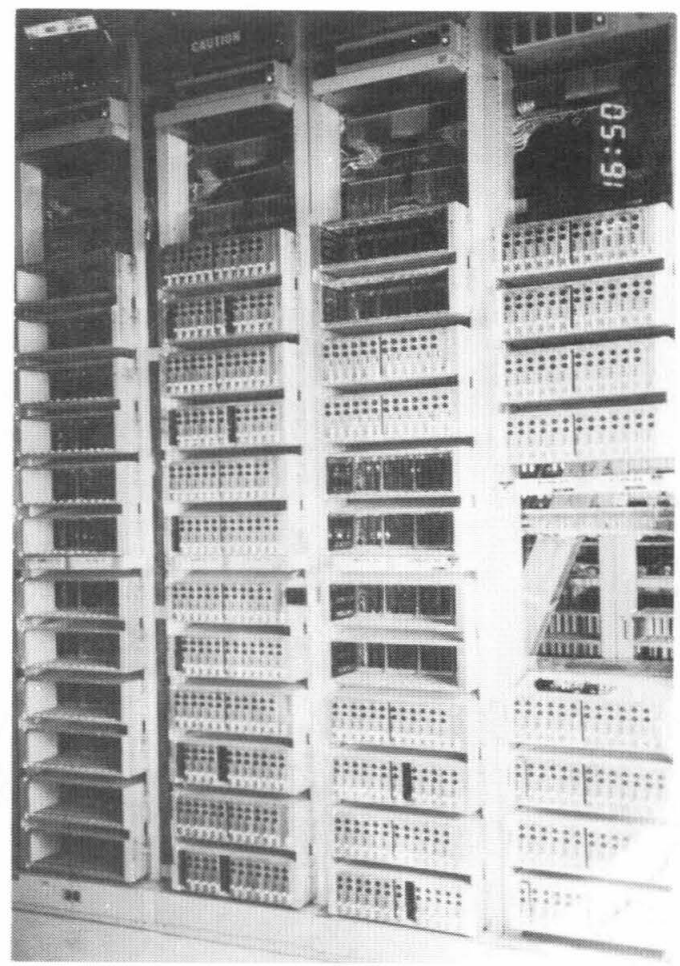

Figure 2-10: Telephone Switching Equipment

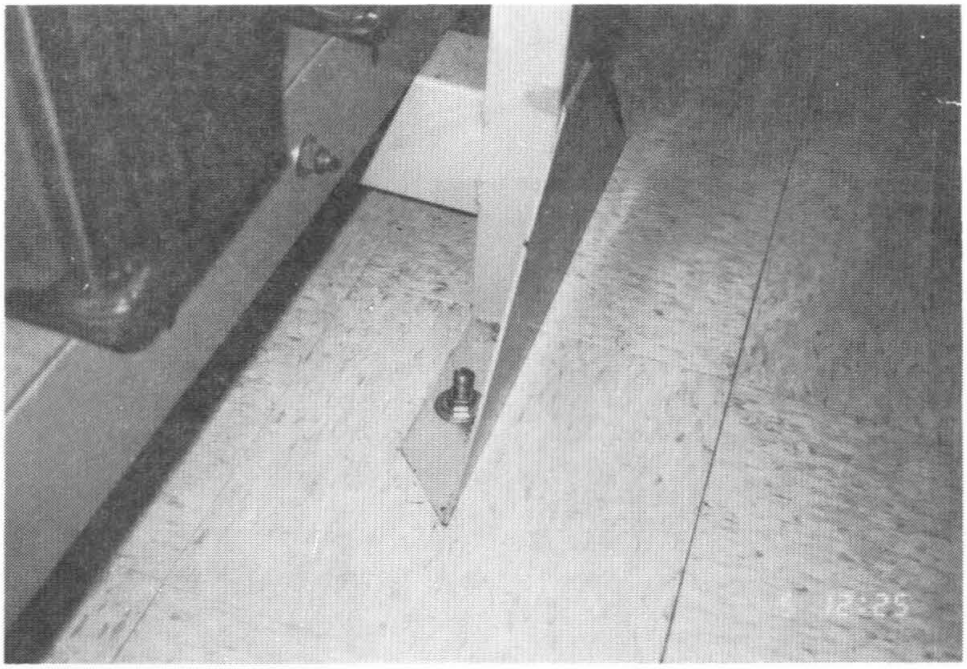

a. To Floor

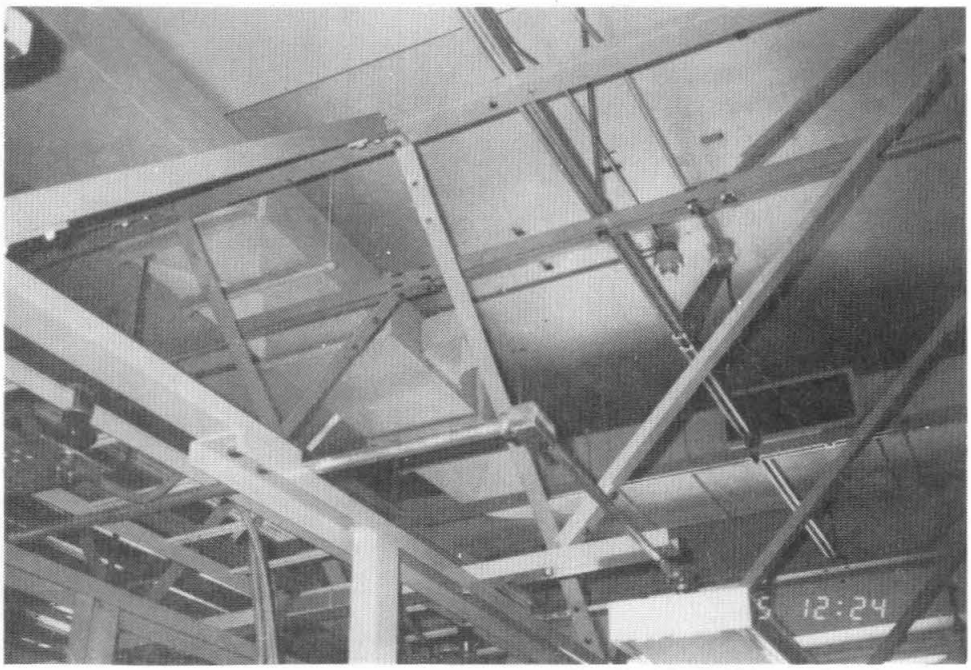

b. To Overhead Framing

Figure 2-11: Equipment Anchorage

a. Ground Floor

b. Fourth Floor

Figure 2-12: Batteries

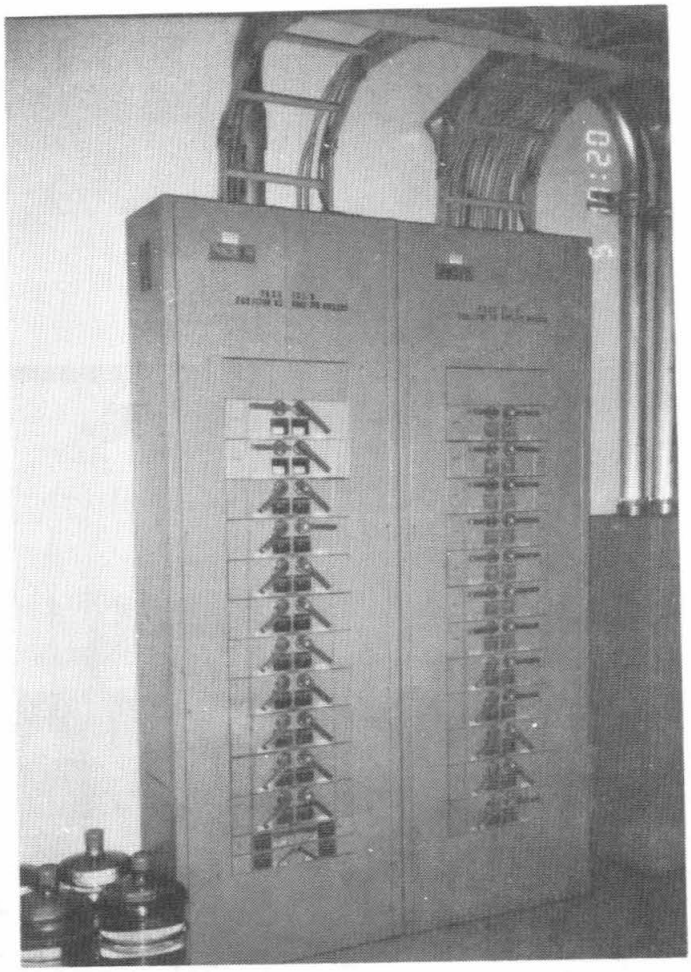

a. 120 Volt AC Distribution Panel

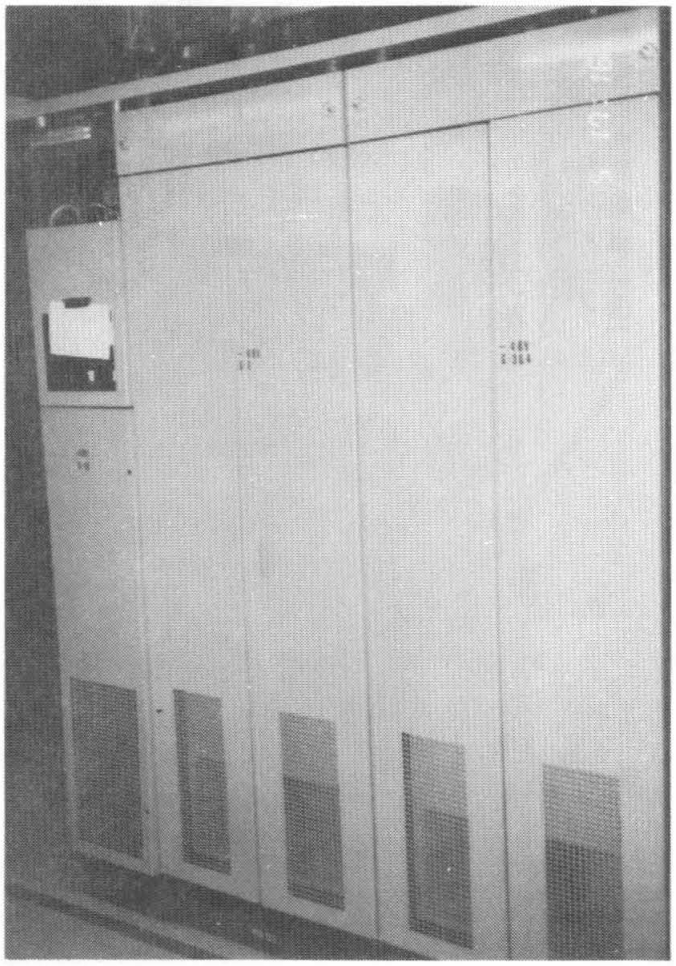

b. Battery Charger

Figure 2-13: Electrical Gear

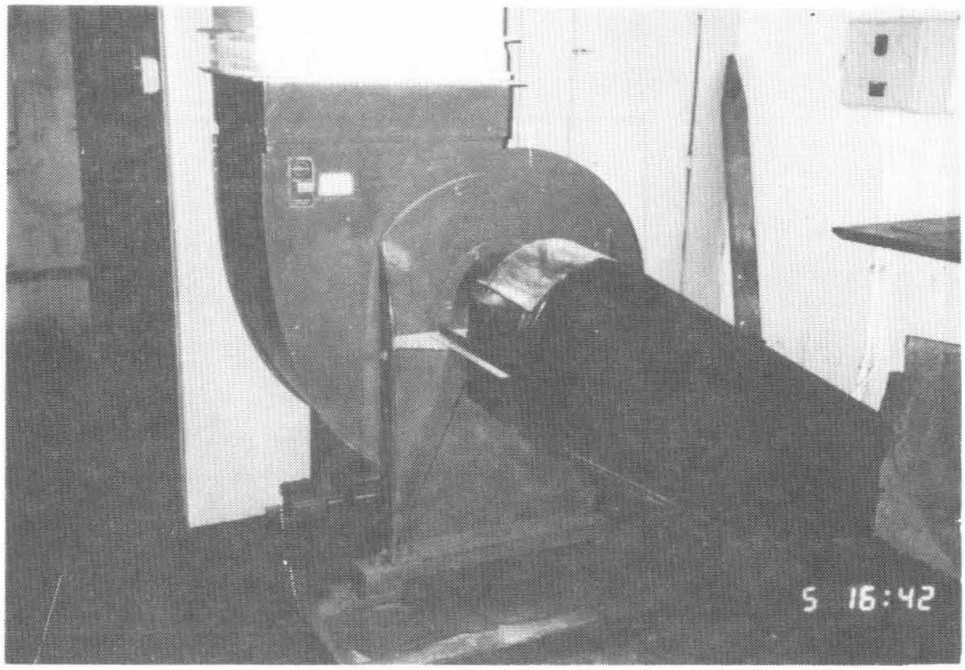

a. Centrifugal Fan

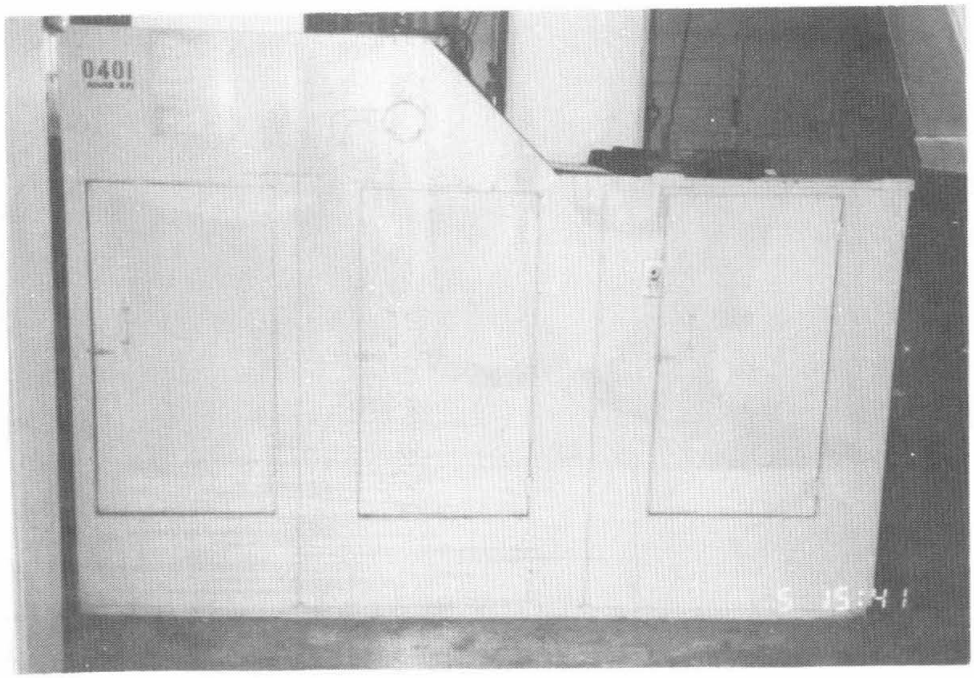

b. Filter

Figure 2-14: Air Handling Equipment

Figure 2-15: Channel 9

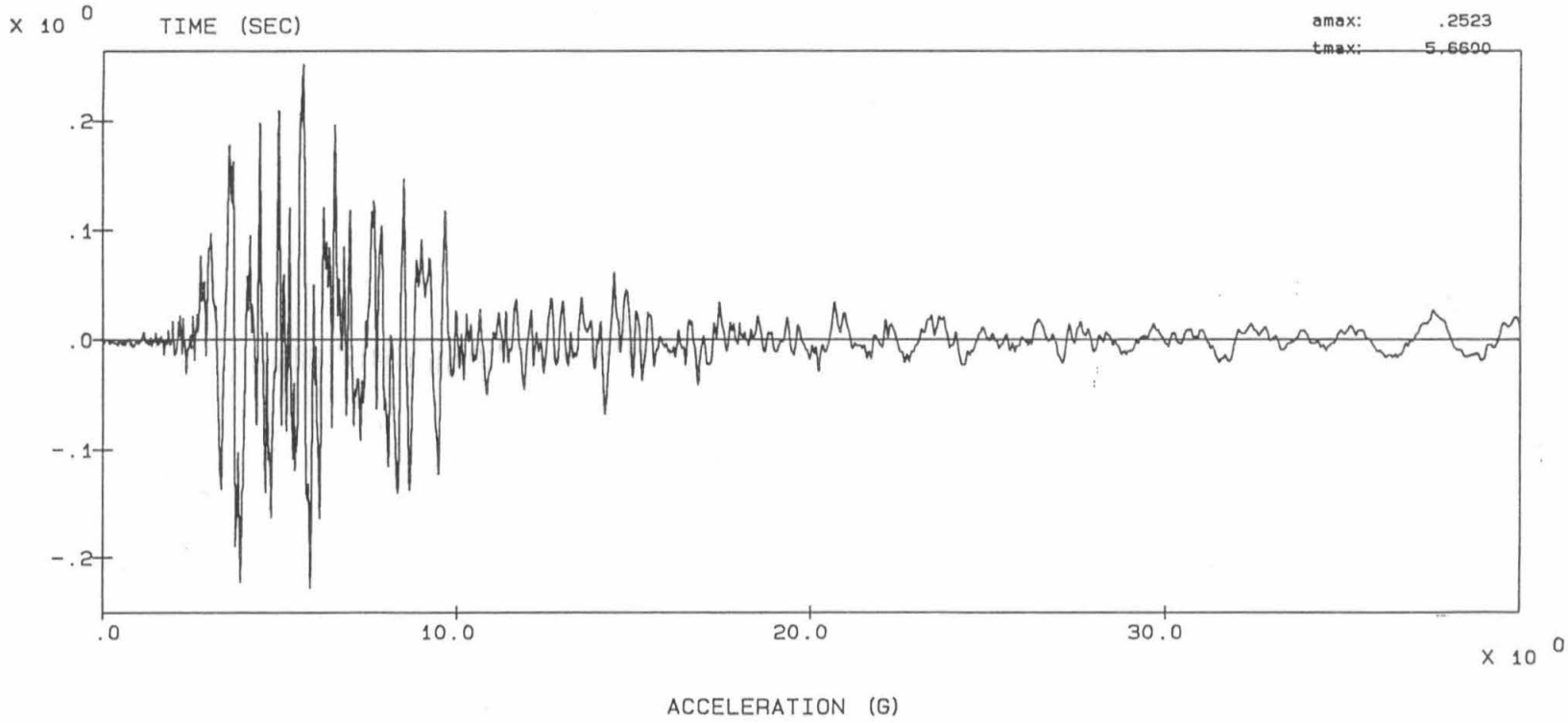

Figure 2-16: Recorded Acceleration Time History, Loma Prieta Earthquake, Ground Floor, N-S Direction (Channel 10)

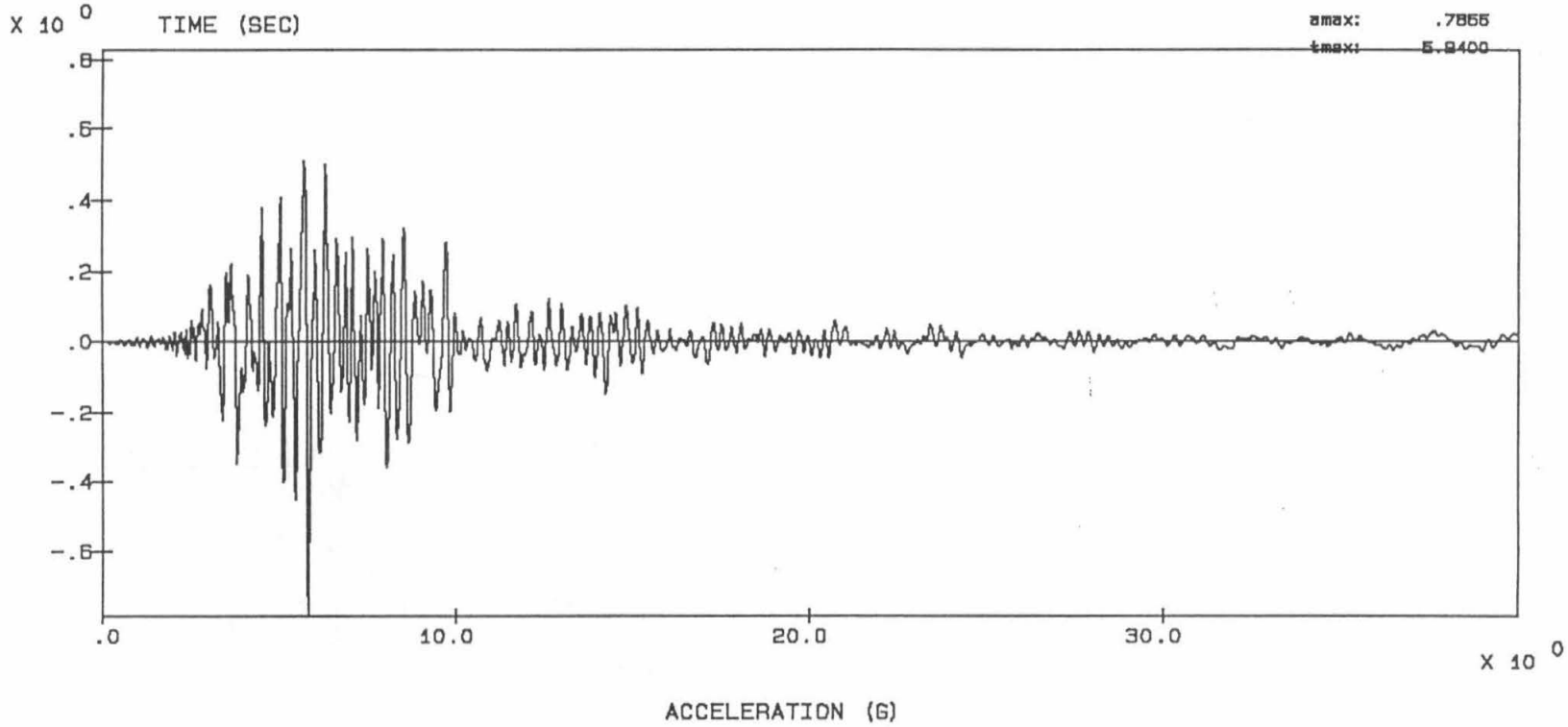

Figure 2-17: Recorded Acceleration Time History, Loma Prieta Earthquake, Roof, N-S Direction (Channel 6)

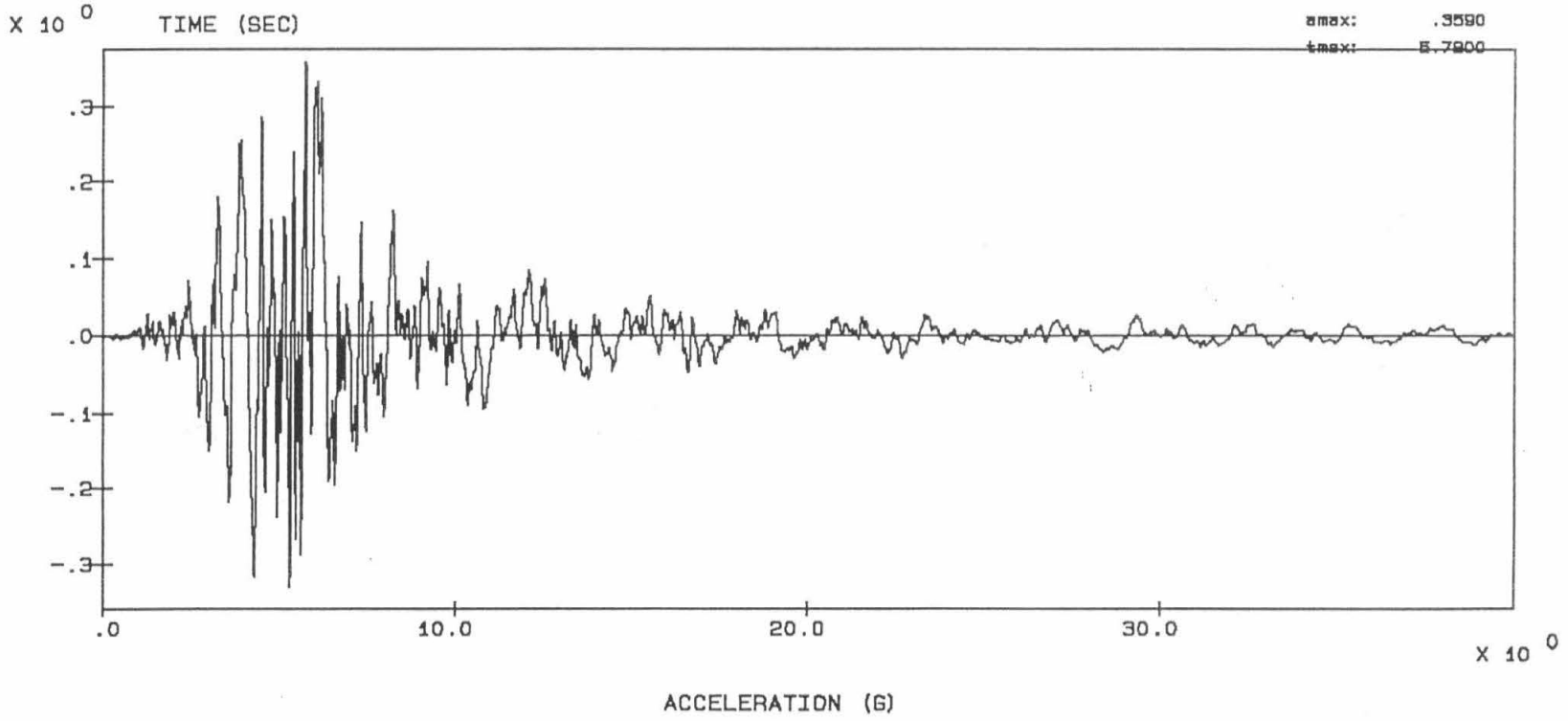

Figure 2-18: Recorded Acceleration Time History, Loma Prieta Earthquake, Ground Floor, E-W Direction (Channel 13)

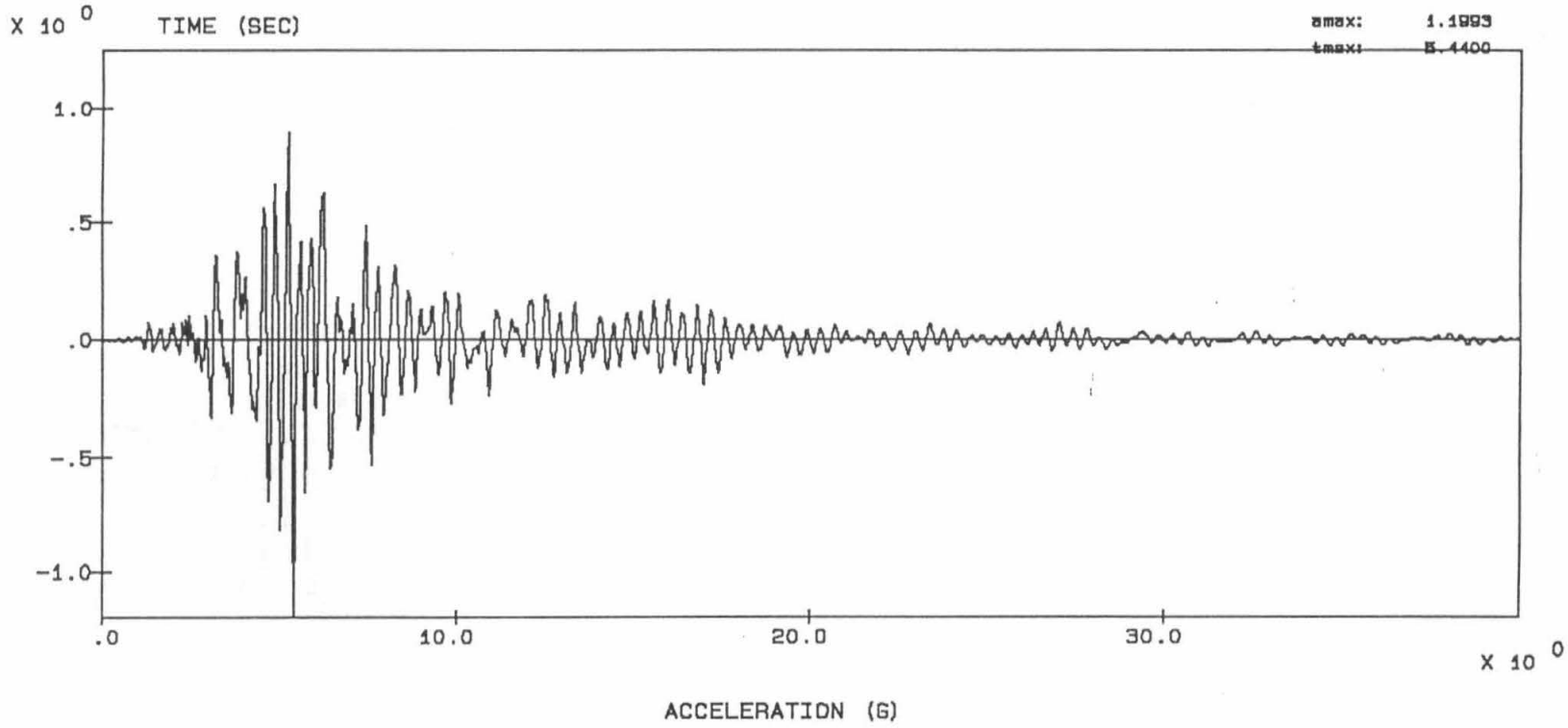

Figure 2-19: Recorded Acceleration Time History, Loma Prieta Earthquake, Roof, N-S Direction (Channel 11)

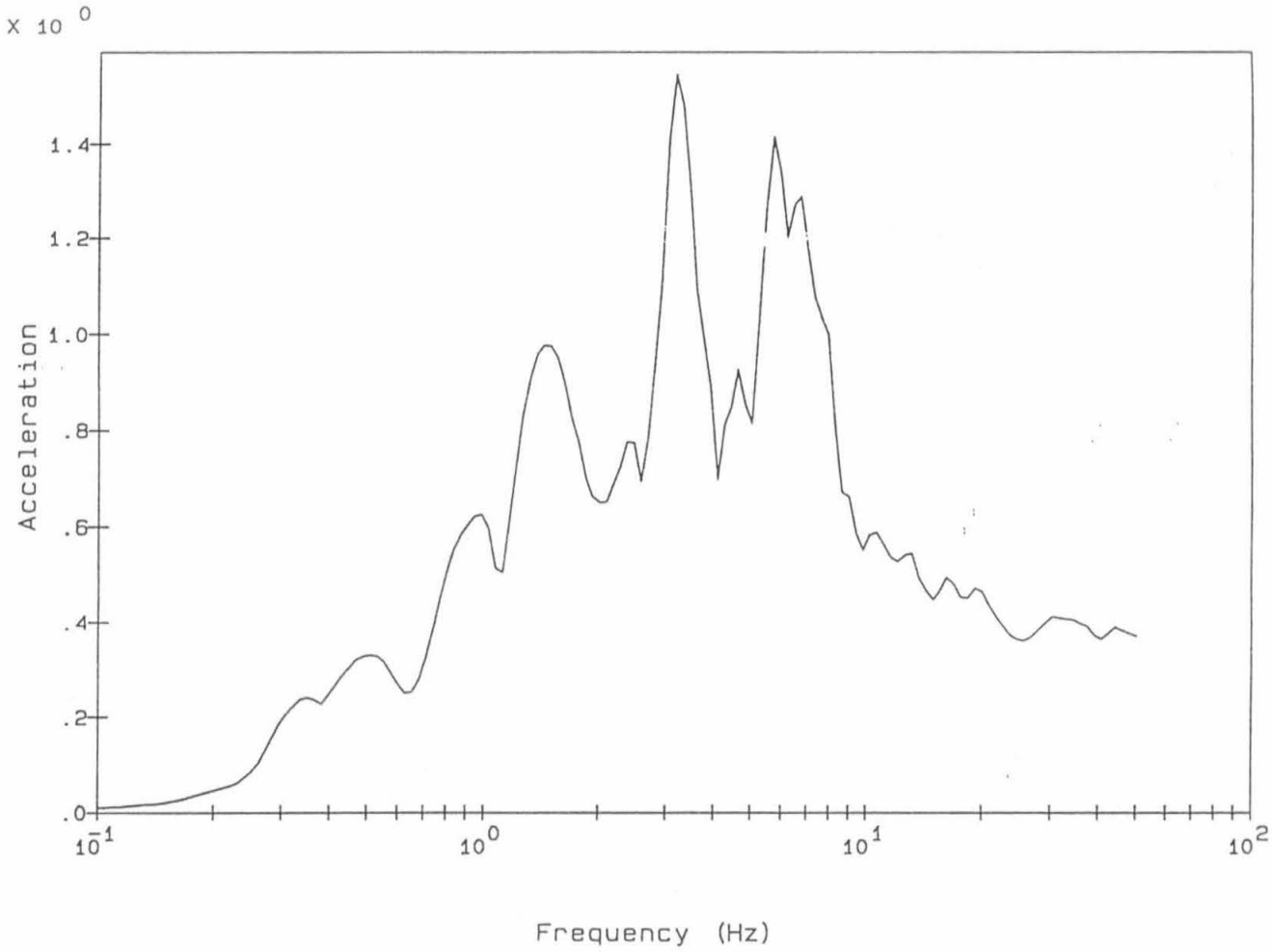

Legend:

Channel 13 Rec.

Notes:

Ground Floor E-W Translation
Acceleration (g)
Spectra calculated at 5% damping

Figure 2-20: 5% Damped Response Spectrum, E-W Direction, Channel 13, Loma Prieta Earthquake

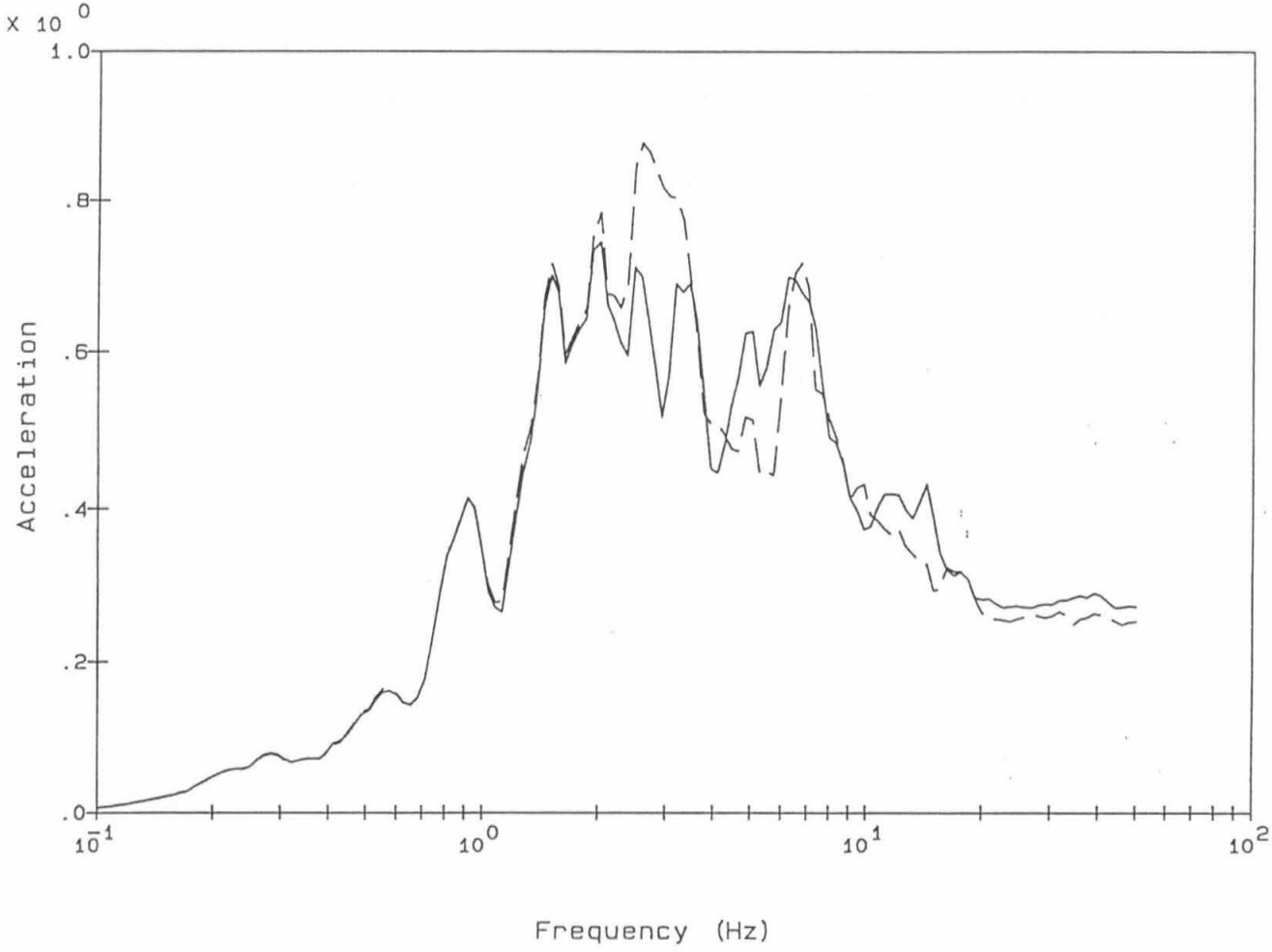

Legend:

Channel 9 Rec. ————————

Channel 10 Rec. — — — — —

Notes:

Ground Floor N-S Translation

Acceleration (g)

Spectra calculated at 5% damping

Figure 2-21: 5% Damped Response Spectra, N-S Direction, Channels 9 and 10, Loma Prieta Earthquake

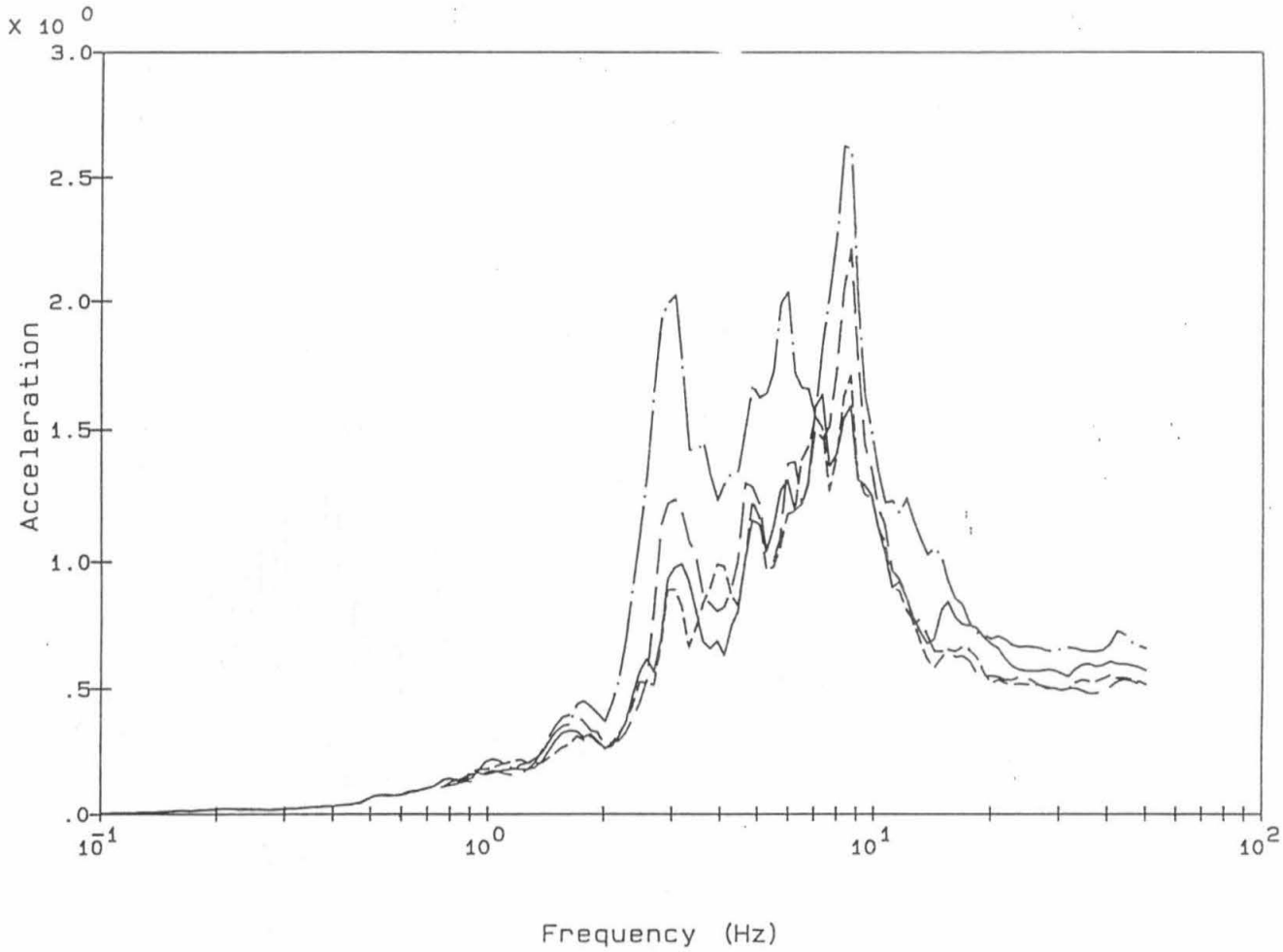

Legend:

Channel 1 Rec.

Channel 2 Rec.

Channel 3 Rec.

Channel 4 Rec.

Notes:

Ground Floor Vertical Translation Acceleration (g)

Spectra calculated at 5% damping

Figure 2-22: 5% Damped Response Spectra, Vertical Direction, Channels 1 to 4, Loma Prieta Earthquake

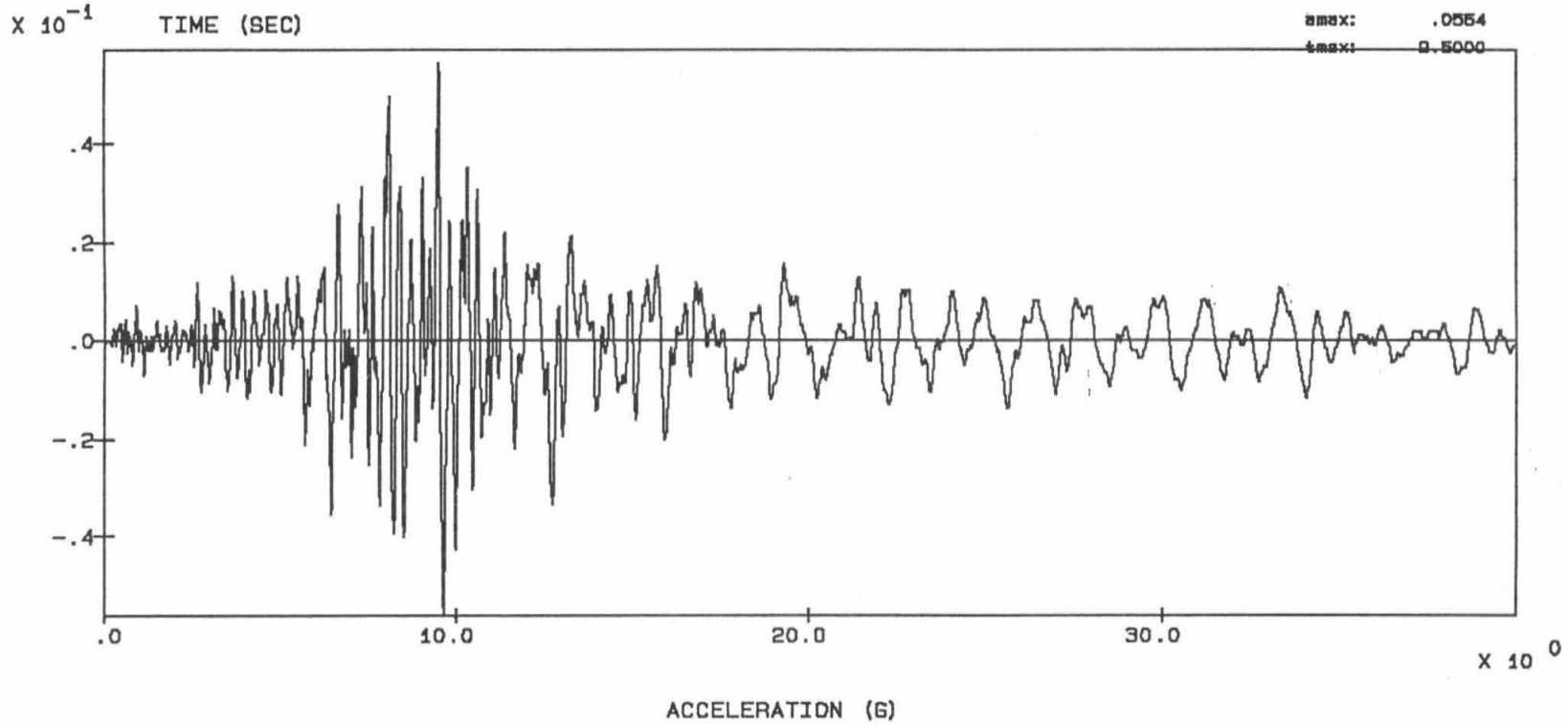

Figure 2-23: Recorded Acceleration Time History, Morgan Hill Earthquake, Ground Floor, N-S Direction (Channel 10)

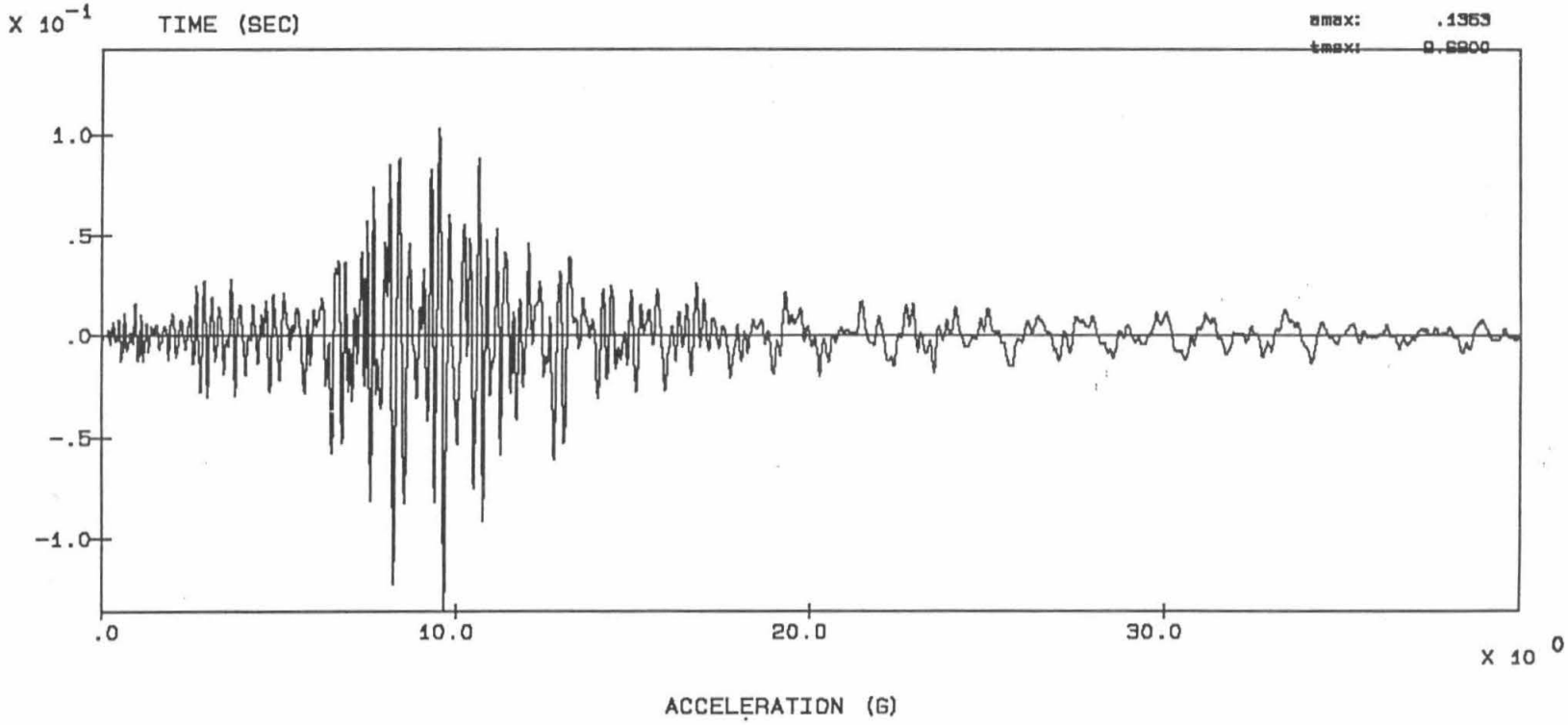

Figure 2-24: Recorded Acceleration Time History, Morgan Hill Earthquake, Roof, N-S Direction (Channel 6)

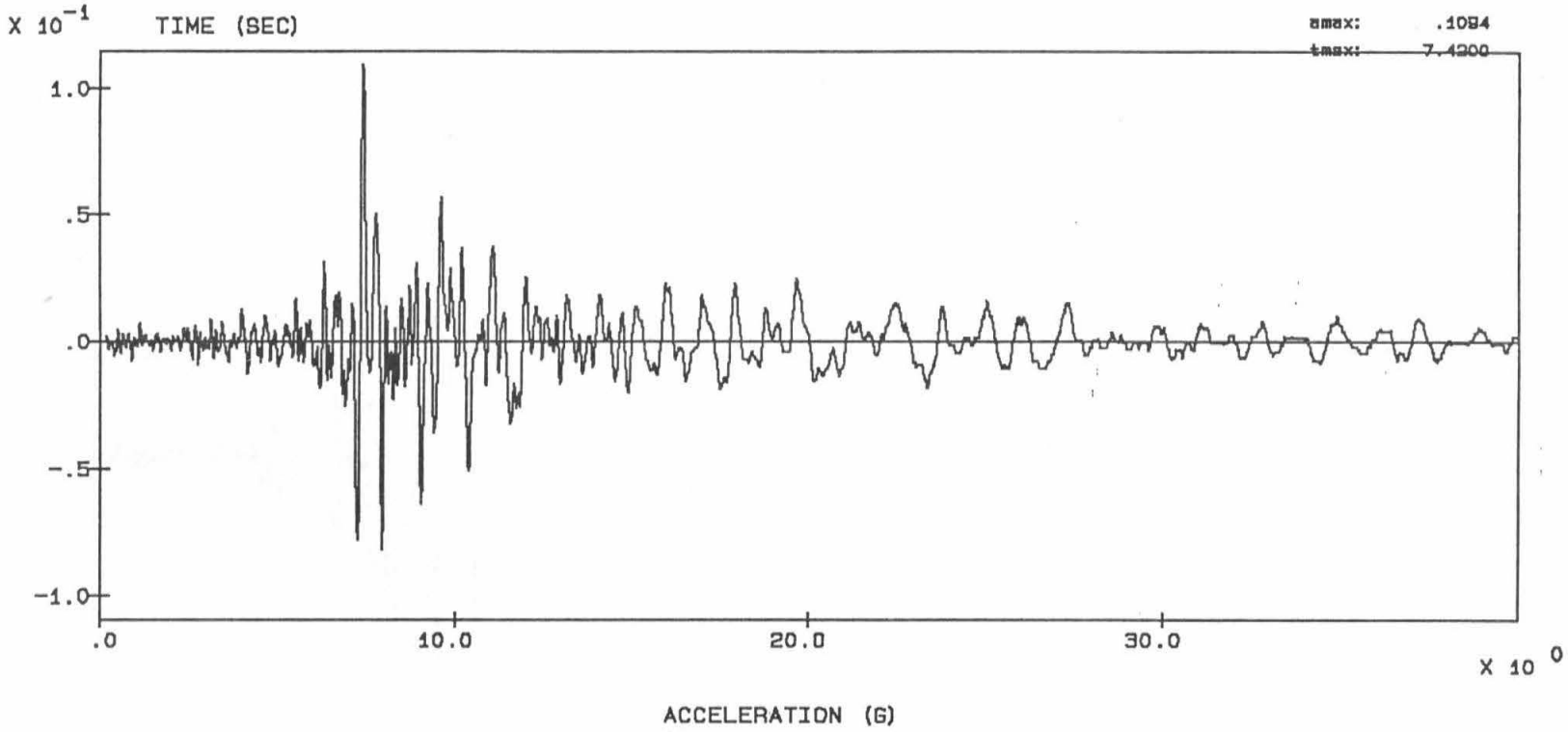

Figure 2-25: Recorded Acceleration Time History, Morgan Hill Earthquake, Ground Floor, E-W Direction (Channel 13)

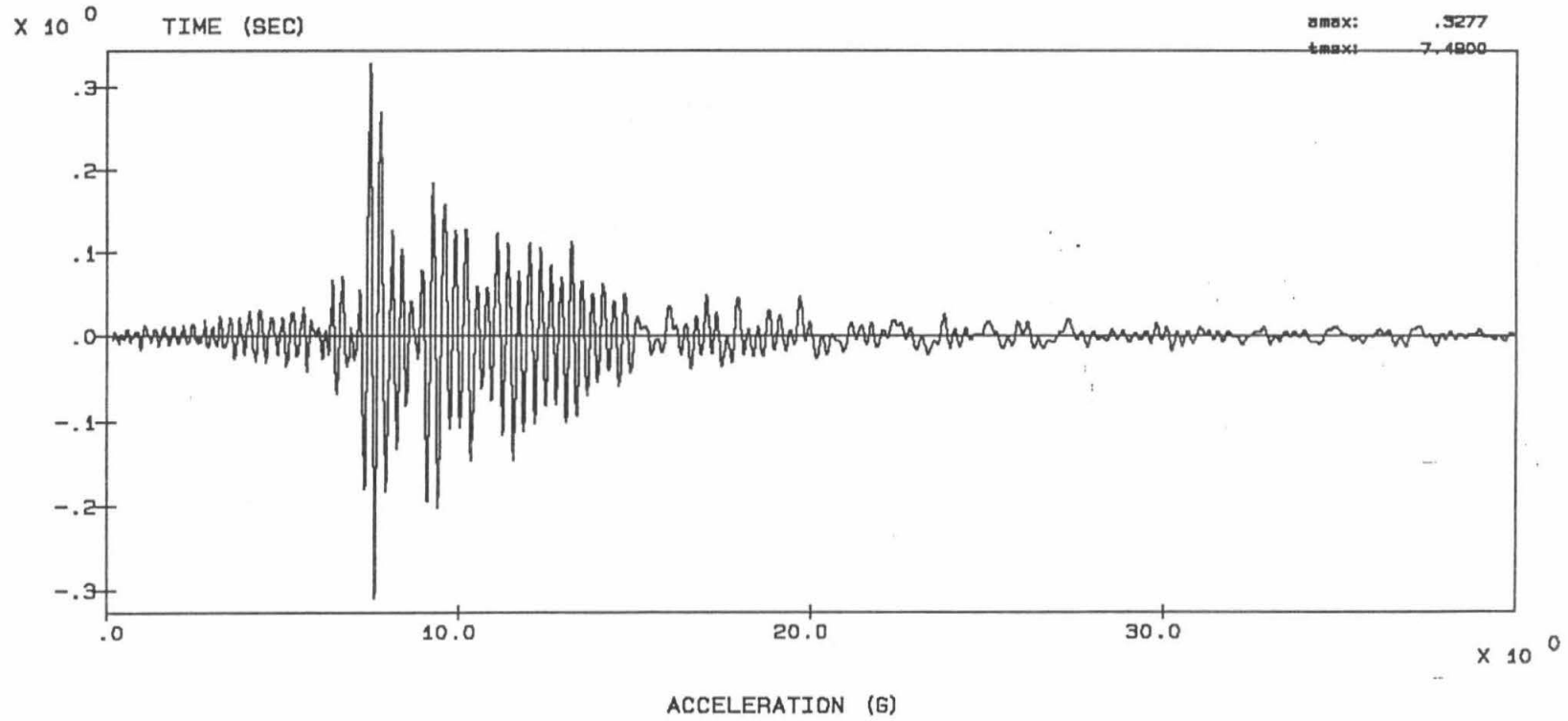

Figure 2-26: Recorded Acceleration Time History, Morgan Hill Earthquake, Roof, N-S Direction (Channel 11)

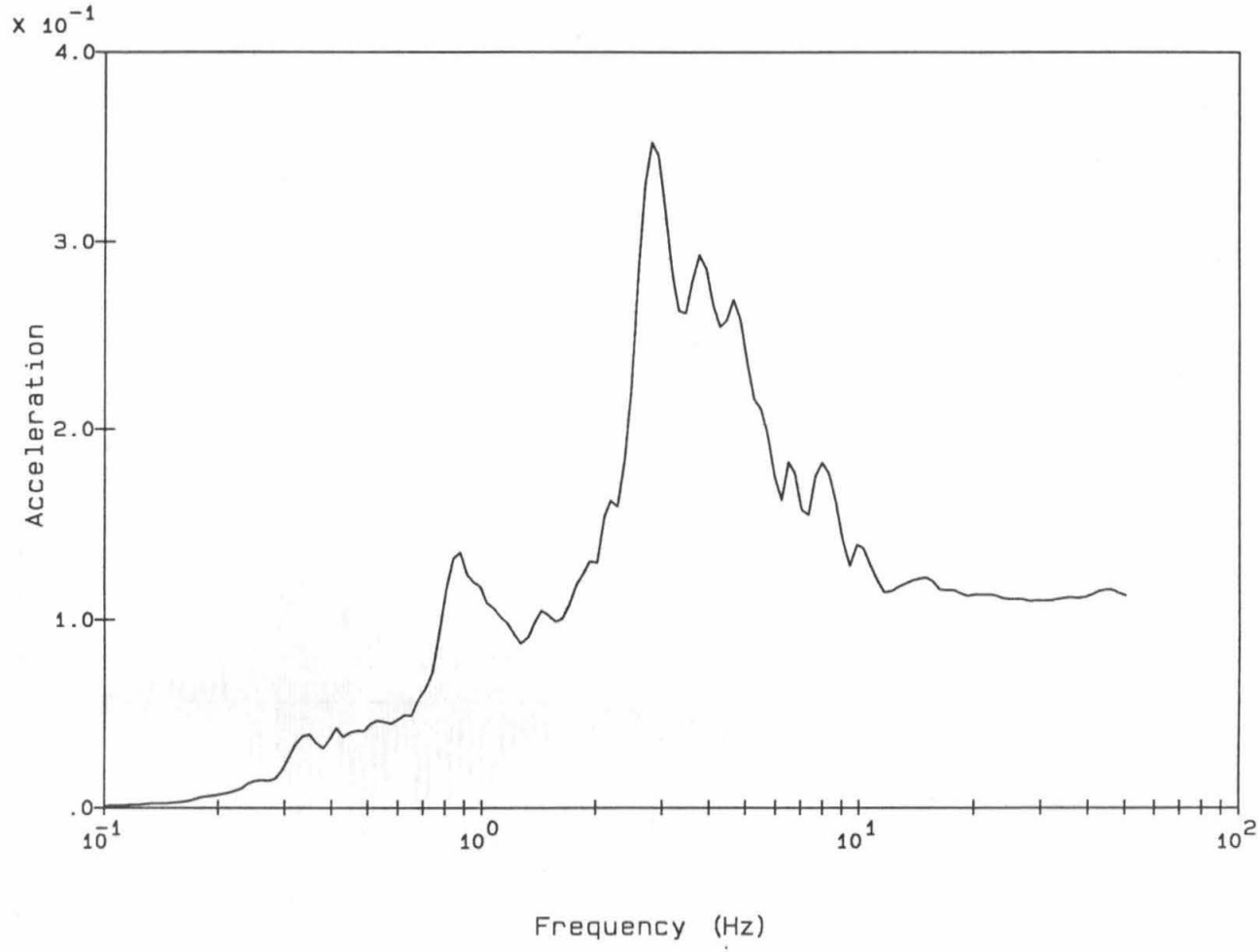

Legend:

Channel 13 Rec.

Notes:

Ground Floor E-W Translation
Acceleration (g)
Spectra calculated at 5% damping

Figure 2-27: 5% Damped Response Spectrum, E-W Direction, Channel 13, Morgan Hill Earthquake

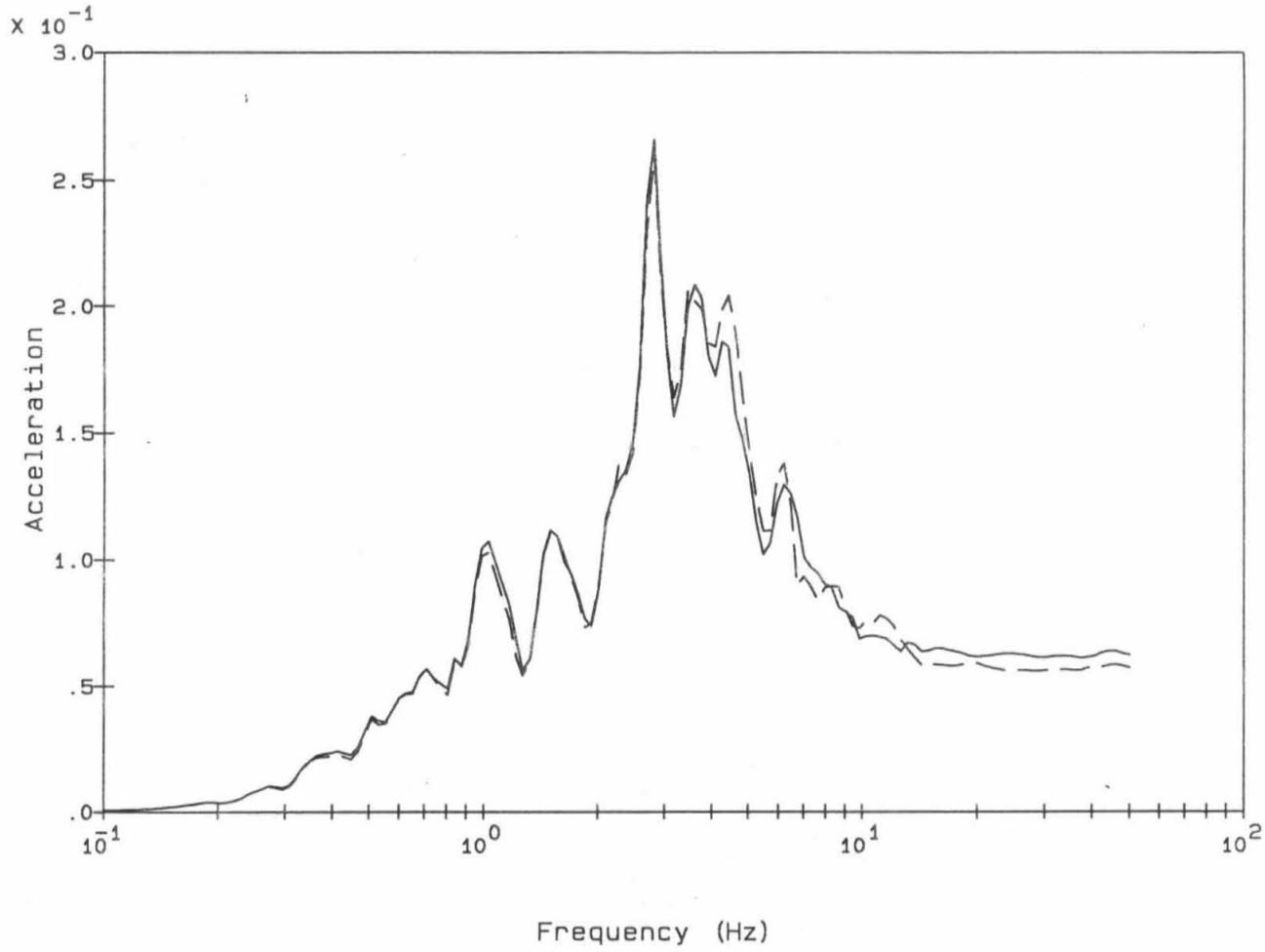

Figure 2-28: 5% Damped Response Spectra, N-S Direction, Channels 9 and 10, Morgan Hill Earthquake

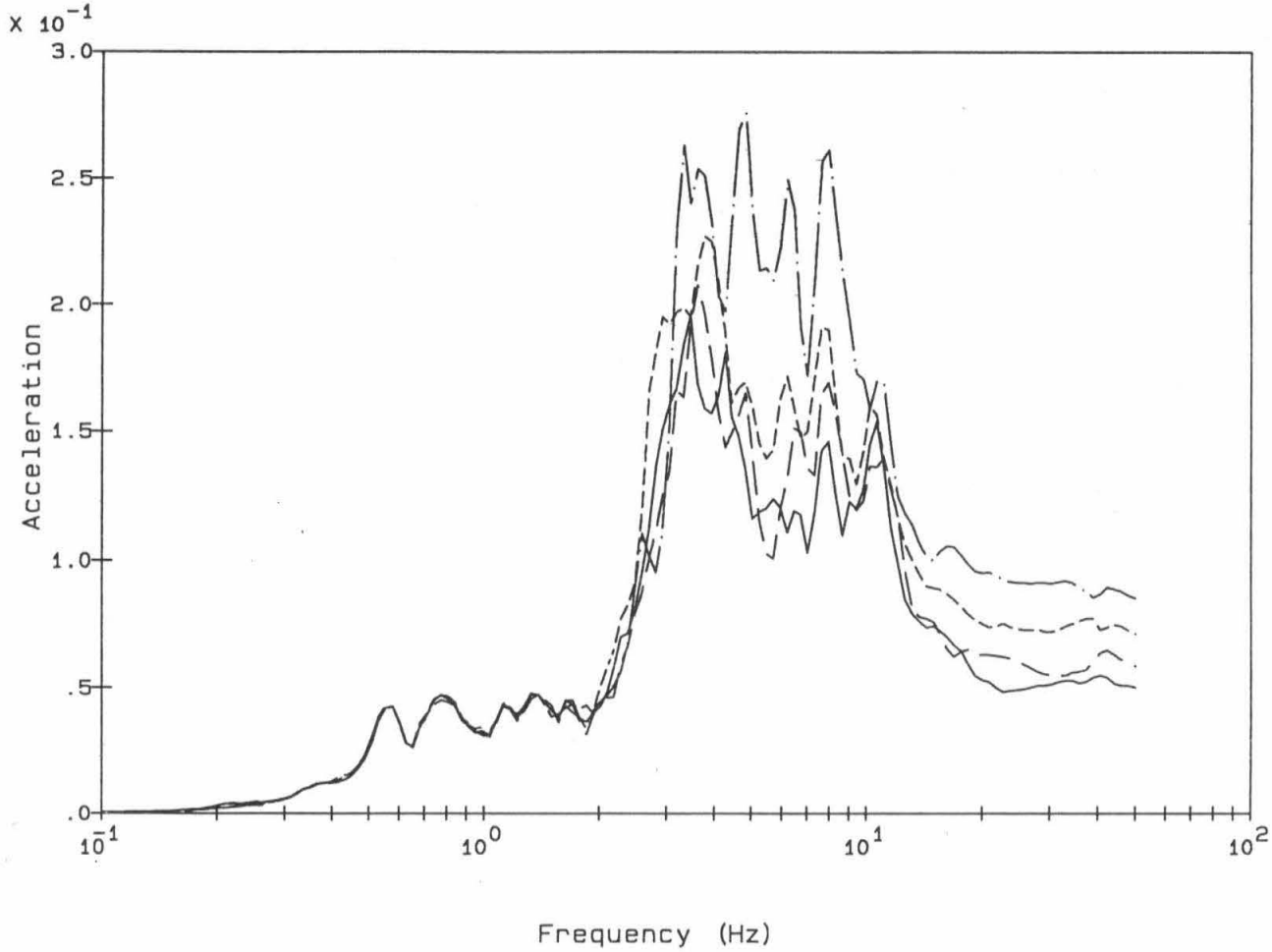

Figure 2-29: 5% Damped Response Spectra, Vertical Direction, Channels 1 to 4, Morgan Hill Earthquake

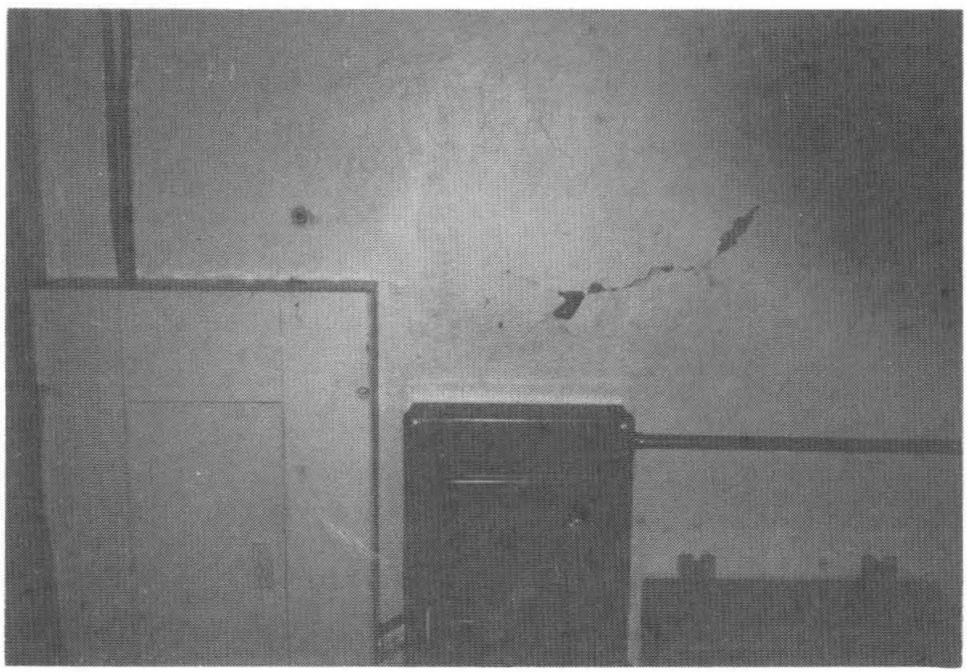

Figure 2-30: Diagonal Cracking in Central E-W Interior Wall, First Story

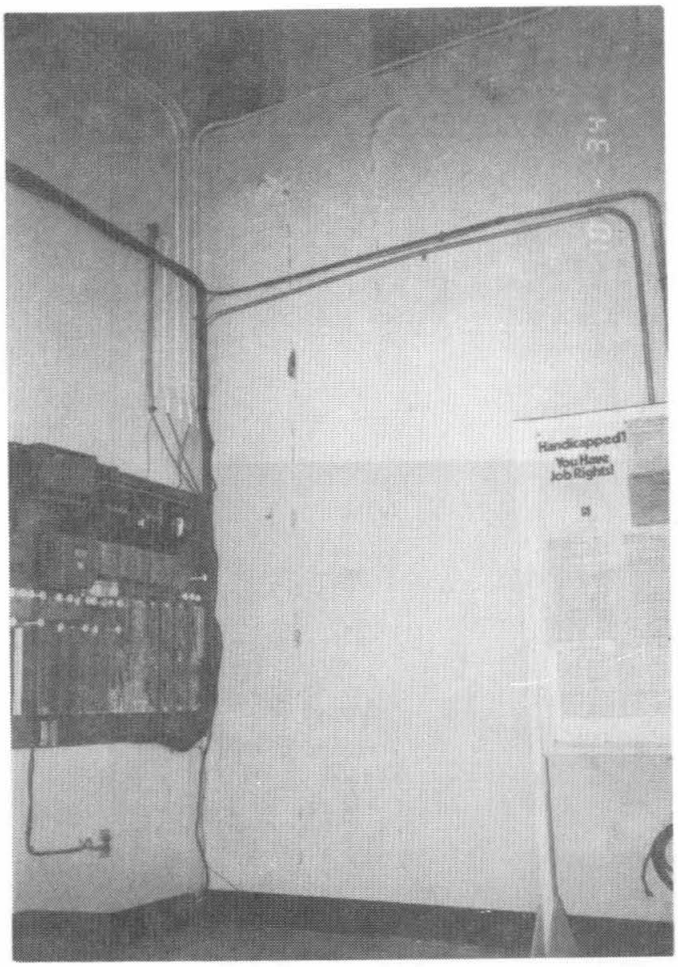

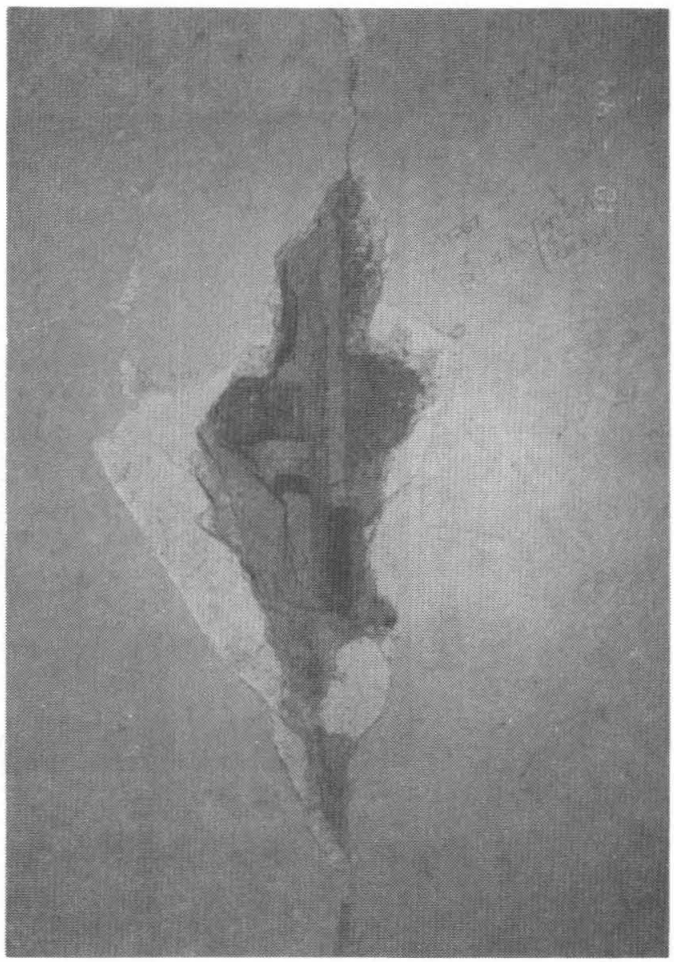

Figure 2-31: Relative Slip Between Masonry In-Fill and Surrounding Structure at the South Wall

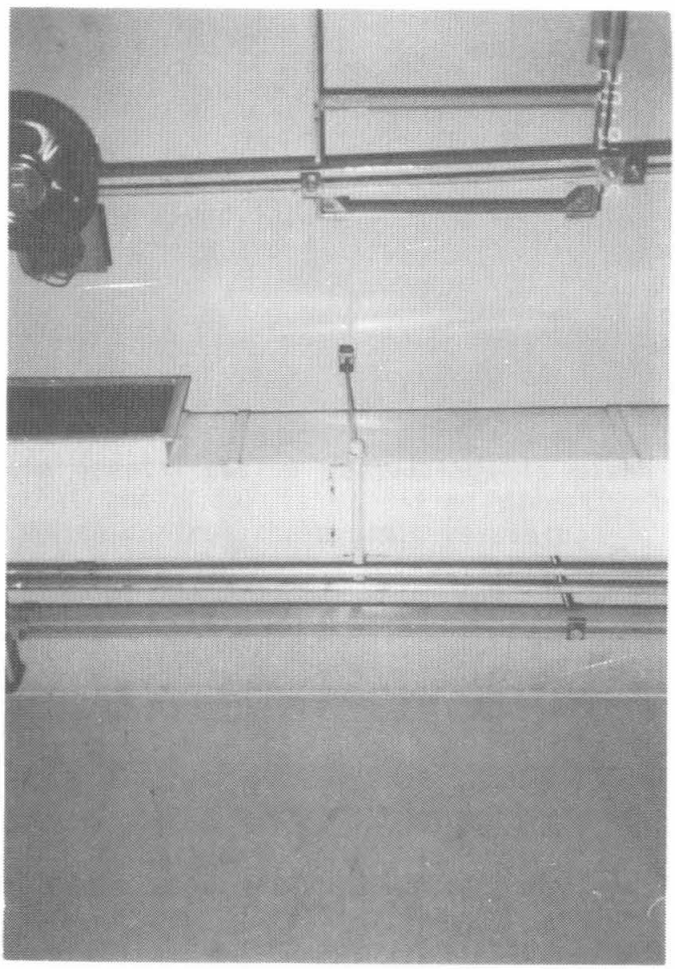

Figure 2-32: Relative Slip Between HVAC Duct and Support

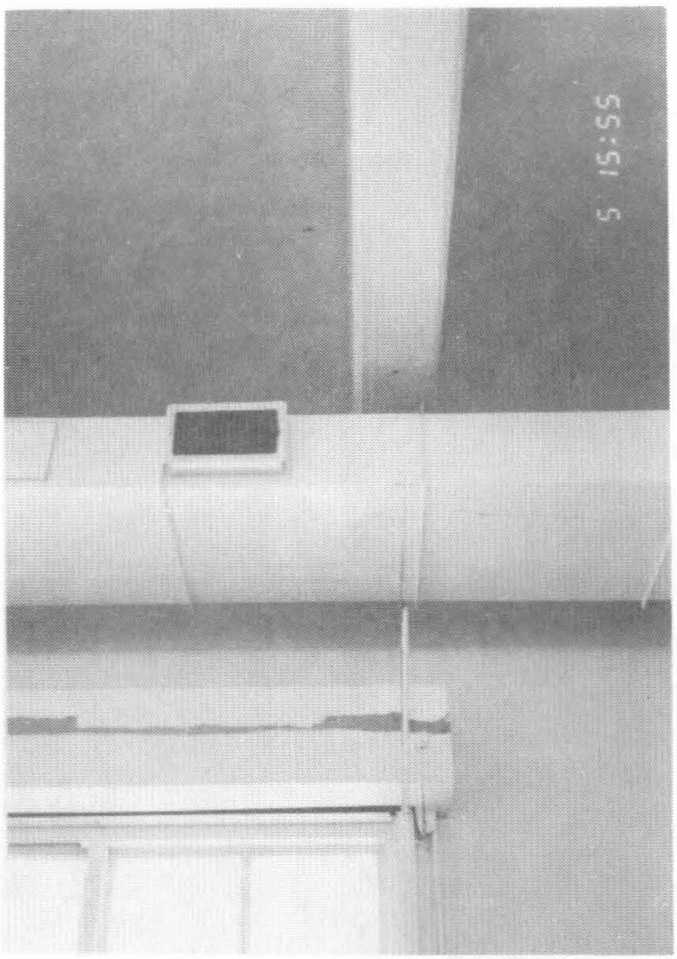

Figure 2-33: HVAC Duct Support Failure

3. MODAL IDENTIFICATION

A modal identification methodology was applied to the measured earthquake accelerations from the Watsonville telephone building to estimate its modal frequencies, equivalent viscous damping ratios, participation factors and modeshape components. This methodology and results obtained from its implementation are described in this section.

3.1 Modal Identification Methodology

3.1.1 Program MODE-ID

The modal identification method used in this project was originally developed by Beck [1978], and later extended by him to handle multiple inputs (excitation channels) and multiple outputs (response channels), as described in Werner, et al [1987]. The method is implemented in the computer program MODE-ID, which estimates the modal parameters from recorded motions based only on the assumptions of linear dynamics and classical normal modes; in particular, MODE-ID does not require a structural model involving mass and stiffness matrices to be specified. The model used by MODE-ID is summarized in Appendix A and a detailed description of the identification methodology is given in Appendix B. It can be seen that the model is specified directly in terms of the modal parameters which control the dynamic response.

The parameters estimated for each mode contributing to the response are the natural frequency, equivalent viscous damping ratio (as a percentage of critical damping), participation factors for each input or support degree of freedom, modeshape components for each output degree of freedom, and initial modal displacements and velocity (if the chosen time window of the data does not begin with the structure at rest). Only the modeshape components for the degrees of freedom at which the response is measured are identified, since the "missing" modeshape components cannot be determined without introducing a structural model. Pseudostatic response can be included to account for the quasi-static contributions to the structural motions induced by the support ("base") motions ignoring inertial and damping effects. In this case, an influence matrix that relates structural response at the output channels to the support motions must either be specified based on theory, or be estimated from the measured motions along with the dynamic modes (see Appendices A and B). The modes representing the dynamic contributions to the structural response then correspond to the "fixed-base" modes where all support degrees of freedom are held fixed. The simplest "pseudostatic mode" or "quasi-static" response is due to rigid body motion, which is the mode evaluated here.

In MODE-ID, the modal parameters are estimated by nonlinear least-squares matching of the model and measured response at each output degree of freedom; that is, the mean-square output error is minimized using all the channels of data corresponding to response signals over a prescribed time interval. The optimal parameters computed in this way can be viewed as the most probable values given the data [Beck, 1990].

The optimization algorithm used in MODE-ID is described in Beck [1978] and Werner, et al [1987] (See Appendix B).

Initial estimates for the modal parameters must be provided, but MODE-ID is very robust to the choice of all parameters except the initial modal frequencies, which must be chosen judiciously in order not to miss contributing modes, since the program tends to converge to the set of modes whose frequencies are close to the initial values. Fourier amplitude spectra of the measured input and output motions, and structural models if available, can be useful to guide the choice of the initial estimates for the modal frequencies.

MODE-ID has been successfully applied to the analysis of earthquake records from buildings [Beck and Jennings, 1980; McVerry and Beck, 1983], a bridge [Werner, et al, 1987], and an offshore platform [Mason, et al, 1989]. In addition to determining the appropriate modal parameters for a "time-invariant" linear model using the entire duration of the recorded motions, the time variation of the equivalent linear parameters can also be studied by applying MODE-ID to smaller time windows of the earthquake data. This can provide insight into the extent and nature of the nonlinearities in the response.

3.1.2 Measurement Noise and Model Error

MODE-ID produces the best estimates of the modal parameters that can be obtained for the linear model in the presence of both measurement noise in the data and model error due to inadequacies in the assumed modal model. These errors must be considered when interpreting the results.

Measurement noise consists of those errors arising during measuring, recording and digitizing which account for the differences between the actual structural motions and the digitized versions available for analysis. For measurement noise, the identified parameters are only affected by the noise spectrum near the frequencies of the contributing modes. Even then, the estimated modal parameters are not very sensitive to measurement noise, with the modal frequencies being the least sensitive [Beck and Beck, 1985]. For the levels of measurement noise expected in the CDMG accelerograms (of the order of 10^{-3}g), the induced errors in the modal parameters should be insignificant compared with the effects caused by inadequacies in the model used by MODE-ID at the strong amplitude levels measured in the building during the two earthquakes. For example, these "model errors", discussed in more detail below, cause differences in the estimated modal parameters from one time segment of the data to another which are much greater than errors due to measurement noise. The existence of model error implies that there are no exact or true values of the modal parameters However, MODE-ID produces the best estimates of these parameters within the limitations of the model used.

Another aspect of measurement noise is discussed later; i.e., with regard to difficulties in identifying "fixed-base modes" from response quantities for which rigid body motion has been removed.

Sources of "model error" include the assumption of linear viscous damping and the further idealization that it produces classical uncoupled modes, the assumption of a linear restoring force, and inaccurate or incomplete definition of the input motions to the structure. The estimated damping ratios should be viewed as equivalent viscous damping ratios which are dependent on the strength of the response, since the actual damping is more complex than the linear viscous model assumed, involving material hysteresis, Coulomb friction and radiation damping. The estimated modal frequencies should also be viewed as equivalent linear values for the chosen time window of the data. The MODE-ID results presented later show that these frequencies change substantially from one time window to the next, even in the more modest shaking produced by the Morgan Hill earthquake. Since the mass distribution does not change during an earthquake, the changing modal frequencies reflect changes in the lateral stiffness of the structure due to concrete cracking, loosening of connections between nonstructural components, such as partitions and masonry in-fill, and the structural shear wall system, changes in boundary conditions, and other effects.

An additional source of model error can occur when the pseudostatic response in MODE-ID is based on a specified theoretical pseudostatic influence matrix. For this analysis, the pseudostatic response reduces to rigid body motions because an assumption of a rigid base is made. Therefore, any deformation in the foundation could produce departures of the pseudostatic response from the calculated rigid body response. This in turn might induce errors in the modal parameters if they are altered by MODE-ID to compensate for the errors in the pseudostatic response. A more accurate theoretical pseudostatic matrix could be derived using a detailed theoretical structural model. This model would define support and response degrees of freedom, and a pseudostatic matrix relating these degrees of freedom could be developed for the building. In lieu of developing such a structural model, another approach to investigating the accuracy of the assumed pseudostatic matrix or rigid body transformation is to perform one additional analysis with MODE-ID after the modal parameters have been identified with the theoretical matrix. In this additional analysis, the matrix elements are also estimated by MODE-ID along with all the other parameters. If the new estimates of the modal parameters and the new pseudostatic response do not change significantly, then one can have confidence that the theoretical pseudostatic matrix is not biasing the estimates of the modal parameters. It will be seen later that this is indeed what happens when using the Morgan Hill earthquake data, but not when the Loma Prieta data is used.

3.1.3 Different Cases of Input-Output Definition

When program MODE-ID was applied to the strong-motion records obtained from the 1984 Morgan Hill and 1989 Loma Prieta earthquakes to identify the modal parameters for the building, a number of input-output channel combinations were considered. Only two cases were selected for final presentation in this report:

Case	Description	Input Channels	Output Channels
A	Fixed Base	9,10,13,z,r_y,r_x	7,8,5,6,12,11,1,2,3,4
B	Rocking Base	9,10,13,z	7,8,5,6,12,11,1,2,3,4

where z, r_y, r_x are the upwards vertical translation at the center of the base, the upwards contribution to Channel 3 from the base rocking about a N-S axis (y-axis) and the downwards contribution to Channel 3 from the base rocking about an E-W axis (x-axis) (Positive r_y and r_x were chosen to correspond to the top of the building moving to the east and to the north, respectively, rather than to correspond to positive angular rotations in the usual "right-hand" sense). The three values z, r_y, r_x at time t were computed from a least-squares fit to the vertical base Channels 1, 2, 3, and 4 at time t, assuming that the base is rigid. This assumption is only an approximation since the predicted rigid-base accelerations of Channels 1, 2, 3, and 4 using z, r_y, r_x are very close to, but do not match exactly, those recorded during the two earthquakes.

Other input-output cases considered include those defining 2-D models where the N-S input and output channels and E-W input and output channels were used separately. These 2-D models allowed for efficient exploration of the frequency parameter space to identify the natural frequencies of N-S and E-W modes, respectively, for both the fixed-base and rocking base cases. Only the fundamental modes could be identified, indicating that the higher modes made little contribution to the seismic response of the building.

A theoretical pseudostatic response was initially assumed in MODE-ID since past experience has shown that, when soil-structure interaction occurs, simultaneous estimation of the pseudostatic and modal parameters may be ill-conditioned. That is, small changes in input may induce large changes in the estimated parameters. The theoretical pseudostatic influence matrices were based on geometrical arguments using the precise locations of the accelerometers and the assumption that the base does not deform but only undergoes rigid-body motions. That is, the foundation gives a "rigid" base. These theoretical matrices are presented in Table 3-1 for both fixed base (Case A) and rocking base (Case B) cases.

Channels 9 and 10 were used directly as inputs, rather than the overall N-S translation of the base and the rotation of the base about a vertical axis, which can be computed from Channels 9 and 10 under the assumption of a rigid base. If the latter had been selected as inputs instead, the first two columns of the pseudostatic influence matrices in Table 3-1 would be different. The resulting pseudostatic responses, however, would be identical to those given by the matrices in Table 3-1 using Channels 9 and 10 as inputs.

Fixed base case runs of MODE-ID give the dynamic modal properties of the building with the base at rest, under the assumption of a "rigid" base. For this case, contributions to the building response from rocking of the base are given by the pseudostatic response obtained by multiplying the vector of input time histories by the pseudostatic influence matrix

given in Table 3-1. Initially, for the fixed base case, Channels 1, 2, 3 and 4 were used as input, along with Channels 9, 10, and 13, in order to account for the contributions to the structural response of rocking of the base. The output corresponded to Channels 7, 8, 5, 6, 12 and 11. After these runs of MODE-ID were performed, it was felt that it was better to use the four vertical channels to define the two rocking motions and overall vertical motion of the assumed rigid base, and then include the vertical channels in the set of output channels for MODE-ID. In this way, departures from the rigid-base assumption are detected as non-zero modeshape components identified for Channels 1, 2, 3 and 4.

The rocking base case gives the modal properties of the building with the assumed rigid base free to rock about any horizontal axis, but fixed against horizontal motions and overall vertical translation. Rocking of the base shows up as non-zero modeshape components at Channels 1, 2, 3, and 4. Departures from the rigid-base assumption show up as departures from the expected rigid-base pattern for the modeshapes at the vertical base channels. An additional assumption in the rocking base case, which is not needed in the fixed base case, is that the rocking is due to soil-structure interaction and not due to wave passage effects. The latter contribution, if important, cannot be separated out with the array of instrumentation installed in the building.

3.2 MODE-ID Results

For both the Morgan Hill and Loma Prieta earthquakes, the modal parameters for the fixed base and rocking base cases were identified from the complete digitized records (0 to 40 seconds). The corresponding dynamic models are called the "time-invariant" optimal linear models since the identified modal parameters, which give the best fit to the recorded response, are constant over the entire duration of the response. To investigate the extent of nonlinearities in the response, MODE-ID was also applied to several time windows for each earthquake. If the response was indeed linear, only small differences in the estimated modal parameters from different time windows would be observed, since studies with simulated data shows that the estimation process is not sensitive to measurement noise [Beck and Beck, 1985]. Significant changes in the modal parameters from one time window to another, therefore, indicate the nonlinearities in the response. In this case, the "time-invariant" parameters tend to reflect the equivalent linear values effective during the strongest motions.

3.2.1 Identification with the Theoretical Pseudostatic Matrices

3.2.1.1 Frequency Estimates

The identified fundamental E-W and N-S modal frequencies and damping values for time-invariant models and models for various time windows are presented in Tables 3-2 and 3-3 for the Morgan Hill and Loma Prieta earthquakes, respectively. The theoretical pseudostatic matrices based on rigid body transformations which are given in Table 3-1 for the fixed base and rocking base cases were used in MODE-ID. The quantity J given

in the last column of Tables 3-2 and 3-3 is a measure of fit of the model response to the recorded response. It is equal to the ratio of the mean-square acceleration output-error to the mean-square recorded acceleration response. A value of J of 5% or less, as obtained by the identified Morgan Hill models, represents an excellent match of the recorded response by the model, as can be seen in the time-history plots presented later. Values of J of 10% or more were obtained for the time-invariant models from the Loma Prieta earthquake. This indicates the greater difficulty experienced in matching the recorded response to this earthquake, presumably because of stronger nonlinear behavior.

As shown in Table 3-2, the fixed base time-invariant model identified from the Morgan Hill records gives frequencies of 4.03 Hz and 5.51 Hz for the E-W and N-S modes, respectively. However, non-linearities occur even in the case of the moderate Morgan Hill earthquake, since the modal parameters vary significantly from one time window to the next. In particular, the modal frequencies tend to decrease as the response amplitudes increase, as expected. For example, the fixed base fundamental N-S frequency changes from 5.88 Hz to 5.26 Hz, and then to 5.65 Hz, for the 0-7, 7-14, and 14-21 time windows, respectively. These frequency variations indicate that a reduction of structure stiffness occurs as the building motions increase to their peak values, which occur in the 7-14 second window. As the seismic response diminishes, the building stiffness increases, although this stiffness recovery does not appear to be complete.

Somewhat surprisingly, the modal frequencies identified for the Loma Prieta earthquake are relatively stable. As shown in Table 3-3, the identified E-W and N-S frequencies for the different time windows show little deviation from their time-invariant values, which are 2.72 Hz and 4.23 Hz, respectively. It appears that the building lost substantial stiffness in the first few seconds of the Loma Prieta response, but then suffered very little further stiffness reduction. The substantial drop in modal frequencies from the later time intervals for Morgan Hill to the 0-10 second interval for Loma Prieta suggests that a large decrease in stiffness was produced by the latter earthquake, since there was no other strong earthquake between these two events. Unfortunately, attempts to identify the modal parameters over the 0-3 second interval prior to the onset of the large-amplitude Loma Prieta response were not successful, except for a planar (2-D) E-W model. This model gave a negative damping but the identified model frequency was 3.82 Hz which is close to the E-W model frequency of 3.85 Hz for the 14-21 second interval of the Morgan Hill response (Table 3-2).

For the 21-40 second interval of the Morgan Hill earthquake, the identified modal parameters are considered unreliable for the fixed base case. The E-W fixed base mode identified by MODE-ID appears to correspond to the E-W rocking base mode, and the N-S fixed base frequency appears to be too low. As discussed later, the identification of the fixed base modes is somewhat ill-conditioned and this problem may have been accentuated over the 21-40 second interval because the two fundamental modes make a small contribution compared to the pseudostatic response over this interval. A similar problem occurs for the 21-40 second interval of the Loma Prieta earthquake where the N-S fixed base

mode could not be identified at all. Although the 21-40 second interval results are considered unreliable, this does not suggest errors in the time-invariant results which, as previously noted, tend to be influenced primarily by the strongest portions of the building responses.

3.2.1.2 Damping Estimates

A surprising result for the damping estimates in Table 3-2 and 3-3 is that the fundamental E-W and N-S mode damping values are substantially different, with the N-S damping values generally being much larger than the E-W values for both the fixed and rocking base cases. For example, for the Morgan Hill earthquake, time-invariant damping values of 4.9% and 11.6% were estimated for the fixed base E-W and N-S modes, respectively. This occurs despite the fact that motions in the E-W direction are much larger than in the N-S direction (Table 2-1). Although the reason for this is not clear, it seems to be a real effect since the identified models fit the data extremely well in the Morgan Hill case.

The E-W mode damping estimated for the fixed base case from the Morgan Hill records in the 0-7 second time window is negative (-2%). Usually this means that there are other inputs exciting the mode which were not provided as input channels to MODE-ID. However, in this particular case, all the inputs have been represented quite well by the input channels selected for MODE-ID (Table 3-1). In fact, there is evidence to suggest that the appropriate damping for the E-W mode over the 0-7 second interval might be larger than 5%. As shown in Figure 3-3, the response at Channel 11 over 0-7 seconds that is calculated by the fixed base time-invariant model exceeds the recorded response. This suggests that the actual damping value over this interval should be greater than the identified value of 4.9%. After the largest response between 7 and 8 seconds, the time-invariant response tends to be less than the recorded response for Channel 11. This suggests that the actual damping is less than 4.9% after the peak response. Also, a fixed base case analysis of MODE-ID using a 5-15 second time window gave an E-W damping value of 4.7% in contrast to 2.4% for 7-14 seconds, whereas the corresponding E-W frequencies of 4.02 Hz and 4.06 Hz were virtually unchanged. The implication is that the E-W damping in the fixed base case was more than 5% until after the peak E-W response between 7 and 8 seconds when it dropped to around 2%. This explains why the time-invariant case gives 4.9% damping even though the E-W damping estimates for 7-14 seconds and 14-21 seconds in Table 3-2 are much lower (As mentioned earlier, the value of 8.3% damping for 21-40 seconds is not considered meaningful for the fixed base E-W mode). As a final comment, note from Table 3-2 that the damping for the rocking base E-W mode for the 0-7 second interval is also larger than the damping for the time-invariant model (6.3% compared with 6.1%). This is consistent with the variation of the fixed base E-W modal damping noted above.

The identified fixed base modal parameters for the E-W mode, Loma Prieta earthquake, are suspect. For example, the time-invariant damping of 17% is unusually high, although possible if significant "damage" has occurred. However, it should be smaller than the corresponding rocking

base damping of 8%, since the latter includes additional damping from radiation and material damping in the soil. Also, the modal frequencies for the rocking base case should be less than those for the fixed base case because of the additional flexibility. However, the fixed base modal frequency is almost identical to that for the rocking base case (2.72 Hz and 2.65 Hz for the time-invariant models for the fixed and rocking base cases respectively).

These unexpected results for the fixed base E-W mode in the Loma Prieta earthquake are thought to be due to an inherent ill-conditioning in identifying "subsystem" modes in the presence of strong "system" modes which is accentuated by the larger model error for the Loma Prieta response. In theory, subsystem modes such as the fixed base modes, can be identified with an appropriate choice of input motions, even though it is the overall soil-structure system modes which are quasi-resonantly excited by the earthquake. However, the identification is somewhat ill-conditioned, since the subsystem frequencies are close to minima in the Fourier amplitude spectrum (F.A.S.), in contrast to the overall system frequencies which are close to maxima in the F.A.S. (The location of the maxima and minima are also influenced by the spectral behavior of the excitation in the frequency domain). The subsystem modal parameters are therefore more influenced by noise and model error than the overall system modal parameters. Significant model error coupled with the inherent ill-conditioning, may cause the optimization process to converge on the rocking base modal frequency even though a rocking pseudostatic contribution has been included in order to try to force convergence to the fixed base modes.

The larger model error for the Loma Prieta response compared with the Morgan Hill response, which accentuates the ill-conditioning in identifying the fixed base modes, could conceivably arise from two sources. The first possibility is stronger nonlinear behavior because of the larger response amplitudes. The second possibility is that there are significant errors in the theoretical rocking pseudostatic response due to the assumption of a rigid base. Although the pseudostatic matrix assumed in the Loma Prieta case is the same as that used for the Morgan Hill earthquake where it produces good results, the much larger response amplitudes may cause the assumption of a rigid base to be a poorer approximation for the stronger Loma Prieta response. In either of these cases (i.e., a strong nonlinear dynamic contribution or a non-rigid body pseudostatic response), the identified equivalent linear model may give such a poor match for frequencies near an overall fundamental soil-structure system "mode" that the residual error for this "mode" swamps the nearby fixed base (subsystem) "mode". However, as shown later by examining the model and recorded motions in the frequency domain, the rigid base assumption still seems to yield a good overall response even for the Loma Prieta earthquake. The stronger nonlinear behavior for this earthquake is, therefore, the likely source for the difficulties in identifying the E-W fixed base mode.

3.2.1.3 Mode Shapes

The identified fixed base E-W modeshapes for time-invariant models and models for the same time windows as in Tables 3-2 and 3-3 are presented in Tables 3-4 and 3-5 for the Morgan Hill and Loma Prieta earthquakes, respectively. The corresponding fundamental N-S modeshapes are given in Tables 3-6 and 3-7. The modeshape components given in these tables correspond to all the output channels, although those components corresponding to the vertical channels at the ground floor of the building are presented in the form of the rocking components at the base of each of the four walls.

One point to note is that, although non-linearities in the response apparently lead to the observed changes in the identified modeshapes for the different time windows, these changes are not large. Furthermore, the changes occurring during the Morgan Hill and Loma Prieta responses are of the same magnitude, and the modeshapes are mostly similar for the two earthquakes, particularly for the dominant components. One significant difference is that the overall N-S component at the third floor (the average for Channels 7 and 8), is about 20% greater in the Loma Prieta earthquake than in the Morgan Hill earthquake. This suggests that the loss of stiffness in the lower two stories relative to the upper two stories was greater during the Loma Prieta response than during the Morgan Hill response. Although it is the overall loss of stiffness which primarily controls the changes in modal frequencies during the response, it is the relative loss of stiffness from one story to another which primarily controls the changes in the modeshapes.

The modeshapes in Tables 3-4 to 3-7 are clearly three-dimensional, but the orthogonal translational components for the E-W modeshape (i.e. the averages of N-S Channels 7 and 8 and of Channels 5 and 6) are only a few percent of the E-W roof component. The orthogonal translational components for the N-S modeshape (i.e. E-W Channels 12 and 11) range up to 25% of the dominant N-S roof component, but they behave rather erratically from one time window to the next. The ill-conditioned nature of the identification of the fixed base ("subsystem") modes may be responsible for the erratic behavior of these modeshape components, although it is not clear why the N-S mode is more affected than the E-W mode.

The torsional components of both the E-W and N-S modeshapes are approximately +5% at the third floor (half the difference of Channels 8 and 7) and +10% at the roof (half the difference of Channels 6 and 5) relative to the dominant roof component, except for the E-W modeshape identified from the Loma Prieta records during the strongest shaking (0-10 second interval) where the torsional components are less than half these values. These torsional motions of the fundamental modes are accompanied by compatible rocking components at the bases of the walls. For example, the west wall rocks to the south while the east wall rocks to the north when the building moves to the north in the N-S mode of vibration. The "overall" N-S rocking motion of the ground floor in the N-S-mode is given by summing the two N-S rocking components in Tables 3-6 and 3-7, and it is +1% or less of the dominant N-S roof component in all cases. Similar results hold for rocking of the walls in the E-W

mode, with the "overall" E-W rocking motion of the ground floor now less than 1/2% of the E-W roof component.

These results indicate some flexibility of the foundation. For example, as shown in Table 3-6 for the fixed base N-S mode, the east wall (Channels 6 and 8) apparently experiences greater translation than the west wall (Channels 5 and 7) when the structure as a whole translates to the north. This is accompanied by a rotation at the base of the east wall relative to the assumed rigid foundation (Channels 2 and 4) that tends to increase the translation of this wall at the upper floors. In contrast, the rotation at the base of the west wall relative to the assumed rigid foundation (Channels 1 and 3) tends to decrease the upper floor translations of the wall. This behavior likely occurs because the east wall is solid and thus stiffer than the west wall, which has openings. As a result, the east wall experiences greater base rotation than the west wall, since the foundation is not sufficiently rigid to fully constrain these rotations. This is reflected in the identified modeshapes by positive and negative rotations at the bases of the east and west walls, relative to the plane of the assumed rigid foundation (Table 3-6) (Note that rigid body motion of the building, which includes overall rocking of the foundation, is included in the pseudostatic contribution to total response). The combination of base rotations and wall deformations result in total translations of the east wall that are greater than those of the west wall. These translations imply a torsional modeshape component that is opposite to what would be expected if the foundation were truly rigid. In the latter case, since the west wall with its openings is more flexible than the east wall, it would be expected to undergo greater deformation in the N-S direction.

3.2.1.4 Effective Participation Factors

An effective participation factor is the product of a participation factor and a modeshape component; there is one for each input-output channel pair (see Appendix A). These parameters are invariant with respect to the modeshape scaling and are important modal parameters controlling the dynamic response, along with the modal frequencies and damping values. The fixed base E-W mode effective participation factors at the roof for time-invariant models and for models for selected time windows are presented in Tables 3-8 and 3-9 for the Morgan Hill and Loma Prieta earthquakes respectively. The N-S mode effective participation factors are given in Tables 3-10 and 3-11. The values in Tables 3-8 to 3-11 are based on the dominant modeshape component at the roof of the building and the input channels corresponding to the columns in the tables are defined in Figure 2-1 and Section 3.1.3. The values at other output degrees of freedom can be obtained by simply multiplying the values in these tables by the appropriate modeshape component in Tables 3-4 to 3-7. As noted earlier, the estimated parameters for the intervals 21-40 second and 20-40 second for the Morgan Hill and Loma Prieta earthquakes respectively, are unreliable because of ill-conditioning in the identification of the fixed base modes along with the low signal for the modal contributions over these intervals.

Consider first the time-invariant values in Table 3-8 for the fixed base E-W mode identified from the Morgan Hill earthquake. As expected for the E-W mode, the largest effective participation factor corresponds to the E-W input Channel 13. This value of -1.22 is close to that of -1.27 for a shear beam. The other large value of -1.05 corresponds to the rocking motion r_y of the foundation about a N-S axis. Transforming this to an angular measure yields a value of approximately 43, which is somewhat different from the theoretical value for a shear beam of 0.81 times the height, or 53, for this building. Also, because of the torsional motion and the N-S translation of the E-W mode, the effective participation factors for the N-S inputs, Channels 9 and 10, are nonzero. The sum of the values for these channels corresponds to excitation of the E-W mode by the overall N-S motion of the foundation, while the difference between Channel 10 and 9 corresponds to excitation of the E-W mode by torsional motion of the foundation. Similar behavior is observed in the results for the different time windows in Table 3-8, but the values identified vary somewhat, particularly for Channels 9 and 10 and for the rocking motion r_y.

It should be noted that some ill-conditioning can be expected in the estimation of participation factors corresponding to input motions which are very similar, such as Channels 9 and 10 for the building during the Morgan Hill earthquake. In this case, it is the sum of the corresponding participation factors which primarily controls the excitation of the modes, and not their individual values. As a consequence, the sum of these participation factors, but not their individual values, will be accurately estimated. If, as an extreme case, Channels 9 and 10 had identical accelerations over the time window chosen, only the sum of their participation factors would be estimated, with the individual values being completely non-unique in the estimation process. Another way to state this result is that the individual values of the participation factors for Channels 9 and 10 can only be identified if there is significant torsional motion of the foundations, so that the motions at Channels 9 and 10 are significantly different. However, for the Morgan Hill earthquake, this does not occur, as illustrated by the nearly identical response spectra for Channels 9 and 10 in Figure 2-28.

For the models identified from the Loma Prieta records, Table 3-9 shows that the largest effective participation factor again corresponds to the E-W input Channel 13, and it has the same value of -1.22 for the time-invariant model as for the Morgan Hill earthquake. However the values for the N-S input Channels 9 and 10 and for the rocking motion r_y are significantly different from those in Table 3-8. In particular, for 0-40 seconds and 0-10 seconds, the values corresponding to r_y from the Loma Prieta earthquake are opposite in sign to those from the Morgan Hill earthquake. As mentioned earlier, the identified modal parameters for the fixed base E-W mode from the Loma Prieta records appear to be influenced by the strongly-excited rocking base E-W mode.

The effective participation factors for the fixed base N-S mode given in Tables 3-10 and 3-11 show that the largest values are for the N-S input Channels 9 and 10 and the rocking motion r_x of the foundation about an E-W axis, as expected. The sum of the values for Channels 9 and 10

corresponds to excitation of the N-S mode by the overall N-S motion of the foundation. For the Morgan Hill earthquake (Table 3-10), this sum is within 10% of unity in magnitude for all the models reliably identified, giving values which are 15% to 25% smaller than expected. If these values were scaled up to -1.22 to agree with the time-invariant value for the E-W mode, the damping for the N-S mode would have to be increased proportionally [Huang, et al, 1985] by 15% to 25% to obtain a model response which is comparable to the recorded N-S response at Channel 5, 6, 7 and 8. Since the damping of the N-S mode is already higher than expected, it seems unlikely that a trade-off between the participation factors and the damping during identification is the reason for the low participation factors for the N-S motion of the foundation, despite the fact that this trade-off is known to be a possibility [Beck, 1978].

It is of interest that for the time-invariant model and the model identified from the 0-10 second interval of the Loma Prieta records where the response amplitudes are largest, the sum of the effective participation factors for Channels 9 and 10 (Table 3-11) for the fixed base N-S mode is -1.31, which is close to that of -1.27 for a shear beam. However, for the 10-20 second interval, where the response amplitudes are comparable to those during the Morgan Hill earthquake, the sum of the values for Channels 9 and 10 drops about 20% to 1.06, which is in the range of the values of the sum for the models identified from the Morgan Hill records. This suggests that the variations in these values for the fixed base N-S mode could be due to nonlinearities, although it is not clear why the N-S mode should exhibit this effect while the fixed base E-W mode does not.

It should be noted that the linear model used in the modal identification has the participation factors as "free" parameters (see Appendix A). It is necessary to estimate these parameters along with the other "free" modal parameters because the complete modeshapes are not determined, since only the components at the measured output degrees of freedom are estimated. If a structural model with M degrees of freedom was known, then the participation factors would be derived from the mass matrix of order M and the M components of the complete modeshape vector. The linear modal model used in program MODE-ID is therefore more general than that derived from a linear structural model, because of these additional free parameters. As shown later in Section 5.2, if a simplified 24 degree-of-freedom structural model is modified to match the fixed base fundamental E-W and N-S frequencies and modeshapes identified from the Morgan Hill records, then the derived participation factors have values close to what might be expected. In particular, the derived participation factors for the fixed base N-S mode are significantly higher than the identified values using MODE-ID, but this leads to calculated N-S responses of the modified structural model which are too large compared with the recorded N-S responses.

3.2.1.5 Response Comparisons

Comparisons of the time-invariant model roof accelerations and recorded roof accelerations for the two earthquakes are shown in Figures 3-1 to

3-9. In these plots, the solid curve is always a recorded response and the dashed curve is the corresponding quantity calculated using the time-invariant model with only two contributing modes, the fundamental E-W and N-S modes, and with the theoretical pseudostatic response. The comparison plots for the Morgan Hill earthquake are given in Figures 3-1 to 3-3 for the fixed base identified models and Figures 3-4 to 3-6 for the rocking base case identified models. Only the time window from 4 to 16 seconds is shown. The models in both cases give very good matches of the recorded roof accelerations, as expected from the low values of the measure of fit J in Table 3-2. The matches for the fixed base case are slightly better than for the rocking base case, possibly because excitation of the building due to rocking of the foundation by the vertical ground motion is not included in the latter case, where it is assumed that rocking of the foundation is only due to soil-structure interaction.

The comparison plots for the Loma Prieta earthquake are given in Figures 3-7, 3-8, and 3-9 for the roof Channels 5, 6 and 11 respectively. Only the results for the fixed base time-invariant model are presented, but to show more detail, the 0-40 second interval is presented in three plots in each of Figures 3-7 to 3-9, covering 0-10 seconds, 10-20 seconds and 20-40 seconds. It is clear that the matches of the recorded roof accelerations by the time-invariant model are not as good in this case as in the Morgan Hill earthquake. This is supported by the larger values of the measure of fit J in Table 3-2. Apparently, the large amplitudes produced by the Loma Prieta earthquake caused strong nonlinear behavior which the linear models can not adequately represent.

Figure 3-10 to 3-15 again show the quality of the match of the recorded roof response for the Morgan Hill earthquake by the time-invariant models for both the fixed and rocking base cases, but this time the comparison is in the frequency domain. For these plots, a three-mode model was used, where the additional mode was an identified torsional mode. For the fixed base torsional mode, the estimated frequency and damping were 8.02 Hz and 9.7% respectively. For the rocking base torsional mode, the estimated frequency and damping were 7.77 Hz and 7.5%. The addition of the torsional mode improves the frequency domain match in the 5 Hz to 8 Hz range for the N-S output channels, but has little effect below 5 Hz. In the time domain, the torsional mode makes only a small contribution to the response and it has little effect on the time-history comparisons. In Figures 3-10 to 3-15, the frequency-domain match is good up to about 8 Hz and is very good up to about 3 Hz. The model response below 3 Hz is dominated by the pseudostatic response, since the lowest mode is at 4 Hz and 3.5 Hz in the fixed and rocking base cases, respectively.

Figures 3-16 to 3-21 give a frequency-domain comparison for the Loma Prieta earthquake using the time-invariant models for both the fixed and rocking base cases, respectively. For these plots, only a two-mode model was used, since the torsional mode could not be identified. The quality of the frequency-domain match is not as good as in the Morgan Hill earthquake, as expected. Note that, once again, the match is best in the range where the pseudostatic contribution dominates the response, which is for frequencies less than about 2 Hz. This suggests that the

theoretical pseudostatic influence matrices for the fixed and rocking base cases work nearly as well for the Loma Prieta earthquake as they did for the Morgan Hill earthquake.

In Figures 3-22 to 3-24, the recorded roof accelerations over the 10-20 second interval of the Loma Prieta earthquake are compared with the accelerations computed using a fixed base two mode model identified from this interval. This interval is of interest since the response amplitudes are comparable to those during the Morgan Hill earthquake. The match of the recorded accelerations shown in Figures 3-22 to 3-24 is good, although not as good as in Figures 3-1 to 3-3 for the Morgan Hill earthquake. Note that the value of J for the fixed base case, 10-20 seconds, in Table 3-3 is substantially smaller than for 0-10 seconds, where the amplitudes are much larger, but it is larger than for the time-invariant model in Table 3-2 (Morgan Hill earthquake). Note also that the modal damping values for the fixed base case, 10-20 seconds, in Table 3-3 are comparable to those for the time-invariant model in Table 3-2, showing that, at least in these cases, comparable response amplitudes give comparable modal damping values.

3.2.2 Identification Including Estimation of Pseudostatic Matrix

To examine whether some of the unexpected results described in Section 3.2.1 for the fixed base case might be due to an inaccurate assumption of a rigid base in calculating the theoretical pseudostatic response, additional analyses of MODE-ID were performed as described in Section 3.1.2. That is, the program was directed to identify the pseudostatic influence matrix as well as the modal parameters for a time-invariant model. The initial estimates supplied to MODE-ID were those presented in Section 3.2.1 for the time-invariant fixed base model.

The MODE-ID results for the Morgan Hill earthquake are presented in Table 3-12. The estimated pseudostatic matrix in Table 3-12 can be compared with the corresponding theoretical matrix in Table 3-1 for the fixed base case. Although the identified pseudostatic response may be reliable for the Morgan Hill earthquake, the individual elements in the identified influence matrix are not expected to be because of ill-conditioning in their estimation by MODE-ID. For example, input Channels 9 and 10 have very similar acceleration time histories, and so their contribution to the pseudostatic response is being controlled primarily by the sum of the elements corresponding to Channels 9 and 10 in each row of the influence matrix, rather than by the individual values of these elements. As a consequence, the sum of these elements, but not their individual values, will be accurately estimated. In the extreme case of Channels 9 and 10 having identical accelerations over the time window chosen, only the sum of the corresponding elements in each row of the matrix can be estimated, with the individual values being completely non-unique in the estimation process. This ill-conditioning is very similar to that which occurs in the estimation of the participation factors corresponding to similar input motions, such as Channels 9 and 10, which was discussed in Section 3.2.1. If just the sum of the first two columns of the pseudostatic matrix corresponding to input Channels 9 and 10 in Table 3-12 is considered, then it can be seen

to be indeed close to the corresponding sum of the first two columns in the theoretical pseudostatic matrix in Table 3-1.

Another type of ill-conditioning in the estimation of the pseudostatic matrix elements can arise because there are contributions to the input motions from the modes of the complete building-soil system due to soil-structure interaction. These "system" modes therefore contribute to both the input and output motions. If there was no other contribution of the input than from these modes, such as during free vibrations of the building, it is clear that with a sufficient number of elements to be estimated in the pseudostatic matrix, this matrix could be altered during the estimation process so that the output was completely accounted for by a fictitious "pseudostatic" response. This incorrect pseudostatic response would account for the output motions by a linear combination of the input motions, since both would be due to a linear combination of the "system" modes. When the input motions also have an external contribution, as in the Morgan Hill and Loma Prieta earthquakes, it is still possible to have a trade-off to some extent between the modal parameters and the elements of the pseudostatic matrix during the identification process. This is because, in the presence of model error and measurement noise, the pseudostatic response and dynamic modal contributions can be partially traded-off without significantly changing their sum, the total response, as long as there are "system" modes which contribute to both the input and the output motions.

In view of this possible ill-conditioning, the elements in the identified pseudostatic matrix in Table 3-12 are reasonably close to their theoretical counterparts in Table 3-1. But an even more important result is that the pseudostatic responses computed using the input motions from the Morgan Hill earthquake and the pseudostatic matrices in Tables 3-1 and 3-12 are very close, despite the differences in these matrices. This implies that the dynamic contributions, which are the sums of the fixed base modal contributions, are also close in the two cases, since the total model responses are nearly the same. Indeed, the measure of fit J decreases from 0.033 when the theoretical pseudostatic matrix is used to 0.028 when this matrix is identified, a very small decrease, supporting the fact that the model responses are nearly the same in the two cases.

The modal parameters in Table 3-12 can be compared with their counterparts in Tables 3-2, 3-4, and 3-6. The modal frequencies change by about 1% and the modal dampings change by less than 4%. The dominant components of the modeshapes change by less than 2% for the E-W mode and by less than 20% for the N-S mode.

The overall impression gained by these results for the Morgan Hill earthquake is that there is no substantial change in the identified modal parameters in the two cases which would cast doubt on the assumption of a rigid base used in computing the theoretical pseudostatic response. Therefore, the estimates of the modal parameters given in Tables 3-2, 3-4, and 3-6 for the time-invariant case can be used with confidence as the representative equivalent linear parameters for the building for the Morgan Hill earthquake, and also for other

strong-motion similar in intensity to the shaking during this earthquake.

The situation is completely different for similar runs of MODE-ID using the Loma Prieta earthquake records. For these data, the identified pseudostatic matrix, modal frequencies and modal damping values are substantially different from the corresponding results for the time-invariant model. In particular, the identified N-S mode frequency changed from 4.23 Hz when the theoretical pseudostatic matrix was used to 3.13 Hz when the pseudostatic matrix was estimated simultaneously with the modal parameters. A surprising result is that despite this large change in the N-S mode frequency, the corresponding modeshapes are quite close.

It is felt that for the Loma Prieta earthquake, the ill-conditioning described earlier, in the presence of a large model error due to the strong nonlinear dynamics of the building, causes a strong interaction between the modal parameters and the estimated pseudostatic matrix elements by a trade-off between the dynamic and pseudostatic parts of the response. This is also consistent with the fact that the optimization algorithm in MODE-ID took many times longer to converge in the Loma Prieta case than in the Morgan Hill case.

Thus, simultaneous estimation of the modal parameters and the pseudostatic matrix cannot be done reliably from the Loma Prieta records. Since the theoretical pseudostatic matrix for the fixed base case in Table 3-1 was shown to give good results in the case of the Morgan Hill earthquake, the best that can be done is to assume that the rigid base assumption continues to be a good one so that the same matrix is applicable. That is, the pseudostatic response continues to be described by rigid body motions even though the dynamic part of the response may be much more nonlinear than in the Morgan Hill earthquake. This assumption is supported by previously mentioned good match in the frequency domain at low frequencies where the pseudostatic response dominates the total response to the Loma Prieta earthquake.

3.3 Concluding Remarks

The overall impression gained from the modal identification of the building is that the modal parameters for the Morgan Hill earthquake are accurate, and can be used with confidence in assessing structure response characteristics as described in the following sections. However, the corresponding results from the Loma Prieta earthquake, particularly for the E-W fixed base mode, are less reliable. The identified modal models for both the fixed base and rocking base cases for the Morgan Hill earthquake give a very good match of the recorded response. The corresponding models for the Loma Prieta earthquake do not do as well in matching the recorded response of the building.

It appears that model error due to nonlinearities in the building's response to the Loma Prieta earthquake accentuates the inherent ill-conditioning in the identification of the fixed base ("subsystem") modes. In particular, the very strong E-W response of the fundamental

E-W mode of the overall building-soil system appears to prevent program MODE-ID from reliably identifying the fixed base E-W mode. On the other hand, the results for the fixed base N-S mode from Loma Prieta earthquake appear more reasonable. It should be noted that some unpublished work applying MODE-ID to simulated numerical data where there is no model error but white noise is added to the computed signals gives accurate identification of the fixed base "sub system" modes for a simple two-story rocking-building. Furthermore, the accuracy of the identified fixed base modal parameters deteriorates gracefully as the signal-to-noise ratio decreases.

The time-varying models produce results which are generally consistent with expectations, such as modal frequencies which decrease with increasing response amplitudes and modeshapes which do not change greatly with changing amplitude levels. There are a few exceptions, such as a case of negative damping (Table 3-2, 0-7 seconds) and results which are suspect for the time intervals 21-40 seconds and 20-40 seconds for the Morgan Hill and Loma Prieta earthquakes respectively.

There are also several puzzling results shared by the time-invariant and time-varying models which, despite being unexpected, appear to be reliable estimates for the equivalent linear parameters during each earthquake. The first of these is the high N-S mode damping (10% or more) compared with that of the E-W mode (about 5% or less) despite the higher responses in the E-W direction during both earthquakes. The second puzzling result is the low participation factors for the fixed base N-S mode for response during the Morgan Hill earthquake, as wells as during time intervals of the Loma Prieta earthquake during which response amplitudes were experienced which were comparable to those in the Morgan Hill earthquake. Finally, the identified "fixed base" modeshapes show that parallel walls of the building actually rock in opposite directions during vibrations in either of the fundamental modes. This rocking causes torsional rotations of the floors which are in the opposite direction to what would be expected if only the unequal resistance of the walls was considered.

Table 3-1

THEORETICAL PSEUDOSTATIC INFLUENCE MATRICES USED IN MODE-ID

Fixed Base Case

Output Channels	Input Channels 9	10	13	z	r_y	r_x
7	1	0	0	0	0	1.03712
8	0	1	0	0	0	1.03712
5	1	0	0	0	0	1.99873
6	0	1	0	0	0	1.99873
12	0	0	1	0	0.96826	0
11	0	0	1	0	1.86601	0
1	0	0	0	1	0.99177	1.01447
2	0	0	0	1	-1	0.72121
3	0	0	0	1	1	-1
4	0	0	0	1	-1	-1.02329

Rocking Base Case

Output Channels	Input Channels 9	10	13	z
7	1	0	0	0
8	0	1	0	0
5	1	0	0	0
6	0	1	0	0
12	0	0	1	0
11	0	0	1	0
1	0	0	0	1
2	0	0	0	1
3	0	0	0	1
4	0	0	0	1

Table 3-2

IDENTIFIED MODES FROM MORGAN HILL: FREQUENCY (Hz), DAMPING (%), J (%)*

Time Segment	Fundamental E-W						Fundamental N-S					
	Case A: Fixed Base			Case B: Rocking Base			Case A: Fixed Base			Case B: Rocking Base		
0-40	4.03	4.9	3.3	3.62	6.1	5.2	5.51	11.6	3.3	4.73	14.7	5.2
0-7	4.47	-2.2**	2.8	3.90	6.3	4.9	5.88	8.8	2.8	4.98	13.9	4.9
7-14	4.06	2.4	2.0	3.57	5.0	3.2	5.26	12.7	2.0	4.67	14.6	3.2
14-21	3.85	1.9	0.8	3.67	4.1	1.5	5.65	10.6	0.8	4.88	14.2	1.5
21-40	3.59**	8.3**	2.4**	3.62	6.7	3.4	5.18**	8.2**	2.4**	4.81	10.5	3.4

* The measure of fit J corresponds to the ratio of the mean-square acceleration output error to the mean-square recorded acceleration response.

** Unreliable results (see text).

Table 3-3

IDENTIFIED MODES FROM LOMA PRIETA: FREQUENCY (Hz), DAMPING (%), J (%)*

Time Segment	Fundamental E-W						Fundamental N-S					
	Case A: Fixed Base			Case B: Rocking Base			Case A: Fixed Base			Case B: Rocking Base		
0-40	2.72	17.2	12.9	2.65	8.1	19.6	4.23	12.7	12.9	3.61	17.8	19.6
0-10	2.74	17.3	12.8	2.69	7.3	19.7	4.23	12.4	12.8	3.58	17.9	19.7
10-20	2.66	6.1	5.2	2.59	7.6	8.7	4.28	10.6	5.2	3.82	15.2	8.7
20-40	2.77**	10.6**	4.7**	2.75	7.6	8.1				3.82	16.9	8.1

* The measure of fit J corresponds to the ratio of the mean-square acceleration output error to the mean-square recorded acceleration response.

** Unreliable results (See text).

Table 3-4

FIXED-BASE IDENTIFIED FUNDAMENTAL E-W MODESHAPE
AT THE OUTPUT CHANNELS: MORGAN HILL EARTHQUAKE

Time	(N-S)		(N-S)		(E-W)		(N-S)*		(E-W)**	
Segment	7	8	5	6	12	11	½(1-3)	½(2-4)	½(1-2)	½(3-4)
0-40	-0.04	0.07	-0.09	0.15	0.64	1.00	-0.04	0.04	-0.04	0.04
0-7	-0.04	0.07	-0.08	0.15	0.59	1.00	-0.03	0.03	-0.03	0.03
7-14	-0.05	0.07	-0.10	0.14	0.64	1.00	-0.04	0.04	-0.04	0.04
14-21	-0.04	0.08	-0.09	0.14	0.66	1.00	-0.04	0.04	-0.04	0.04
21-40	-0.01	0.08	-0.04	0.16	0.67	1.00	-0.02	0.02	-0.02	0.02

* Rocking components in the N-S direction at the base of the west and east walls respectively.

** Rocking components in the E-W direction at the base of the south and north walls respectively.

Table 3-5

FIXED-BASE IDENTIFIED FUNDAMENTAL E-W MODESHAPE
AT THE OUTPUT CHANNELS: LOMA PRIETA EARTHQUAKE

Time	(N-S)		(N-S)		(E-W)		(N-S)*		(E-W)**	
Segment	7	8	5	6	12	11	½(1-3)	½(2-4)	½(1-2)	½(3-4)
0-40	-0.00	0.04	-0.02	0.04	0.63	1.00	-0.02	0.02	-0.02	0.02
0-10	-0.00	0.04	-0.02	0.03	0.63	1.00	-0.02	0.02	-0.02	0.02
10-20	-0.01	0.06	-0.01	0.15	0.68	1.00	-0.02	0.03	-0.03	0.03
20-40	-0.01	0.06	-0.01	0.12	0.68	1.00	-0.02	0.02	-0.02	0.02

* Rocking components in the N-S direction at the base of the west and east walls respectively.

** Rocking components in the E-W direction at the base of the south and north walls respectively.

Table 3-6

FIXED-BASE IDENTIFIED FUNDAMENTAL N-S MODESHAPE
AT THE OUTPUT CHANNELS: MORGAN HILL EARTHQUAKE

Time	(N-S)		(N-S)		(E-W)		(N-S)*		(E-W)**	
Segment	7	8	5	6	12	11	½(1-3)	½(2-4)	½(1-2)	½(3-4)
0-40	0.46	0.56	0.82	1.00	0.02	-0.07	-0.08	0.09	-0.09	0.09
0-7	0.44	0.55	0.77	1.00	0.07	0.07	-0.08	0.09	-0.09	0.09
7-14	0.48	0.57	0.85	1.00	-0.09	-0.25	-0.08	0.09	-0.09	0.09
14-21	0.51	0.57	0.91	1.00	0.07	-0.03	-0.08	0.09	-0.09	0.09
21-40	0.52	0.58	0.86	1.00	0.01	0.11	-0.04	0.04	-0.04	0.04

* Rocking components in the N-S direction at the base of the west and east walls respectively.

** Rocking components in the E-W direction at the base of the south and north walls respectively.

Table 3-7

FIXED-BASE IDENTIFIED FUNDAMENTAL N-S MODESHAPE
AT THE OUTPUT CHANNELS: LOMA PRIETA EARTHQUAKE

Time	(N-S)		(N-S)		(E-W)		(N-S)*		(E-W)**	
Segment	7	8	5	6	12	11	½(1-3)	½(2-4)	½(1-2)	½(3-4)
0-40	0.54	0.66	0.80	1.00	-0.11	-0.16	-0.05	0.06	-0.05	0.05
0-10	0.53	0.65	0.80	1.00	-0.10	-0.15	-0.05	0.06	-0.05	0.05
10-20	0.63	0.70	0.89	1.00	0.01	-0.13	-0.03	0.04	-0.03	0.03
20-40	0.62	0.67	0.85	1.00	-0.00	-0.09	-0.05	0.06	-0.05	0.05

* Rocking components in the N-S direction at the base of the west and east walls respectively.

** Rocking components in the E-W direction at the base of the south and north walls respectively.

Table 3-8

FIXED BASE FUNDAMENTAL E-W MODE EFFECTIVE PARTICIPATION FACTORS AT CHANNEL 11 IDENTIFIED FROM MORGAN HILL EARTHQUAKE

Time Segment	Input Channels 9	10	13	z	r_y	r_x
0-40	0.22	-0.40	-1.22	-0.03	-1.05	-0.02
0-7	0.05	-0.09	-1.19	0.01	-1.67	-0.10
7-14	0.14	-0.32	-1.27	-0.08	-1.37	0.02
14-21	0.07	-0.11	-1.02	-0.04	-0.62	-0.14
21-40*	0.03	-0.04	-0.88	0.12	0.38	-0.08

Table 3-9

FIXED BASE FUNDAMENTAL E-W MODE EFFECTIVE PARTICIPATION FACTORS AT CHANNEL 11 IDENTIFIED FROM LOMA PRIETA EARTHQUAKE

Time Segment	Input Channels 9	10	13	z	r_y*	r_x*
0-40	-0.15	-0.05	-1.22	0.05	0.64	-0.04
0-10	-0.16	-0.02	-1.21	0.05	0.62	-0.03
10-20	-0.16	-0.02	-1.20	0.11	-0.12	0.05
20-40*	-0.03	-0.11	-1.32	0.14	0.76	0.15

* Unreliable results (See Text)

Table 3-10

FIXED BASE FUNDAMENTAL N-S MODE EFFECTIVE PARTICIPATION FACTORS AT CHANNEL 6 IDENTIFIED FROM MORGAN HILL EARTHQUAKE

Time Segment	Input Channels 9	10	13	z	r_y	r_x
0-40	-0.33	-0.69	-0.05	0.01	0.04	-0.44
0-7	-0.44	-0.66	-0.01	0.00	0.11	-0.71
7-14	-0.34	-0.58	-0.06	-0.02	0.01	-0.24
14-21	-0.25	-0.70	-0.06	0.05	0.05	-0.43
21-40*	-0.24	-0.48	-0.00	-0.00	0.02	-0.03

Table 3-11

FIXED BASE FUNDAMENTAL N-S MODE EFFECTIVE PARTICIPATION FACTORS AT CHANNEL 6 IDENTIFIED FROM LOMA PRIETA EARTHQUAKE

Time Segment	Input Channels 9	10	13	z	r_y	r_x
0-40	-0.79	-0.52	0.12	0.07	-0.02	-0.56
0-10	-0.85	-0.46	0.14	0.07	-0.02	-0.60
10-20	-0.36	-0.70	-0.07	0.03	-0.16	-0.29
20-40*	-0.54	-1.20	-0.18	0.24	-0.50	1.18

* Unreliable results (See Text)

Table 3-12

IDENTIFIED TIME-INVARIANT FIXED BASE MODAL PARAMETERS AND PSEUDOSTATIC MATRIX FOR THE MORGAN HILL EARTHQUAKE

PSEUDOSTATIC INFLUENCE MATRIX

Output Channels	Input Channels 9	10	13	z	r_y	r_x
7	1.42	-0.43	0.05	0.03	-0.02	0.91
8	-0.39	1.39	0.05	0.02	0.05	0.62
5	1.79	-0.81	0.02	0.03	-0.14	2.06
6	-0.64	1.54	0.07	-0.01	0.24	1.91
12	-0.28	0.37	1.16	0.03	1.21	-0.21
11	-0.62	0.68	1.18	0.07	2.10	-0.34
1	0.12	-0.11	0.00	1.00	0.91	0.95
2	-0.14	0.12	0.00	1.00	-0.90	0.79
3	-0.12	0.11	0.00	1.00	1.08	-0.94
4	0.14	-0.12	0.00	1.00	-1.09	-1.10

MODAL PARAMETERS

	Frequency	Damping
First E-W	4.06 Hz	4.7%
First N-S	5.46 Hz	11.8%

Table 3-12 (Continued)

IDENTIFIED TIME-INVARIANT FIXED BASE MODAL PARAMETERS AND PSEUDOSTATIC MATRIX FOR THE MORGAN HILL EARTHQUAKE

MODESHAPE COMPONENTS

Output Channels	7	8	5	6	12	11	1	2	3	4
First E-W	-0.03	0.04	-0.03	0.06	0.52	0.85	-0.01	0.02	0.01	-0.02
First N-S	0.31	0.46	0.47	0.68	0.02	-0.02	-0.04	0.05	0.04	-0.05

PARTICIPATION FACTORS

Input Channels	9	10	13	z	r_y	r_x
First E-W	0.27	-0.52	-1.33	-0.01	-1.18	0.02
First N-S	-0.61	-1.05	-0.07	0.00	0.07	-0.68

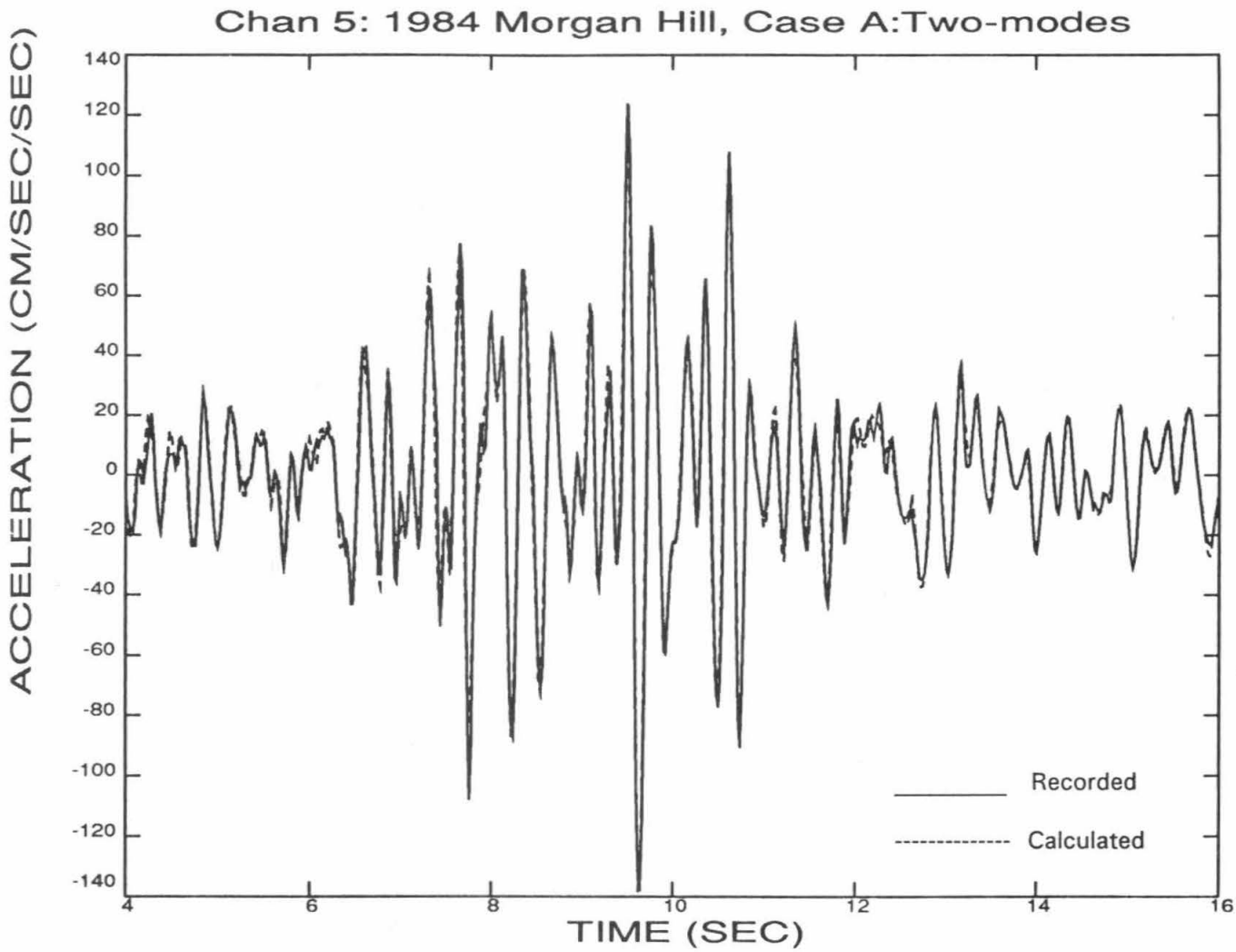

Figure 3-1: Comparison of Recorded Response and Calculated Response for the Identified Fixed Base Time-Invariant Model, Morgan Hill Earthquake, Channel 5

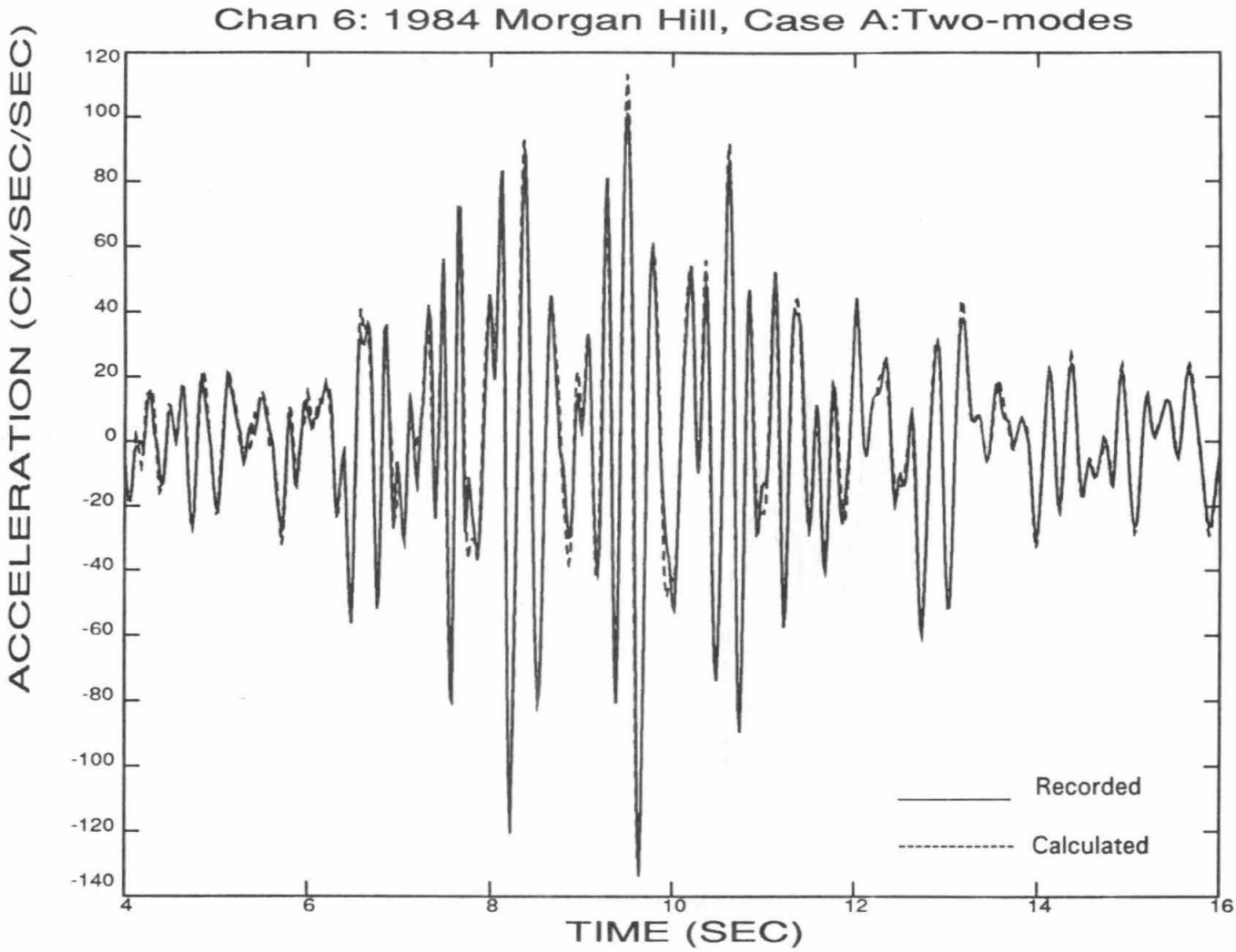

Figure 3-2: Comparison of Recorded Response and Calculated Response for the Identified Fixed Base Time-Invariant Model, Morgan Hill Earthquake, Channel 6

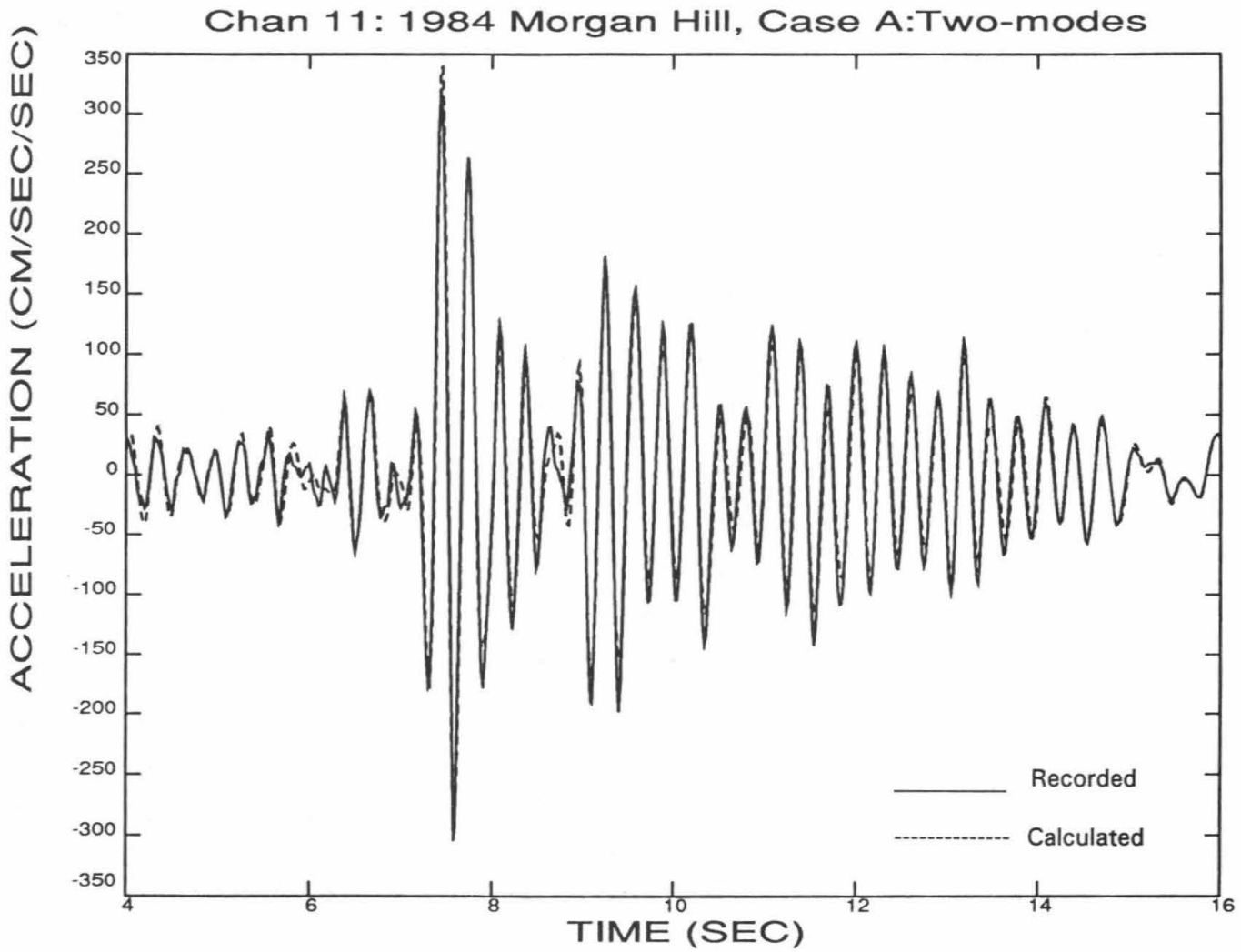

Figure 3-3: Comparison of Recorded Response and Calculated Response for the Identified Fixed Base Time-Invariant Model, Morgan Hill Earthquake, Channel 11

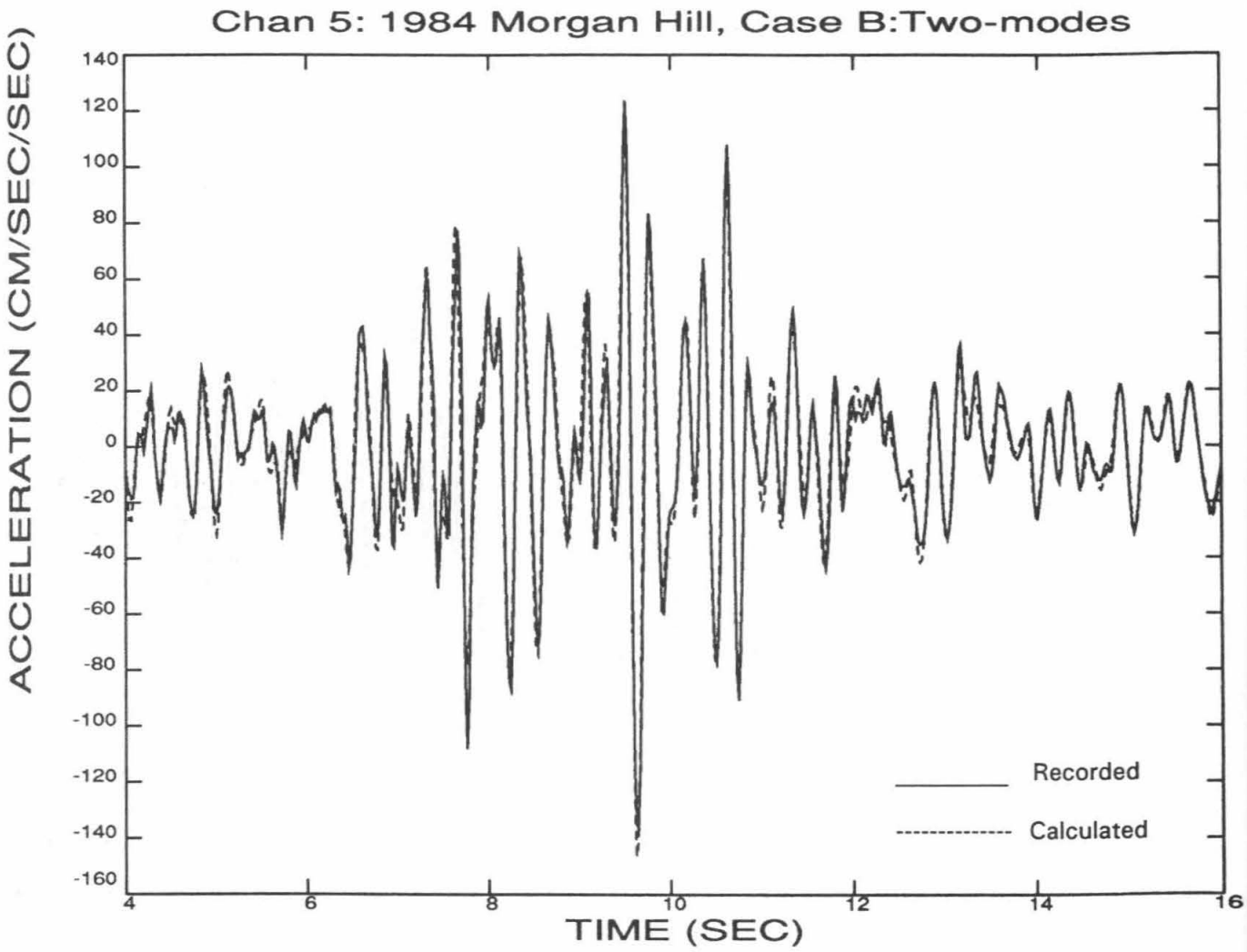

Figure 3-4: Comparison of Recorded Response and Calculated Response for the Identified Rocking Base Time-Invariant Model, Morgan Hill Earthquake, Channel 5

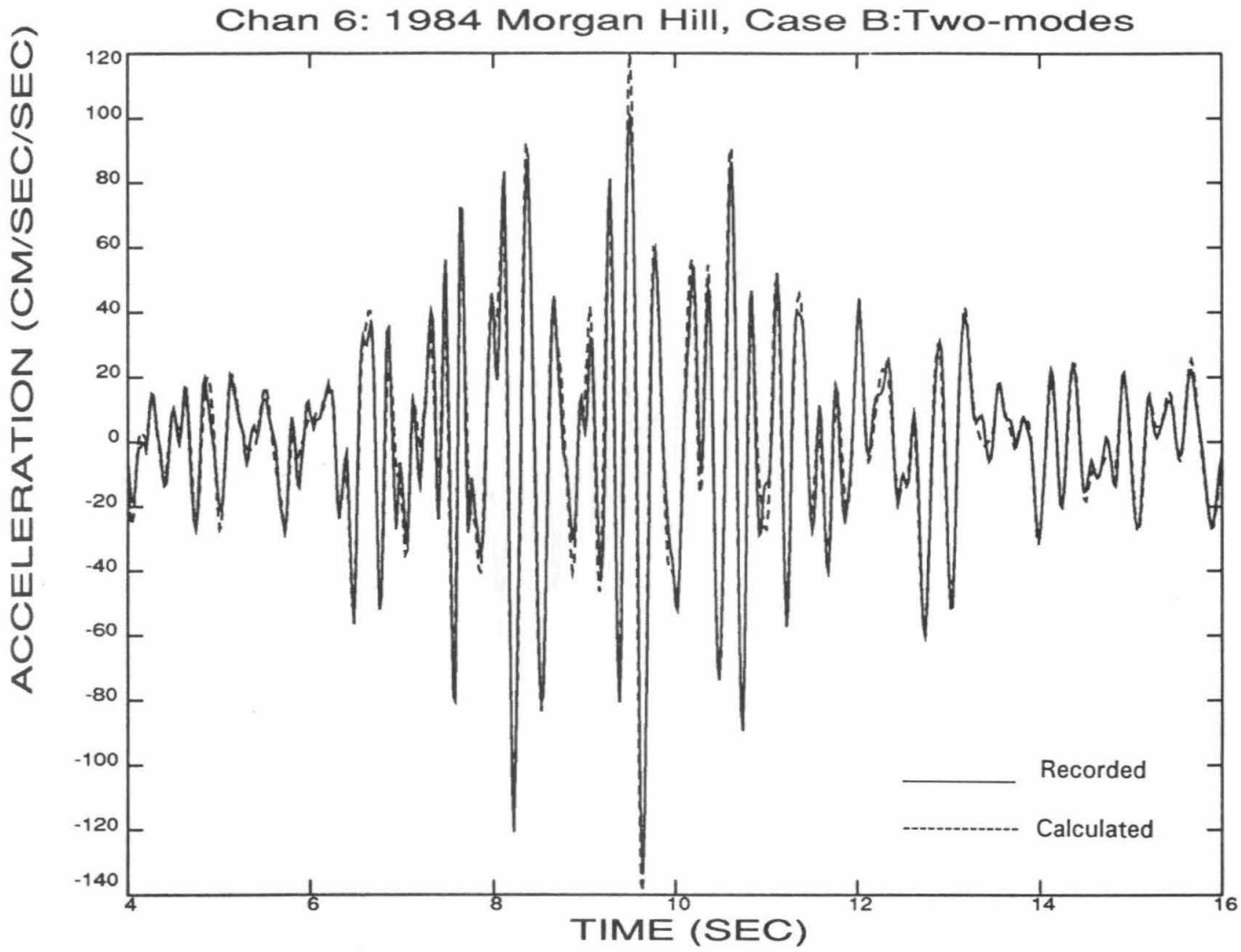

Figure 3-5: Comparison of Recorded Response and Calculated Response for the Identified Rocking Base Time-Invariant Model, Morgan Hill Earthquake, Channel 6

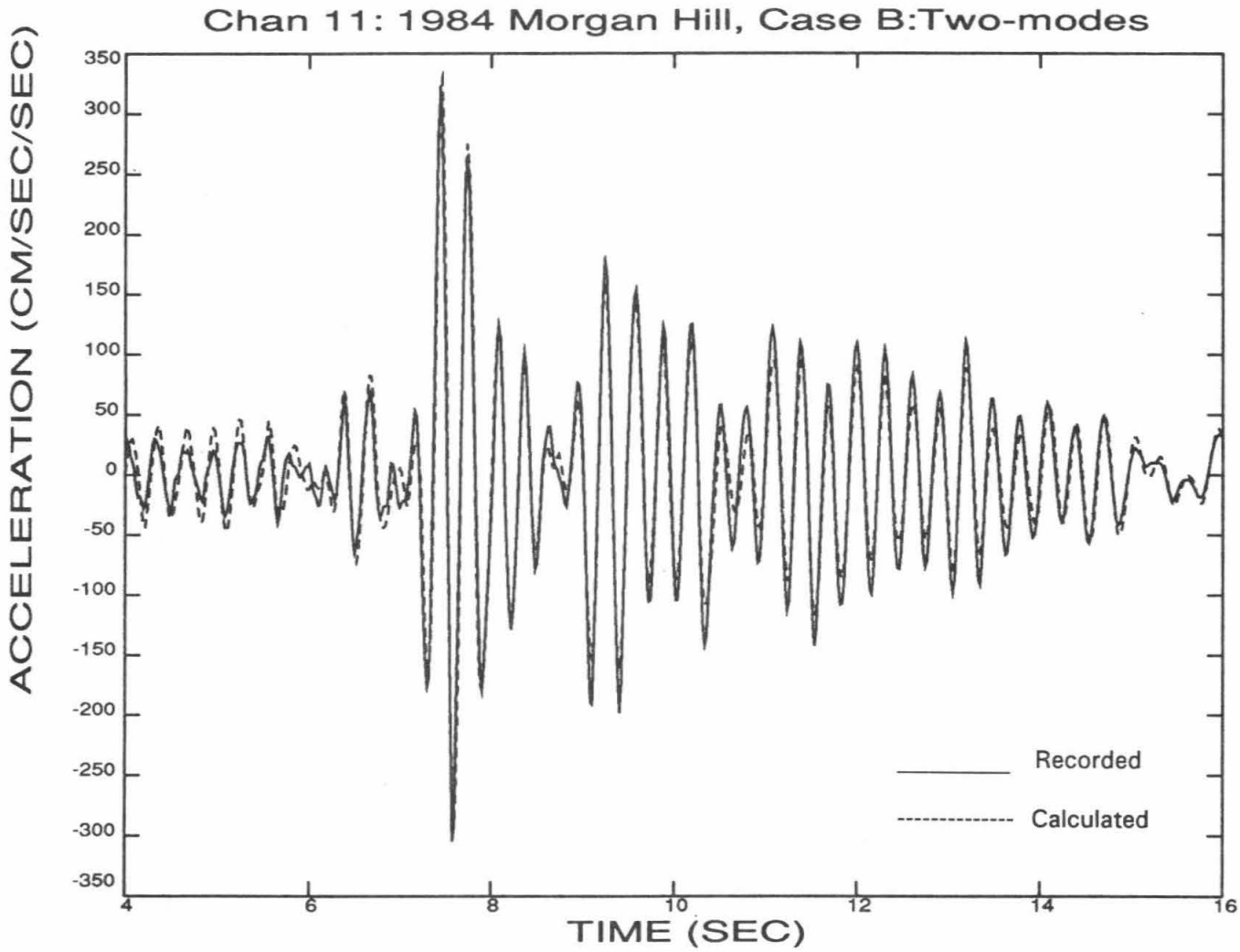

Figure 3-6: Comparison of Recorded Response and Calculated Response for the Identified Rocking Base Time-Invariant Model, Morgan Hill Earthquake, Channel 11

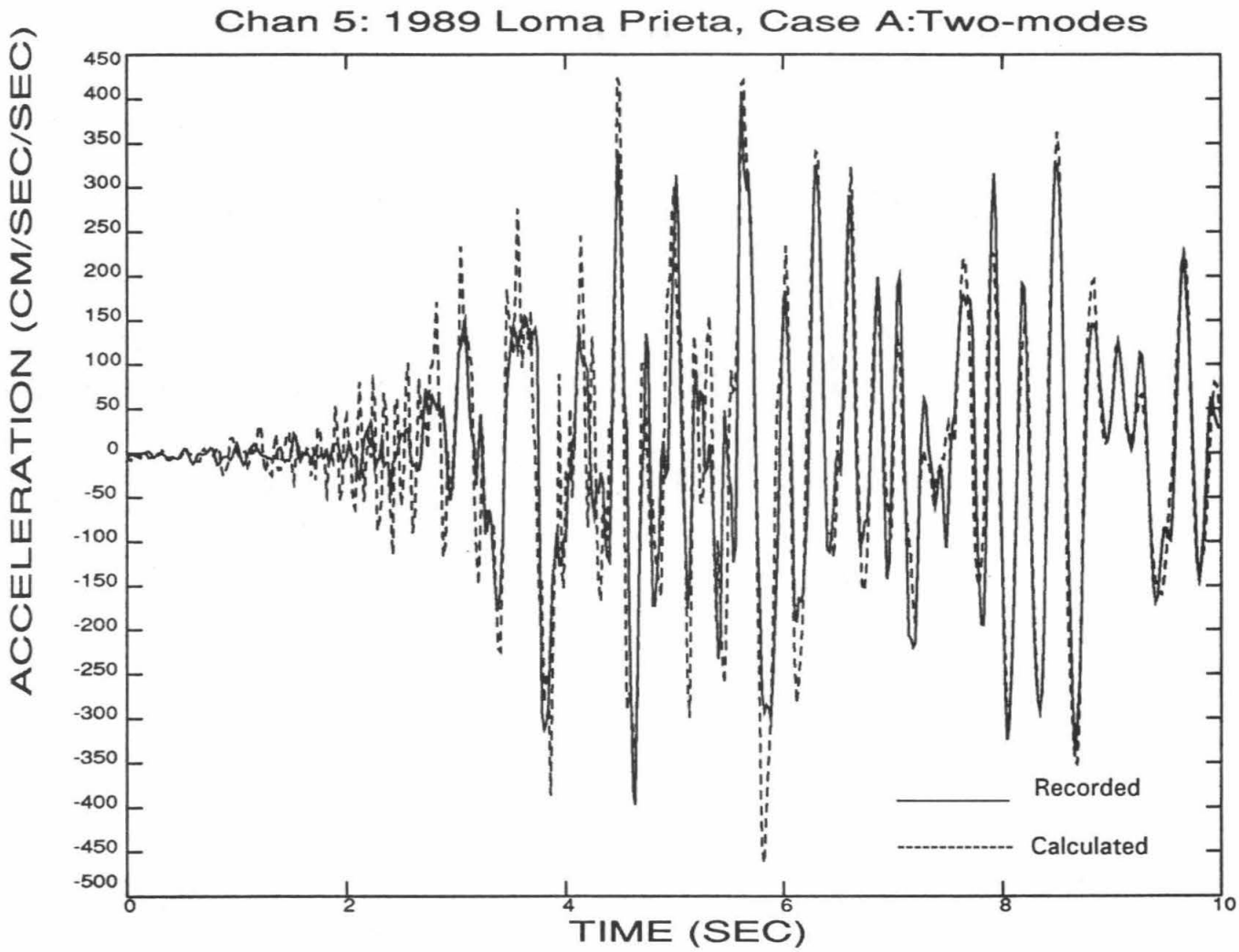

Figure 3-7a: Comparison of Recorded Response and Calculated Response for the Identified Fixed Base Time-Invariant Model, Loma Prieta Earthquake, Channel 5, [0, 10] Seconds

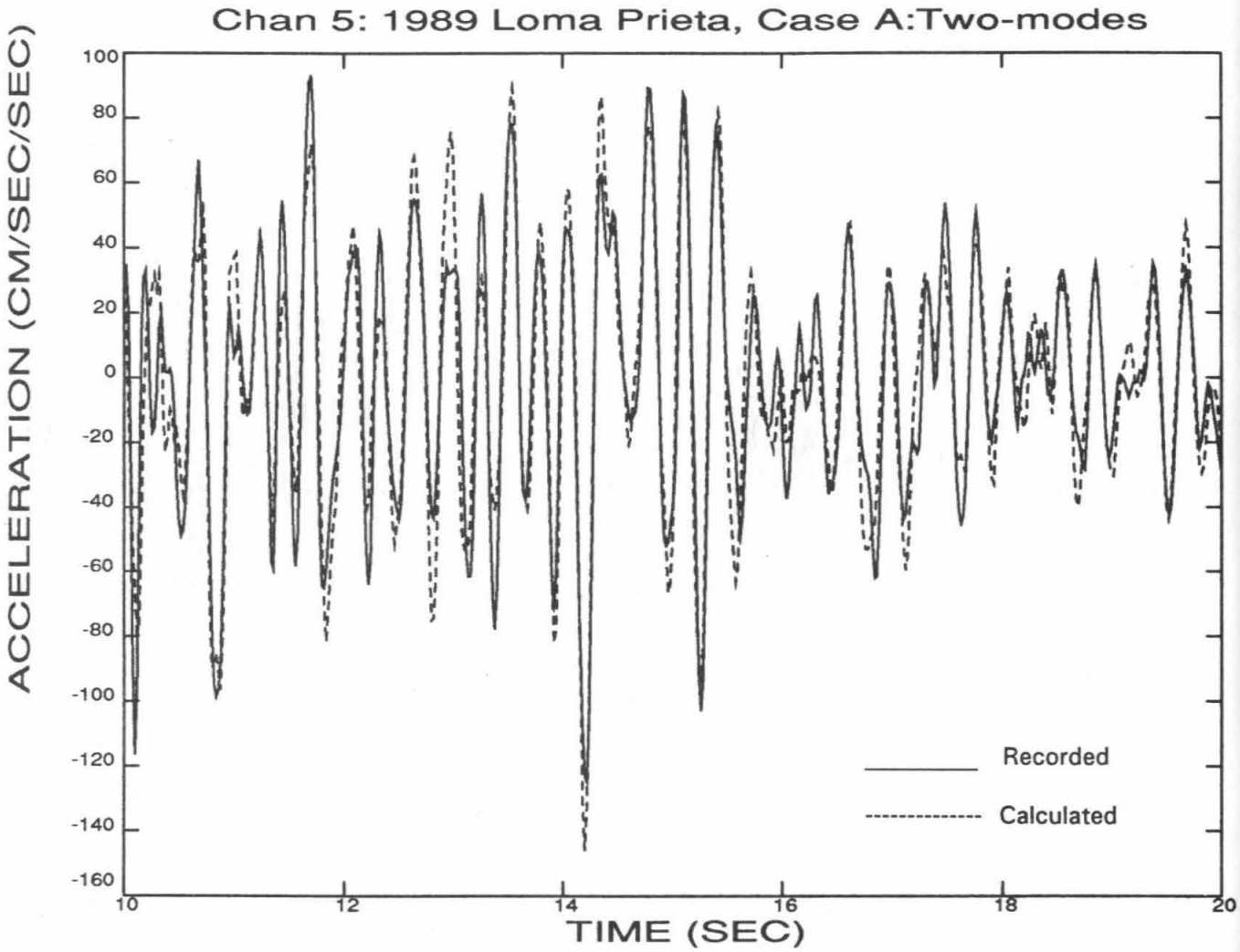

Figure 3-7b: Comparison of Recorded Response and Calculated Response for the Identified Fixed Base Time-Invariant Model, Loma Prieta Earthquake, Channel 5, [10, 20] Seconds

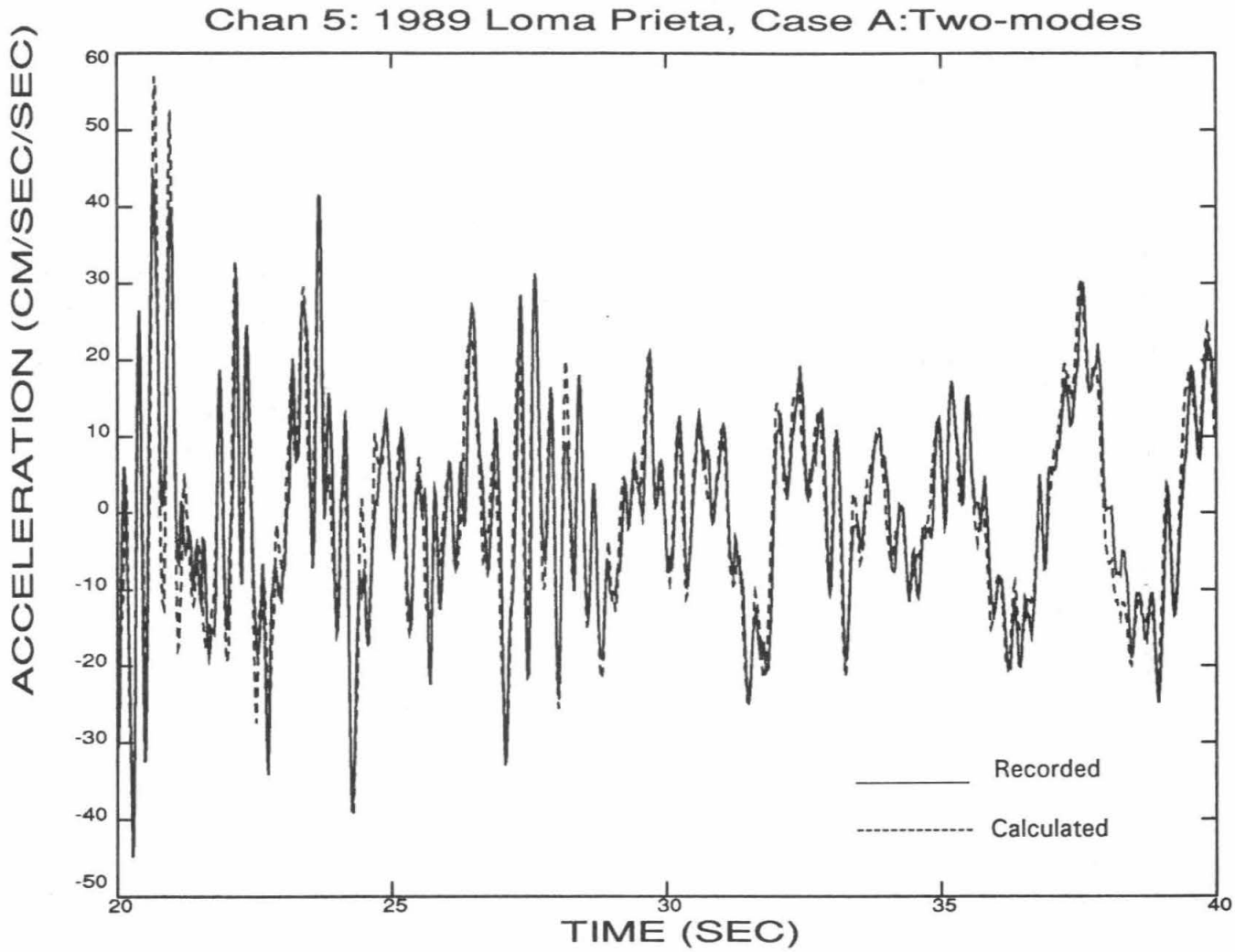

Figure 3-7c: Comparison of Recorded Response and Calculated Response for the Identified Fixed Base Time-Invariant Model, Loma Prieta Earthquake, Channel 5, [20, 40] Seconds

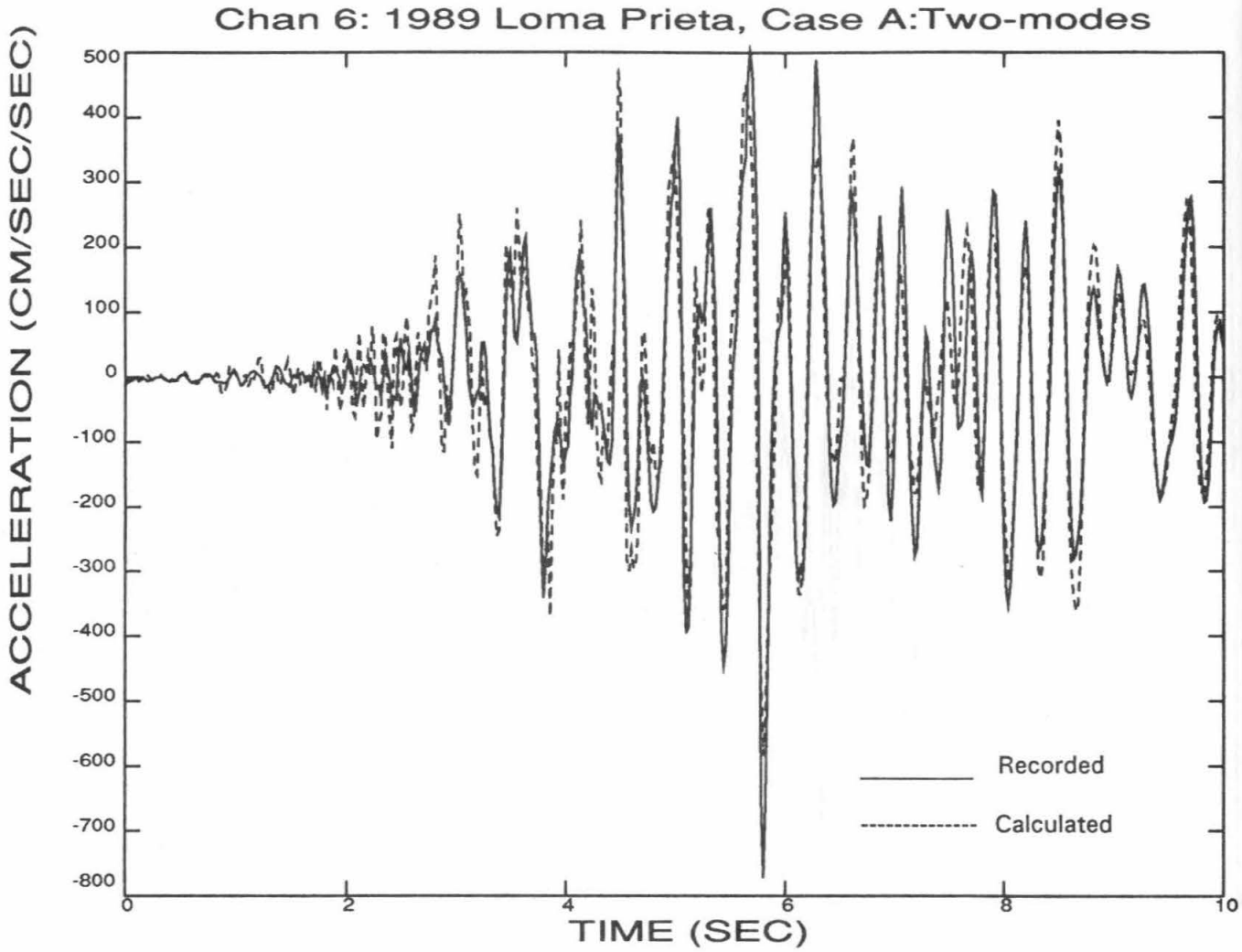

Figure 3-8a: Comparison of Recorded Response and Calculated Response for the Identified Fixed Base Time-Invariant Model, Loma Prieta Earthquake, Channel 5, [0, 10] Seconds

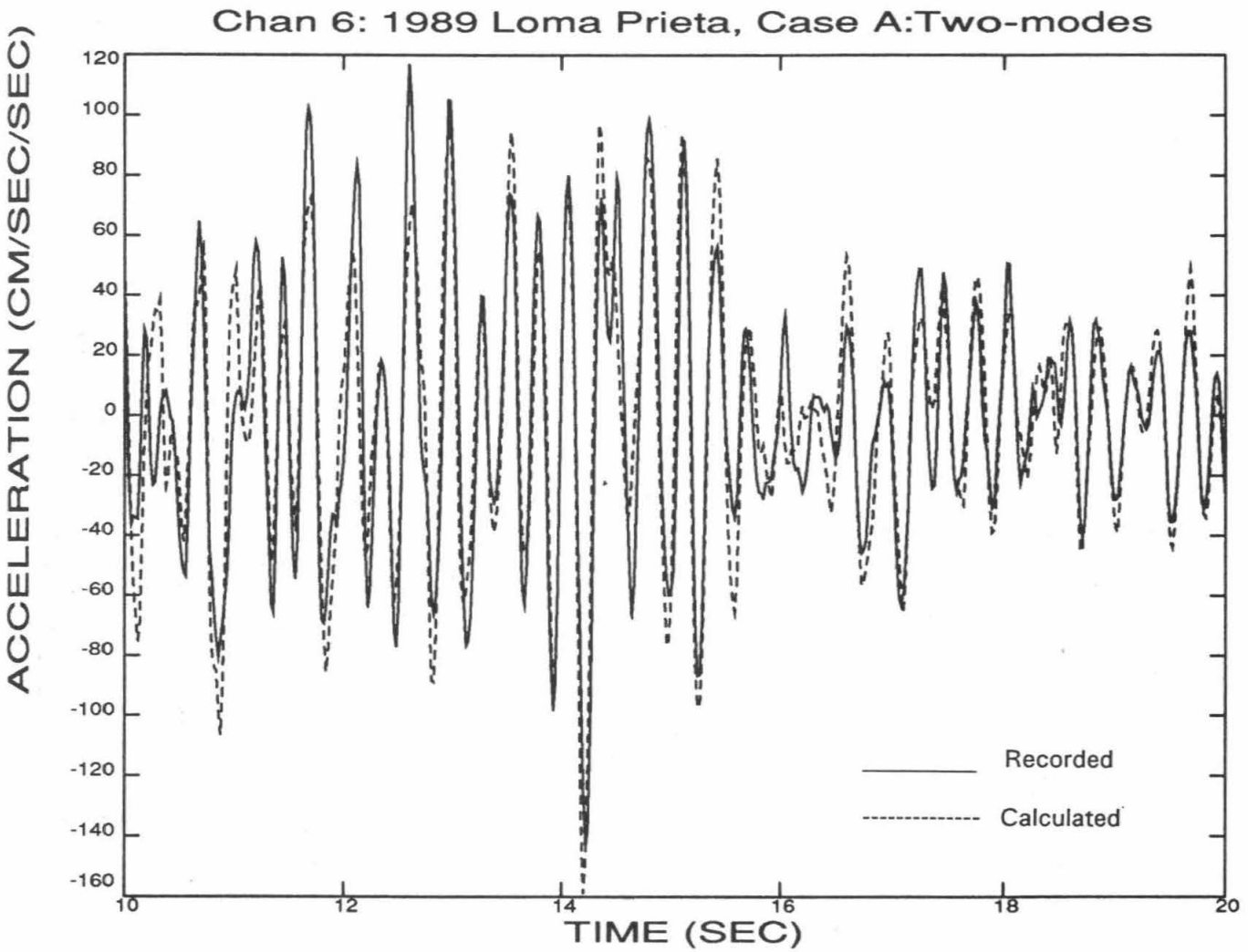

Figure 3-8b: Comparison of Recorded Response and Calculated Response for the Identified Fixed Base Time-Invariant Model, Loma Prieta Earthquake, Channel 6, [10, 20] Seconds

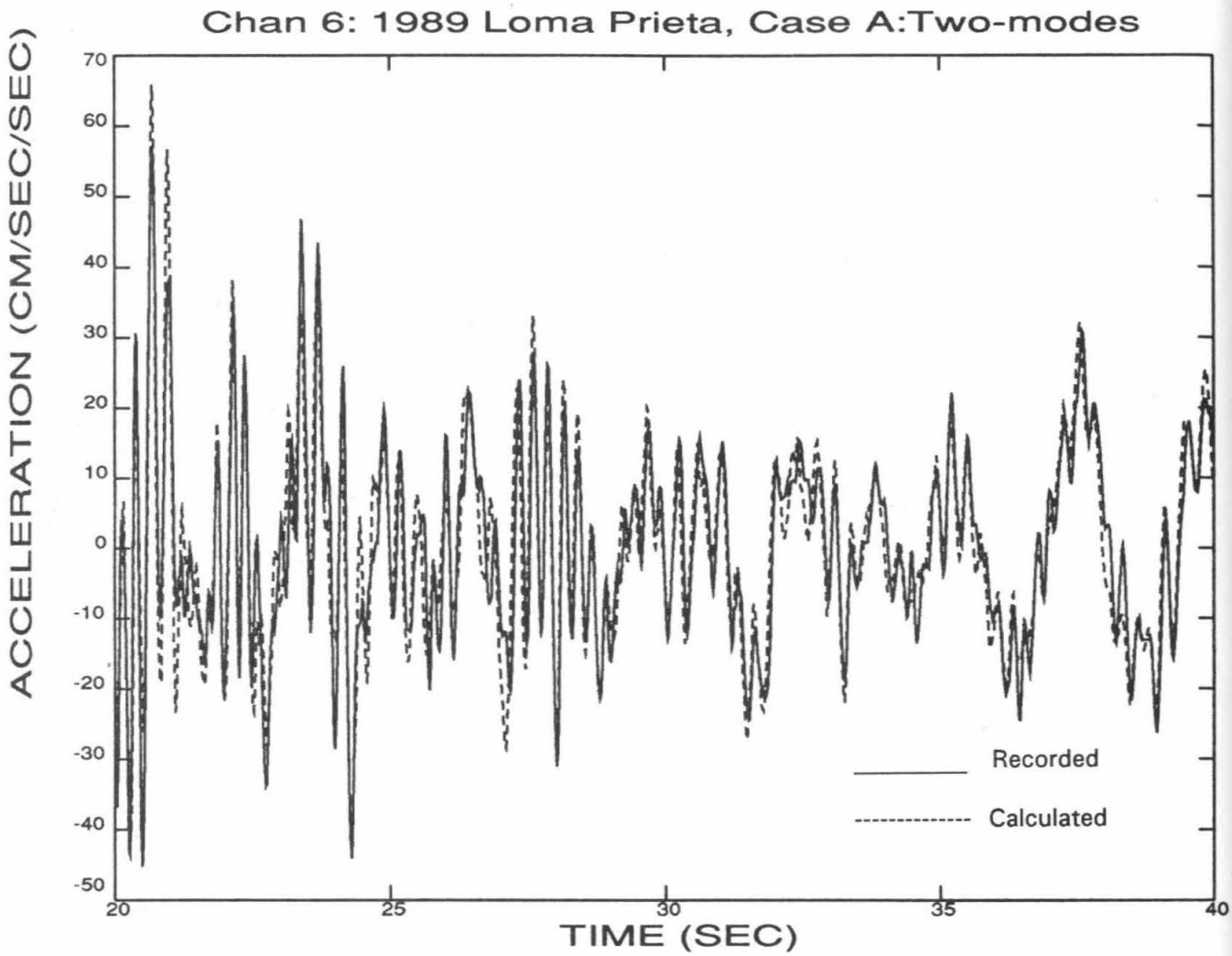

Figure 3-8c: Comparison of Recorded Response and Calculated Response for the Identified Fixed Base Time-Invariant Model, Loma Prieta Earthquake, Channel 6, [20, 40] Seconds

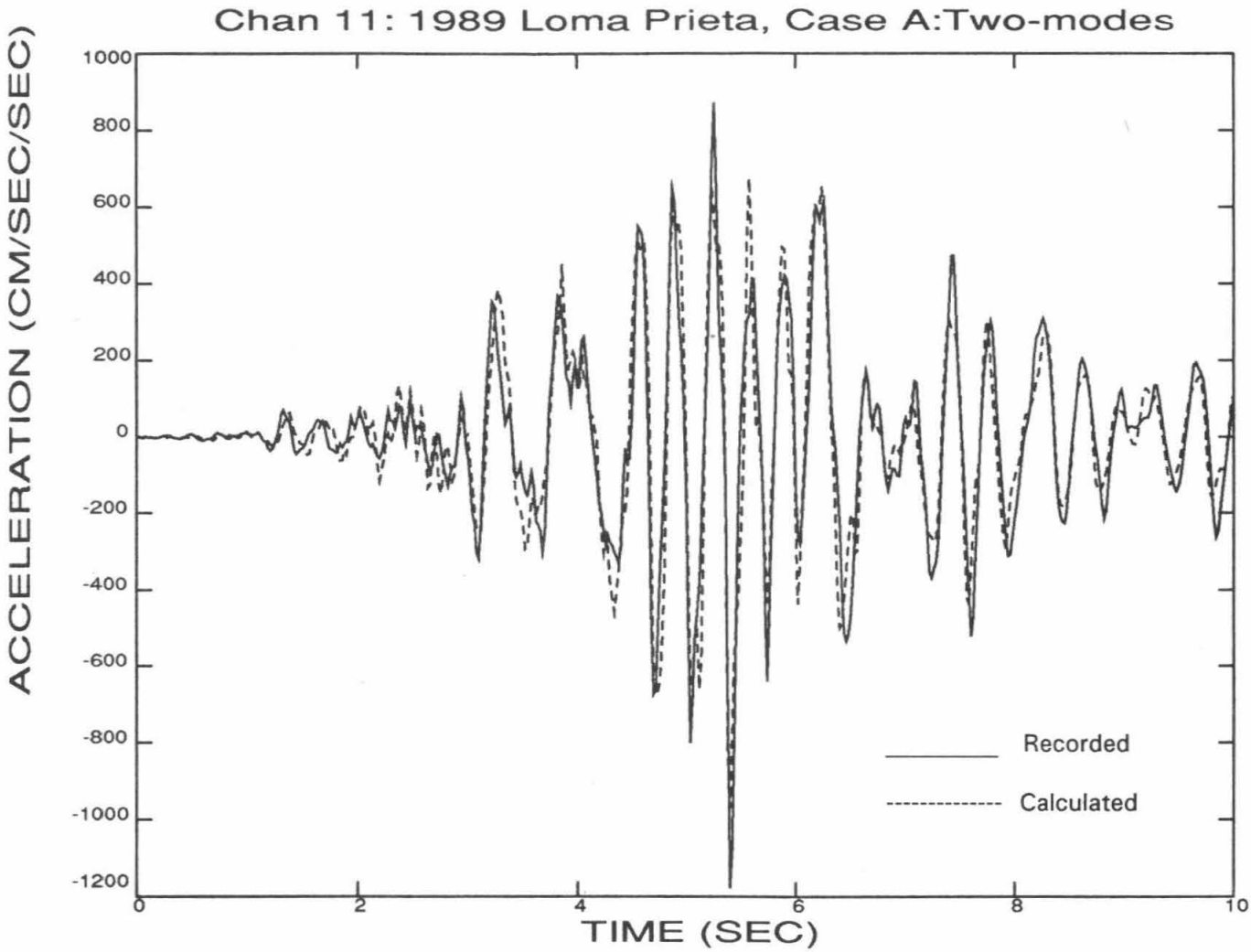

Figure 3-9a: Comparison of Recorded Response and Calculated Response for the Identified Fixed Base Time-Invariant Model, Loma Prieta Earthquake, Channel 11, [0, 10] Seconds

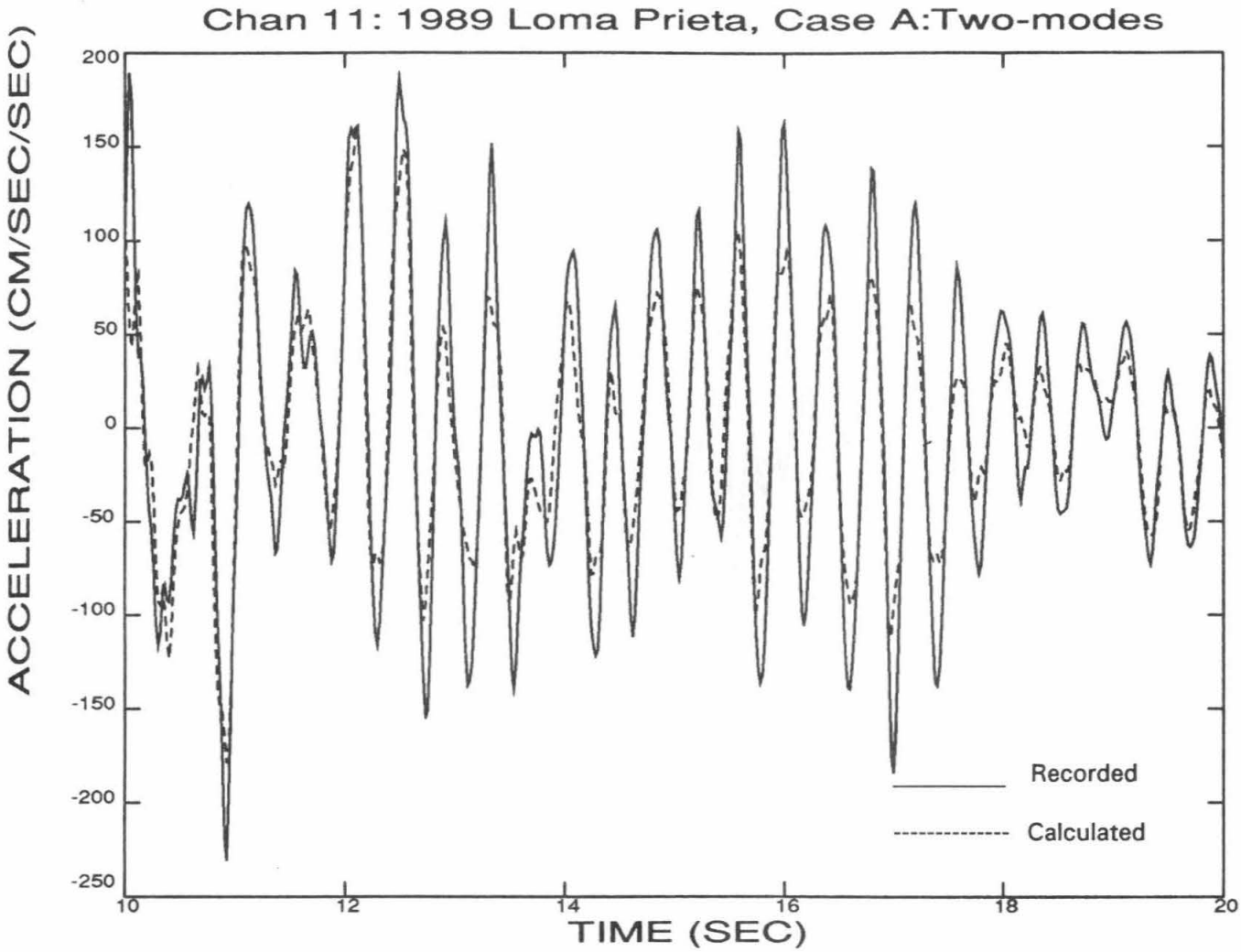

Figure 3-9b: Comparison of Recorded Response and Calculated Response for the Identified Fixed Base Time-Invariant Model, Loma Prieta Earthquake, Channel 11, [10, 20] Seconds

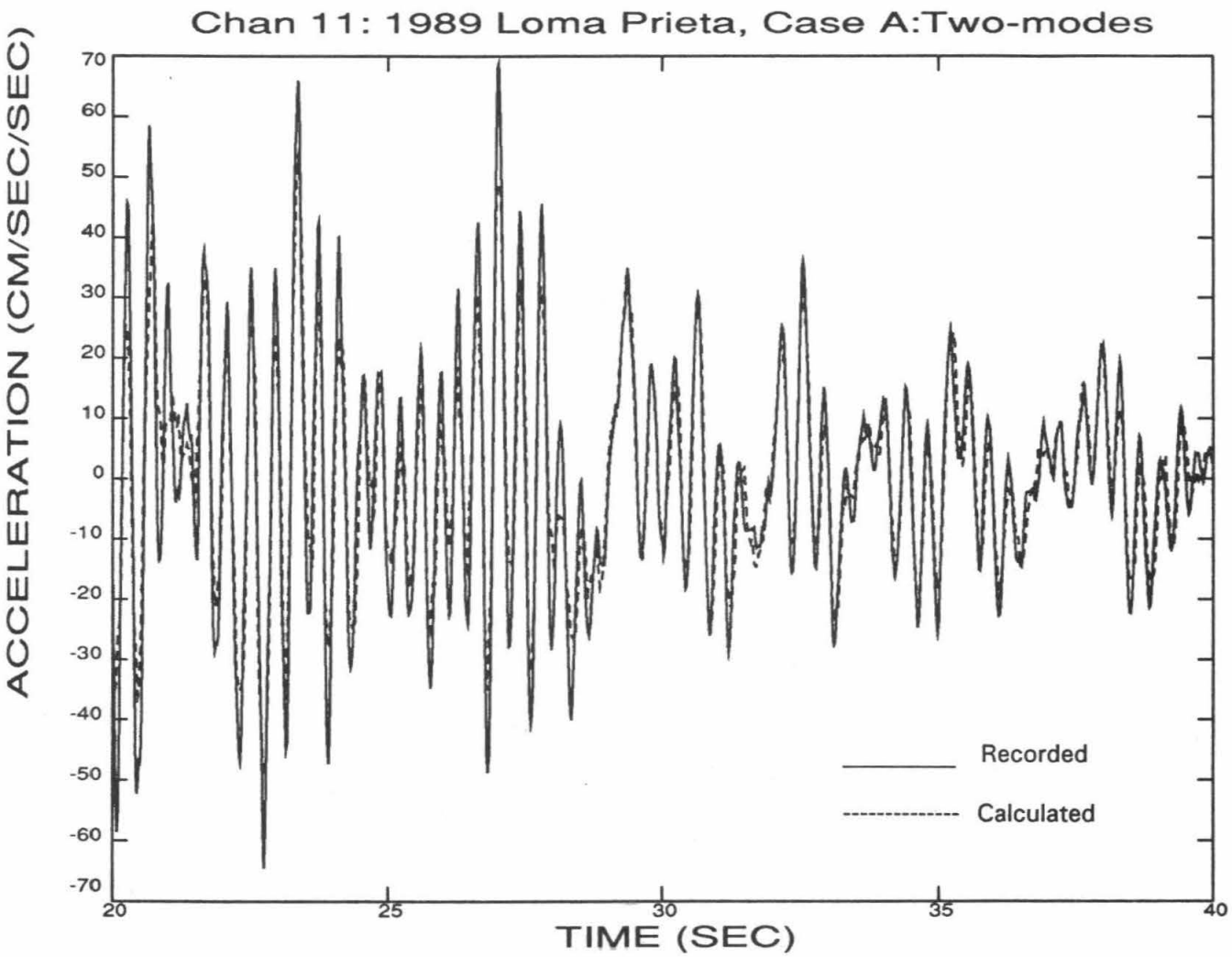

Figure 3-9c: Comparison of Recorded Response and Calculated Response for the Identified Fixed Base Time-Invariant Model, Loma Prieta Earthquake, Channel 11, [20, 40] Seconds

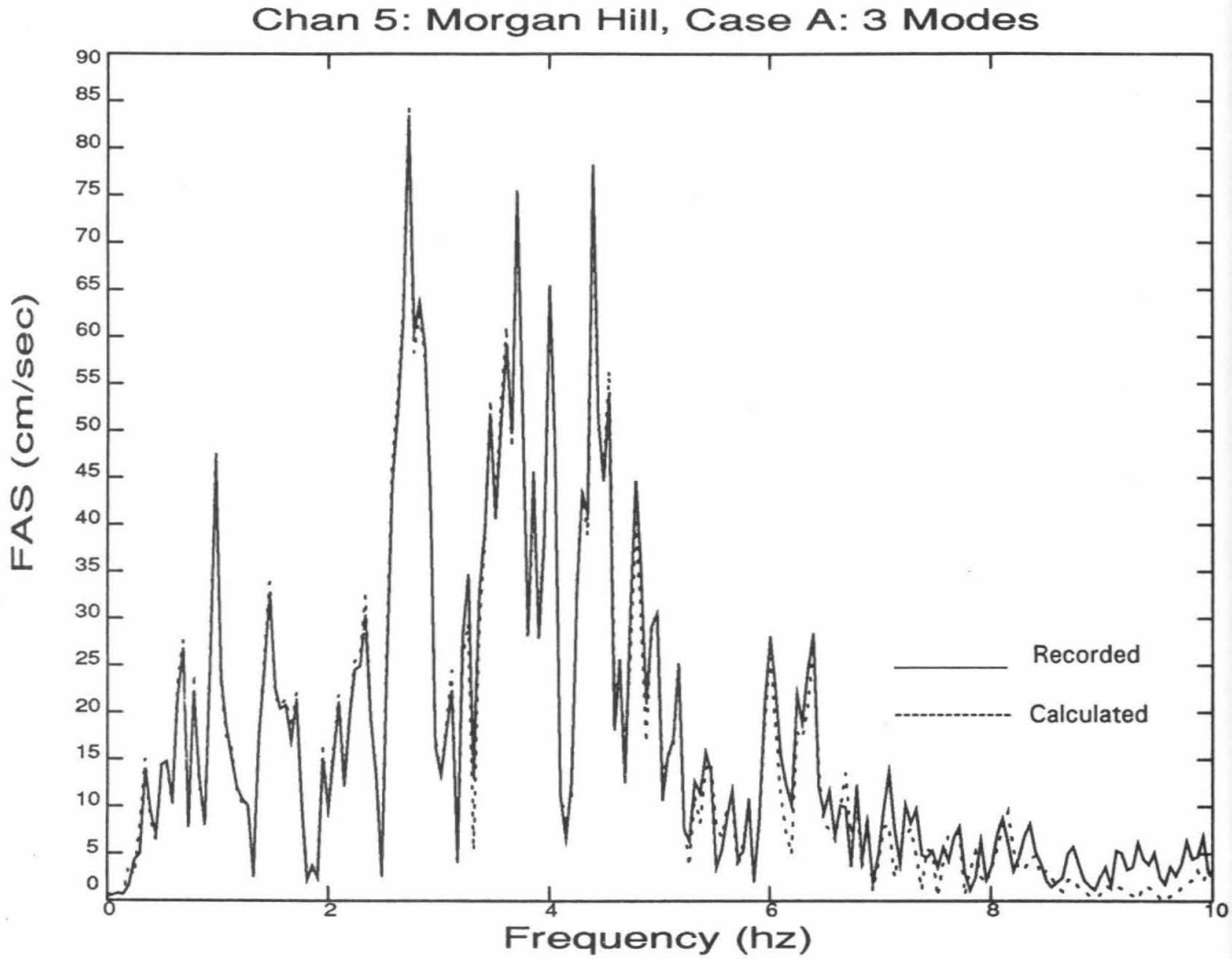

Figure 3-10: Comparison of the Fourier Amplitude Spectra of the Recorded Response and Calculated Response for the Identified Fixed Base Time-Invariant Model, Morgan Hill Earthquake, Channel 5

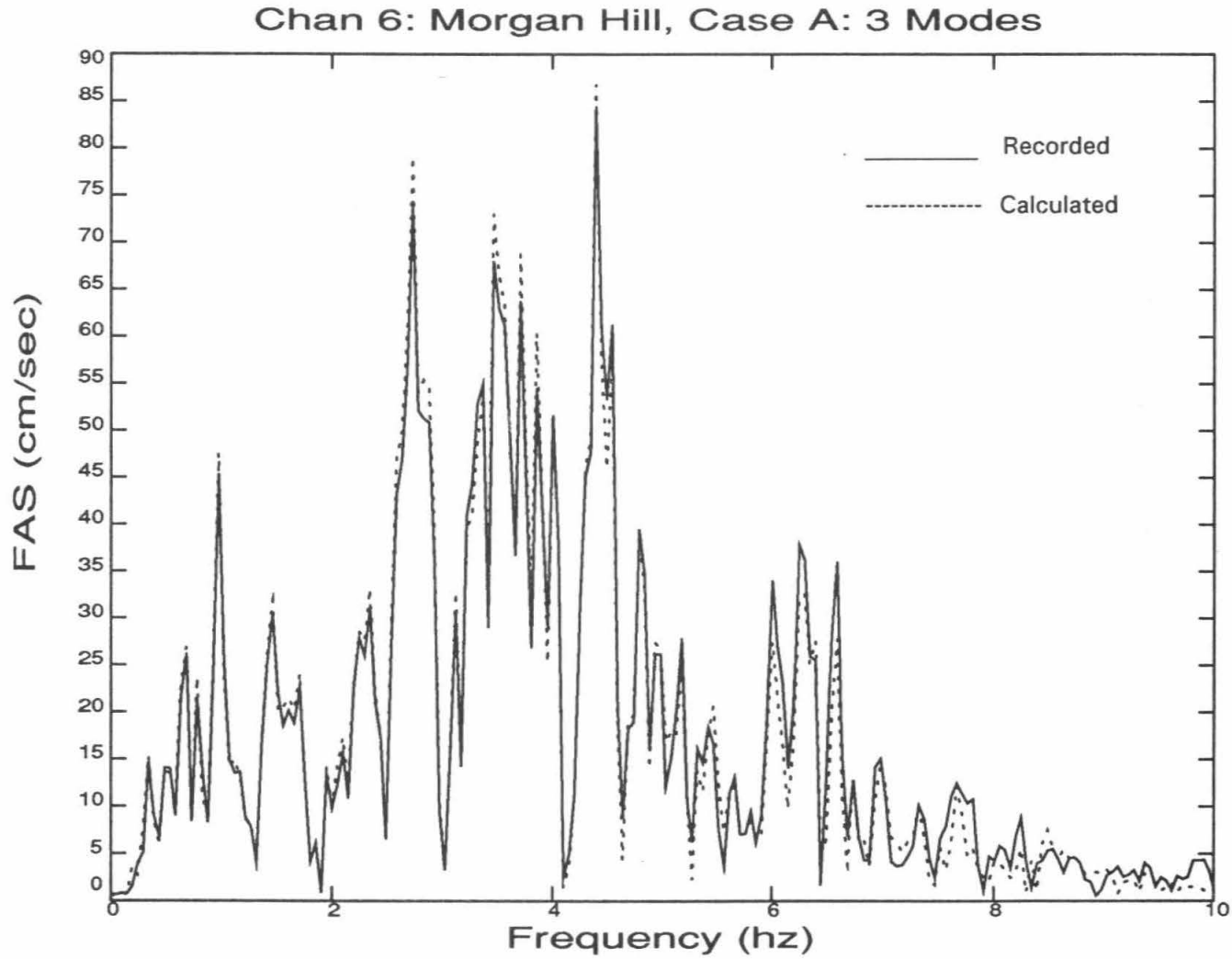

Figure 3-11: Comparison of the Fourier Amplitude Spectra of the Recorded Response and Calculated Response for the Identified Fixed Base Time-Invariant Model, Morgan Hill Earthquake, Channel 6

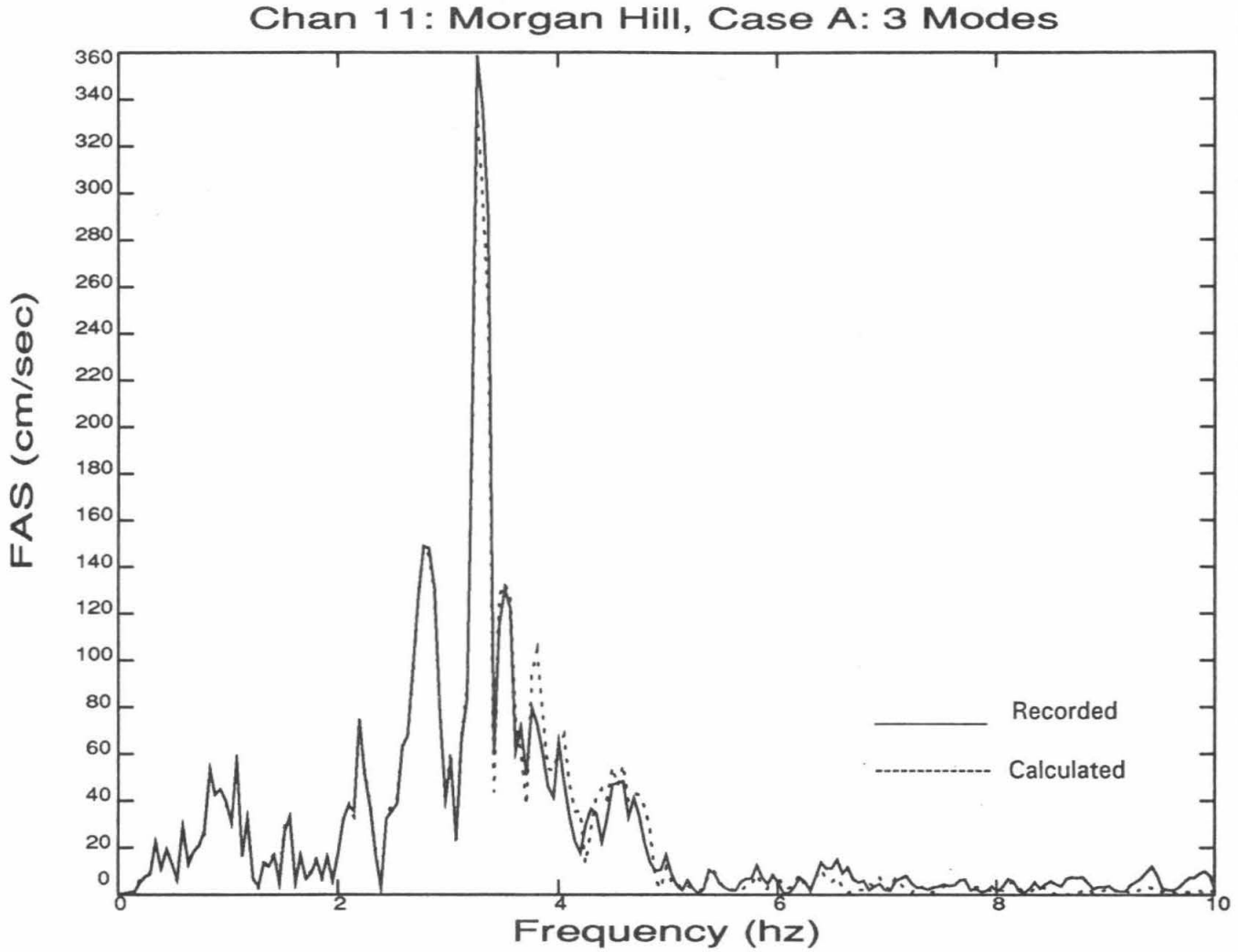

Figure 3-12: Comparison of the Fourier Amplitude Spectra of the Recorded Response and Calculated Response for the Identified Fixed Base Time-Invariant Model, Morgan Hill Earthquake, Channel 11

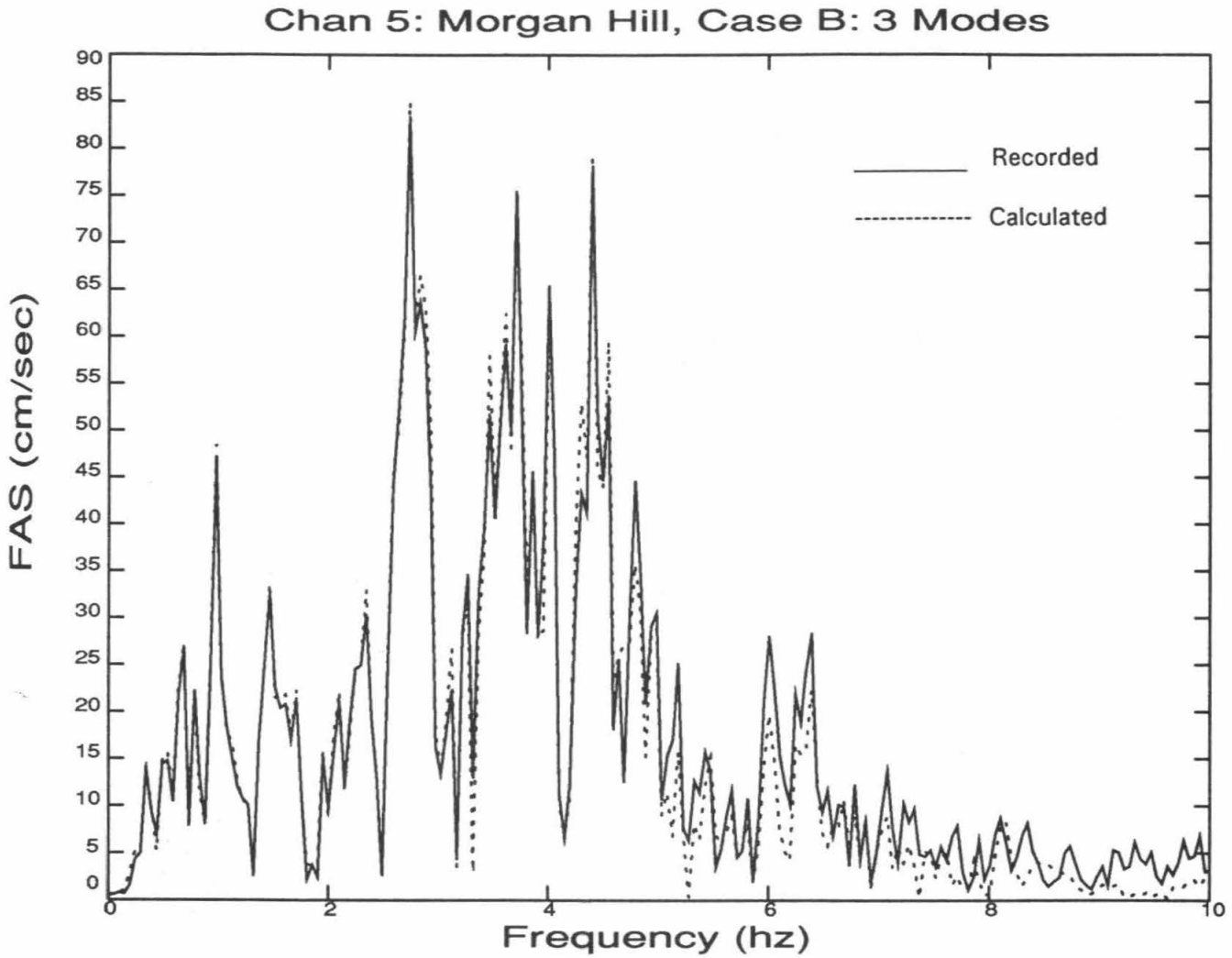

Figure 3-13: Comparison of the Fourier Amplitude Spectra of the Recorded Response and Calculated Response for the Identified Rocking Base Time-Invariant Model, Morgan Hill Earthquake, Channel 5

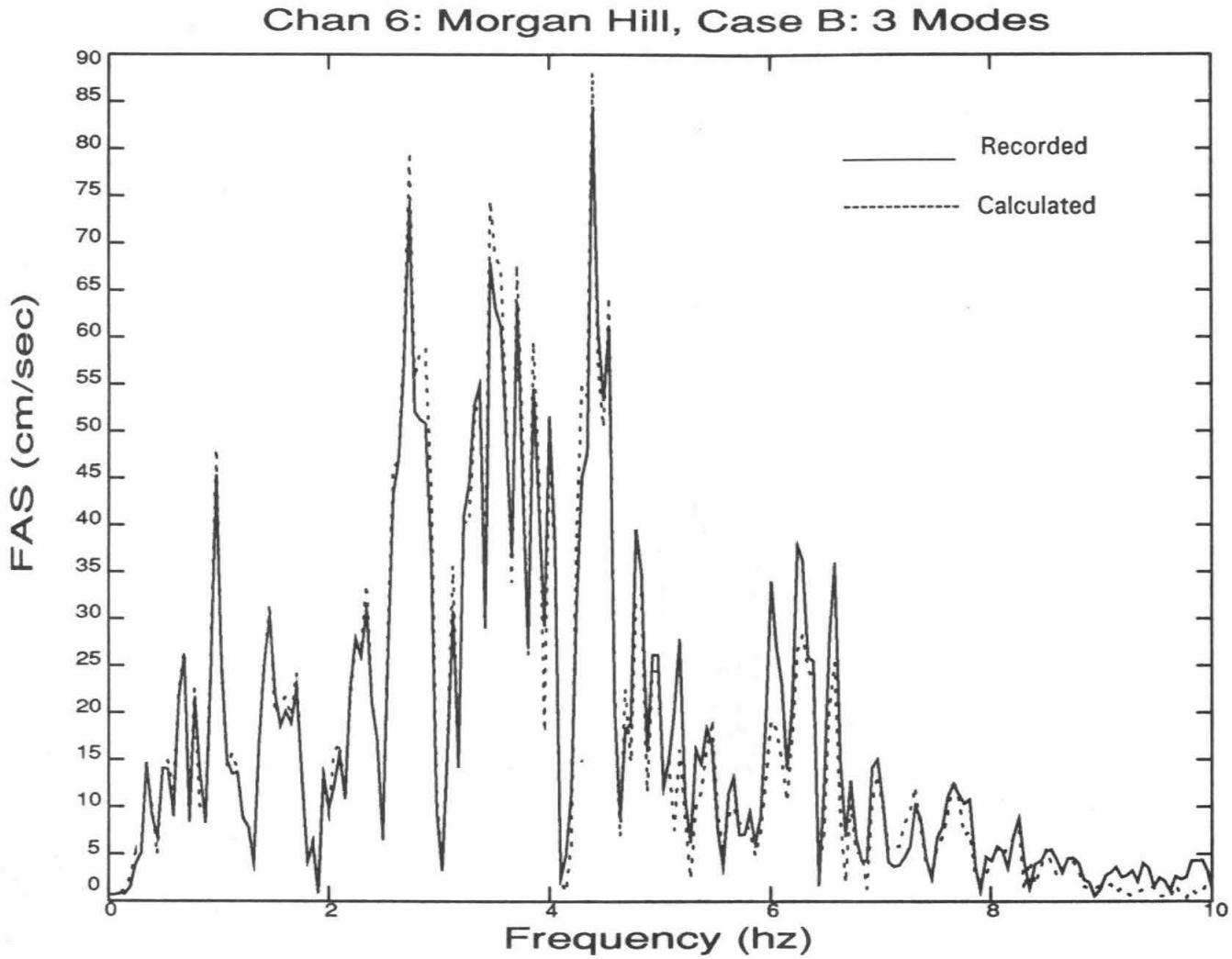

Figure 3-14: Comparison of the Fourier Amplitude Spectra of the Recorded Response and Calculated Response for the Identified Rocking Base Time-Invariant Model, Morgan Hill Earthquake, Channel 6

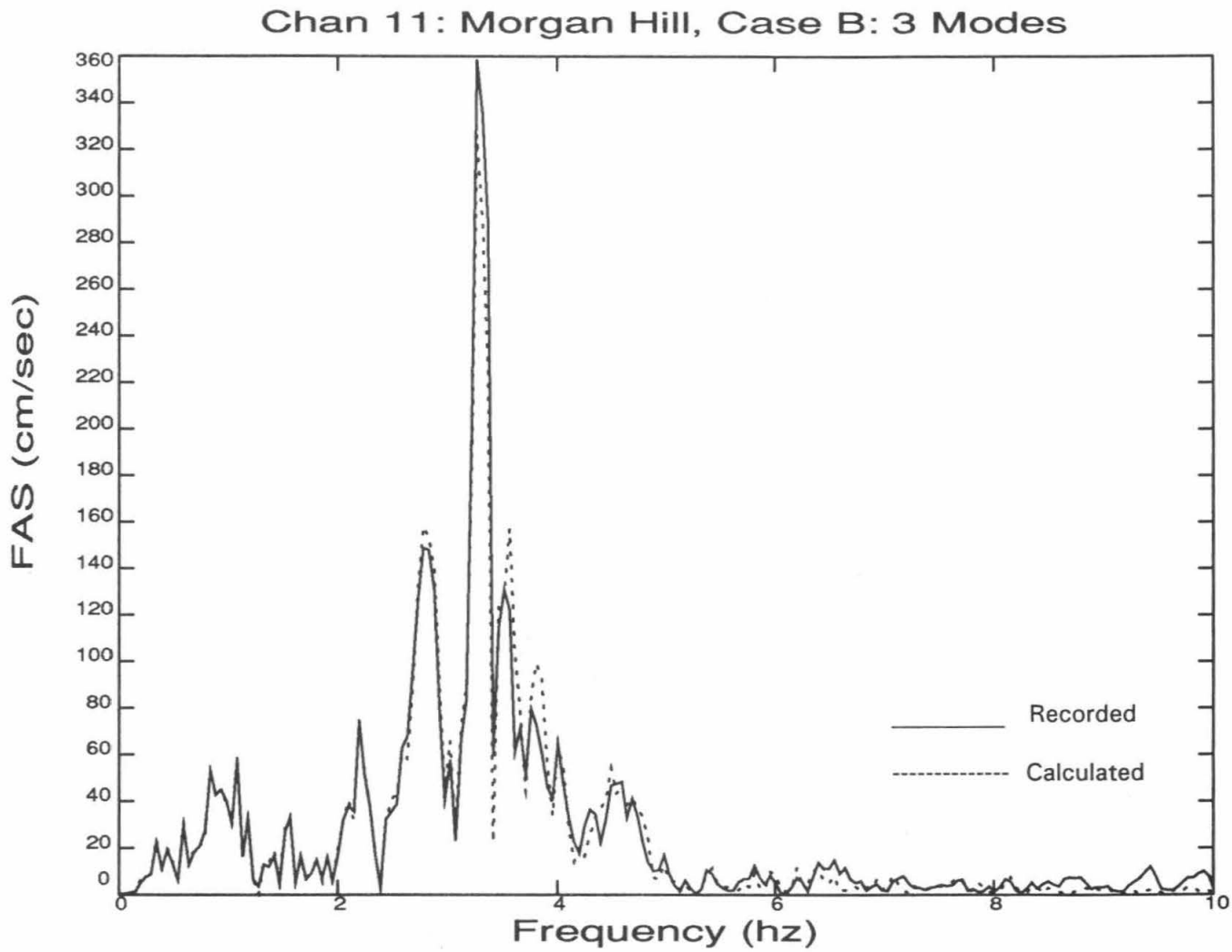

Figure 3-15: Comparison of the Fourier Amplitude Spectra of the Recorded Response and Calculated Response for the Identified Rocking Base Time-Invariant Model, Morgan Hill Earthquake, Channel 11

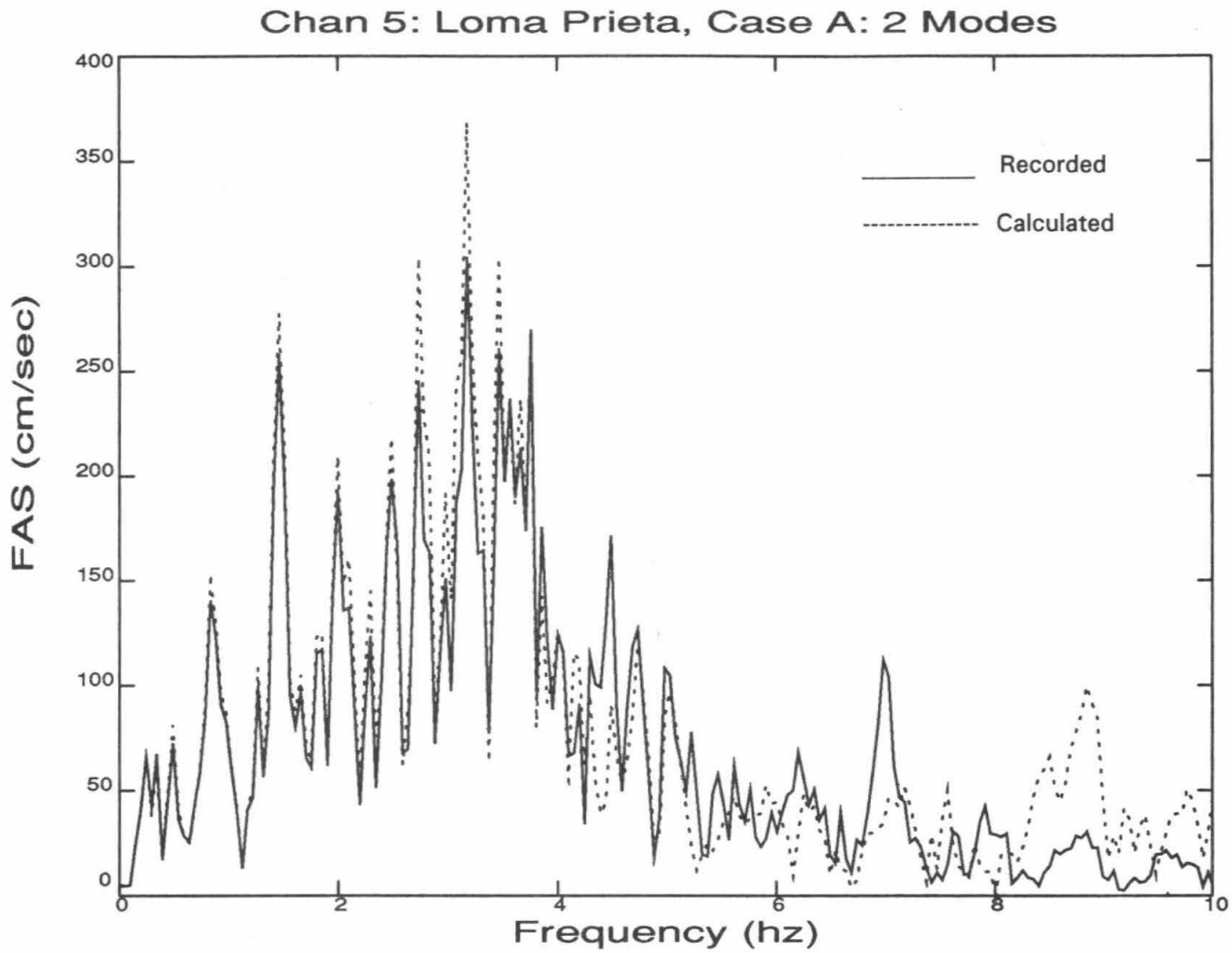

Figure 3-16: Comparison of the Fourier Amplitude Spectra of the Recorded Response and Calculated Response for the Identified Fixed Base Time-Invariant Model, Loma Prieta Earthquake, Channel 5

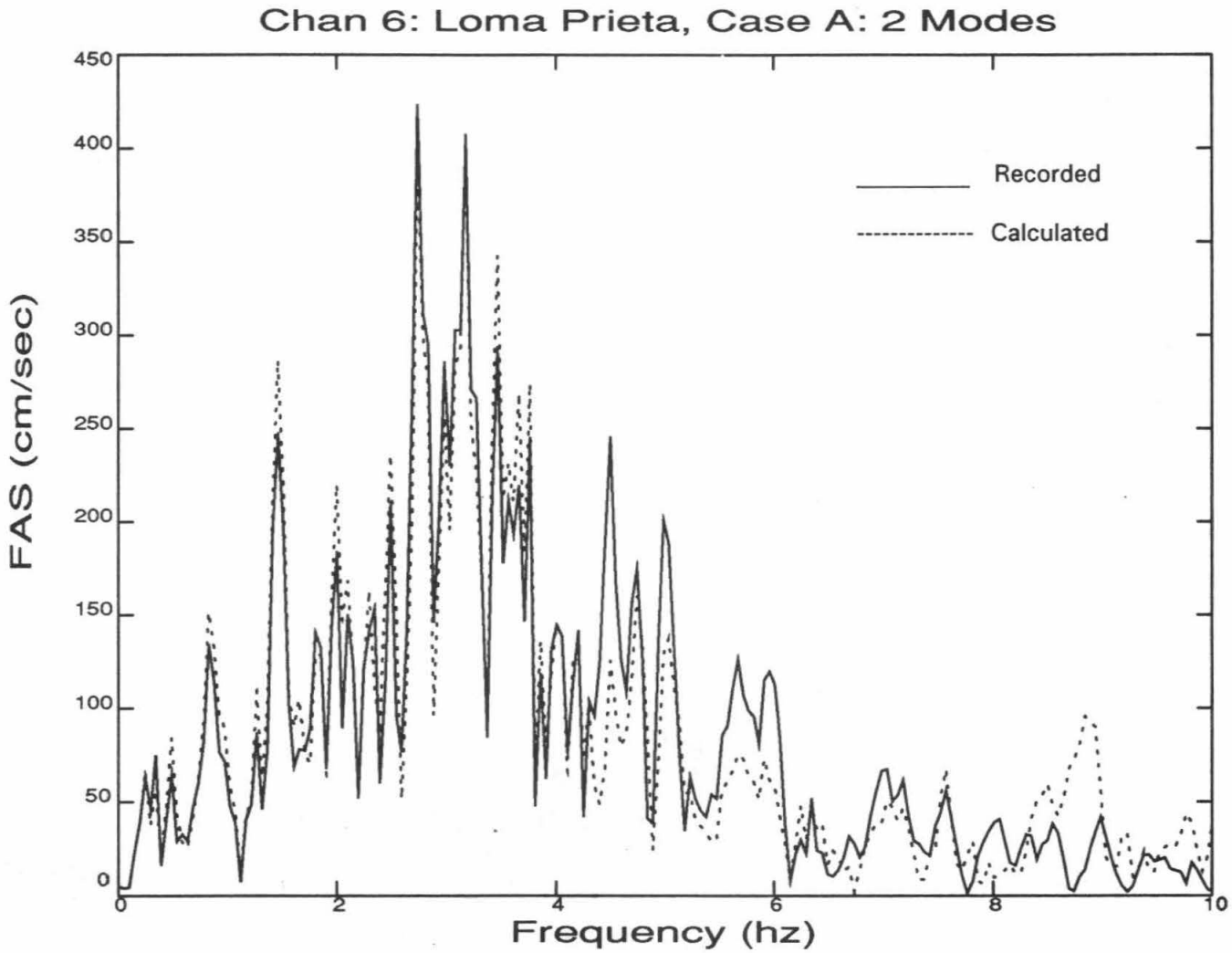

Figure 3-17: Comparison of the Fourier Amplitude Spectra of the Recorded Response and Calculated Response for the Identified Fixed Base Time-Invariant Model, Loma Prieta Earthquake, Channel 6

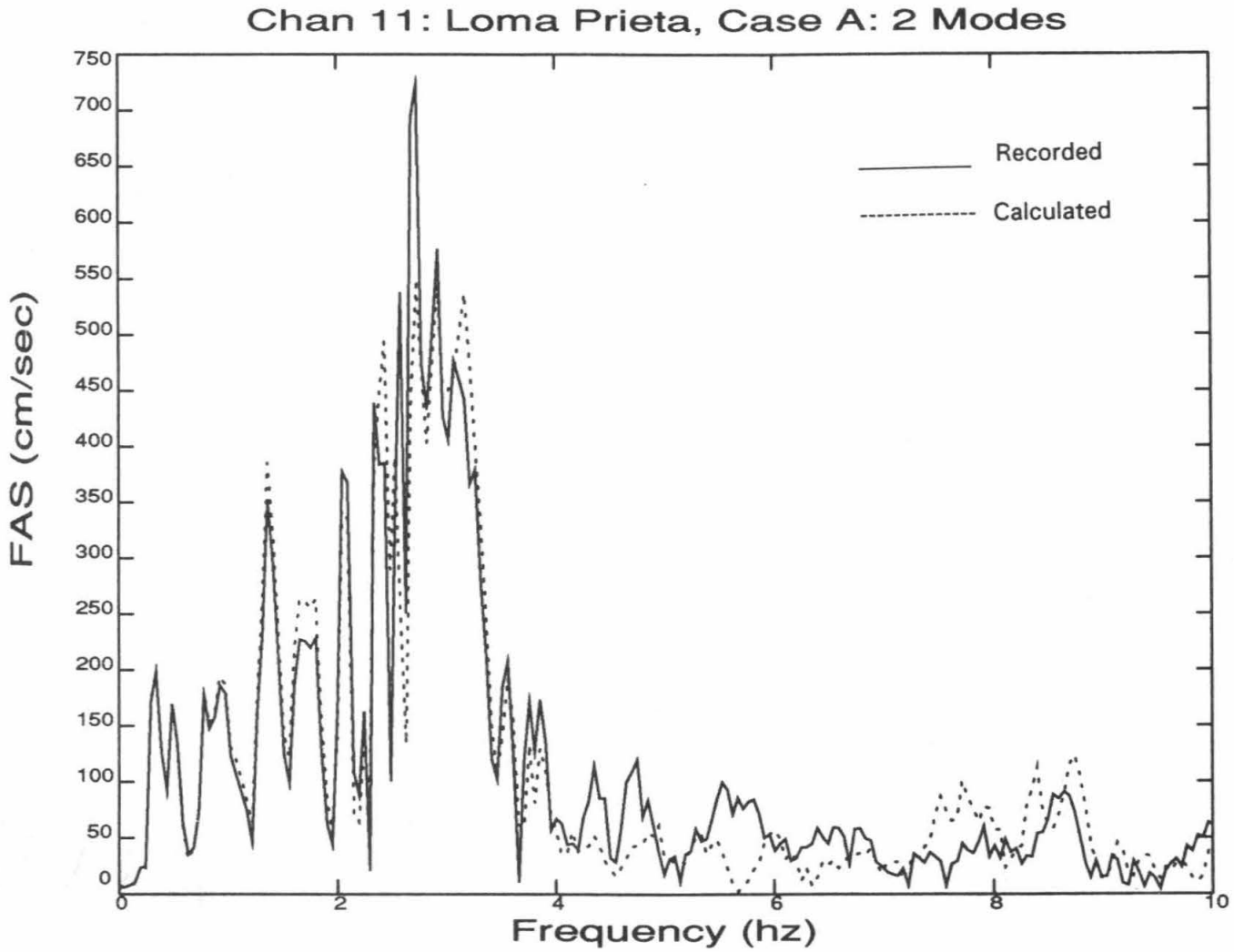

Figure 3-18: Comparison of the Fourier Amplitude Spectra of the Recorded Response and Calculated Response for the Identified Fixed Base Time-Invariant Model, Loma Prieta Earthquake, Channel 11

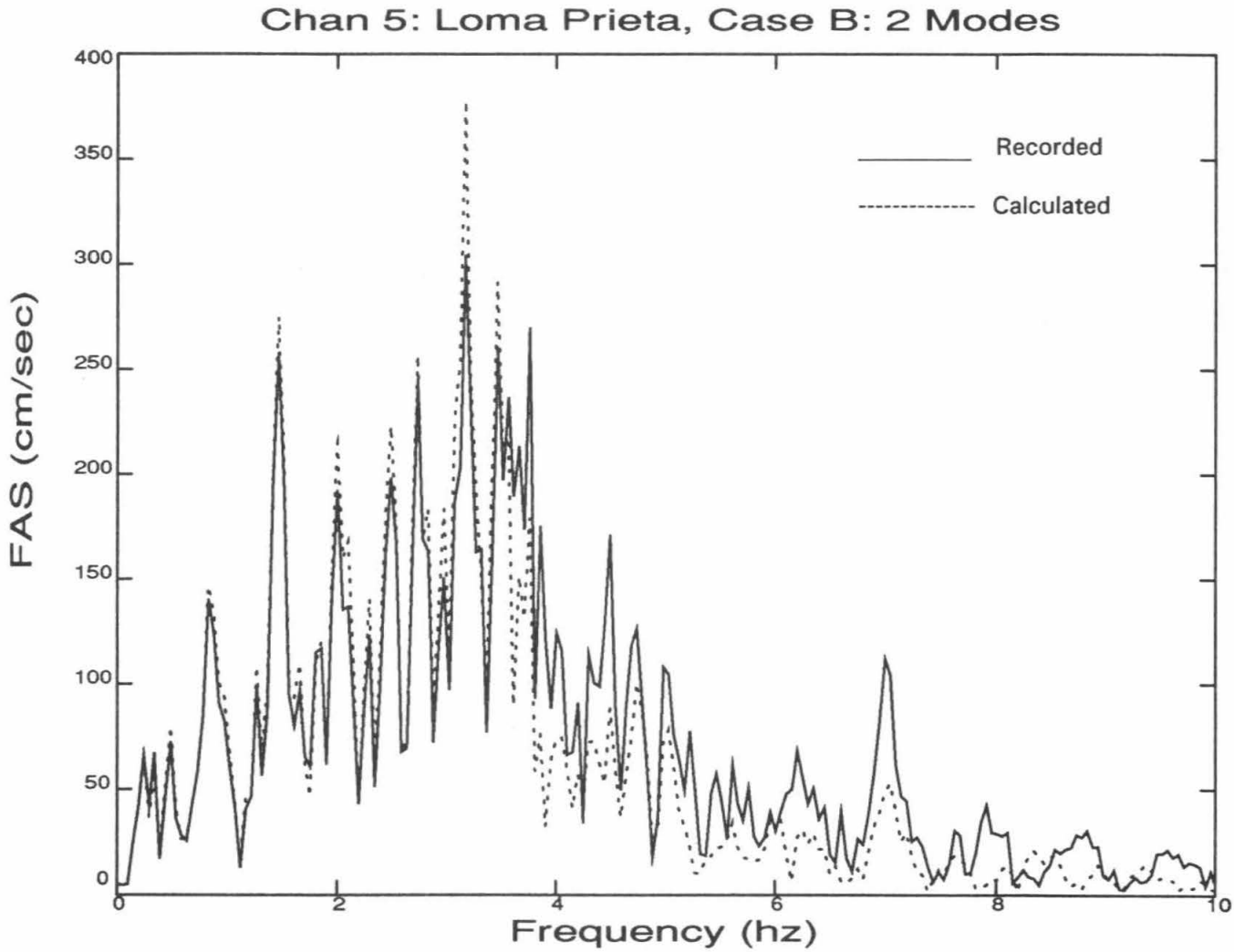

Figure 3-19: Comparison of the Fourier Amplitude Spectra of the Recorded Response and Calculated Response for the Identified Rocking Base Time-Invariant Model, Loma Prieta Earthquake, Channel 5

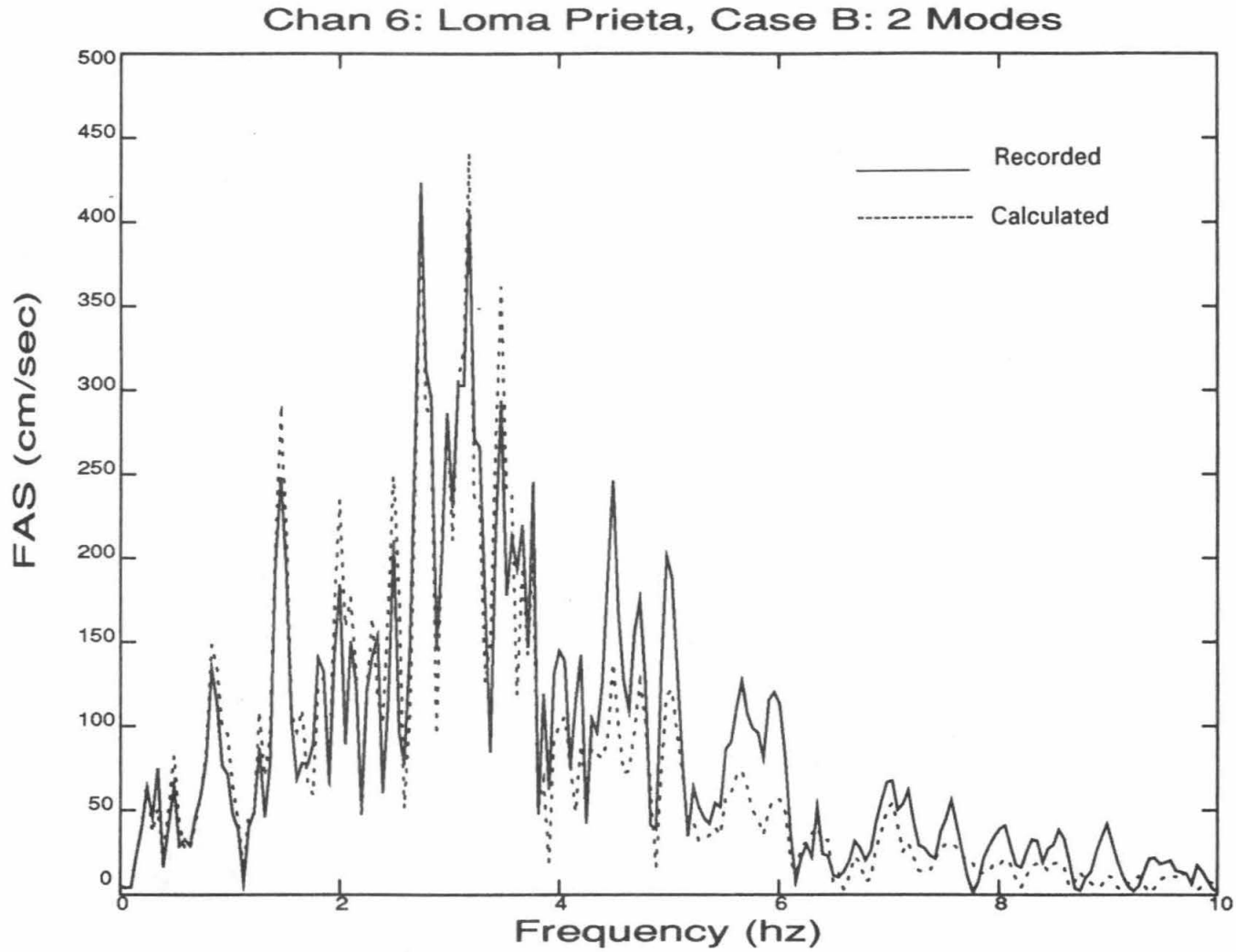

Figure 3-20: Comparison of the Fourier Amplitude Spectra of the Recorded Response and Calculated Response for the Identified Rocking Base Time-Invariant Model, Loma Prieta Earthquake, Channel 6

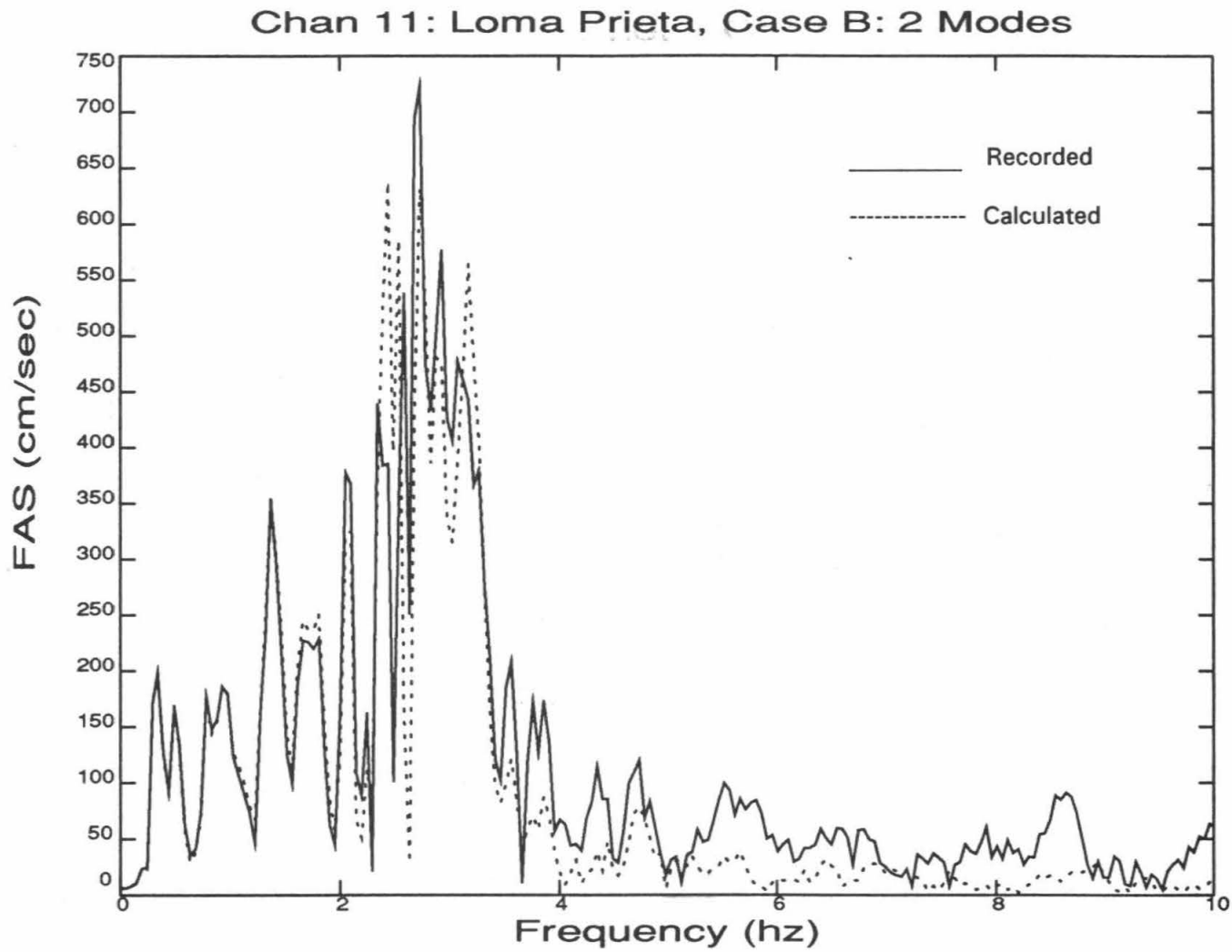

Figure 3-21: Comparison of the Fourier Amplitude Spectra of the Recorded Response and Calculated Response for the Identified Rocking Base Time-Invariant Model, Loma Prieta Earthquake, Channel 11

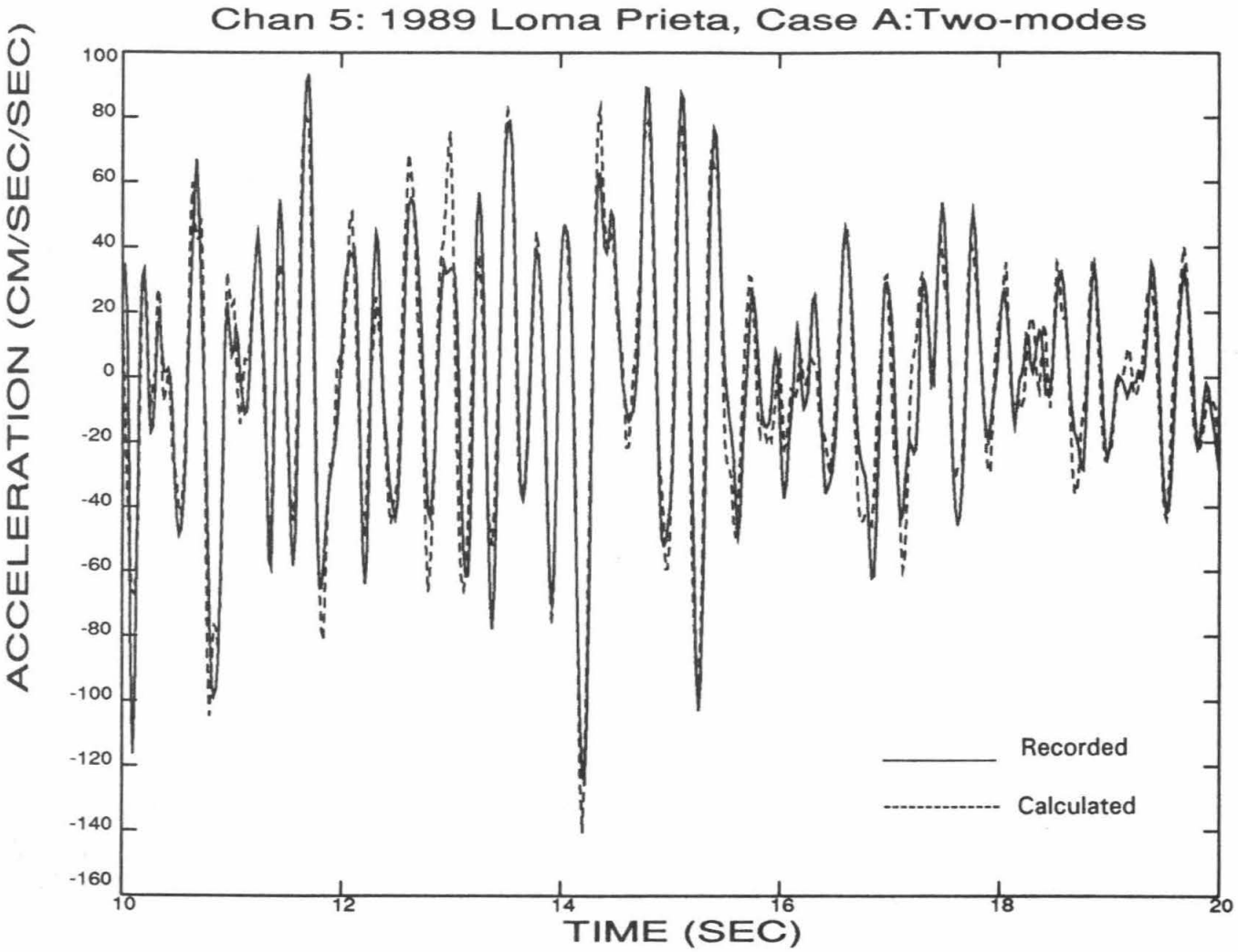

Figure 3-22: Comparison of Recorded Response and Calculated Response for the Fixed Base Model Identified From the Time Segment [10, 20], Loma Prieta Earthquake, Channel 5

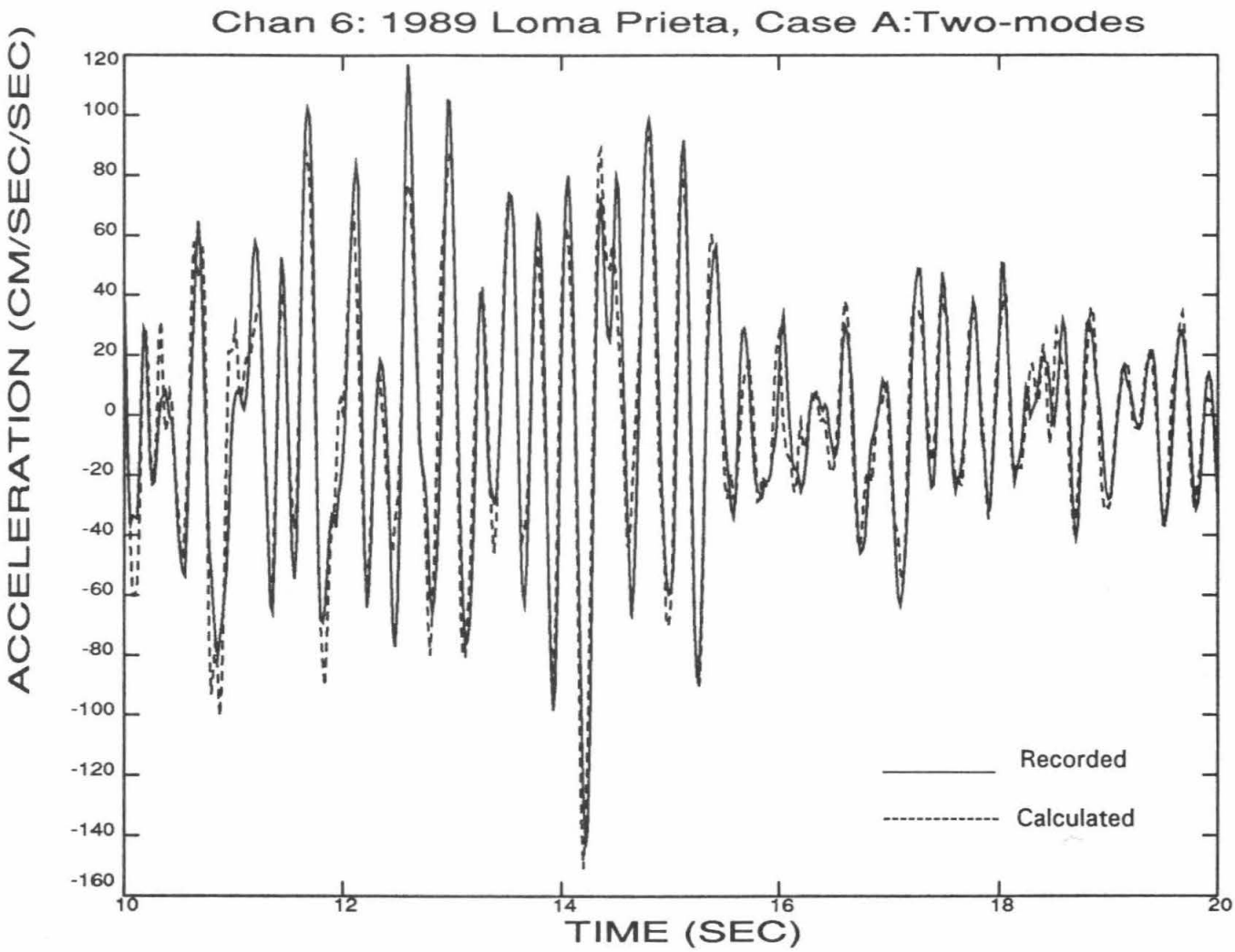

Figure 3-23: Comparison of Recorded Response and Calculated Response for the Fixed Base Model Identified From the Time Segment [10, 20], Loma Prieta Earthquake, Channel 6

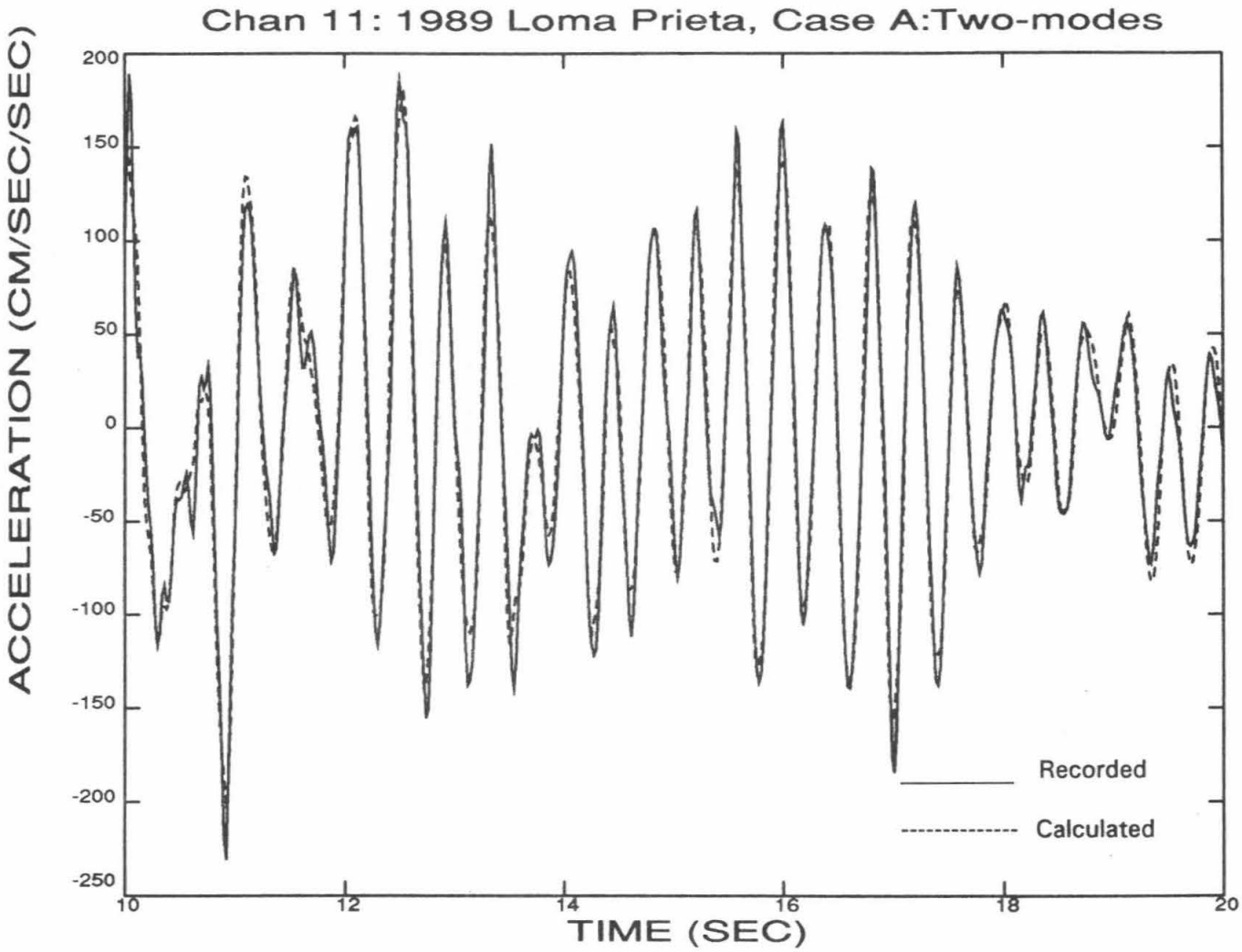

Figure 3-24: Comparison of Recorded Response and Calculated Response for the Fixed Base Model, Identified From the Time Segment [10, 20], Loma Prieta Earthquake, Channel 11

4. ELASTIC ANALYSIS TO CURRENT CRITERIA AND GUIDELINES

In this analysis, structure analytical models were developed, and other analytical input parameters were specified, following current USNRC seismic analysis criteria and industry guidelines. Comparisons of the analytical results to the actual recorded responses and modal identification results provide insight into the adequacy of these criteria and guidelines.

4.1 Analytical Approach

Key elements of the seismic analyses include the following:

- Overall structure model layout
- Modeling of mass
- Modeling of stiffness
- Structure damping
- Seismic input
- Soil-structure interaction
- Time-history analysis

Guidance on treatment of the first four items was obtained primarily from the USNRC Standard Review Plan [U.S. Nuclear Regulatory Commission, 1981] and ASCE Standard 4-86 [American Society of Civil Engineers, 1986]. These documents were supplemented by others noted below for certain specific details.

Seismic input and soil-structure interaction are also key elements of nuclear plant structure seismic analysis. For nuclear plant seismic analysis, the seismic input is typically specified in terms of the ground motion in the free-field. For soil sites, the effective input motion to the structure is modified from the free-field motion by soil-structure interaction. For the analyses performed in this study, seismic input was based upon motions recorded at the ground floor of the building. Assuming that the foundation is rigid, these recorded foundation motions include soil-structure interaction effects and completely describe foundation response. Structure response can then be determined without modeling soil-structure interaction effects.

As described below, the analytical methods adopted for these analyses involve various approximations of the actual structure characteristics or behavior that are frequently employed by the industry. Sensitivity studies were performed to investigate the significance of certain modeling approximations and assumptions. While these approximations introduce uncertainties into the calculated seismic responses, the results obtained are considered sufficiently accurate to achieve the

objectives of this study. These uncertainties can be reduced by more refined analysis in the future, if desired.

4.1.1 Overall Structure Model Layout

The building was represented by a three-dimensional lumped mass model. The base of the model was established at the ground floor, Elevation 0'–0". The floor slabs were judged to be sufficiently stiff in-plane to act as rigid diaphragms. Masses were lumped at the mass centroids of each floor of the building above grade: Second floor, Elevation 17'–10"; Third floor, Elevation 34'-4"; Fourth floor, Elevation 50'–10"; and Roof, Elevation 66'-4". These masses were permitted to have all six degrees of freedom, with the resulting model having a total of 24 dynamic degrees of freedom.

The structure stiffness at each story was represented by a single element. Each element was assigned material and geometric properties to provide the overall horizontal, vertical, rotational, and torsional stiffnesses at each story. They were located at the story centers of horizontal rigidity.

4.1.2 Modeling of Mass

Lumped masses assigned to each floor were based upon best estimates of all tributary masses, including the weights of floor slabs, beams and columns (including concrete fireproofing), walls, equipment, partitions, and other significant masses. Most of the mass was associated with the structure. This is due to the relatively thick concrete walls, extensive concrete encasement around structural steel members, and relatively light weight of attached equipment.

Field walkdown data obtained after the Loma Prieta earthquake were used to establish non-structural masses. Review of the drawings suggest that masses at the time of the Morgan Hill earthquake were not significantly different.

4.1.3 Modeling of Stiffness

Structure stiffness properties were based exclusively on the stiffnesses of the concrete exterior and interior walls. Determination of the wall stiffnesses requires estimates of the concrete modulus of elasticity and treatment of potential stiffness reduction due to cracking. Shear wall stiffness is one of the significant issues investigated in this study. A series of structure models, based on different estimates of shear wall stiffness, were analyzed. These models were all based on uncracked shear wall section properties. Specific differences between the different models are presented in later discussion. Stiffness representation common to all models is discussed here.

Story stiffnesses against horizontal translation and torsional rotation were based on the guidance provided in ASCE Standard 4-86, supplemented by Derecho, et al [1974]. The story stiffness against translation in

each of the horizontal directions was taken as the sum of the story stiffnesses of the individual shear walls loaded in-plane in that direction. Out-of-plane wall stiffnesses were neglected. Centers of rigidity and torsional story stiffnesses were determined following Section 3.1.8.1.3 of ASCE Standard 4-86. These stiffnesses were converted to equivalent shear areas and polar moments of inertia for inclusion in the structure model.

Two different approaches were used to determine horizontal story stiffnesses of the individual shear wall elements. For the east exterior wall, which is solid, and interior walls, which may be perforated by openings that are relatively small, story stiffnesses were determined following the approach recommended in Derecho, et al [1974]. The stiffness is determined by modeling a wall as a vertical beam of rectangular cross-section, and fixed against rotations at the floor levels. Shear and local bending deformations are considered. A wall perforated by openings is discretized into a series of piers, whose individual stiffnesses are determined in the same manner and subsequently combined to obtain the total wall story stiffness.

Openings in the north, south, and west exterior walls separate these walls into piers and spandrels. To more accurately account for the increased flexibility introduced by these openings, two-dimensional finite element models were developed of these walls. These models were used to determine story stiffnesses of each wall.

Vertical and rotational stiffnesses were determined following elementary beam theory, with the walls forming the cross-section of the equivalent beam. This assumes that the floor slabs are rigid and that plane sections remain plane. This approach, although approximate, is sufficiently accurate to capture the overall building response since the global vertical and rotational flexibilities are small in comparison to those associated with horizontal translation and torsion. In a sensitivity study, estimated lower bound vertical and rotational stiffnesses were assigned to the dynamic model as alternative values. This study determined that the dynamic characteristics of the building are not particularly sensitive to the vertical and rotational stiffnesses.

The masonry in-fill was neglected in determining the structural stiffnesses. Accounting for differences in the moduli of elasticity, the masonry in-fill is equivalent in stiffness to about five to seven inches of concrete, which is about half of the thickness of the exterior concrete walls. The effective stiffness of the in-fill is further reduced by the light connectivity to the surrounding concrete. As noted in Section 2.4, relative slip between the in-fill and surrounding concrete at the south wall was observed in the Loma Prieta earthquake. The lack of cracking in the in-fill panels themselves suggests that they did not experience significant seismic load, perhaps because of the flexibility in the joints with the concrete structure. Neglecting the masonry in-fill stiffness was judged to be appropriate, and is customary in nuclear plant seismic analysis. The effect of this approximation was considered in a sensitivity study, which determined that the masonry contributes relatively little additional stiffness to the structure.

Potential interaction between the concrete shear walls and the embedded structural steel framing was also neglected in determining the structural stiffnesses. This approximation has been used in nuclear plant structures with this type of construction. Considering the steel frames as independent seismic load-resisting systems, this approximation is appropriate since their horizontal stiffnesses are very small in comparison to the stiffnesses of the shear walls. However, the steel framing may introduce secondary effects that can influence the shear wall stiffness. As suggested by Gergely [1985] for the Zion Nuclear Power Plant, steel framing embedded in a concrete wall provides restraint for shrinkage strains. This restraint may lead to cracking. Also, there may be increased interaction between the framing and concrete after the latter cracks under seismic load. The potential effects of steel framing-concrete shear wall interaction could not be investigated in the present study, and remain as a source of uncertainty in the analysis.

4.1.4 Structure Damping

Guidance on appropriate equivalent viscous modal damping values was obtained from USNRC Regulatory Guide 1.61 (R.G. 1.61), ASCE Standard 4-86, and EPRI NP-6041, "A Methodology for Assessment of Nuclear Power Plant Seismic Margin [Electric Power Research Institute, 1988]. For reinforced concrete structures, R.G. 1.61 specifies damping values of 4% and 7% for the Operating Basis Earthquake (or 1/2 Safe Shutdown Earthquake) and Safe Shutdown Earthquake (SSE), respectively. R.G. 1.61 notes that lower values should be used if maximum stresses are significantly lower than the yield stress and 1/2 yield stress for the SSE and 1/2 SSE, respectively.

For reinforced concrete structures, ASCE Standard 4-86 recommends damping values of 4% and 7% for Stress Levels 1 and 2, respectively. For the generation of input motions to attached equipment and piping, ASCE Standard 4-86 suggests that the Level 2 value may be used if stresses in the majority of resisting building elements for the applicable loading combination are greater than 50% of ultimate strength for concrete. The Level 1 value should be used if the stresses are 50% or less than the code ultimate strength for concrete in the majority of resisting building elements.

EPRI NP-6041 recommends the use of a "conservative estimate of median damping" for analysis of earthquakes beyond the design basis, rather than conservative values prescribed by R.G. 1.61 and ASCE Standard 4-86. For stresses at about 1/2 yield or below, damping of 3% is recommended for reinforced concrete with slight cracking, and 5% with moderate cracking. For stresses beyond or just below yield, damping for reinforced concrete of 10% is recommended.

In response analyses for Morgan Hill earthquake input motion, 4% damping was assigned to all structure modes, based on the guidance described above. As noted later, maximum ratios of applied loads to available capacities are estimated to be about 0.75 and 0.25 for the E-W and N-S shear walls due to the Morgan Hill earthquake. This would suggest that

a value somewhat higher than 4% could be assigned to E-W modes, while a value somewhat lower could be used for the N-S modes. However, the 4% damping selected is a reasonable value representative of the state of stress in the building and the recommendations available to the industry.

In response analyses for Loma Prieta earthquake input motion, separate analyses using 7% and 10% structure damping were performed. Seven percent damping is the maximum value suggested for design analysis by the Standard Review Plan and ASCE Standard 4-86. As discussed later, applied loads due to the Loma Prieta earthquake were determined to be greater than the available capacities in the main load-resisting shear walls. The 10% damping was based on the recommendations of EPRI NP-6041.

4.1.5 Seismic Input

The seismic input for the building response analyses consisted of the foundation responses. Acceleration time-histories for all six degrees of freedom at a reference point on the foundation, assuming that the foundation is rigid, defined the input. For convenience, the foundation reference point was located near the center of the building, at the intersections of Column Lines 3 and C (see Figure 2-1). Recorded motions from Channels 9, 10, and 13 were used to generate the foundation motions for the N-S and E-W horizontal translations and torsion. The foundation motions for vertical translation and rotation about the N-S and E-W axes are overdefined, since four vertical channels, Channels 1 to 4, are available to determine the input for these three degrees of freedom. Accordingly, input motions to the structure model were based upon a least-squares fit to the motions recorded at the vertical channels. Resulting response spectra at the foundation reference point for both earthquakes are shown in Figures 4-1 to 4-12. For reference in these figures, the X, Y, and Z directions correspond to the E-W, N-S, and vertical directions, respectively.

As noted in Section 3, modal identification determined that the foundation exhibits a slight degree of flexibility, resulting in different rotations at the bases of the wall. The vertical acceleration time-history at Channel 1 generated from foundation motions assuming a rigid foundation is compared to the actual recorded motions in Figure 4-13 for the Loma Prieta earthquake. As shown, there is a slight error through the duration of the strongest input. This aspect of foundation/structure behavior is discussed in more detail in Section 7.

4.1.6 Time-History Analysis

Time-history response analysis of the structure was performed using a version of Computer Program CLASSI [Wong and Luco, 1980]. The foundation motions for all six degrees of freedom, calculated as described in Section 4.1.5, were applied at the base of the structure model. These foundation motions were obtained directly from recorded earthquake motions including soil-structure interaction effects.

Consequently, they include all aspects of soil-structure interaction (kinematic and inertial interaction).

4.1.7 Variation of Shear Wall Stiffness

ASCE Standard 4-86 specifies that the concrete modulus of elasticity be based on the standard ACI Code equation in conjunction with the specified concrete compressive strength. ASCE Standard 4-86 recommends that "Best estimate stiffness properties for elements shall be used, except that reinforced concrete elements may be modeled as uncracked sections, provided that the elements do not crack significantly due to the critical load combination". Because this provision is relatively general, determination of shear wall stiffness requires interpretation and judgement by the analyst. The standard provides additional recommendations on peak broadening and peak amplitude reduction to account for uncertainties in response due to uncertainties in structure frequencies and soil-structure interaction.

To provide more definitive guidance on modeling the stiffness of low aspect ratio concrete shear walls, the Working Group on Stiffness of Concrete Shear Wall Structures of the ASCE Dynamic Analysis Committee was formed. Based upon a review of available data, particularly experimental results obtained by the USNRC's Seismic Category I Structures Program, the ASCE Working Group on Stiffness of Concrete Shear Walls [1991] has recently recommended the following two bounding stiffness estimates for the generation of in-structure response spectra (currently in draft form):

- A lower bound stiffness based on the uncracked section properties and one-half of the best estimate concrete modulus.

- An upper bound stiffness based on the uncracked section properties and the concrete modulus based on the specified f'_c (design concrete compressive strength).

Peak broadening or peak shifting can be used with the in-structure spectra for equipment and piping design. For the upper bound stiffness case, a 10% broadening of the spectral peaks only in the direction of higher frequencies is recommended to account for uncertainties.

Based on this survey, the following three structure models, with different estimates of shear wall stiffness, were developed:

Model 1

This represents the baseline model, which serves as a common reference against which other models can be compared. Best estimates of the uncracked shear wall stiffnesses are used. A best estimate of the concrete modulus of elasticity was determined using the following equation from ACI 349-85 [American Concrete Institute, 1986], in conjunction with a best estimate of the concrete compressive strength:

$$E_c = 57{,}000\ (f'_c)^{1/2} \text{ in psi}$$

Best estimates of the concrete compressive strength were determined by applying factors to the minimum specified values. The ratio of the median concrete compressive strength to the minimum specified value at the time of testing was estimated to be approximately 1.2. This value is reduced slightly below typical values exhibited by nuclear plant concrete to account for potential differences in quality control. An additional factor of 1.2 was included to account for increase in concrete strength from the time of testing to the present. This is a representative value estimated in nuclear plant structural fragility evaluations for concrete tested at 28 days [Wesley and Hashimoto, 1981]. Even though the building was about 40 years old at the times of the earthquakes, no evidence of any significant strength degradation was observed. Applying a total factor of 1.2 x 1.2 = 1.44 to the minimum specified concrete compressive strengths, best estimate strengths of 4,000 psi and 4,700 psi were estimated for the original construction and 1955 addition. The resulting moduli of elasticity have uncertainty associated with accuracy of the ACI formulation for concrete modulus of elasticity and estimated concrete strengths. However, these uncertainties are considered to be small in comparison to the uncertainty in the shear wall stiffness even when the concrete modulus is known.

Model 2

This model corresponds to the best estimate model based on ASCE Standard 4-86 recommendations for reinforced concrete structures that do not crack significantly, and the upper bound stiffness model for the recommendations of the ASCE Working Group on Stiffness of Concrete Shear Wall Structures. This model was also based on uncracked section properties. The concrete moduli of elasticity were based on the ACI code equation in conjunction with the minimum specified concrete compressive strengths.

*Model 3**

This model represents the lower bound structure stiffness following the recommendations of the ASCE Working Group on Stiffness of Concrete Shear Wall Structures. Uncracked section properties were again used. The concrete moduli of elasticity were taken as one-half of the best estimate values used in Model 1.

---

* Subsequent to this study, draft ASCE Working Group recommendations revised the lower stiffness to be 60% of the concrete modulus based on the ACI code equation in conjunction with the minimum specified concrete strength. Resulting concrete moduli for this building are essentially equal to values assigned to Model 3.

Concrete moduli of elasticity for the three models are summarized in Table 4-1. As shown, the values for Models 2 and 3 are 83% and 50% of those for Model 1.

4.2 Response Analysis for the Morgan Hill Earthquake

For the Morgan Hill earthquake, the following two types of comparisons were made:

- Comparison of modal parameters calculated by the structure model to values obtained by modal identification
- Comparison of analytically calculated and actual recorded responses

4.2.1 Comparison of Modal Parameters

The seismic response levels experienced by the building during the Morgan Hill earthquake are well within those for which the criteria and guidelines described above should be applicable. Comparisons of modal parameters calculated by the structure models with the modal identification results provides estimates on the adequacy of these methods.

Fixed base structure frequencies for the first six modes obtained by Models 1, 2, and 3 are listed in Table 4-2. The first two modes dominate the horizontal response, with approximately 80% of the total translational mass participating in these modes.

Table 4-3 compares frequencies for the fundamental E-W and N-S modes calculated by Models 1, 2, and 3 to time-invariant values obtained for the fixed base structure by modal identification using Morgan Hill input and output. Similarly, Tables 4-4 and 4-5 compare mode shapes for the fundamental E-W and N-S modes. Mode shapes for Models 1, 2, and 3 are the same because all models have the same lumped masses, and because the stiffnesses of the model vary by a factor that is the same for all elements of a single model.

Ratios of frequency obtained by Model 1 to frequency obtained by modal identification were determined to be about 1.55 for both the fundamental E-W and N-S modes. Because the masses are considered to be accurate, these results suggest that the actual structure stiffnesses are significantly less than the best estimate, uncracked values, even for the moderate seismic response levels experienced by the building during the Morgan Hill earthquake. On the average, the actual stiffnesses are about 40% of the best estimate, uncracked values. Specific data on structure stiffnesses are reviewed in Section 6.

The same frequency ratios were obtained for the two horizontal directions, even though the peak accelerations and stresses in the E-W direction exceed those in the N-S direction by about a factor of two to three. Because only light concrete cracking was observed after the Loma

Prieta earthquake, it may be that little or no cracking occurred due to the Morgan Hill earthquake. This suggests that the stiffness reductions may have been due to sources of cracking independent of direction, such as concrete shrinkage, rather than seismic load. This phenomenon is discussed in Section 6 in more detail.

Ratios of frequencies obtained by Models 2 and 3 to frequencies calculated by modal identification are about 1.4 and 1.1, respectively. Thus, the upper bound stiffness estimate from the ASCE Working Group recommendations overestimates the actual frequency by about 40%. The lower bound stiffness estimate still slightly overestimates the actual frequency by about 10%. However, the level of overestimation is not considered significant. While the lower bound stiffness recommendation may not be a true lower bound, overestimation of the actual frequency may also be due to approximations and assumptions implicit in the structure model. Thus, the ASCE Working Group recommendations appear to provide reasonable bounding values, although further substantiation could require more detailed analysis.

Comparison of mode shapes for the fundamental E-W mode from modal identification and the structure models in Table 4-4 indicates that the models are able to accurately calculate the structure deformations in the E-W direction. However, it appears that the models overestimate the N-S translations at Channels 5, 7, and 8. The translations at these channels are due primarily to torsion, rather than overall N-S motion. This result is somewhat surprising, since discontinuity of the south wall at the first story would be expected to cause a shift in the center of rigidity away from the centers of mass. The increase in eccentricity would then be expected to lead to significant torsional rotations. However, such torsion is not indicated by modal identification.

As shown in Table 4-5, the fundamental N-S mode shapes have been normalized to a value of 1 at Channel 6 for consistency with the modal identification results presented in Section 3. Averaging the N-S translations at the two channels at the same floor to obtain approximate translations for the centers of mass, the mode shapes obtained by the structural models and modal identification are very close to each other. The structure models obtain greater translation at the west side of the building than the east side. This is because the east exterior wall, which is solid, is stiffer than the west exterior wall, which is perforated by openings, thus shifting the centers of rigidity to the east of the centers of mass, which are located close to the middle of the building. However, the mode shape obtained by modal identification shows torsion in the opposite direction, with translations greater at the east side of the building than the west side.

As discussed in Section 3.2.1, the perceived errors in torsion predicted by the structure model may actually be a consequence of foundation flexibility, rather than errors in the relative wall stiffnesses. For example, the base of the solid, and thus stiffer, east exterior wall rotates relative to the assumed rigid foundation, and this rotation tends to increase positive horizontal translations at Channels 6 and 8, which are attached to this wall. In contrast, the base of the west exterior wall rotates in such a manner as to decrease the overall

translations of this wall. This behavior occurs because the foundation is not sufficiently stiff to fully constrain rotations at the bases of the relatively stiff walls. Because the structure models assume a rigid foundation, this behavior cannot be explicitly represented.

4.2.2 Comparison of Floor Response Spectra

Five percent damped floor response spectra calculated by Models 2 and 3 are compared to spectra corresponding to motions recorded by channels at the 3rd Floor and roof in Figures 4-14 to 4-19. In the E-W direction (Figures 4-14 and 4-15), Model 2 (upper bound stiffness case) underestimates the structure peak accelerations and spectral accelerations at frequencies away from the Model 2 structure E-W frequency. This is because earthquake input at the E-W frequency of Model 2 is less than the input at the actual structure frequency. Peak structure accelerations and floor response spectra in the E-W direction obtained by Model 3 (lower bound stiffness case) are close to those actually recorded, since the model frequency is much closer to the actual frequency. Peak spectral accelerations calculated by Model 3 at frequencies between about 3 to 4 Hz underestimate the actual values somewhat.

Differences between the analytically calculated and actual recorded responses in the N-S direction vary according to the structure model considered, channel location, and frequency (Figures 4-16 to 4-19). Peak accelerations calculated by Model 2 are relatively close to the recorded values. Seismic input at the Model 2 N-S frequency of 7.78 Hz is less than the input at the actual fixed base structure frequency of 5.51 Hz. However, the 4% damping assigned to Model 2 is also significantly less than the time-invariant value of 11.6% obtained by modal identification for the fixed base case. These two differences appear to cancel each other out, resulting in a close comparison between the Model 2 and actual peak accelerations. Peak spectral accelerations in the vicinity of the fundamental N-S frequency of Model 2 (about 8 Hz) significantly exceed the values obtained from the actual recordings. The difference is greater for Channels 5 and 7 at the west side of the building than Channels 6 and 8 at the east side. This is due to the differences between the analytically calculated and actual mode shapes.

The floor response spectra analytically calculated using Model 3 are relatively close to those actually recorded at the east side of the building (Channels 6 and 8). However, Model 3 floor spectra at the west side of the building (Channels 5 and 7) exceed those actually recorded. Again, this result is influenced by the differences in analytically calculated and identified mode shapes.

The current criteria and guidelines followed in these analyses are intended to result in conservative floor response spectra for use in equipment design or evaluation. Review of Figures 4-14 to 4-19 indicate that, without any additional broadening or peak shifting, the bounding stiffness estimates incorporated in Models 2 and 3 result in floor spectra that envelope spectra from the actual recorded motions at most, but not all, frequencies. The calculated floor spectra slightly

underestimate the actual spectra at limited frequency ranges. This underestimation appears to occur primarily because the bounding stiffness estimates, although close, do not completely envelope the actual frequencies. As noted in Section 4.2.1, the bounding stiffness estimates recommended by current guidelines are considered to be reasonable values based on the analyses performed in this study. However, as illustrated in the comparisons above, sufficiently conservative floor spectra require structure stiffness estimates that cover the range of probable values.

4.3 Response Analysis for the Loma Prieta Earthquake

The following comparison of modal parameters and seismic responses for the Loma Prieta earthquake is limited to the fundamental N-S mode. As discussed in Section 3, while modal identification results for both modes are uncertain, the identified parameters for the fundamental E-W mode are more suspect. Furthermore, structure stresses due to E-W response are probably well beyond levels for which the bounding stiffness estimates in Models 2 and 3 were intended. Consequently, discussion in this section is focussed only on the responses in the N-S direction, which are considered more applicable.

4.3.1 Comparison of Modal Parameters

Fixed base fundamental N-S frequencies obtained by modal identification are compared to values calculated using Models 1, 2, and 3 in Table 4-6. Frequency ratios are less than those obtained for the Morgan Hill earthquake. The frequency ratio of 2.0 for Model 1 indicates that stiffness of the shear walls is significantly less than the uncracked values. The bounding stiffness estimates recommended by the ASCE Working Group also result in models that overestimate the identified frequency. The frequency ratio for Model 3, based on the lower bound stiffness estimate, is 1.4.

As with the Morgan Hill results, the structure models obtain a mode shape that suggest torsional rotation in the opposite direction to that obtained by modal identification (Table 4-7). The identified mode shape is closer to that of a uniform shear beam than the mode shape obtained by the structural models.

4.3.2 Comparison of Floor Response Spectra

Analytically calculated 5% damped floor response spectra obtained using Models 2 and 3 are compared to spectra corresponding to the actual recorded motions in Figures 4-20 to 4-31. The floor spectra in Figures 4-20 to 4-25 are based on 7% structure damping, while those in Figure 4-26 to 4-31 are based on 10% structure damping. Peak structure accelerations and peak in-structure spectral accelerations are greater for Model 2 than for Model 3. This appears to be due to significant rocking input about the E-W axis in the 8 Hz range, which corresponds to the fundamental N-S frequency for Model 2. Floor spectra calculated by either structure model significantly exceed the actual spectra for

frequencies greater than about 4 Hz, with slight underestimations in the 2 to 4 Hz range. Floor spectra generated using 10% structure damping are slightly lower than those obtained for 7% structure damping, but significant exceedances of the actual spectra still result.

In general, the calculated N-S floor spectra significantly overestimate the actual spectra. The level of conservatism achieved by the calculated floor spectra would probably be considered excessive for evaluation of equipment against a beyond design basis earthquake. These spectra may also be too conservative for design. Some of this conservatism is introduced into the calculated floor spectra by structure damping, 7% or 10%, that underestimates the actual damping of about 13%, and differences between the calculated and actual frequencies. As discussed in Section 5 in more detail, differences in the effective participation factor also cause the calculated floor spectra to exceed the actual spectra.

Table 4-1

SUMMARY OF CONCRETE MODULI OF ELASTICITY FOR MODELS 1, 2, AND 3

Concrete	Modulus of Elasticity (ksf)		
	Model 1	Model 2	Model 3
Original construction	519,000	430,000	260,000
1955 addition	563,000	468,000	282,000

Table 4-2

SUMMARY OF FREQUENCIES FOR MODELS 1, 2, AND 3

Mode	Description	Frequency (Hz)		
		Model 1	Model 2	Model 3
1	First E-W mode	6.29	5.72	4.45
2	First N-S mode	8.55	7.78	6.05
3	First torsional mode	11.4	10.4	8.06
4	Second E-W mode	17.6	16.0	12.5
5	First vertical mode	19.5	17.7	13.8
6	Coupled vertical and N-S mode	25.0	22.8	17.7

Table 4-3

COMPARISON OF FREQUENCIES OBTAINED BY MODELS 1, 2, 3, AND MODAL IDENTIFICATION FOR THE MORGAN HILL EARTHQUAKE

Mode	Frequency (Hz)			
	Modal ID	Model 1	Model 2	Model 3
1, E-W	4.03	6.29 (1.56)	5.72 (1.42)	4.45 (1.10)
2, N-S	5.51	8.55 (1.55)	7.78 (1.41)	6.05 (1.10)

Note:

( ) Ratio of frequency obtained by the structure model to the frequency obtained by modal identification

Table 4-4

COMPARISON OF MODE SHAPES FOR THE FUNDAMENTAL E-W MODE OBTAINED BY MODELS 1, 2, 3, AND MODAL IDENTIFICATION FOR THE MORGAN HILL EARTHQUAKE

	Channel					
Source	7	8	5	6	12	11
Modal ID	-0.04	0.07	-0.09	0.15	0.64	1.00
Models 1, 2, 3	-0.16	0.11	-0.23	0.14	0.63	1.00

Note:

1. Mode shapes are normalized to a value of 1 at Channel 11

Table 4-5

COMPARISON OF MODE SHAPES FOR THE FUNDAMENTAL N-S MODE OBTAINED BY MODELS 1, 2, 3, AND MODAL IDENTIFICATION FOR THE MORGAN HILL EARTHQUAKE

	Channel					
Source	7	8	5	6	12	11
Modal ID	0.46	0.56	0.82	1.00	0.02	0.07
Models 1, 2, 3	0.73	0.56	1.29	1.00	0.04	0.06

Note:

1. Mode shapes are normalized to a value of 1 at Channel 6

Table 4-6

COMPARISON OF FREQUENCIES OBTAINED BY MODELS 1, 2, 3, AND MODAL IDENTIFICATION FOR THE LOMA PRIETA EARTHQUAKE

Mode	Frequency (Hz)			
	Modal ID	Model 1	Model 2	Model 3
2, N-S	4.23	8.55 (2.02)	7.78 (1.84)	6.05 (1.43)

Note:

( ) Ratio of frequency obtained by the structure model to the frequency obtained by modal identification

Table 4-7

COMPARISON OF MODE SHAPES FOR THE FUNDAMENTAL N-S MODE OBTAINED BY MODELS 1, 2, 3, AND MODAL IDENTIFICATION FOR THE LOMA PRIETA EARTHQUAKE

	Channel					
Source	7	8	5	6	12	11
Modal ID	0.54	0.66	0.80	1.00	-0.11	-0.16
Models 1, 2, 3	0.73	0.56	1.29	1.00	0.04	0.06

Note:

1. Mode shapes are normalized to a value of 1 at Channel 6

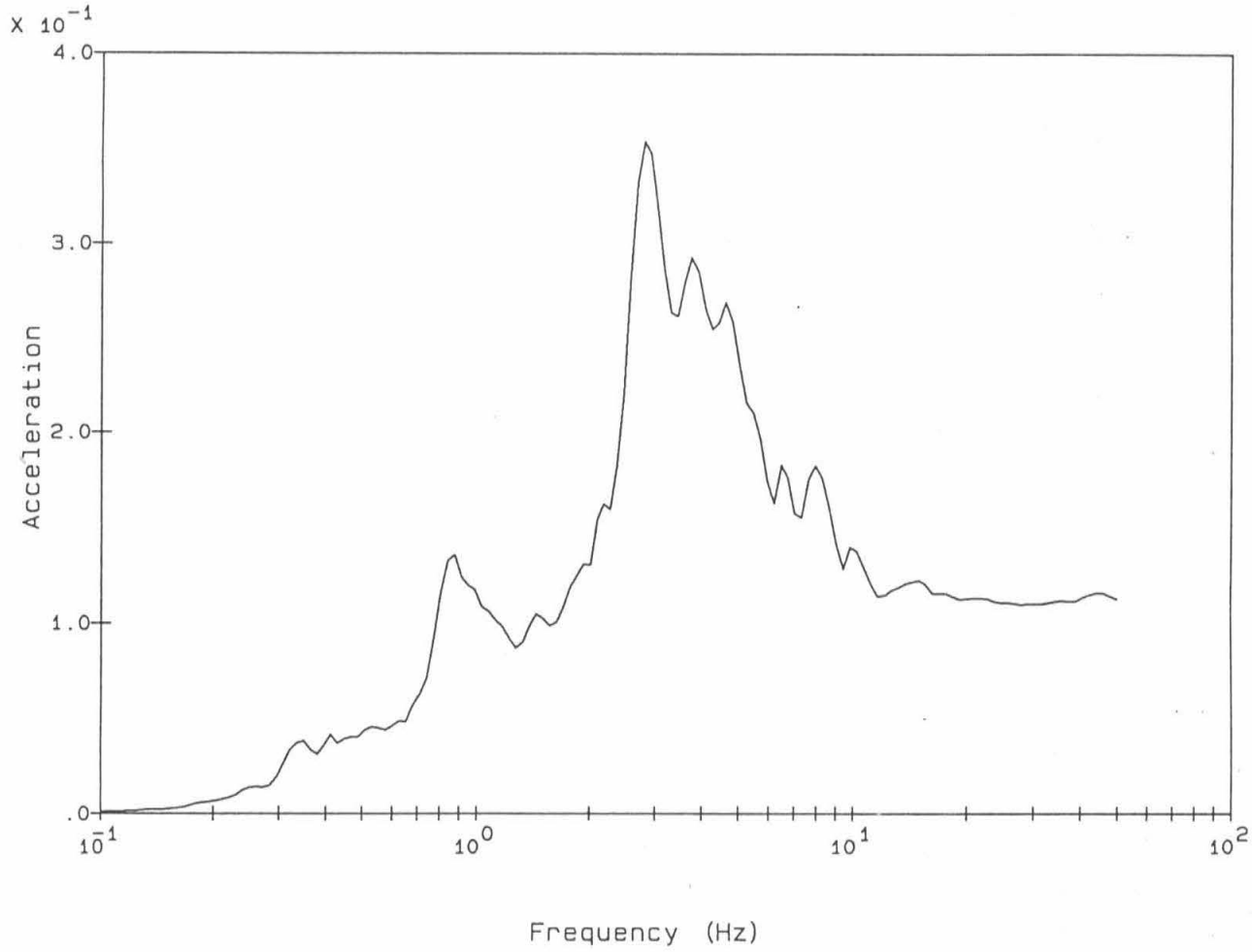

Notes:

X TRANSLATION

Acceleration (g)

Spectra calculated at 5% damping

Figure 4-1: Ground Spectrum at Foundation Reference Point, E-W Translation, Morgan Hill Earthquake

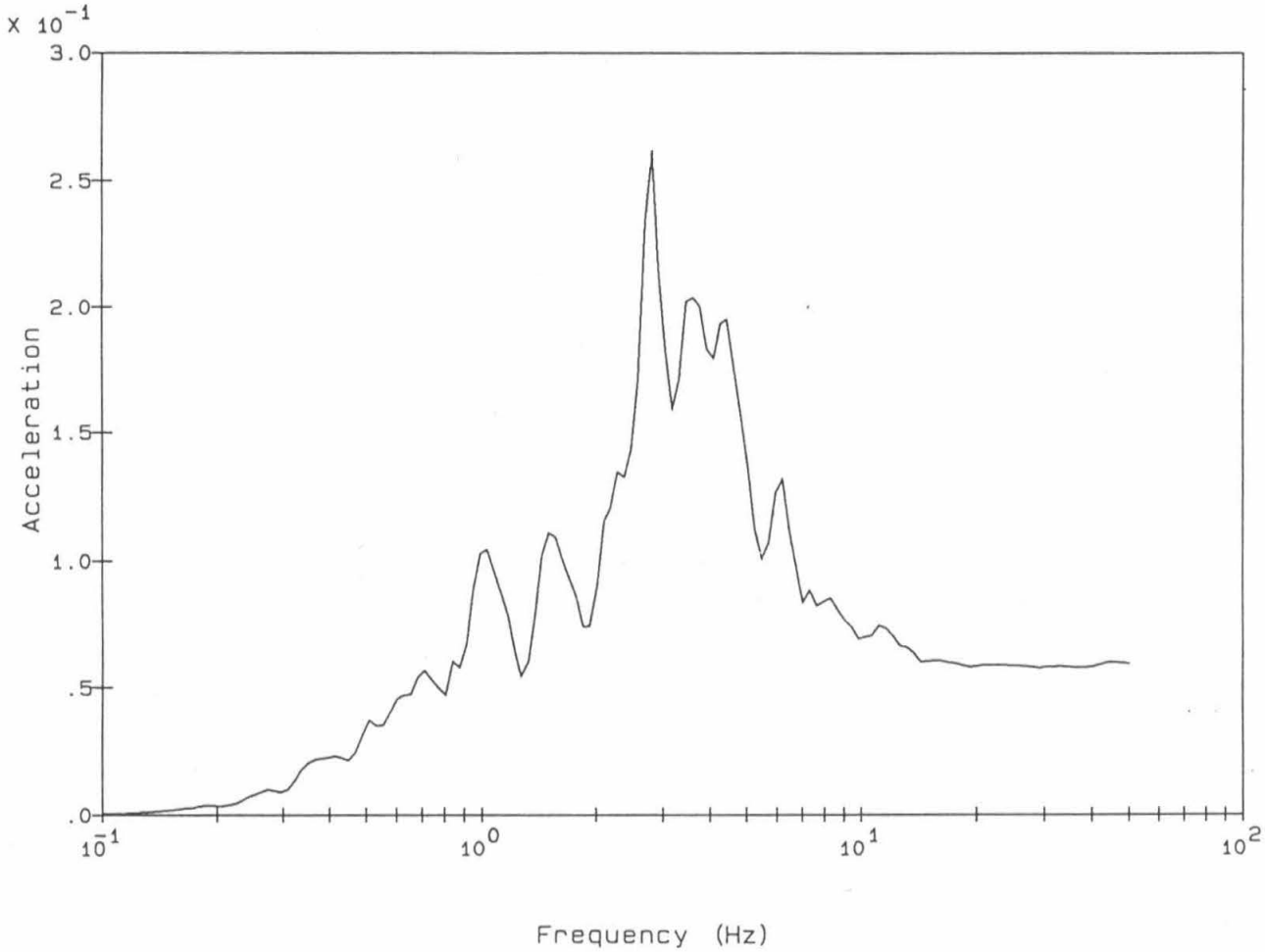

Notes:

Y TRANSLATION

Acceleration (g)

Spectra calculated at 5% damping

Figure 4-2: Ground Spectrum at Foundation Reference Point, N-S Translation, Morgan Hill Earthquake

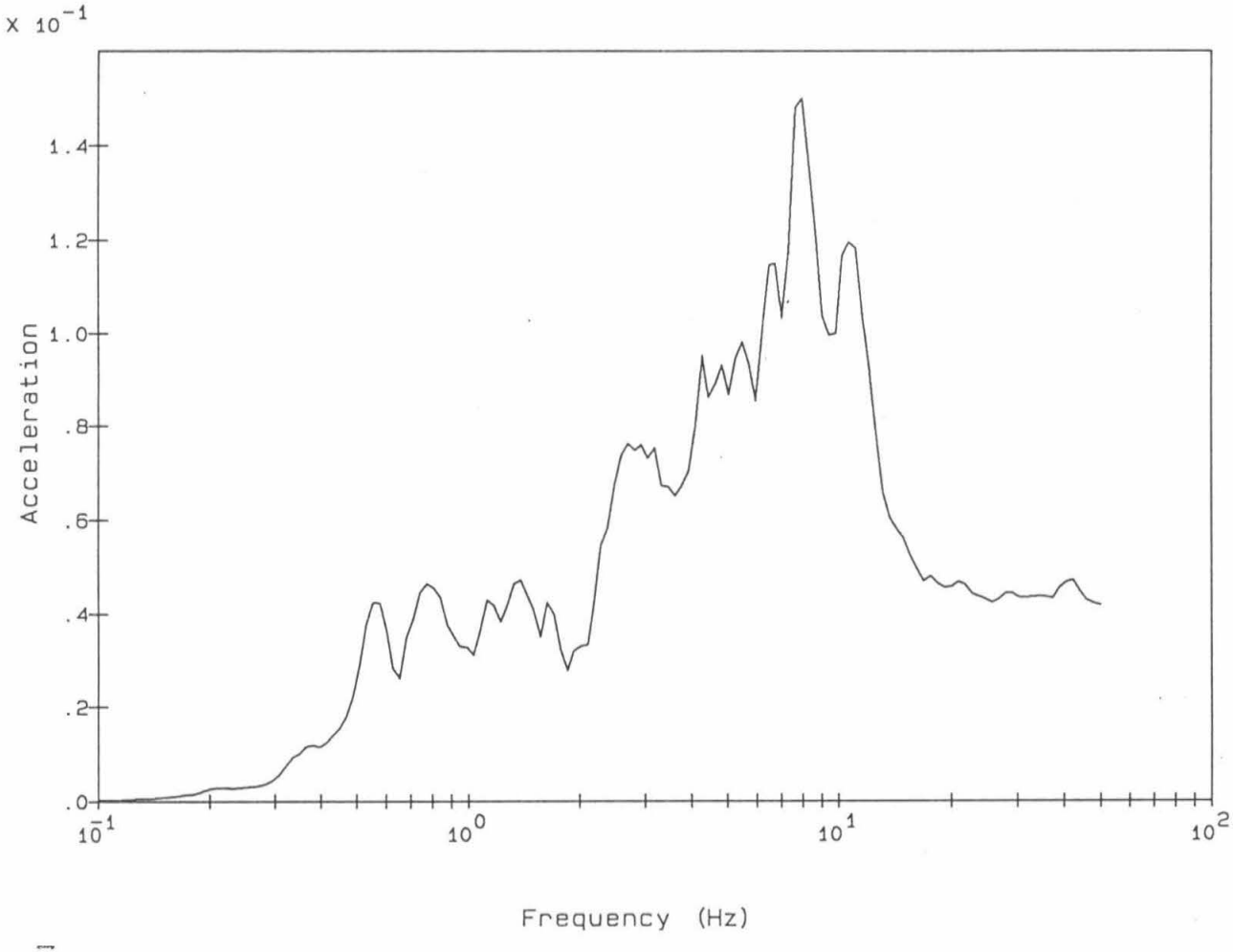

Notes:

Z TRANSLATION

Acceleration (g)

Spectra calculated at 5% damping

Figure 4-3: Ground Spectrum at Foundation Reference Point, Vertical Translation, Morgan Hill Earthquake

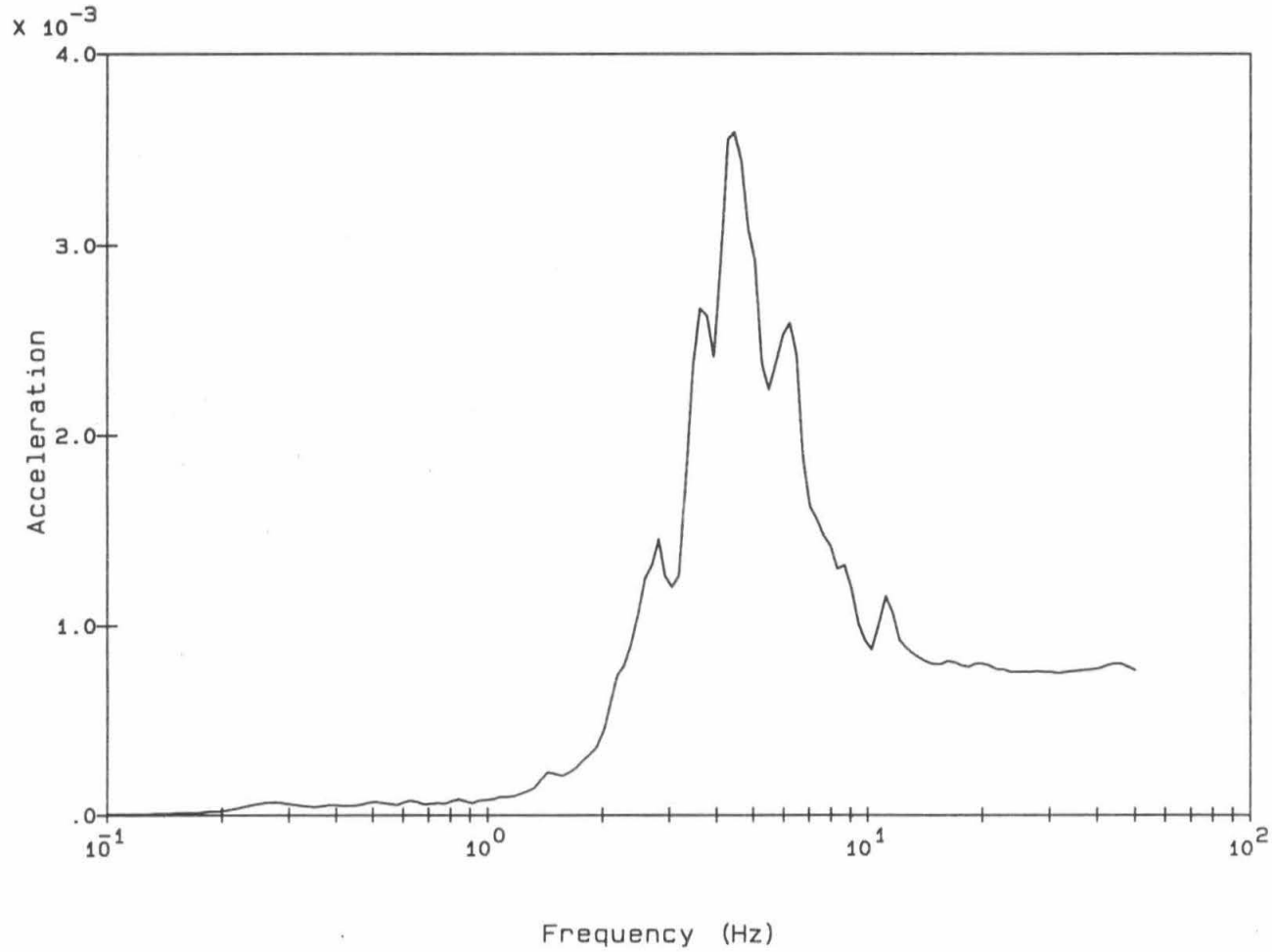

Notes:

XX ROTATION

Acceleration in g/ft

Spectra calculated at 5% damping

Figure 4-4: Ground Spectrum at Foundation Reference Point, Rotation About the E-W Axis, Morgan Hill Earthquake

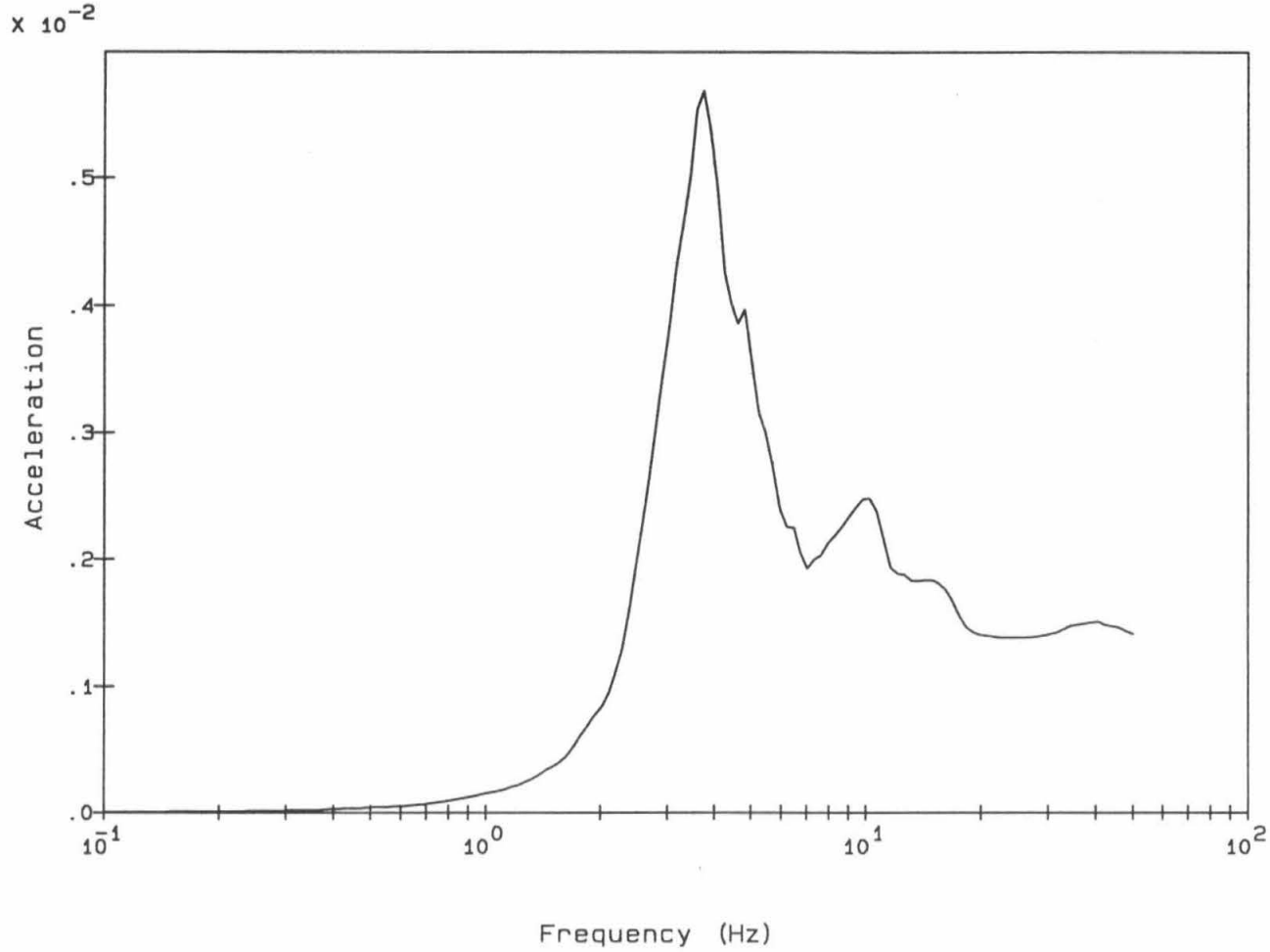

Notes:

YY ROTATION

Acceleration in g/ft

Spectra calculated at 5% damping

Figure 4-5: Ground Spectrum at Foundation Reference Point, Rotation About the N-S Axis, Morgan Hill Earthquake

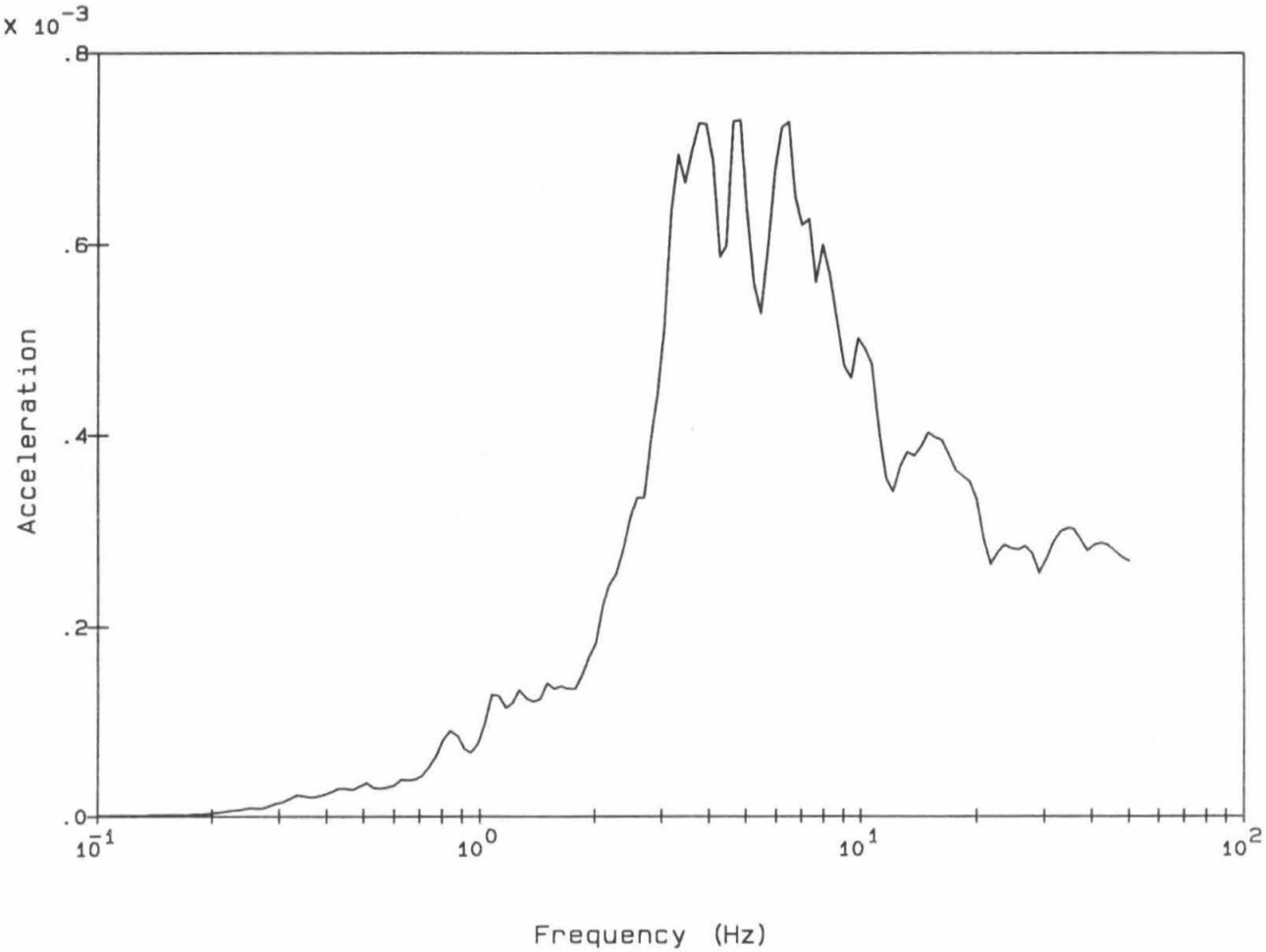

Notes:

ZZ ROTATION

Acceleration in g/ft

Spectra calculated at 5% damping

Figure 4-6: Ground Spectrum at Foundation Reference Point, Rotation About the Vertical Axis, Morgan Hill Earthquake

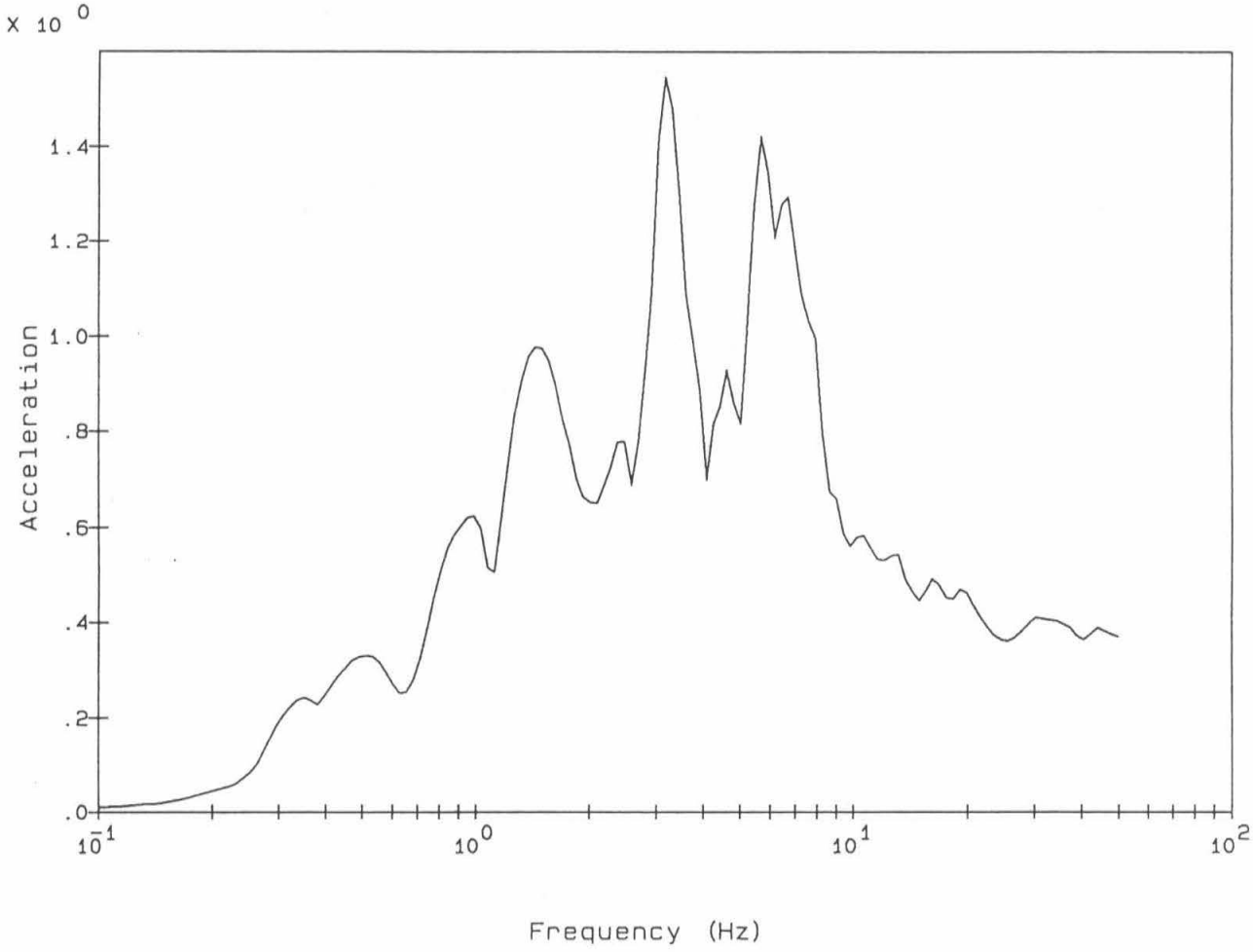

Notes:

X TRANSLATION

Acceleration (g)

Spectra calculated at 5% damping

Figure 4-7: Ground Spectrum at Foundation Reference Point, E-W Translation, Loma Prieta Earthquake

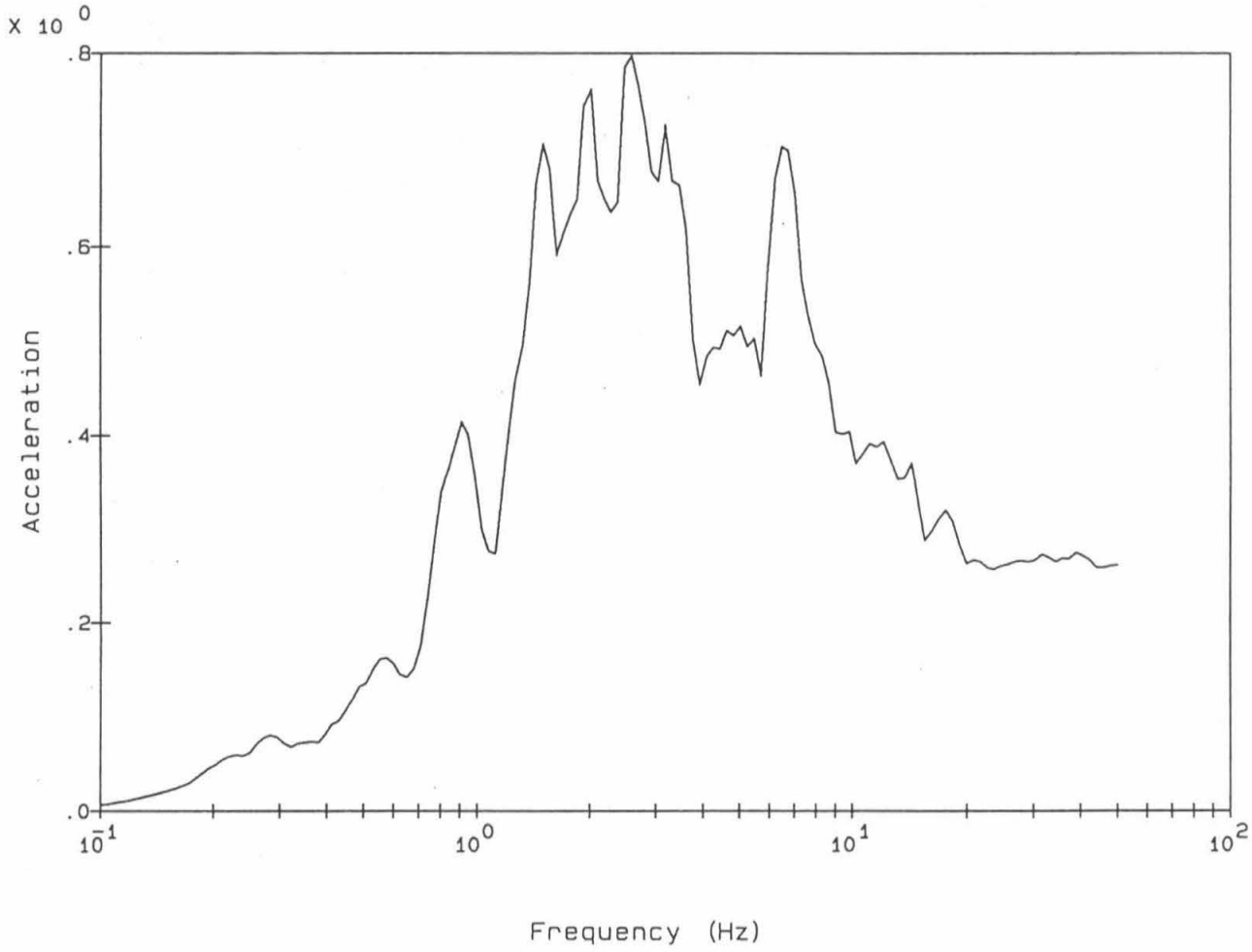

Notes:

Y TRANSLATION
Acceleration (g)
Spectra calculated at 5% damping

Figure 4-8: Ground Spectrum at Foundation Reference Point, N-S Translation, Loma Prieta Earthquake

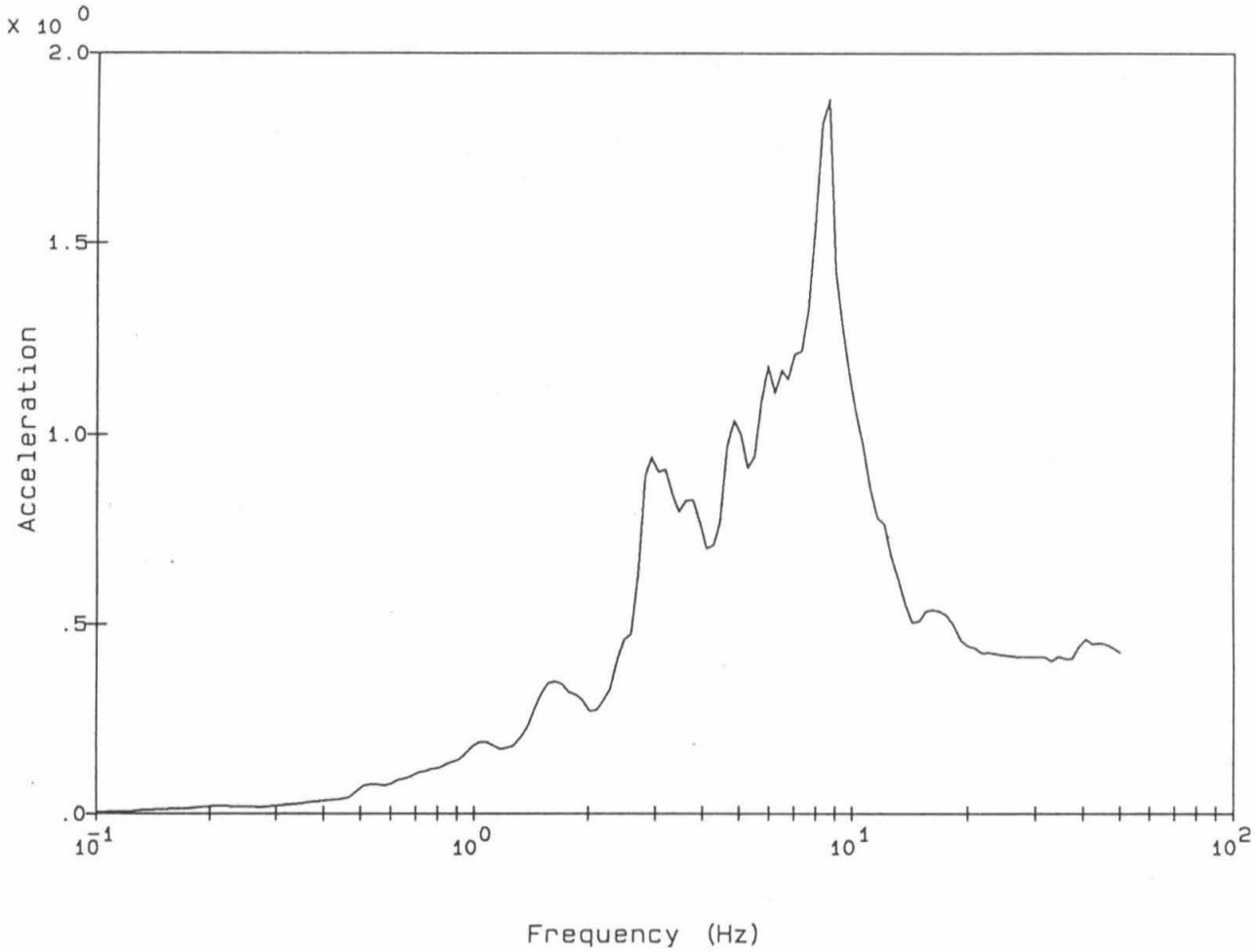

Notes:

Z TRANSLATION

Acceleration (g)

Spectra calculated at 5% damping

Figure 4-9: Ground Spectrum at Foundation Reference Point, Vertical Translation, Loma Prieta Earthquake

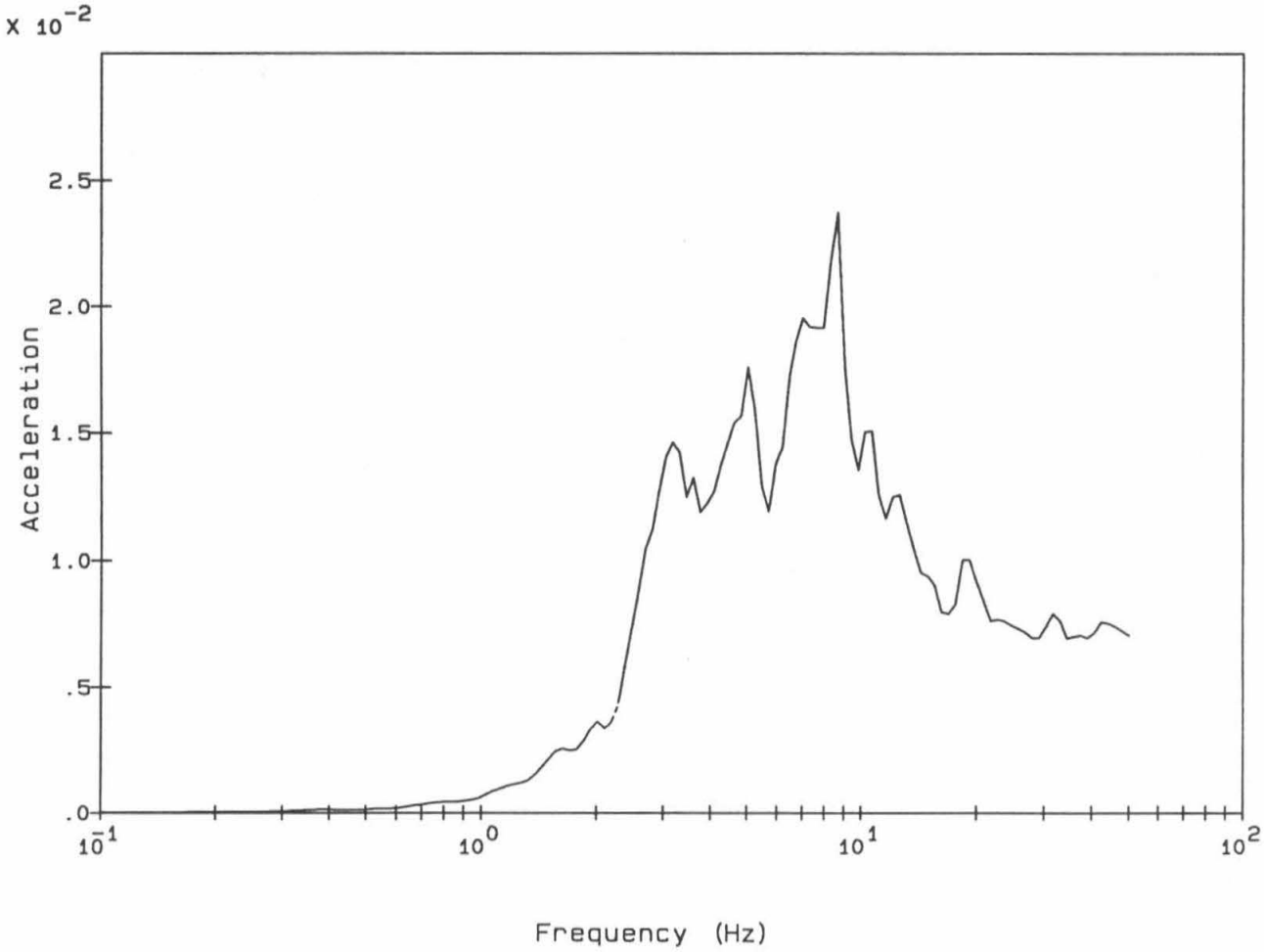

Notes:

XX ROTATION

Acceleration in g/ft

Spectra calculated at 5% damping

Figure 4-10: Ground Spectrum at Foundation Reference Point, Rotation About the E-W Axis, Loma Prieta Earthquake

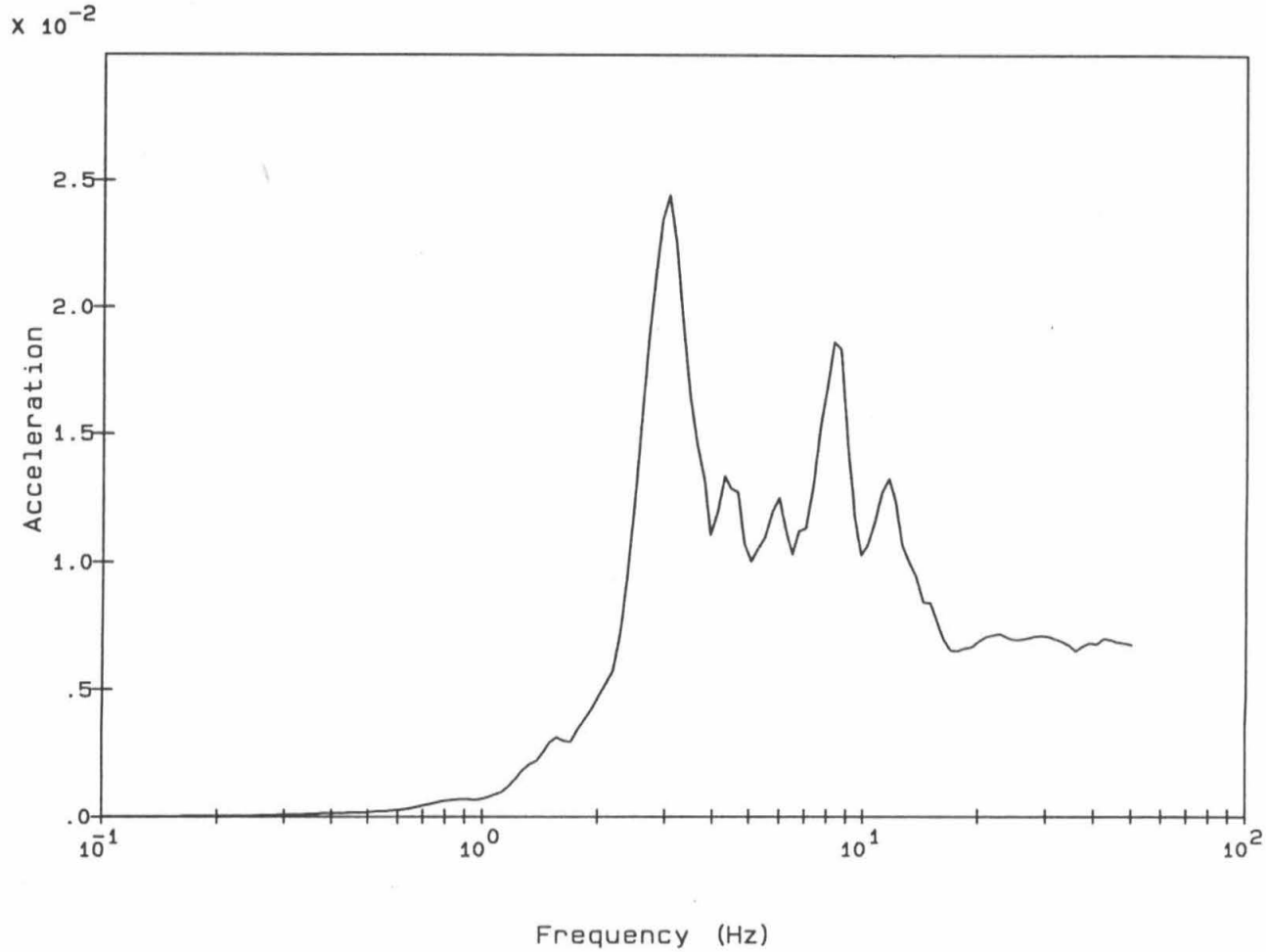

Notes:

YY ROTATION

Acceleration in g/ft

Spectra calculated at 5% damping

Figure 4-11: Ground Spectrum at Foundation Reference Point, Rotation About the N-S Axis, Loma Prieta Earthquake

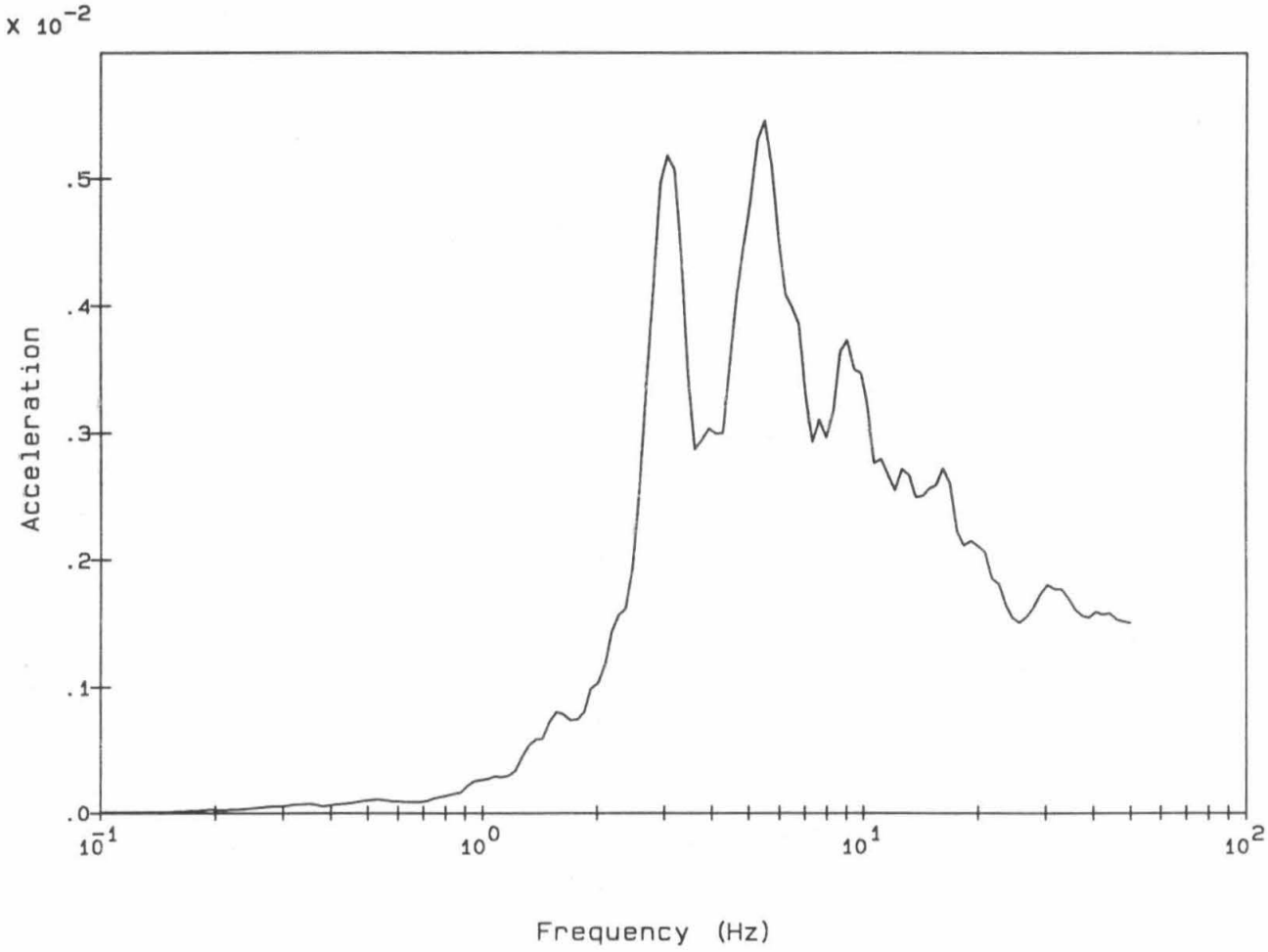

Notes:

ZZ ROTATION

Acceleration in g/ft

Spectra calculated at 5% damping

Figure 4-12: Ground Spectrum at Foundation Reference Point, Rotation About the Vertical Axis, Loma Prieta Earthquake

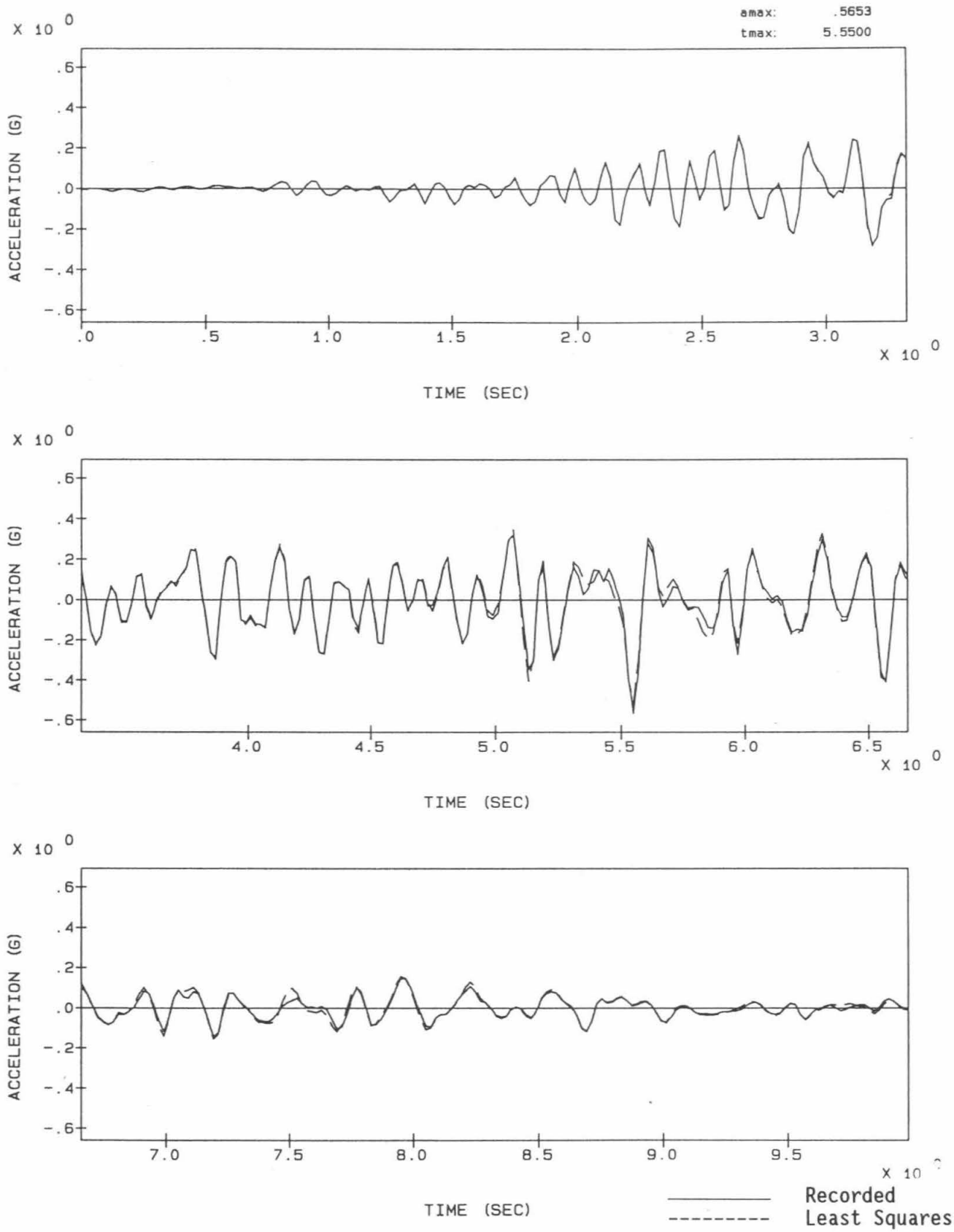

Figure 4-13: Comparison of Calculated and Recorded Vertical Acceleration Time-History at Channel 1, Loma Prieta Earthquake

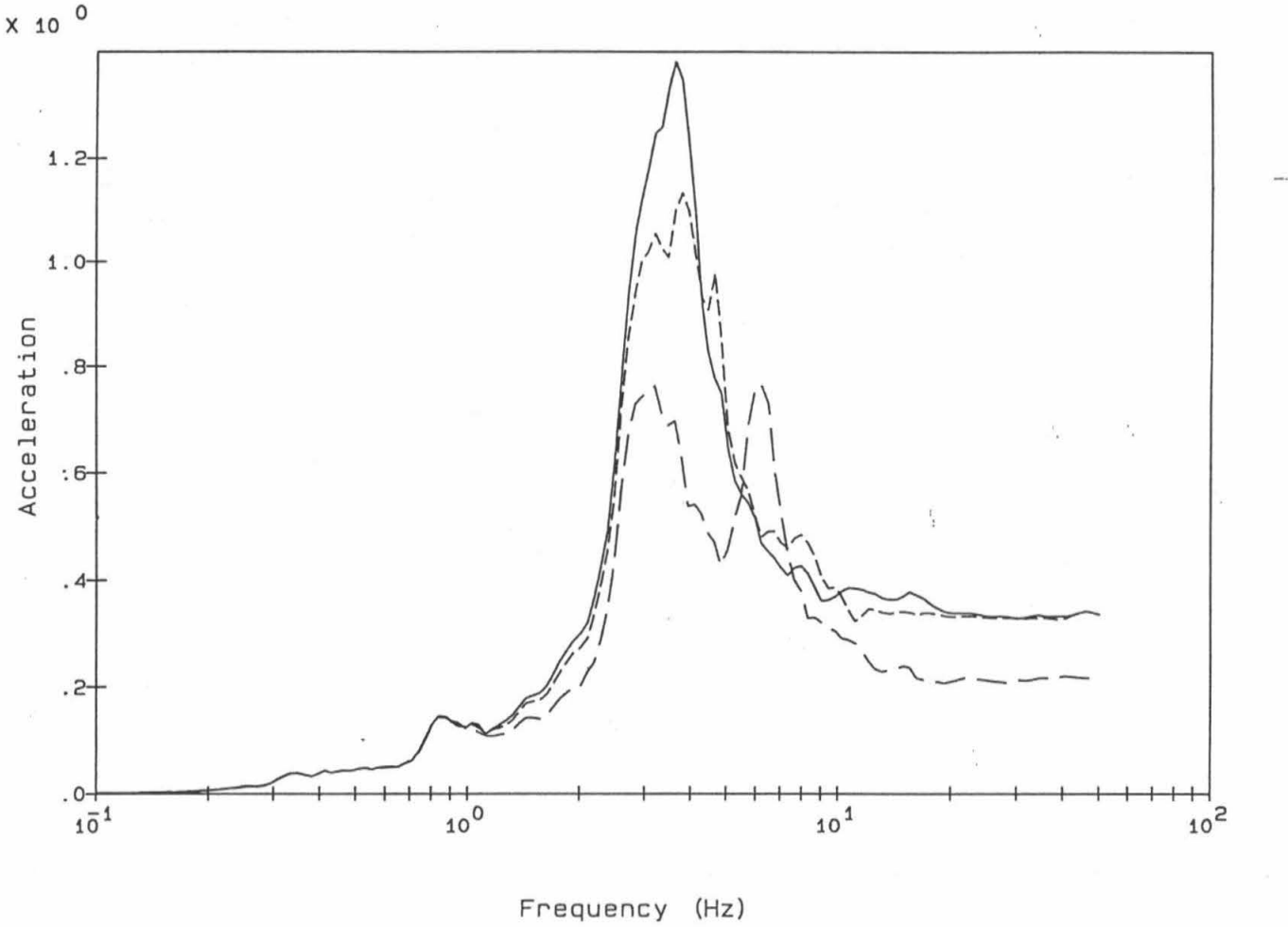

Figure 4-14: Comparison of Floor Response Spectra at Channel 11, Roof, E-W Direction, Morgan Hill Earthquake

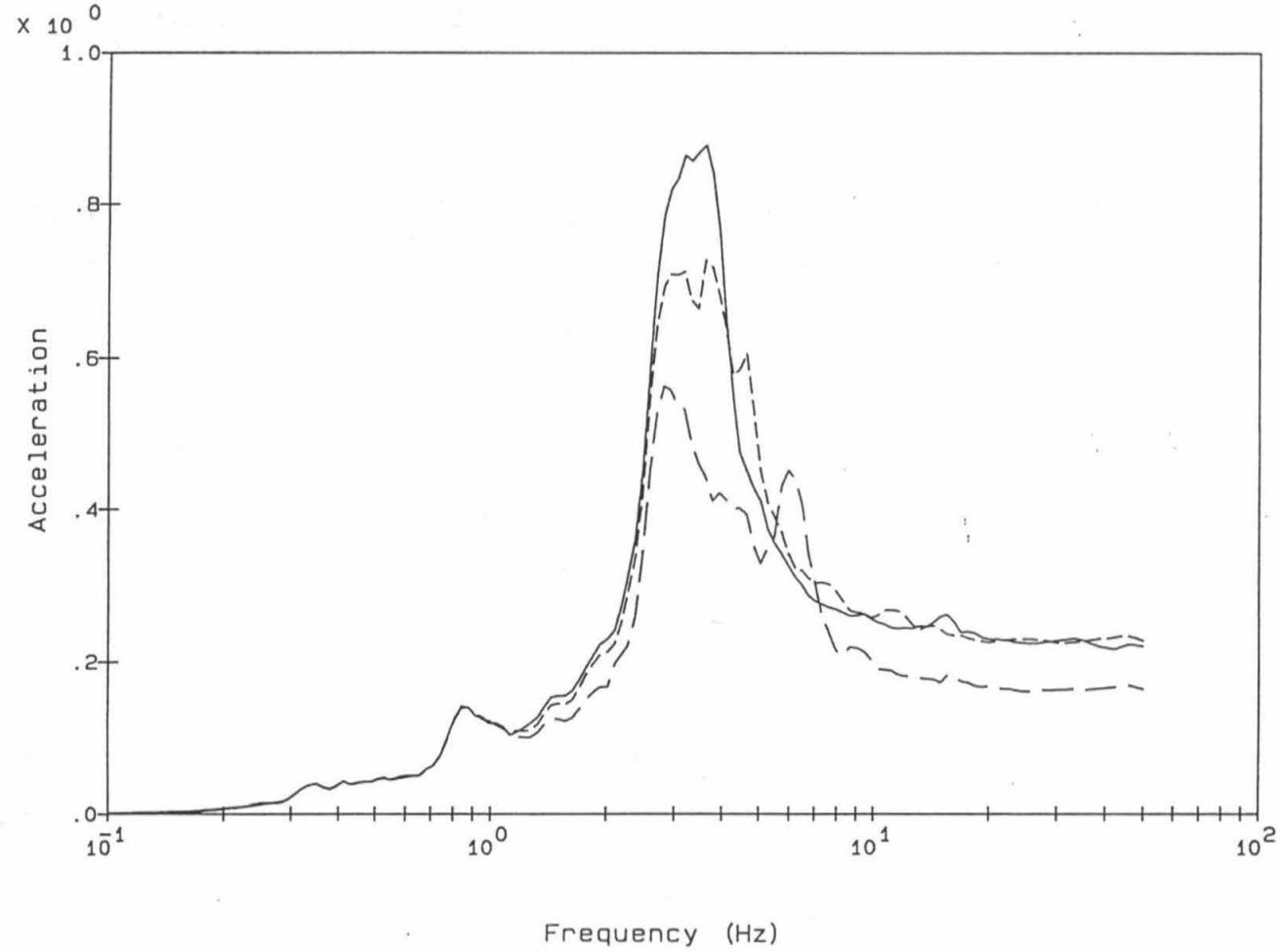

Figure 4-15: Comparison of Floor Response Spectra at Channel 12, Third Floor, E-W Direction, Morgan Hill Earthquake

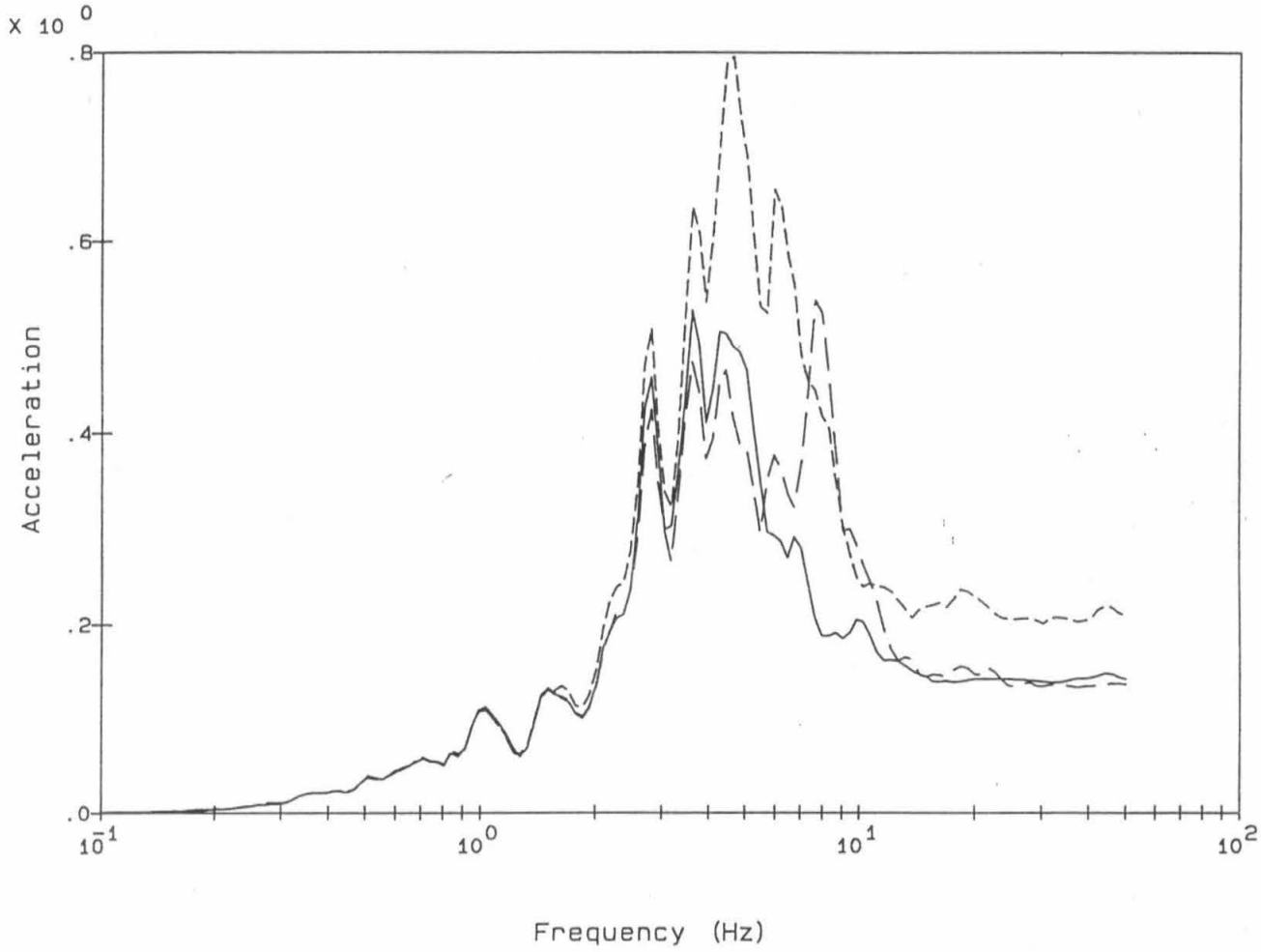

Figure 4-16: Comparison of Floor Response Spectra at Channel 5, Roof, N-S Direction, Morgan Hill Earthquake

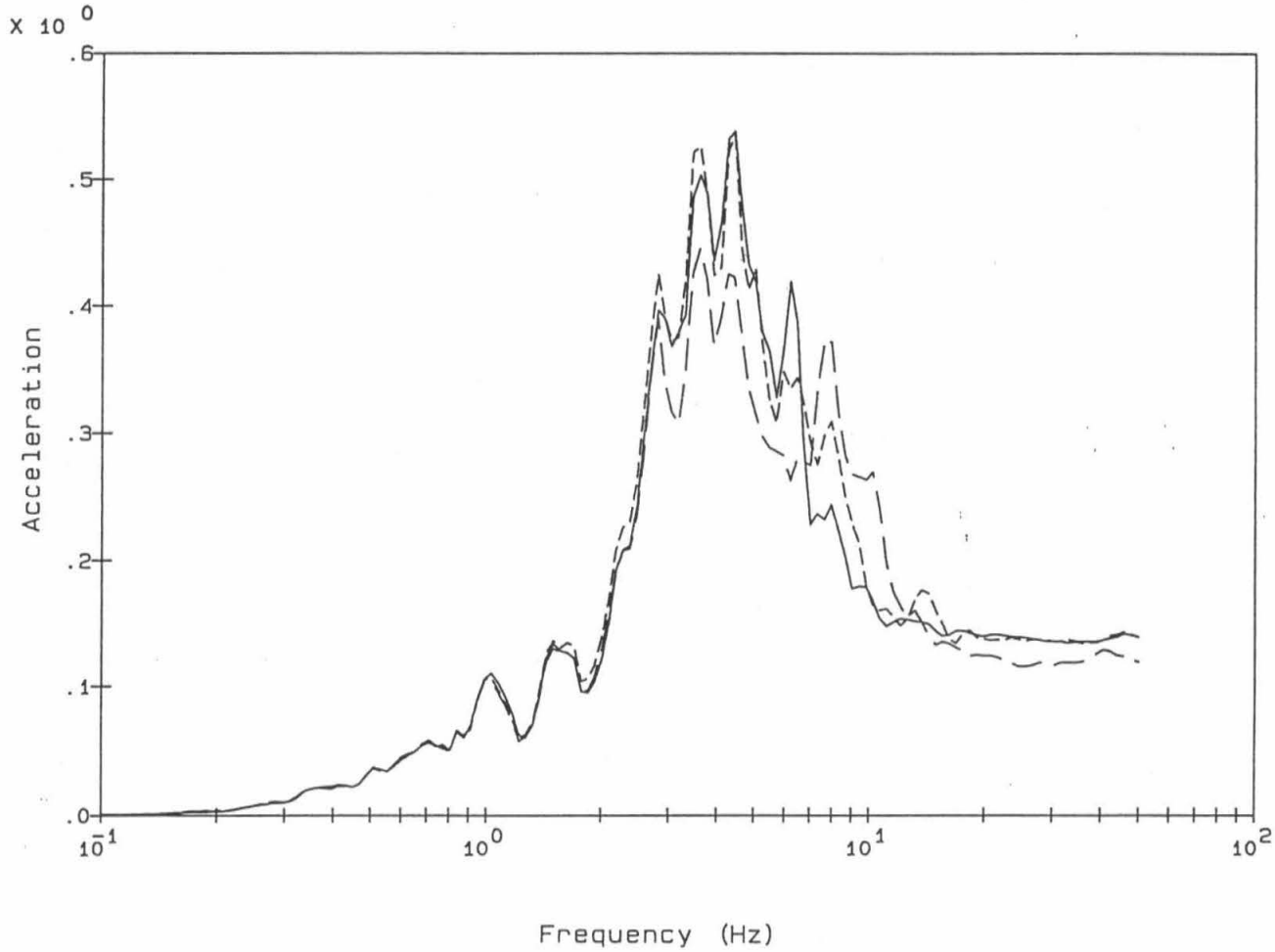

Figure 4-17: Comparison of Floor Response Spectra at Channel 6, Roof, N-S Direction, Morgan Hill Earthquake

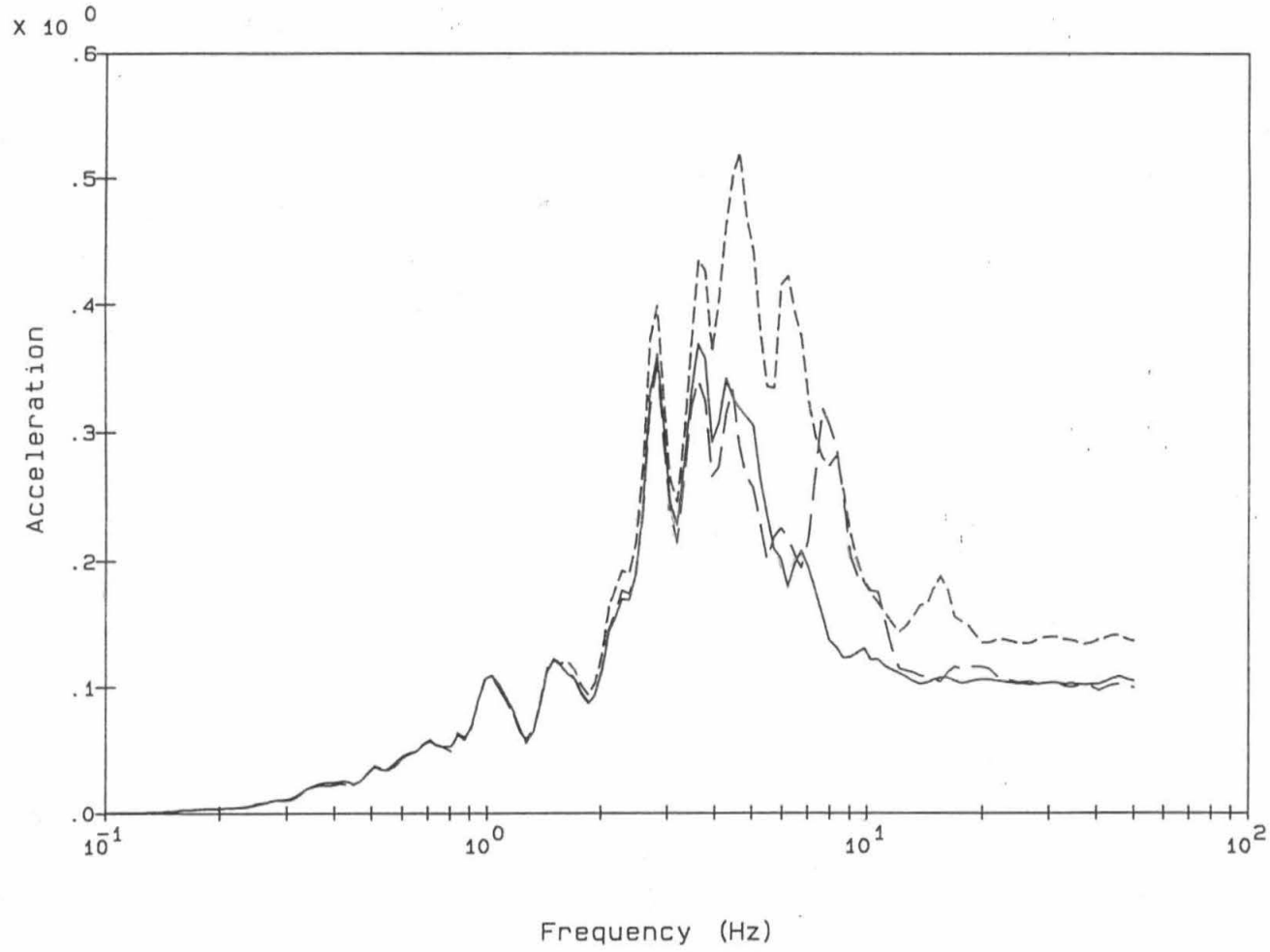

Figure 4-18: Comparison of Floor Response Spectra at Channel 7, Third Floor, N-S Direction, Morgan Hill Earthquake

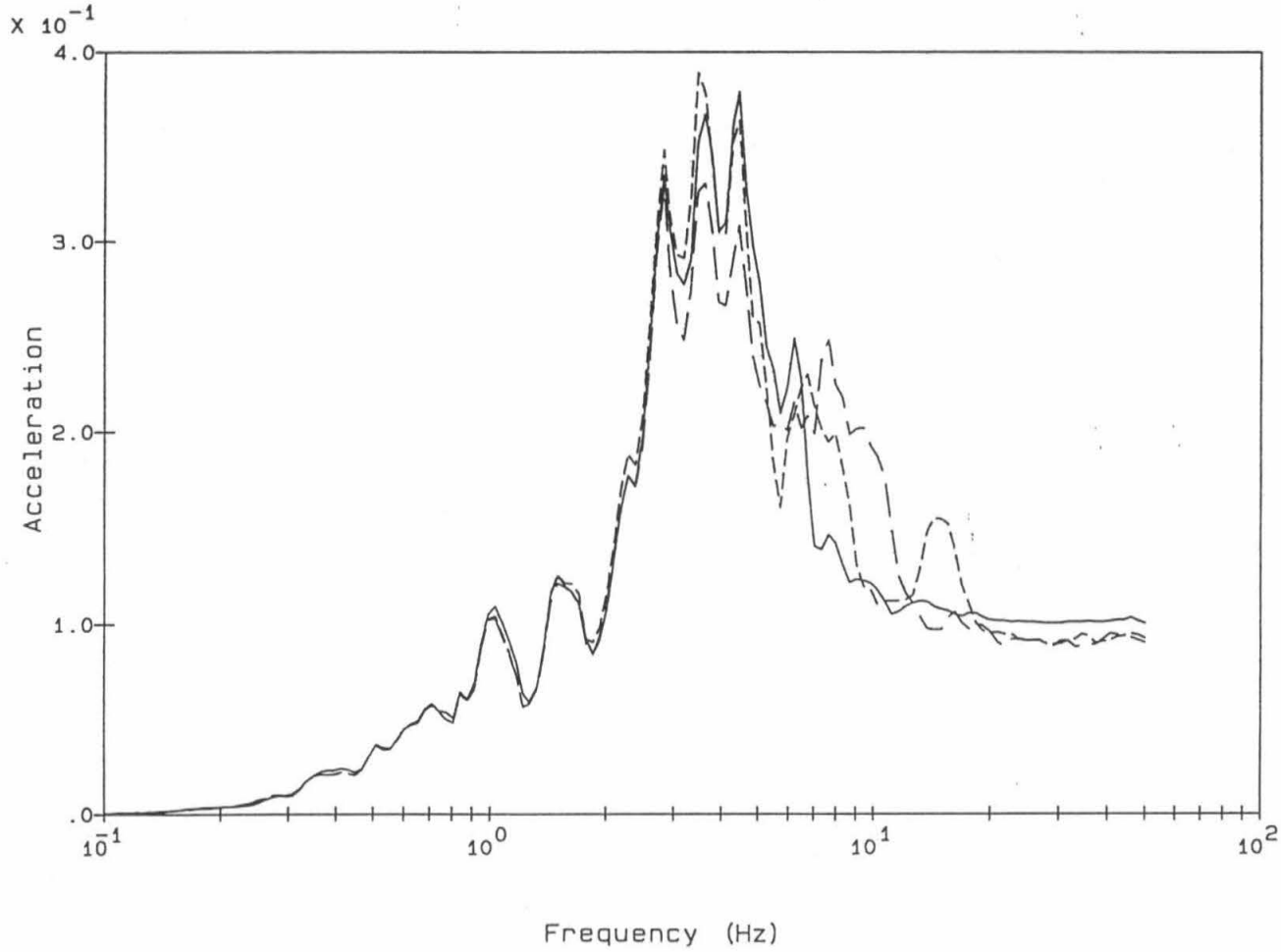

Figure 4-19: Comparison of Floor Response Spectra at Channel 8, Third Floor, N-S Direction, Morgan Hill Earthquake

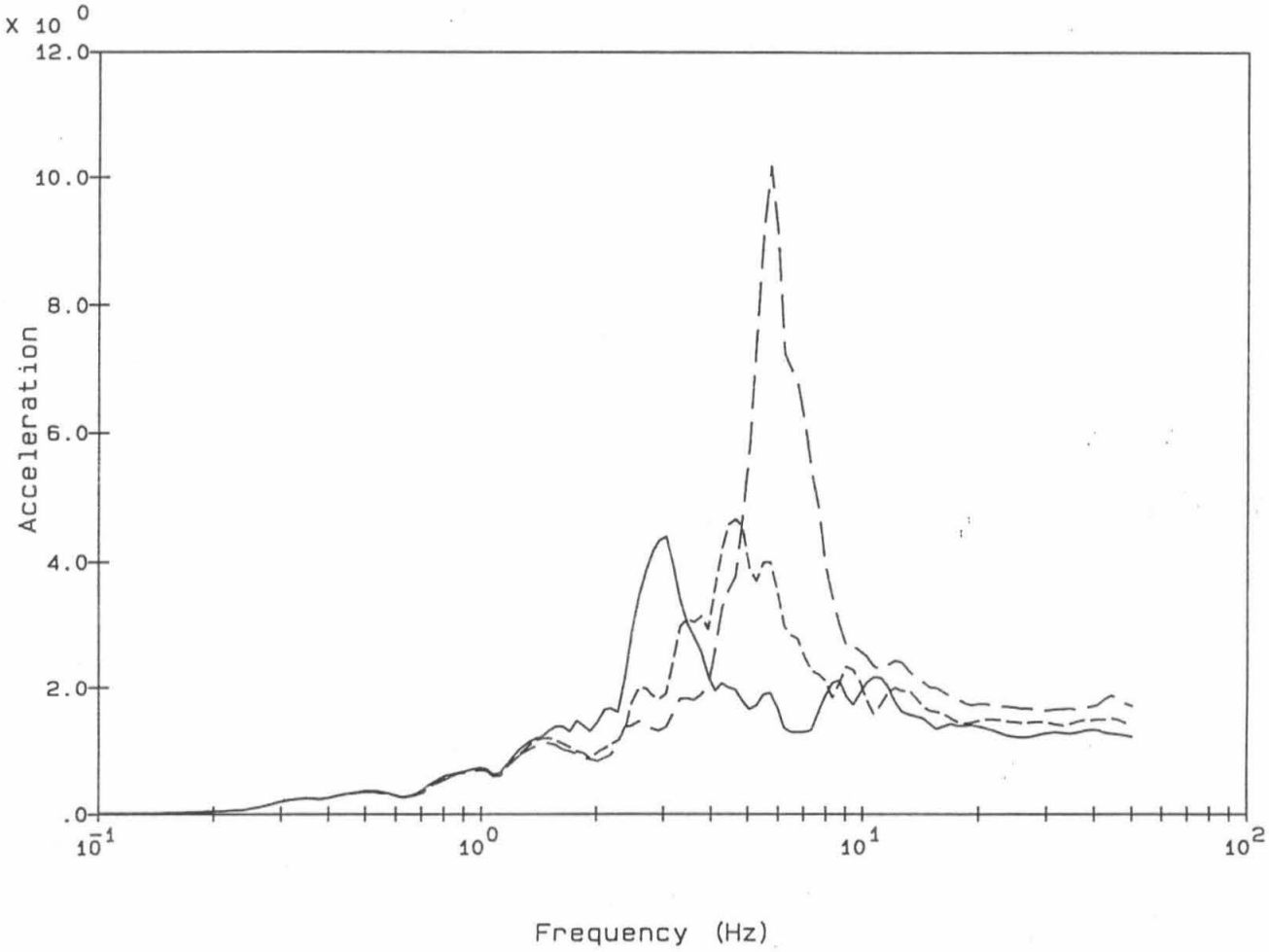

Figure 4-20: Comparison of Floor Response Spectra at Channel 11, Roof, E-W Direction, 7% Structure Damping, Loma Prieta Earthquake

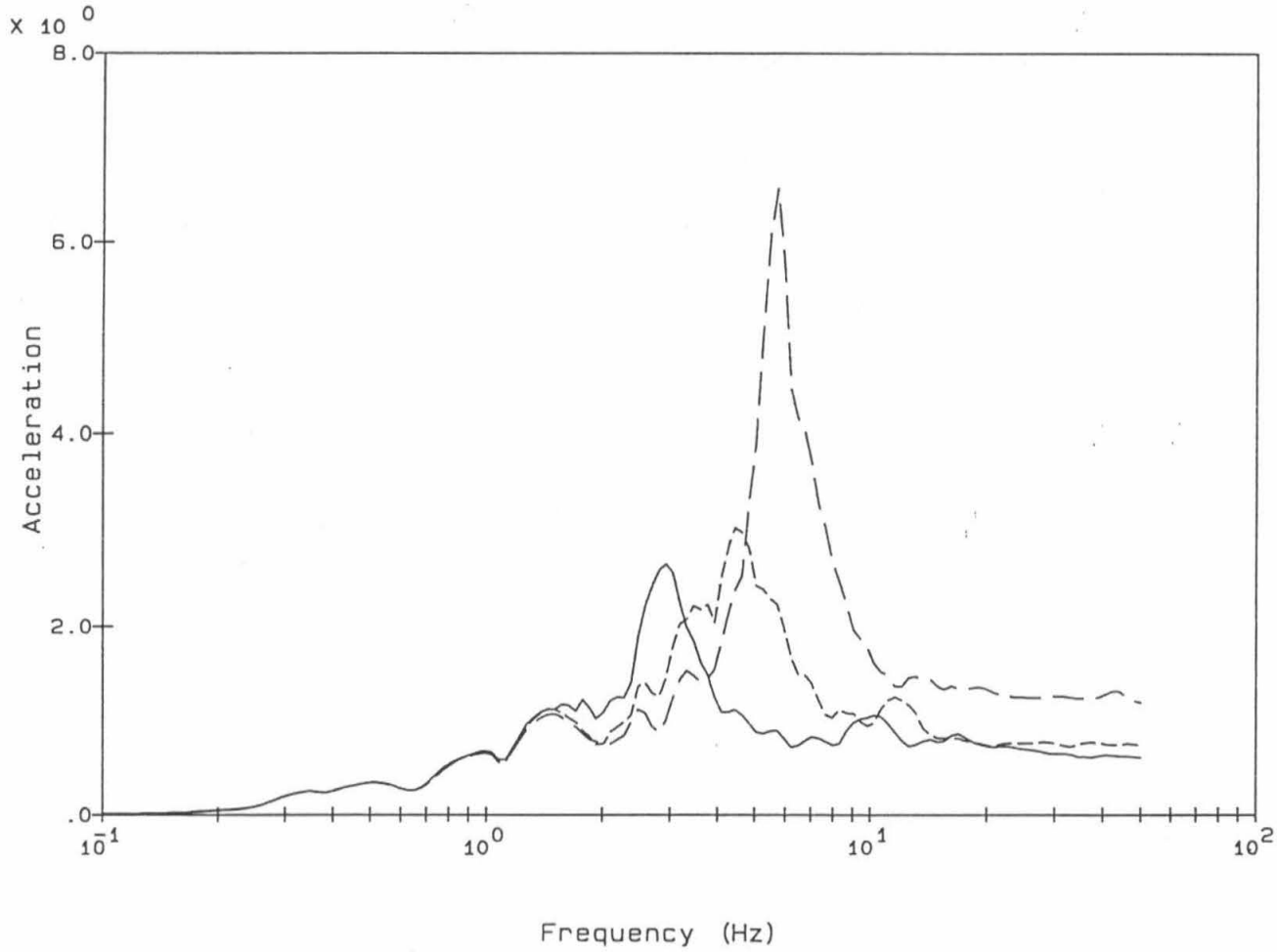

Legend:

Channel 12 Rec.

Model 2

Model 3

Notes:

Acceleration (g)

Spectra calculated at 5% damping

Figure 4-21: Comparison of Floor Response Spectra at Channel 12, Third Floor, E-W Direction, 7% Structure Damping, Loma Prieta Earthquake

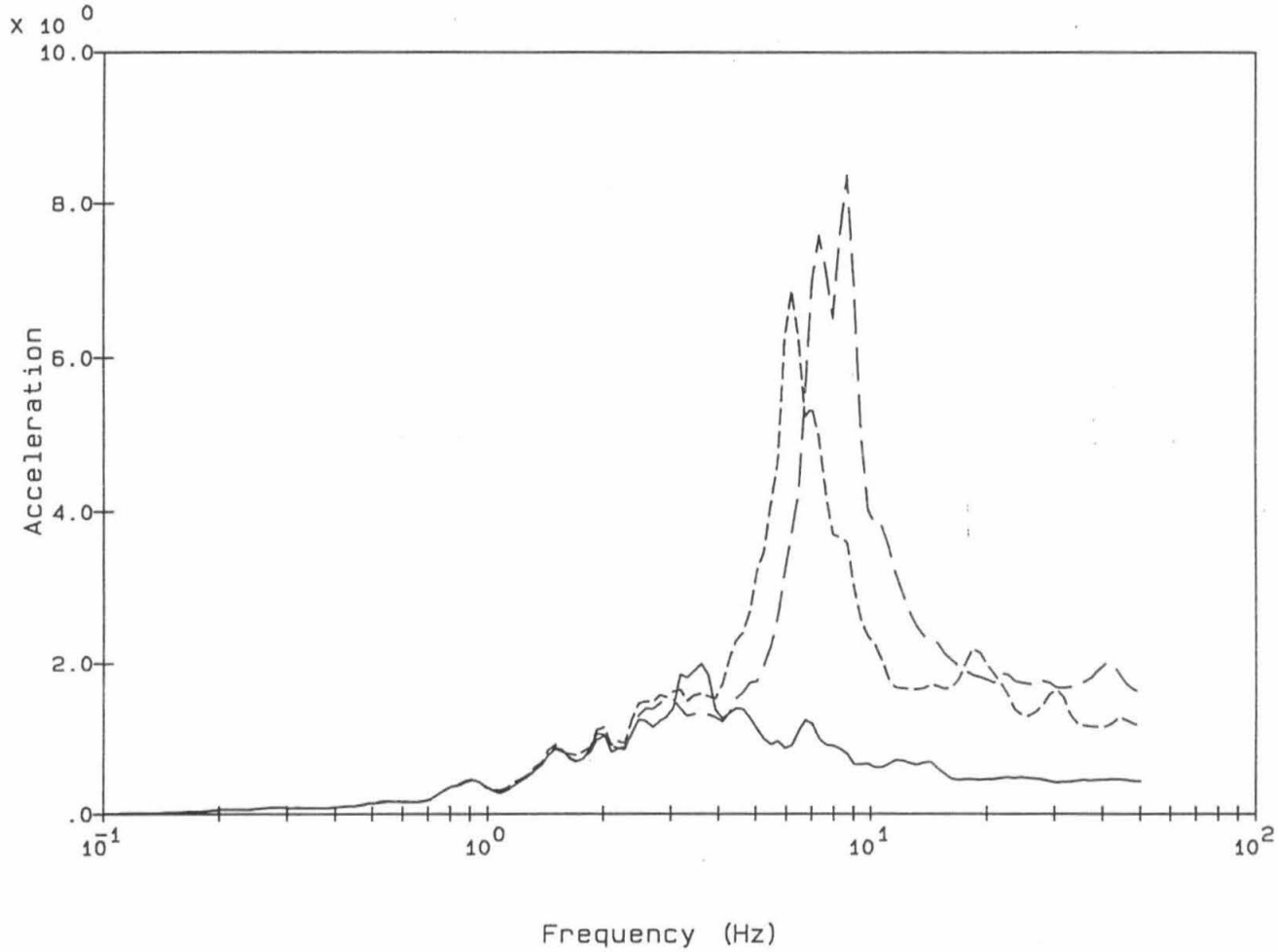

Figure 4-22: Comparison of Floor Response Spectra at Channel 5, Roof, N-S Direction, 7% Structure Damping, Loma Prieta Earthquake

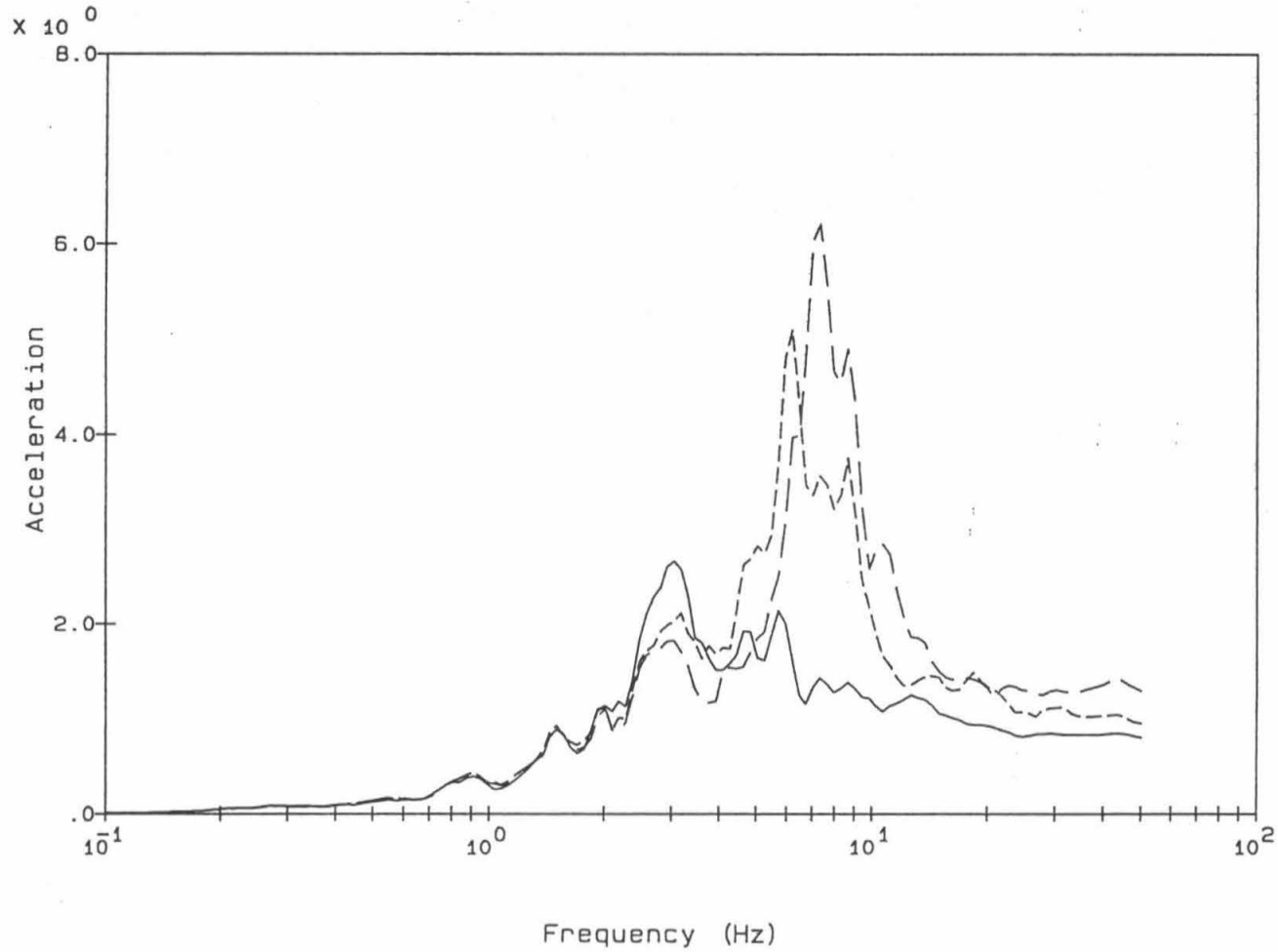

Legend:

Channel 6 Rec.

Model 2

Model 3

Notes:

Acceleration (g)

Spectra calculated at 5% damping

Figure 4-23: Comparison of Floor Response Spectra at Channel 6, Roof, N-S Direction, 7% Structure Damping, Loma Prieta Earthquake

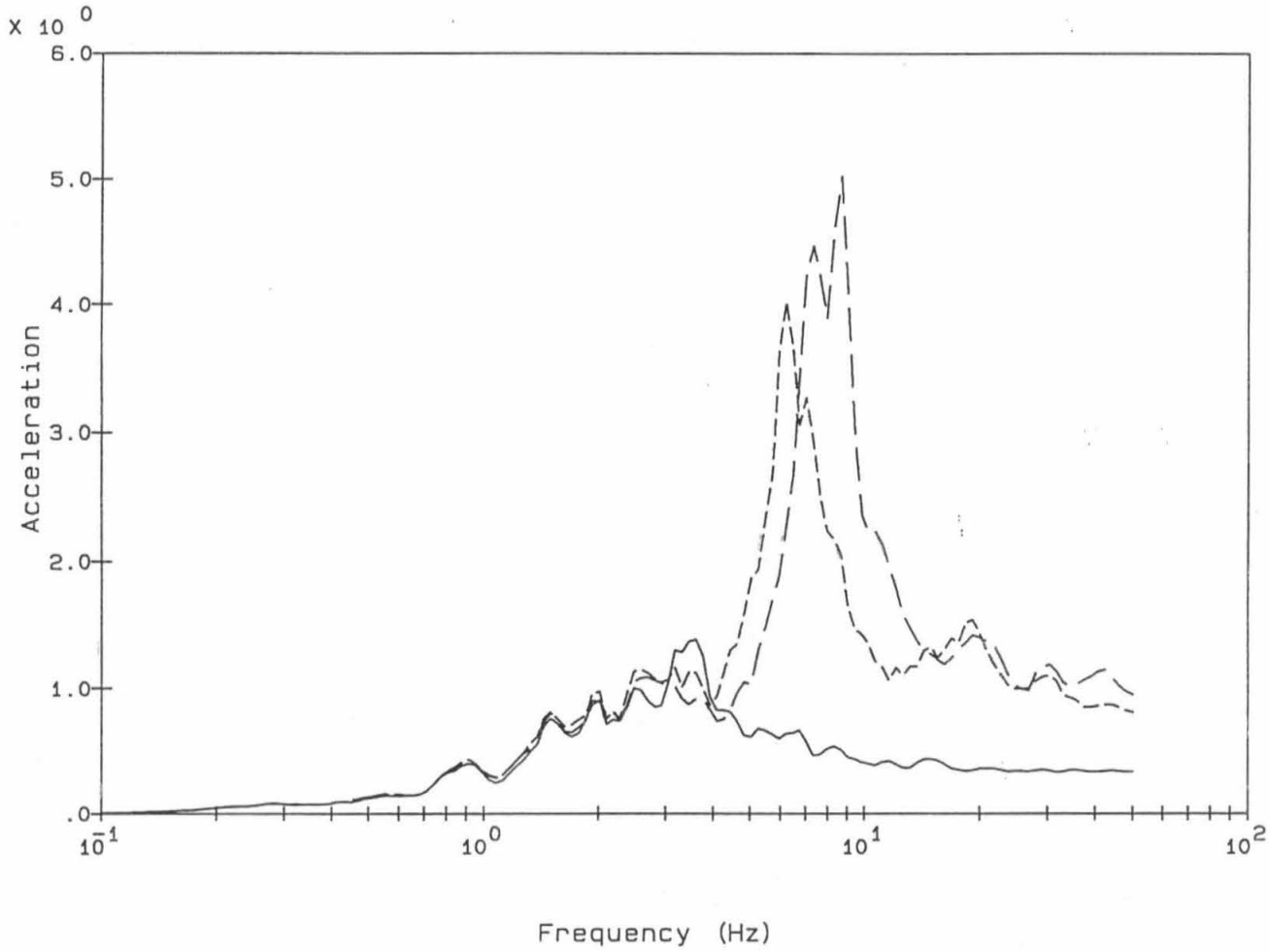

Figure 4-24: Comparison of Floor Response Spectra at Channel 7, Third Floor, N-S Direction, 7% Structure Damping, Loma Prieta Earthquake

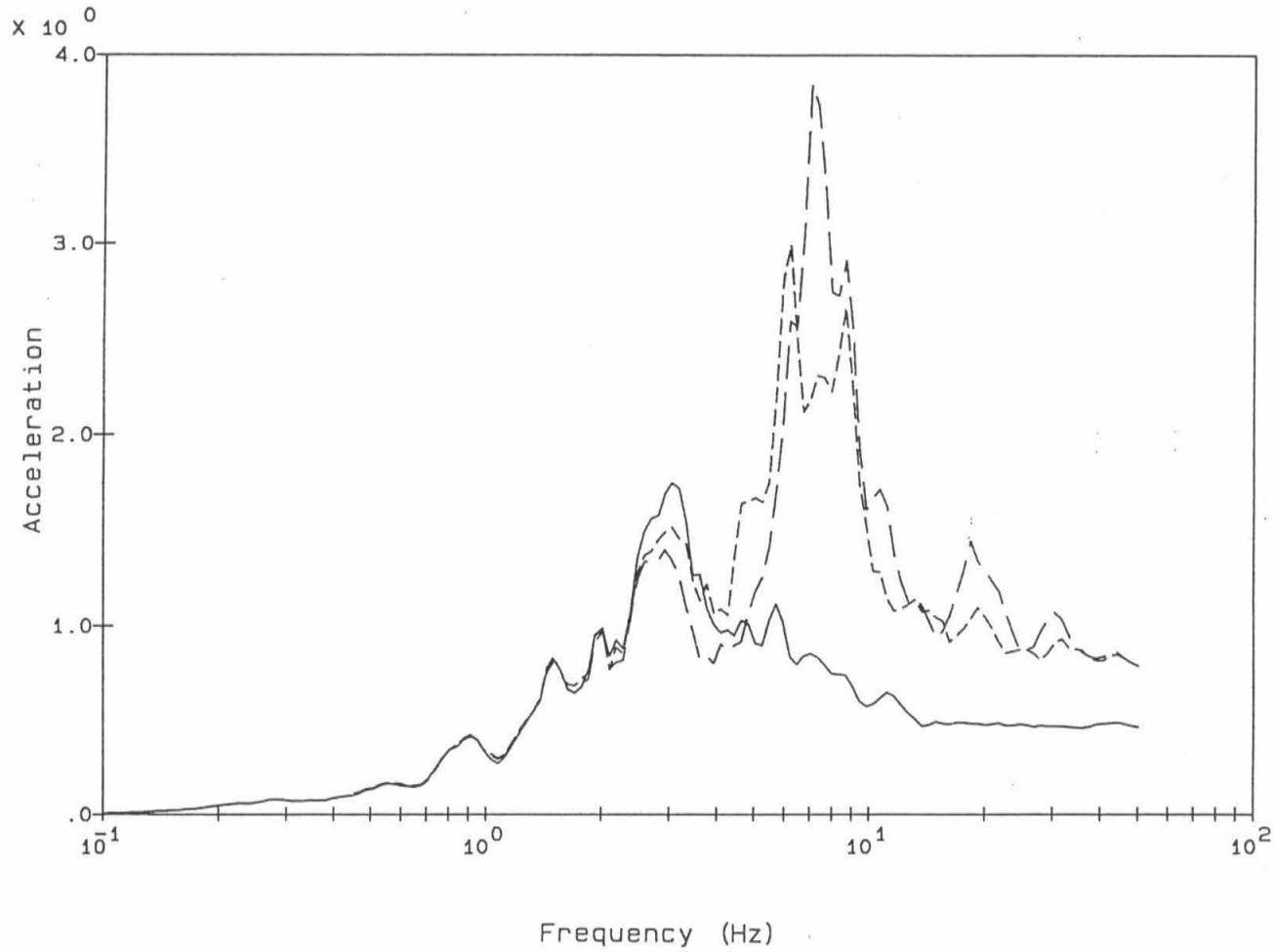

Figure 4-25: Comparison of Floor Response Spectra at Channel 8, Third Floor, N-S Direction, 7% Structure Damping, Loma Prieta Earthquake

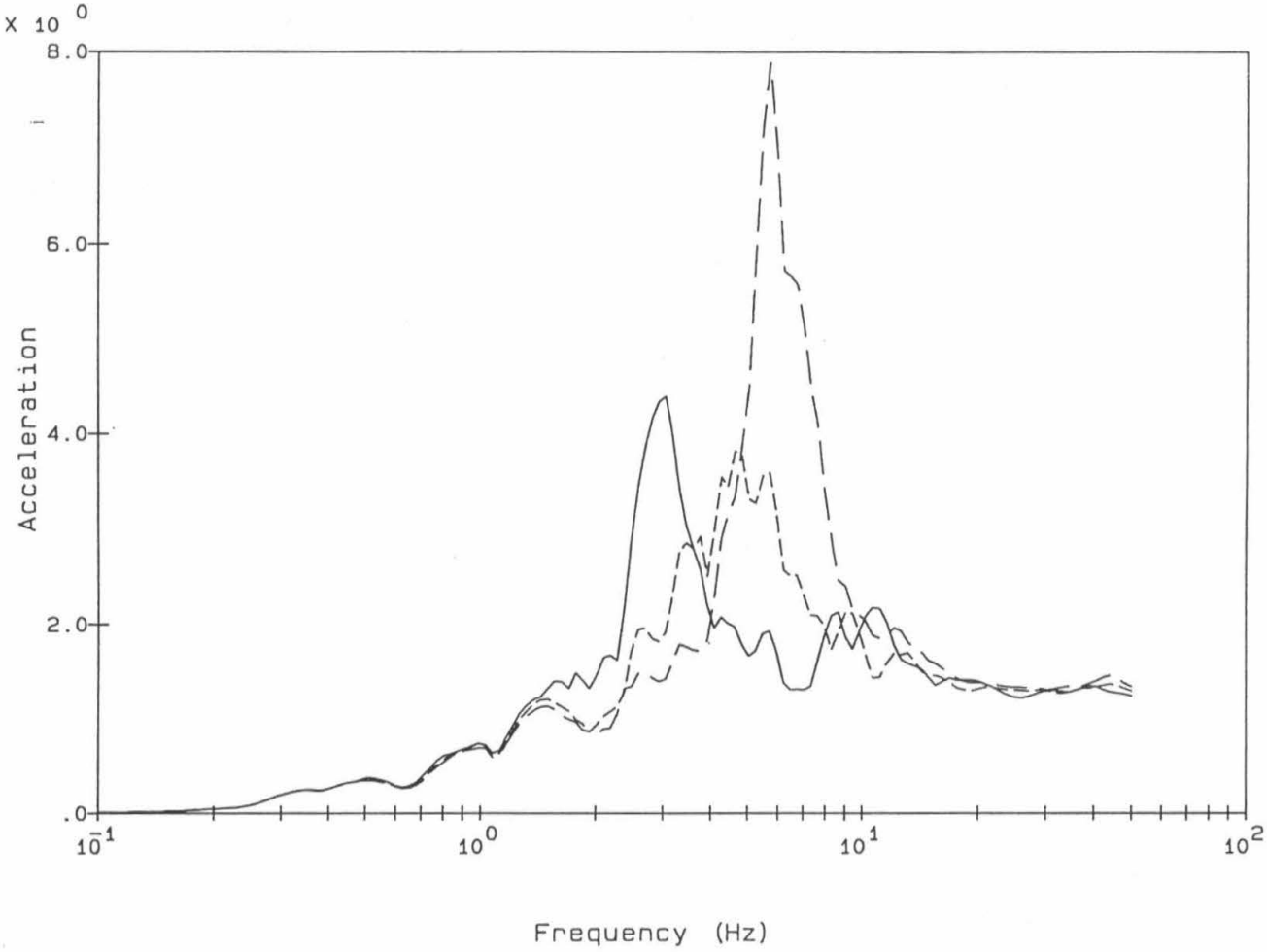

Figure 4-26: Comparison of Floor Response Spectra at Channel 11, Roof, E-W Direction, 10% Structure Damping, Loma Prieta Earthquake

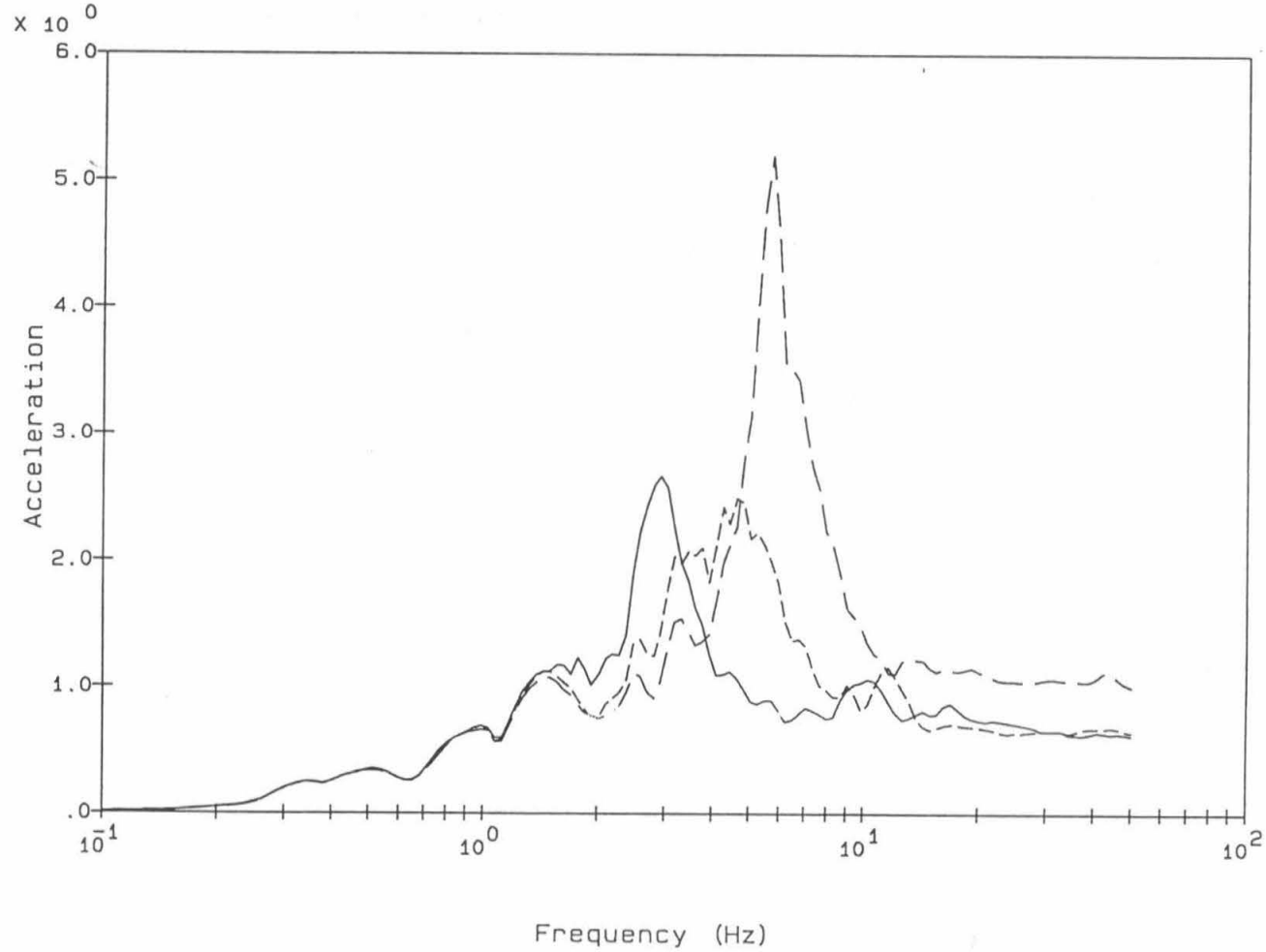

Figure 4-27: Comparison of Floor Response Spectra at Channel 12, Third Floor, E-W Direction, 10% Structure Damping, Loma Prieta Earthquake

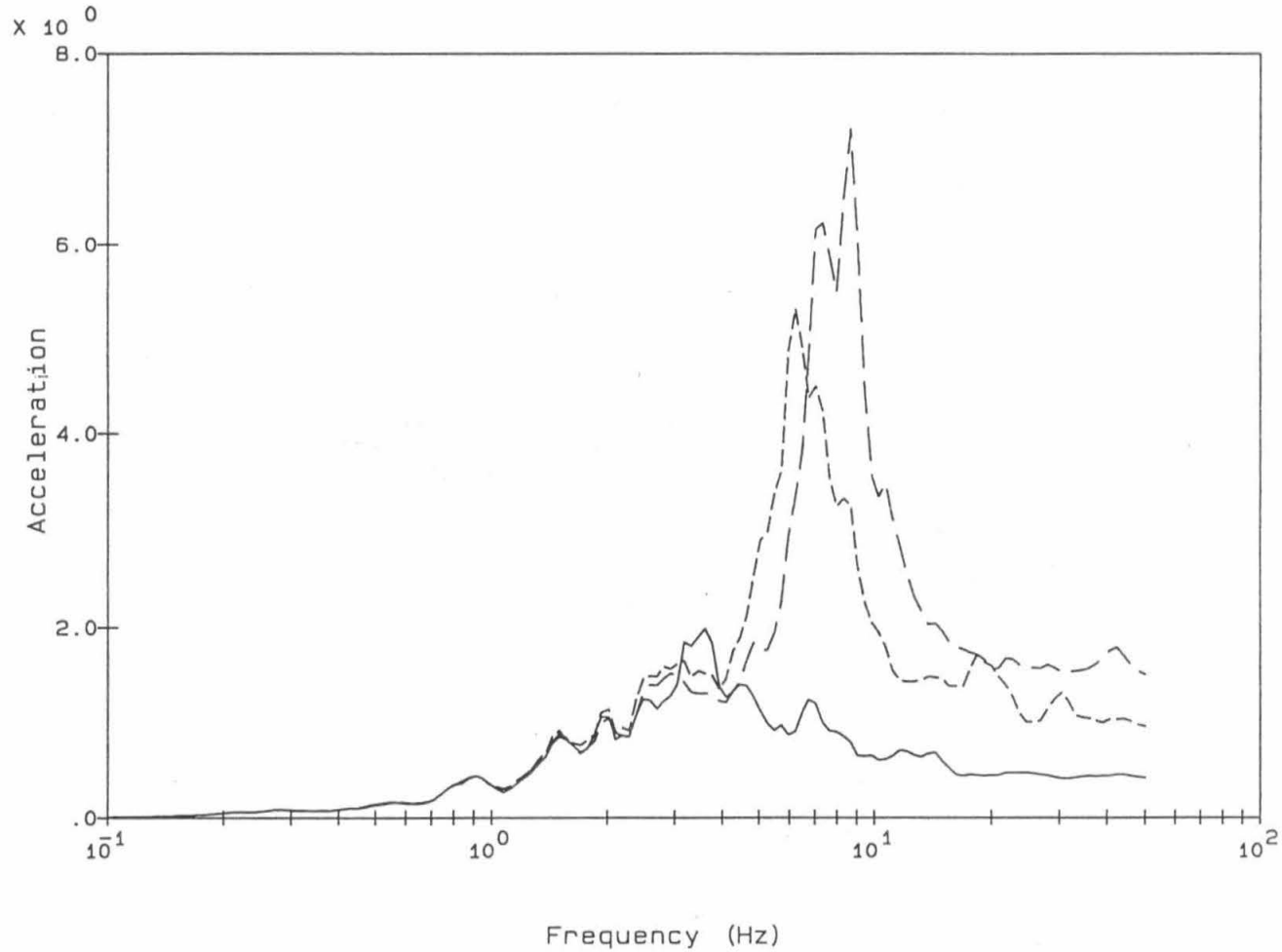

Figure 4-28: Comparison of Floor Response Spectra at Channel 5, Roof, N-S Direction, 10% Structure Damping, Loma Prieta Earthquake

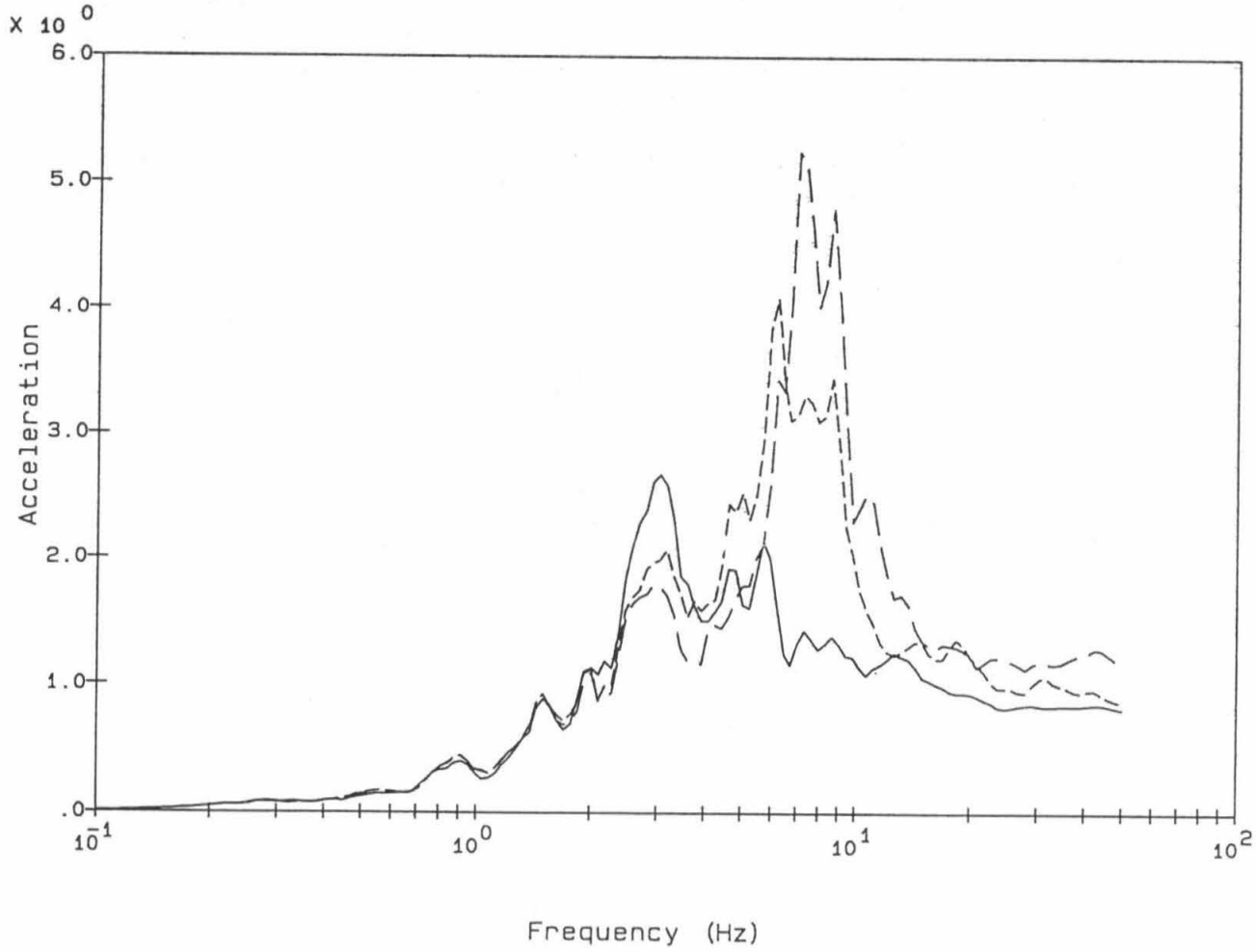

Figure 4-29: Comparison of Floor Response Spectra at Channel 6, Roof, N-S Direction, 10% Structure Damping, Loma Prieta Earthquake

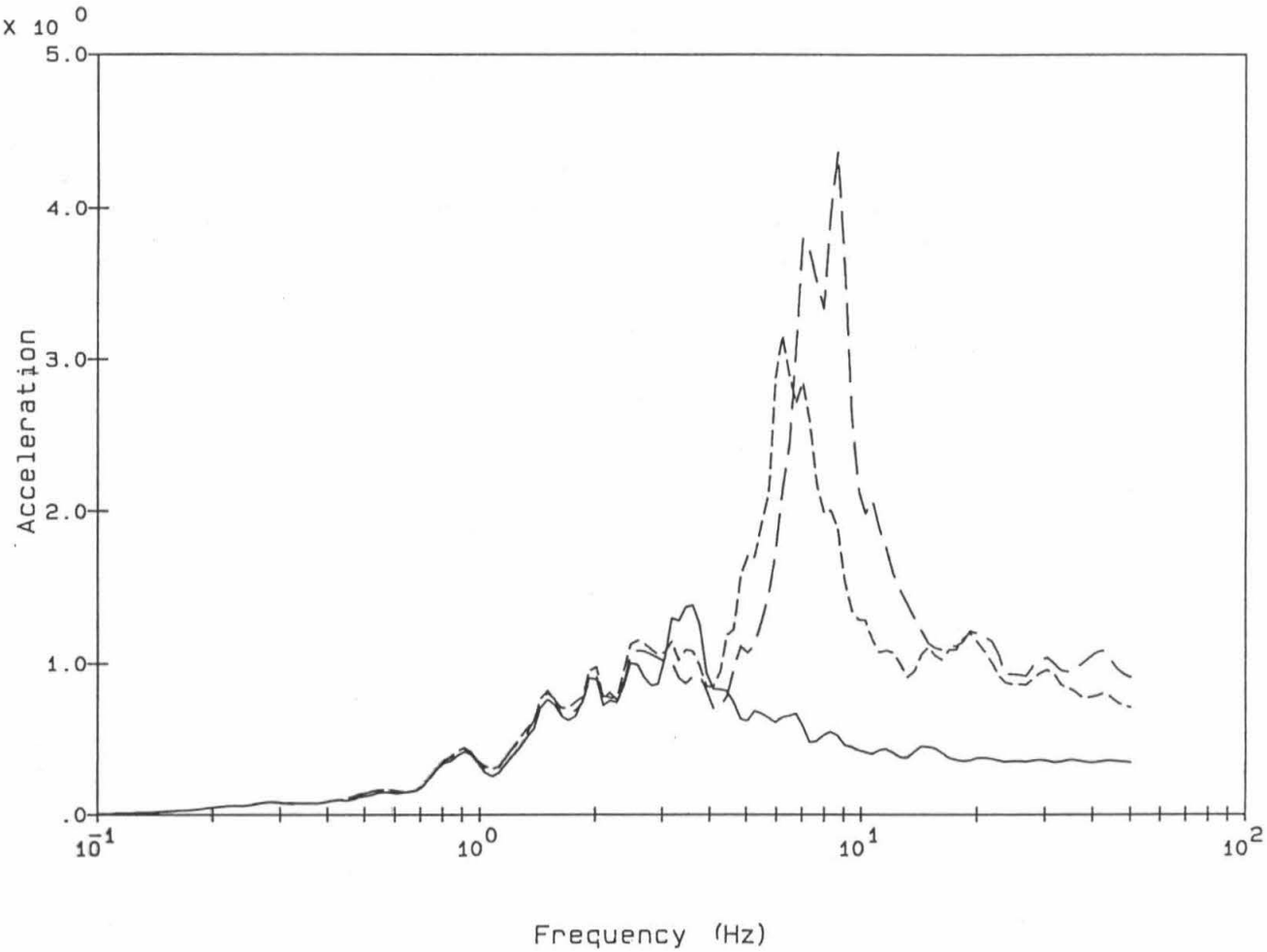

Figure 4-30: Comparison of Floor Response Spectra at Channel 7, Third Floor, N-S Direction, 10% Structure Damping, Loma Prieta Earthquake

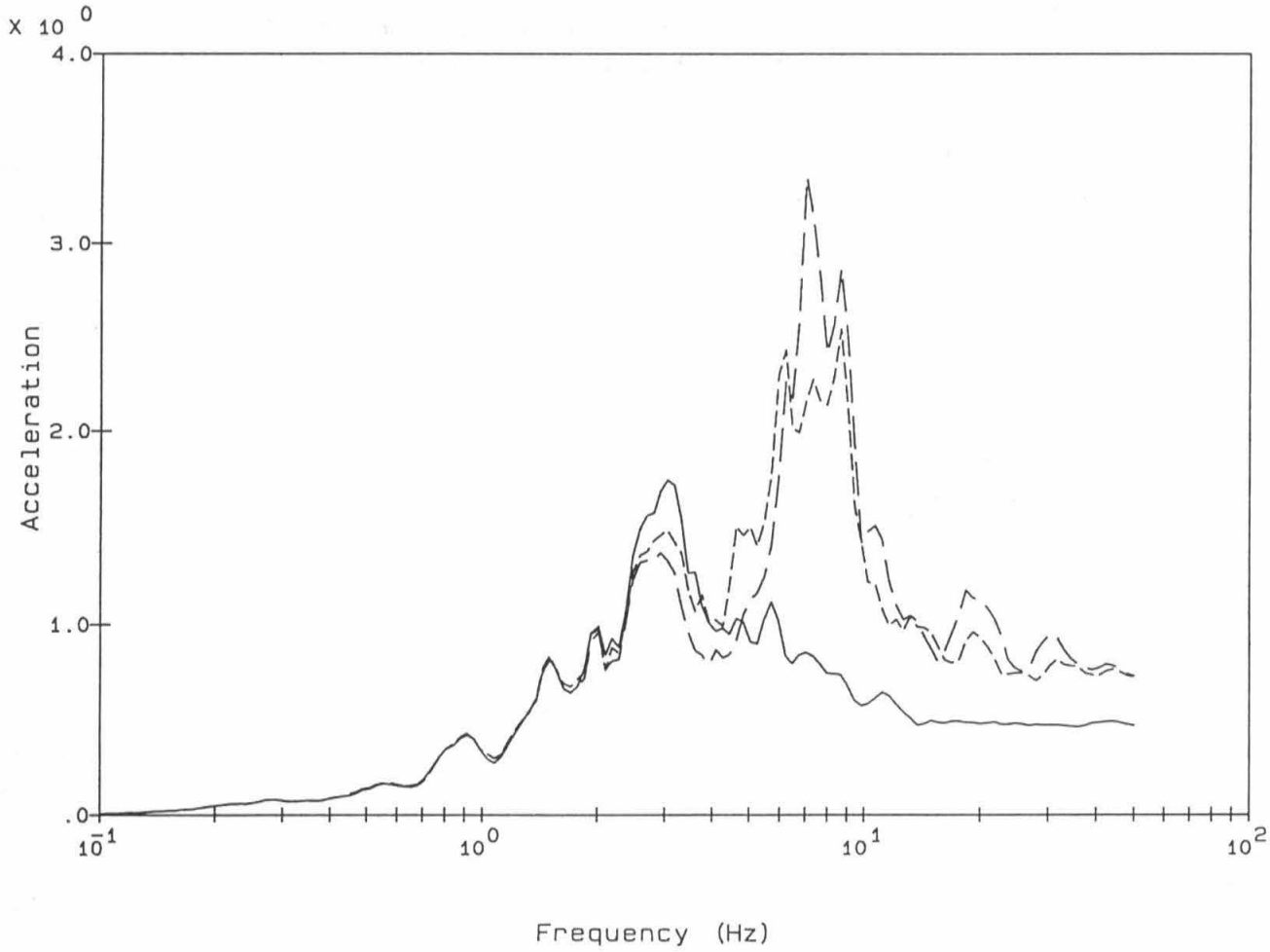

Legend:

Channel 8 Rec.

Model 2

Model 3

Notes:

Acceleration (g)

Spectra calculated at 5% damping

Figure 4-31: Comparison of Floor Response Spectra at Channel 8, Third Floor, N-S Direction, 10% Structure Damping, Loma Prieta Earthquake

5. ELASTIC ANALYSIS TO MATCH RECORDED RESPONSES

These analyses were performed in an attempt to obtain best fits between the analytically calculated and actual recorded seismic responses. The results provide specific data on actual structure properties effective during the earthquakes.

5.1 Analytical Approach

The general analytical approach for these analyses consisted of the following steps:

- Adjustment of structure model stiffnesses to match frequencies and mode shapes obtained by modal identification
- Assignment of structure damping obtained by modal identification
- Comparison of analytically calculated and actual recorded responses
- Comparison of applied loads and allowable capacities for selected shear walls

As discussed in Section 4, frequencies and mode shapes of the structure models based on current criteria and guidelines exhibit variations from values obtained by modal identification. These variations are judged to result primarily from differences between the estimated stiffnesses assigned to the structure models and the actual values. Masses included in the structure models are considered to be more accurate than the stiffnesses.

Accordingly, the stiffnesses of the structure were adjusted by trial and error so that the frequencies and mode shapes calculated by the structure model match those obtained by modal identification for the fixed base structure. As noted in Section 3, modal identification is able to determine modal parameters effective during the Morgan Hill earthquake that provide a very accurate fit to the actual recorded seismic responses of the building. Thus, the stiffnesses of the "matching" structure models should be good estimates of the actual values. Modal parameters identified for the Loma Prieta earthquake are more uncertain. Consequently, the estimated stiffnesses are also more uncertain.

The stiffness estimates for the matching structure models are expressed in terms of stiffness ratios. The stiffness ratio is defined as the ratio of the estimated stiffness to the best estimate, uncracked value (i.e., stiffnesses estimated in Model 1). Because mode shape components are provided at the third floor, but not the second floor, the same stiffness ratio was assigned to the stiffness of the lower two stories. Similarly, the upper two stories were assigned the same stiffness ratio. Because the available data do not provide information on the relative

contributions of horizontal translations and global rotations about the horizontal axes to the total structure deformations, the same stiffness ratios were applied to the horizontal translation and rotational stiffnesses contributing to the structure stiffness in a particular direction (i.e., the same factor is applied to the horizontal translational stiffness in the E-W direction and rotational stiffness about the N-S axis).

Modal damping values obtained by modal identification for the fixed base structure were assigned to the fundamental modes in the E-W and N-S directions. Lacking guidance from modal identification, damping values of 4% and 10% were assigned to the higher modes for the Morgan Hill and Loma Prieta earthquakes, respectively. Because response is dominated by the fundamental modes, these higher mode damping values do not have significant impact on the results.

Seismic response analyses were performed, and analytically calculated and actual recorded responses were compared. These responses should ideally be the same. The existence of differences between the calculated and recorded responses may reflect additional biases in the structural model or a lack of accuracy in the modal identification results.

Seismic load distributions were calculated by distributing the overall structure seismic loads from the response analyses to the individual shear walls in proportion to their relative rigidities. Allowable capacities of selected shear walls were determined in accordance with ACI 349 [American Concrete Institute, 1986], which is currently specified for design of concrete structures by the USNRC Standard Review Plan. Demand to capacity ratios (i.e., ratios of applied loads to allowable capacities) provide measures of the extent to which the building was loaded during the earthquakes.

5.2 Response Analysis for the Morgan Hill Earthquake

Two structure models, Models 4 and 4X, were created to match the responses recorded during the Morgan Hill earthquake. These models differ by the extent to which the coupled horizontal translation-torsional rotation behavior obtained in the modal identification is matched. In Model 4, structure story stiffnesses were adjusted to match the horizontal translations in the principal direction of the mode. For the fundamental E-W mode, E-W translations at Channels 11 and 12 were matched. For the fundamental N-S mode, only the average N-S translations of the two channels at each floor were matched (i.e., Channels 5 and 6 at the roof, Channels 7 and 8 at the third floor). In Model 4X, centers of rigidity were also adjusted to better match the "torsional" rotations that accompany the horizontal translations. These center of rigidity adjustments are somewhat artificial, since one source of the observed "torsion" is foundation flexibility, which is not modeled explicitly. While floor response spectra calculated using Model 4X fit the actual recorded spectra slightly better, the improvement in the fit is not significant. Only Model 4 results are discussed further.

5.2.1 Stiffness Ratios

Stiffness ratios applied to the best estimate, uncracked stiffnesses to provide a match to the frequencies and mode shapes obtained by modal identification are listed in Table 5-1. As shown, the stiffness ratios are nearly identical at about 0.4 for both horizontal directions and all stories. The implications of this observation are addressed in more detail in Section 6.

5.2.2 Floor Response Spectra

Comparisons of 5% damped floor response spectra calculated using Model 4 with floor spectra generated from the actual recorded motions are presented in Figures 5-1 to 5-6. As shown in Figures 5-1 and 5-2, the match between the analytically calculated and actual E-W floor spectra is generally good. The calculated E-W peak accelerations slightly exceed the actual recorded values, but the difference is not significant. The calculated peak spectral accelerations exceed the actual values by about 20%

As shown in Figures 5-3 to 5-6, the analytically calculated N-S floor spectra significantly exceed the actual spectra at frequencies of about 3 Hz and greater, where the dynamic structure response begins to dominate over the rigid body contribution. One possible source of this difference may be the effective modal participation factor for the fundamental N-S mode. As presented in Section 3.2.1 and Appendix A, the effective modal participation factor is independent of mode shape scaling, and is an important parameter controlling dynamic response.

Effective modal participation factors associated with horizontal translation input motion obtained by modal identification and Model 4 are compared in Table 5-2. In this table, effective modal participation factors obtained by modal identification for E-W Channels 11 and 12 are based on the fundamental E-W mode participation factor for input Channel 13. Similarly, values for N-S Channels 5 to 8 are based on the sum of fundamental N-S mode participation factors for input Channels 9 and 10. The effective modal participation factors obtained at Channels 11 and 12 for the fundamental E-W mode are very close. This is consistent with the relatively good match between the analytically calculated and recorded E-W floor response spectra. The value of about 1.2 obtained at the roof by modal identification and Model 4 is close to the value of 1.27 for a uniform shear beam. However, significant differences exist between the effective modal participation factors for Channels 5 to 8 for the fundamental N-S mode. Averaging values from the two channels at a floor, it is apparent that the effective participation factors from Model 4 exceed those from modal identification by almost 40%. The average effective participation factor at the roof obtained by Model 4 of 1.28 is almost identical to the value for a uniform shear beam. However, the value of 0.93 obtained by modal identification is unexpectedly less than 1. While not reported here, differences in effective participation factors associated with rotational input motion are even greater, with values from modal identification being only about 20% of those calculated by Model 4.

Overestimation of the N-S structure response by Model 4 appears to stem from differences in effective modal participation factors. The effective modal participation factors calculated by Model 4 are constrained by other model properties, including the masses, which are based upon accurate data, and the stiffnesses, which have been estimated to match the identified frequencies and mode shapes. These properties, along with the modal damping values which are based upon the modal identification results, determine the magnitude of structure seismic response. Because the E-W effective modal participation factors from modal identification and Model 4 are close, the seismic response calculated by Model 4 is close to the recorded motions. However, because of the difference in effective modal participation factor for the given modal damping, the N-S seismic response calculated by Model 4 significantly overestimates the actual recorded responses.

In the modal identification procedure, the frequencies, mode shapes, damping values, and effective modal participation factors are identified parameters free to take on values that provide the best fit between the recorded input and response motions. The effective modal participation factors are not constrained by the mode shapes, in contrast to the structure models.

The overestimation of the response obtained by Model 4, given the identified modal parameters, suggests that either Model 4 or modal identification, or both, do not reflect the true N-S properties of the building. The structure model calculates effective modal participation factors that would meet conventional expectations for this building. However, this model may not be sufficient to adequately represent N-S building response characteristics suggested by the modal identification results. As noted in preceding discussion, this model was derived using various simplifying approximations and assumptions, which may introduce inadvertent bias into the analytical results.

On the other hand, it may be that modal identification underestimates the effective modal participation factor of the fundamental N-S mode. This value is much less than conventional expectations. Also, there is no readily apparent physical reason why it is so much less than the effective modal participation factor of the fundamental E-W mode. An increase in the effective modal participation factor would require an increase in the damping value to obtain the excellent fit to the recorded response from modal identification. However, the identified damping value for the fundamental N-S mode of 12% is already higher than expected.

5.2.3 Capacity Evaluation

Capacity evaluation of the most heavily loaded structural elements was performed to obtain estimates of applied loads to allowable capacities permitted by USNRC Standard Review Plan criteria (demand to capacity ratios). Values greater than 1 would suggest that the structure was overstressed against the design acceptance criteria. Calculated demand to capacity ratios should be considered approximate values due to

various approximations included in the capacity evaluation as well as the seismic response analyses.

Seismic load distributions to the individual shear walls were based on overall structure story loads generated by the response analysis. To account for differences between the analytically calculated and actual recorded responses, the structure loads were scaled by factors based on the ratios of measured and calculated peak structure accelerations. Load distributions to the piers and spandrels of the exterior walls with openings were determined using the previously described detailed finite element models. Seismic loads were combined with non-seismic loads, with load factors of 1 applied to all individual load cases.

Based on a review of the structure seismic load distributions, configuration, and detailing, the following structural elements were selected for capacity evaluation:

- North exterior wall
- East exterior wall
- West exterior wall
- Central E-W interior wall
- Fourth floor diaphragm connection to the east exterior wall at cable ducts
- Second and third floor diaphragm connections to the west exterior wall at duct, stair, and elevator openings

These elements were evaluated for in-plane shear, axial load, and moment based on allowable capacities permitted by ACI 349 [American Concrete Institute, 1986] acceptance criteria. A maximum demand to capacity ratio for structural elements resisting E-W seismic load of about 0.75 was estimated for one of the first story piers of the central E-W interior wall subjected to in-plane shear. A maximum demand to capacity ratio for structural elements resisting N-S seismic load of about 0.25 was estimated for one of the second floor spandrels of the west exterior wall subjected to in-plane shear.

Base shear coefficients were estimated to be about 0.23 and 0.10 for the E-W and N-S directions, respectively. Even though the former value is well in excess of the equivalent static coefficient of 0.08 considered in the original seismic design, a maximum demand to capacity ratio less than 1 was obtained. The relatively large seismic resistance available in the current configuration may be due to the original design being intended for a larger building.

5.3 Response Analysis for the Loma Prieta Earthquake

Similar to Models 4 and 4X for the Morgan Hill earthquake, Models 5 and 5X were developed to match the responses recorded during the Loma Prieta earthquake. Because significant uncertainty is associated with the E-W modal parameters, the following discussion is focussed primarily on N-S structure properties and responses.

5.3.1 Stiffness Ratios

Stiffness ratios applied to the best estimate, uncracked stiffnesses for Model 5 are listed in Table 5-3. Stiffness ratios for Model 5X were nearly identical. These results indicate that reductions in N-S stiffness at the lower two stories were more significant than those for the upper two stories. The N-S stiffness ratio for the lower two stories reduced from 0.41 in the Morgan Hill earthquake to 0.22 in the Loma Prieta earthquake. The N-S stiffness ratio increased from 0.42 in the Morgan Hill earthquake to 0.47 in the Loma Prieta earthquake, which is not expected. This may be due to the difficulty in fitting the Loma Prieta responses that was experienced by the modal identification. Alternatively, the coarse distribution of stiffness ratios used (i.e, only two different values applied to four building stories) may introduce some error, as has been observed in similar studies. However, the difference is only about 10%, which is relatively small in comparison to other uncertainties implicit in these analyses, and is not considered significant. These results indicate that stiffness reduction associated with the N-S response to the Loma Prieta earthquake was concentrated in the lower two stories.

5.3.2 Floor Response Spectra

Comparisons of 5% damped floor response spectra calculated using Model 5 with floor spectra generated from the actual recorded motions are shown in Figures 5-7 to 5-12. Focussing on the N-S spectra, the analytically calculated spectra significantly exceed the actual recorded spectra in general. The calculated spectra have significant amplifications resulting from higher modes with frequencies in the 7 to 12 Hz range. These amplifications do not exist in the actual spectra. Somewhat better correlations to the actual recorded responses are obtained by Model 5X, as shown in Figures 5-13 to 5-18, which are probably due to the better match of the building torsional behavior in this model. However, the analytically calculated floor spectra still exhibit significant differences from the actual spectra.

Effective effective modal participation factors associated with horizontal translation input motion for Models 5 and 5X are compared to those obtained by modal identification for the fixed base case in Table 5-4. As shown, the effective modal participation factors for Model 5X are nearly identical at all channels.

Even though the fit to the identified Loma Prieta modal parameters obtained by the structural models (specifically Model 5X) is better than the match obtained for Morgan Hill, significant differences between the

analytically calculated and actual recorded floor response spectra still exist. Sources of this difference include errors in both the modal identification results and the structure model. As noted in Section 3, modal identification experienced difficulty in providing a good match to the recorded responses due to nonlinearities and ill-conditioning.

5.3.3 Capacity Evaluation

Allowable capacities based upon current acceptance criteria were compared to applied loads for the most heavily loaded structural elements. Of the structural elements resisting E-W seismic loads, a maximum demand to capacity ratio of about 2 was obtained for certain piers of the central E-W interior wall and the north exterior wall. A maximum demand to capacity ratio of about 1.2 was obtained for the east and west exterior walls, which provide the primary resistance to N-S seismic loads. The difference between ratios for the E-W and N-S structural elements reflects the difference in responses between these two directions.

The demand to capacity ratio of 2 for the E-W shear walls indicates that these walls were overstressed against the conservative acceptance criteria by the Loma Prieta earthquake. As noted in Section 2.4, only light cracking was observed in the central E-W interior wall. The lack of significant damage experienced, despite the relatively high demand to capacity ratio, demonstrates the conservatism implicit in the current acceptance criteria. Sources of conservatism include material strengths, member capacity formulations, and elastic load distributions. Actual concrete compressive and reinforcement yield strengths are typically greater than the minimum specified values. For example, the actual compressive strength for the original construction concrete is estimated to be about 4,000 psi, in comparison to the minimum specified value of 2,750 psi. Member capacities permitted by current codes and standards are generally conservative, lower bound values. For example, the in-plane shear strength of low aspect ratio shear walls permitted by the ACI Code has been shown to be very conservative in comparison to available test data [Wesley and Hashimoto, 1981; Electric Power Research Institute, 1988]. Demand to capacity ratios in this capacity evaluation have been based on seismic load distributions assuming elastic behavior, as is conventional in the design of concrete structures at nuclear plants. However, even shear walls have sufficient ductility to withstand deformations past initial yielding. Seismic loads will tend to redistribute to other, less heavily loaded walls, after initial yielding. This load redistribution provides additional structure capacity.

Table 5-1

STIFFNESS FACTORS FOR THE MORGAN HILL EARTHQUAKE

Direction	1st and 2nd Stories	3rd and 4th Stories
E-W	0.41	0.42
N-S	0.41	0.42

Table 5-2

COMPARISON OF EFFECTIVE PARTICIPATION FACTORS, MORGAN HILL EARTHQUAKE

	Fundamental E-W Mode				Fundamental N-S Mode			
	Ch. 11	Ch. 12	Ch. 5	Ch. 6	Chs. 5 and 6	Ch. 7	Ch. 8	Chs. 7 and 8
Modal ID	1.21	0.77	0.80	1.05	0.93	0.45	0.59	0.52
Model 4	1.24	0.78	1.44	1.11	1.28	0.81	0.62	0.72

Table 5-3

STIFFNESS FACTORS FOR THE LOMA PRIETA EARTHQUAKE

Direction	1st and 2nd Stories	3rd and 4th Stories
E-W	0.19	0.19
N-S	0.22	0.47

Table 5-4

COMPARISON OF EFFECTIVE MODAL PARTICIPATION FACTORS, LOMA PRIETA EARTHQUAKE

	Fundamental E-W Mode					Fundamental N-S Mode		
	Ch. 11	Ch. 12	Ch. 5	Ch. 6	Chs. 5 and 6	Ch. 7	Ch. 8	Chs. 7 and 8
Modal ID	1.22	0.77	1.05	1.31	1.18	0.71	0.86	0.78
Model 5	1.22	0.81	1.40	1.04	1.22	0.94	0.68	0.81
Model 5X	1.28	0.81	1.07	1.36	1.22	0.71	0.92	0.82

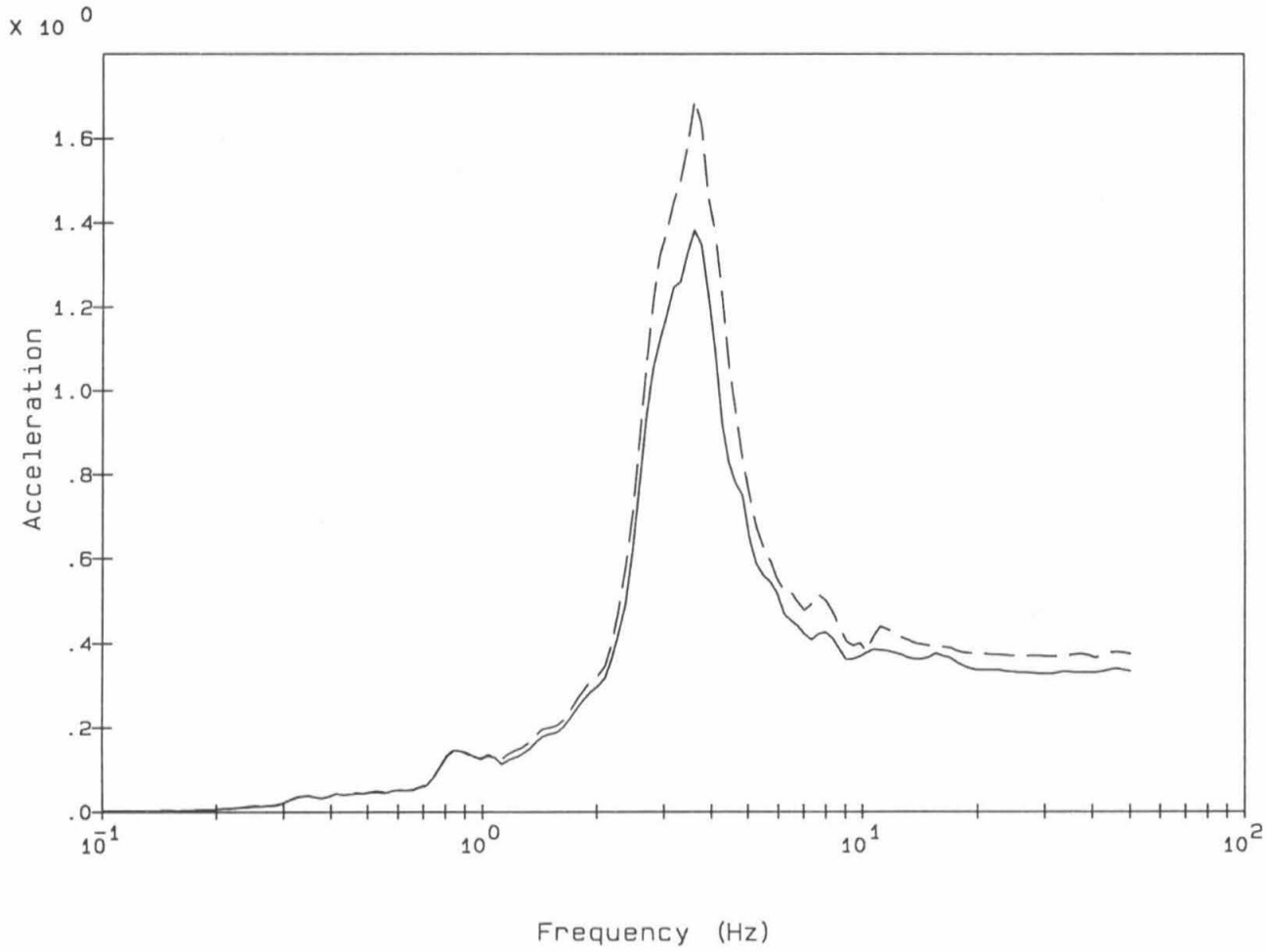

Legend:

Channel 11 Rec. ————————

Node 18 Calc. — — — — -

Notes:

Acceleration (g)

Spectra calculated at 5% damping

Figure 5-1: Comparison of Actual Recorded and Analytically Calculated 5% Floor Response Spectra At Channel 11, Morgan Hill Earthquake

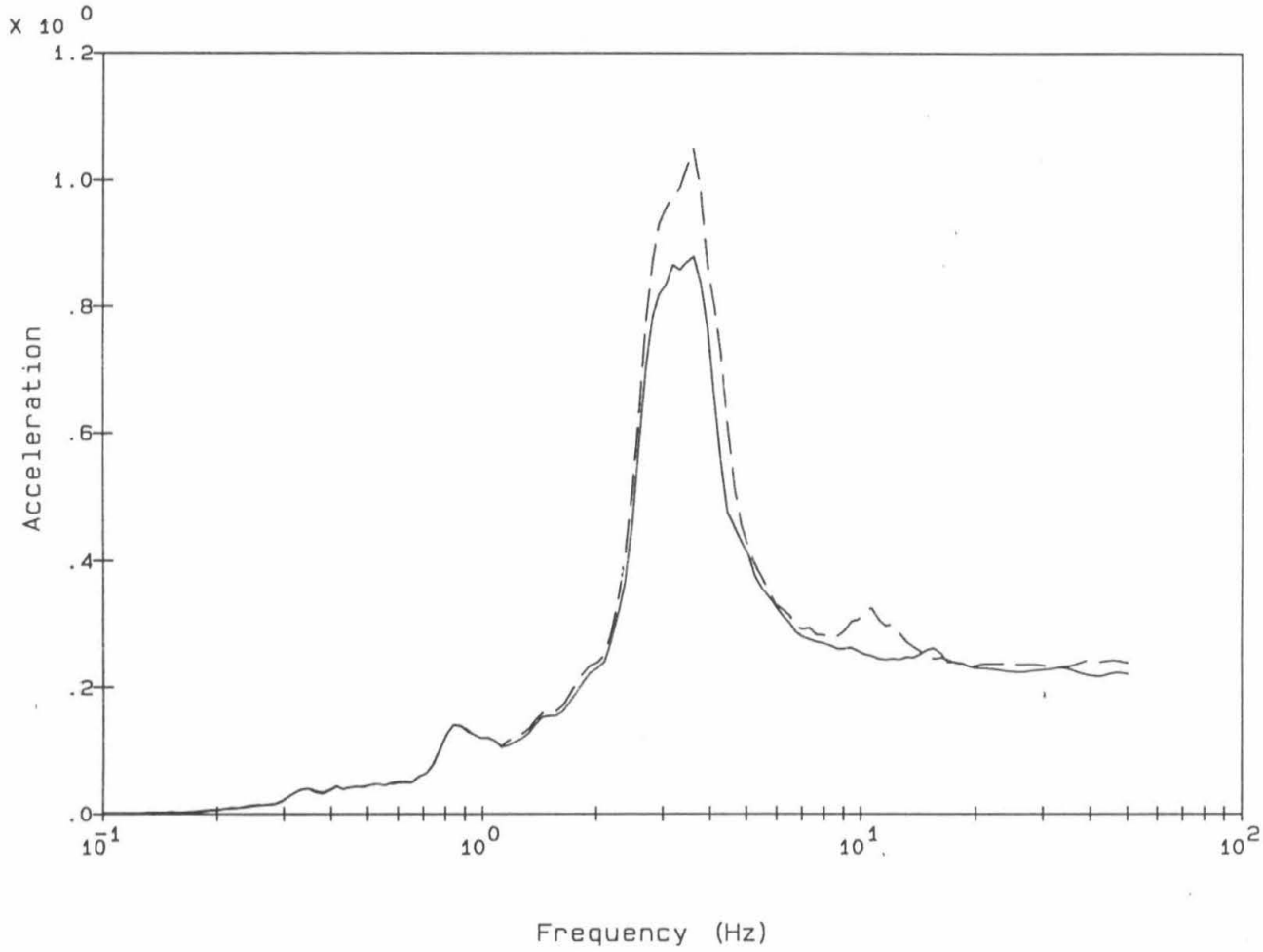

Figure 5-2: Comparison of Actual Recorded and Analytically Calculated 5% Floor Response Spectra At Channel 12, Morgan Hill Earthquake

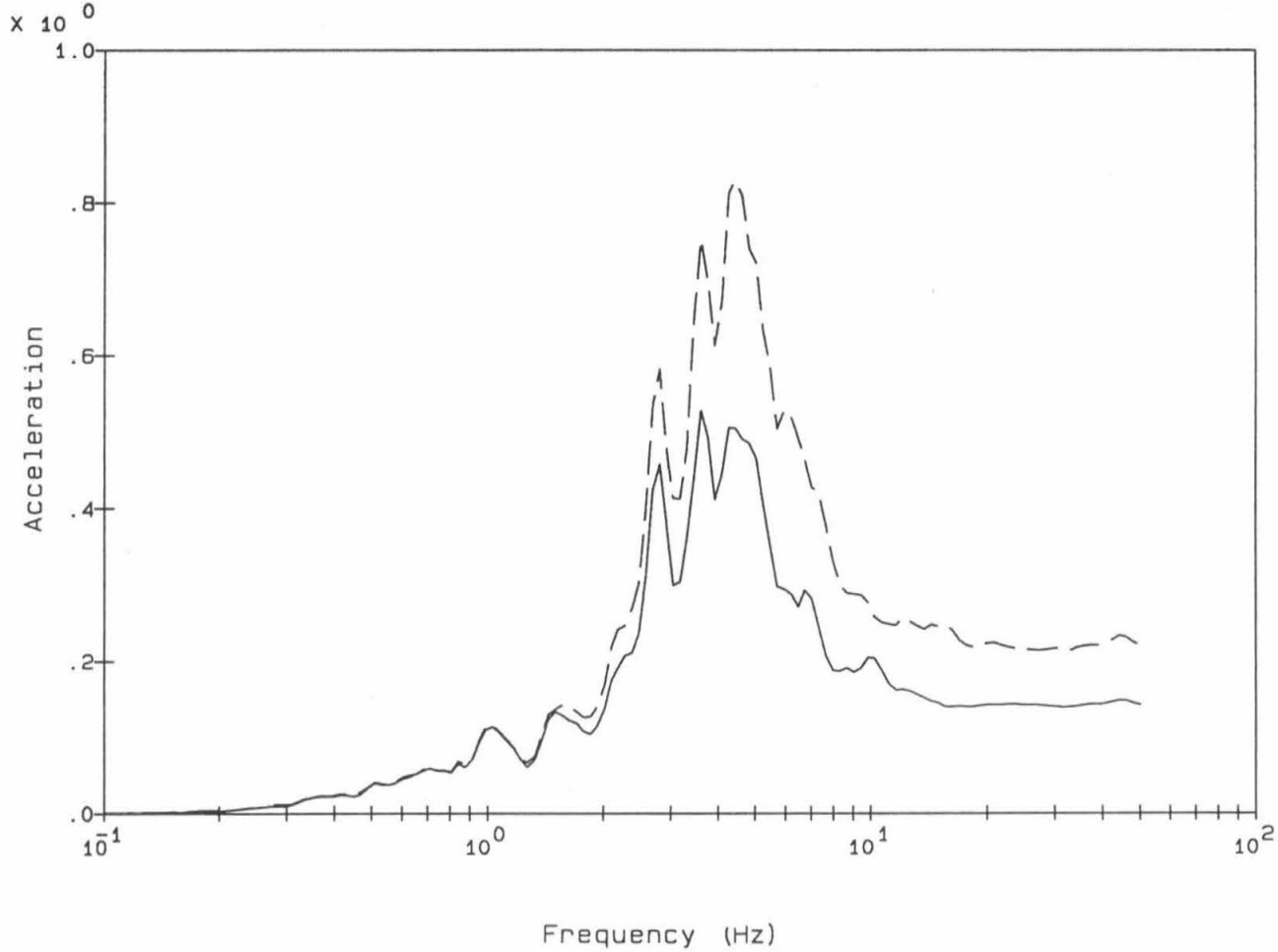

Legend:

Channel 5 Rec. ————————

Node 16 Calc. — — — — -

Notes:

Acceleration (g)

Spectra calculated at 5% damping

Figure 5-3: Comparison of Actual Recorded and Analytically Calculated 5% Floor Response Spectra At Channel 5, Morgan Hill Earthquake

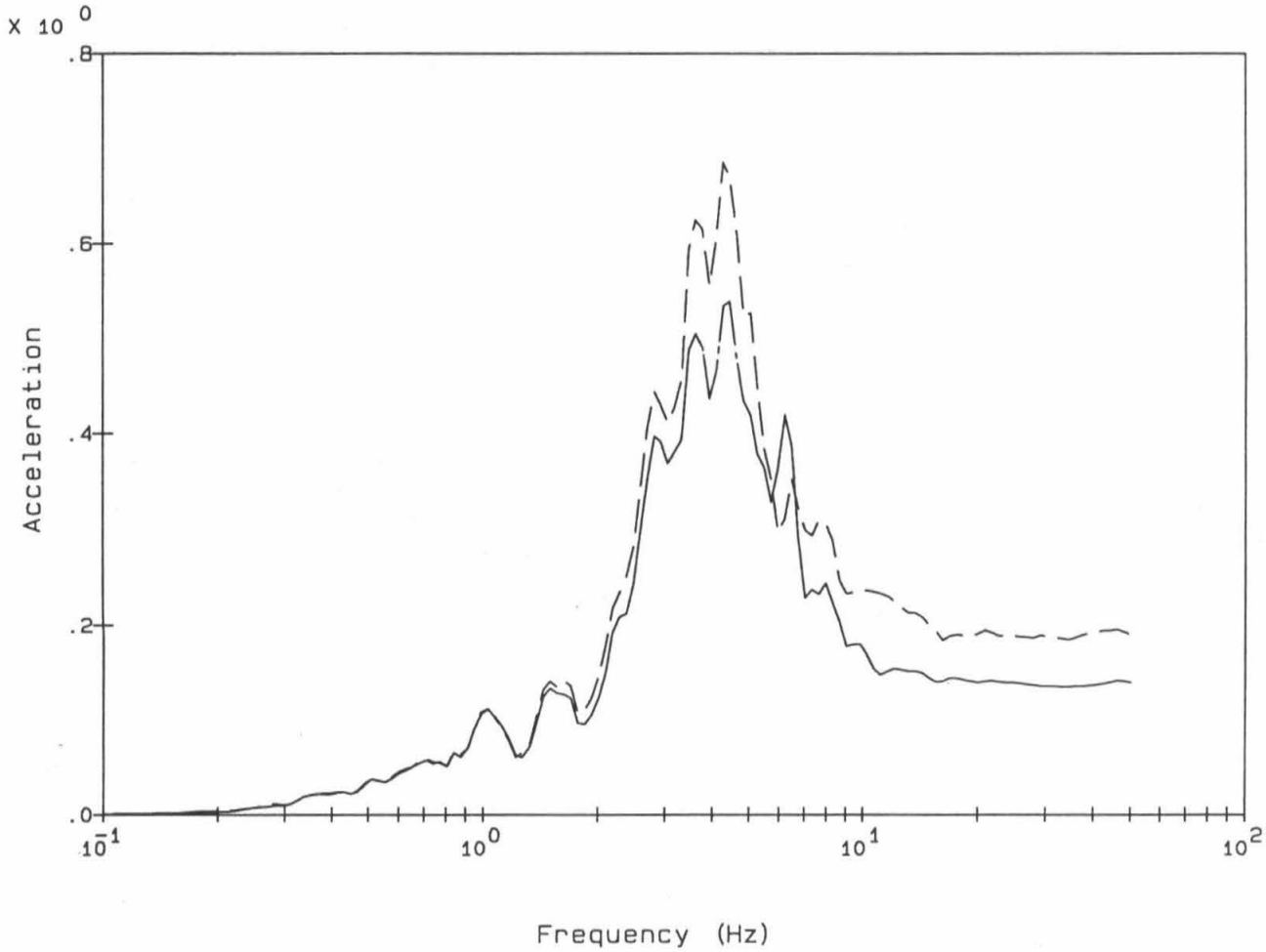

Figure 5-4: Comparison of Actual Recorded and Analytically Calculated 5% Floor Response Spectra At Channel 6, Morgan Hill Earthquake

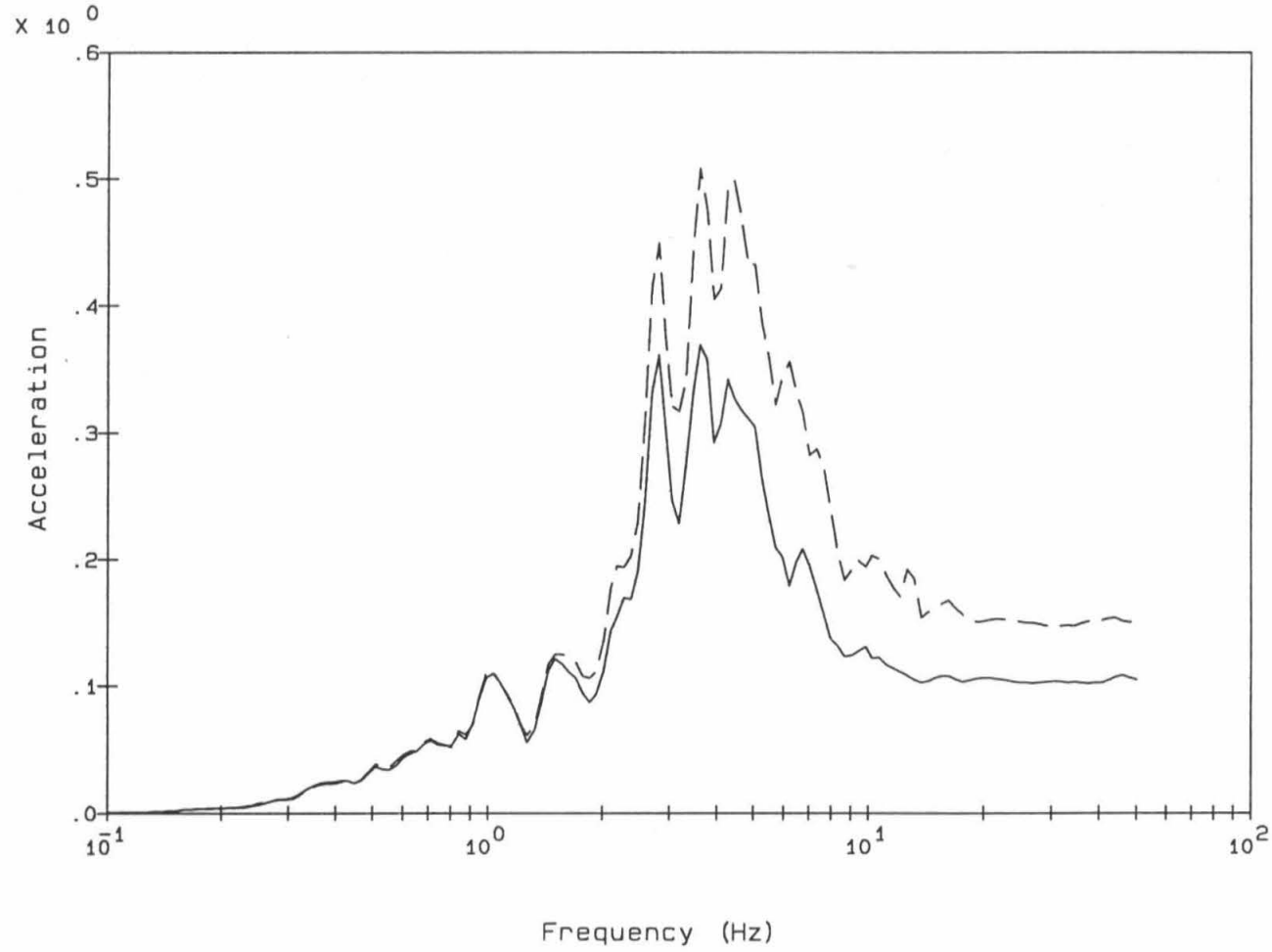

Figure 5-5: Comparison of Actual Recorded and Analytically Calculated 5% Floor Response Spectra At Channel 7, Morgan Hill Earthquake

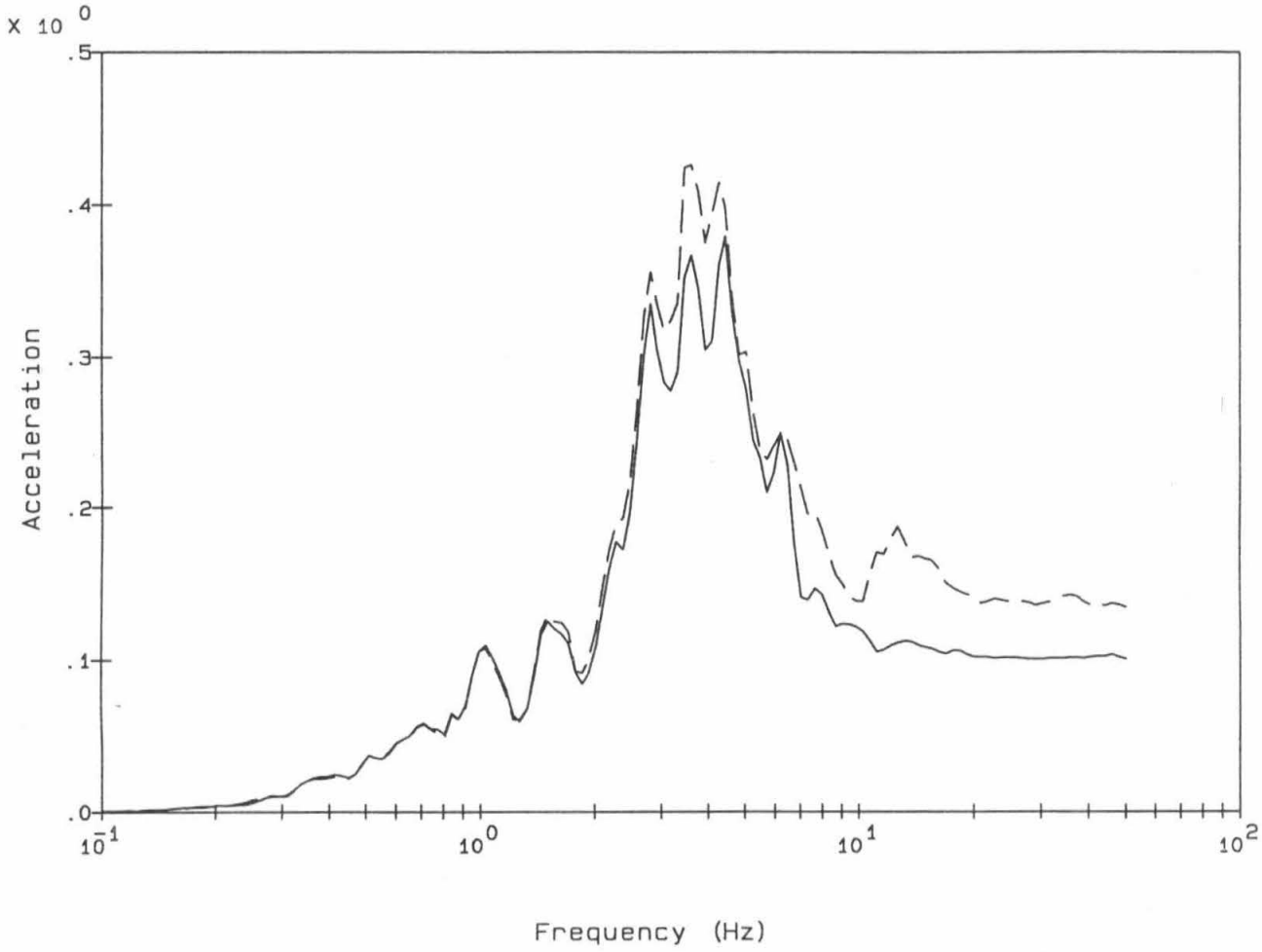

Figure 5-6: Comparison of Actual Recorded and Analytically Calculated 5% Floor Response Spectra At Channel 8, Morgan Hill Earthquake

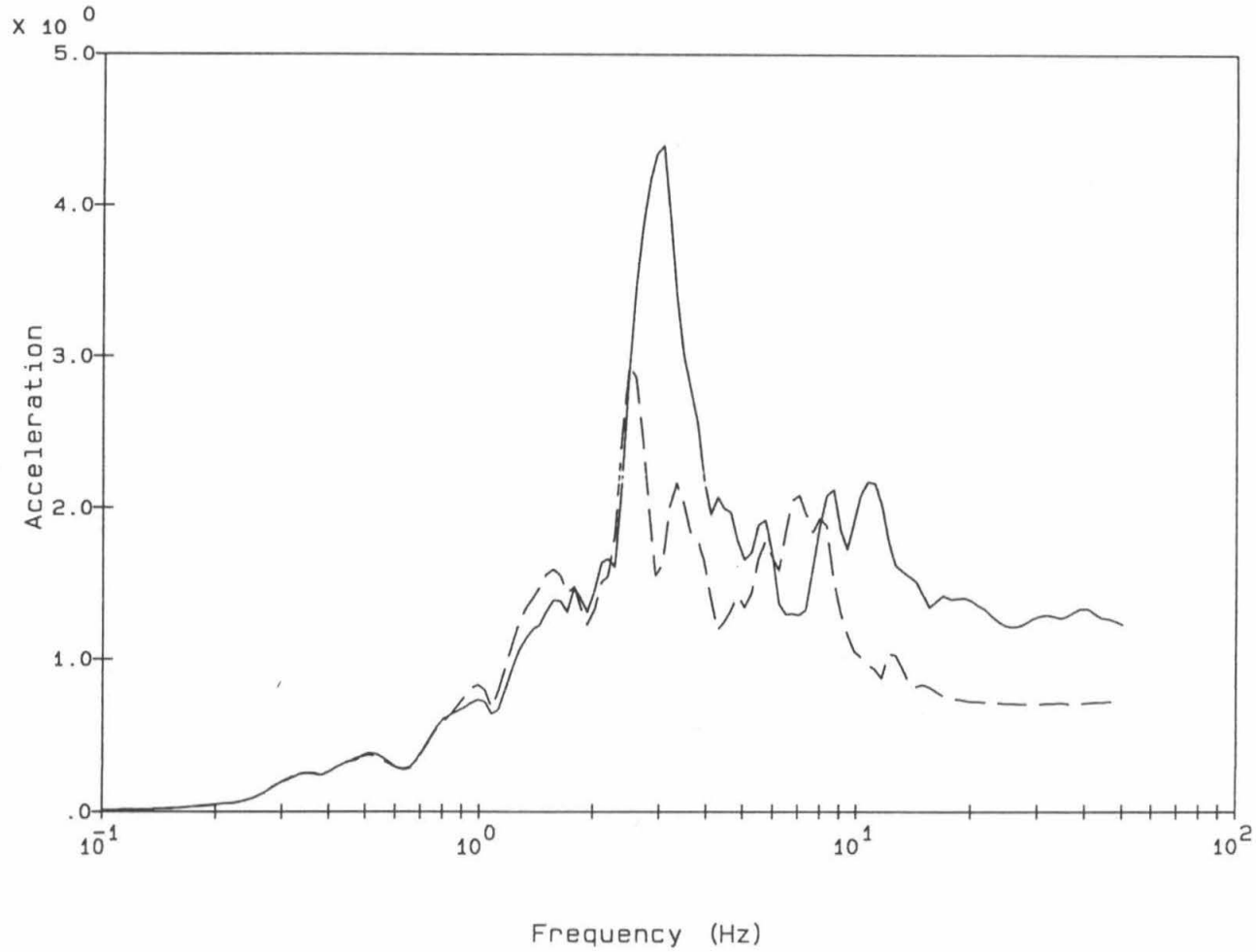

Legend:

Channel 11 Rec. ————————

Node 18 Calc. — — — — —

Notes:

Acceleration (g)

Spectra calculated at 5% damping

Figure 5-7: Comparison of Actual Recorded and Analytically Calculated 5% Floor Response Spectra Using Model 5 At Channel 11, Loma Prieta Earthquake

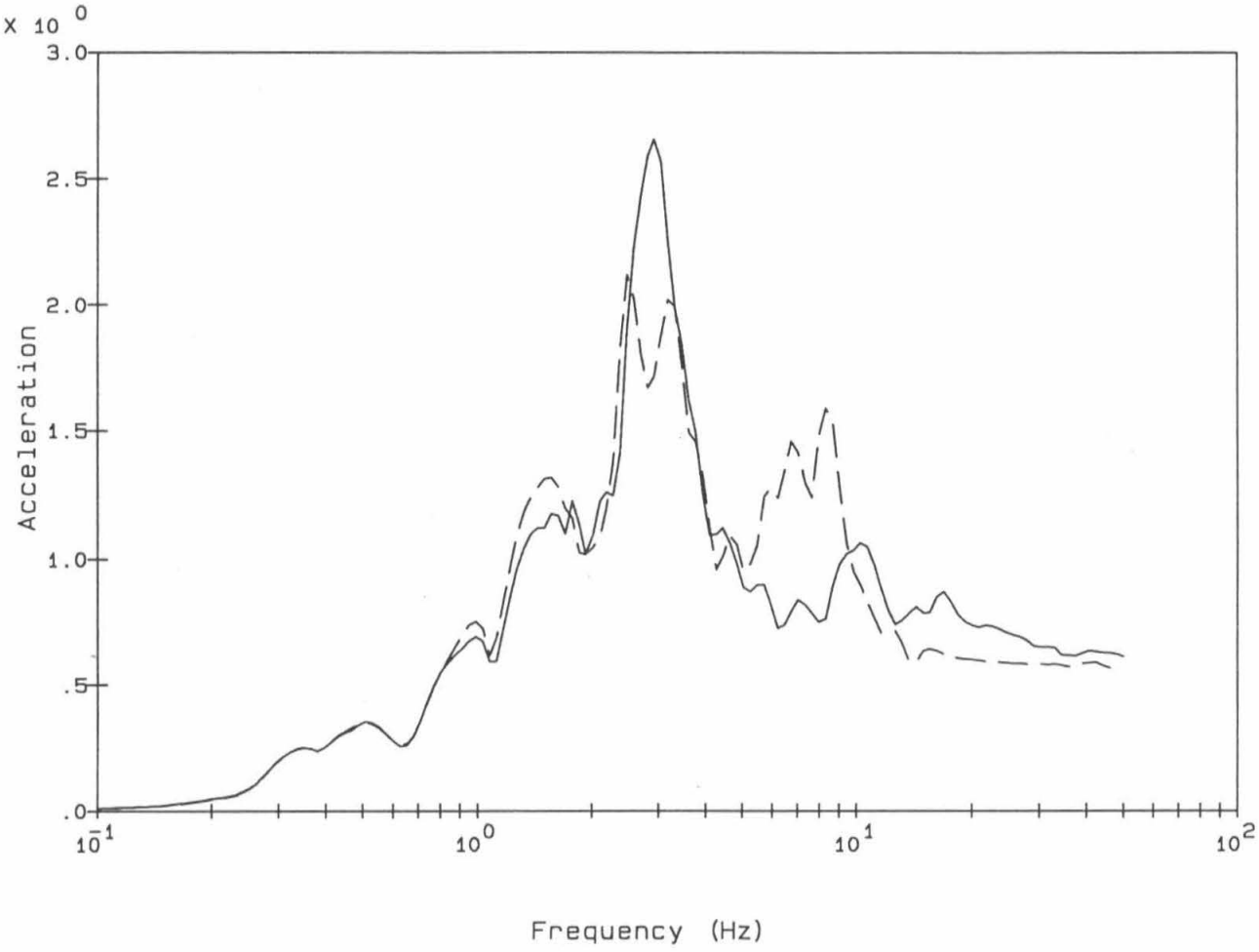

Figure 5-8: Comparison of Actual Recorded and Analytically Calculated 5% Floor Response Spectra Using Model 5 At Channel 12, Loma Prieta Earthquake

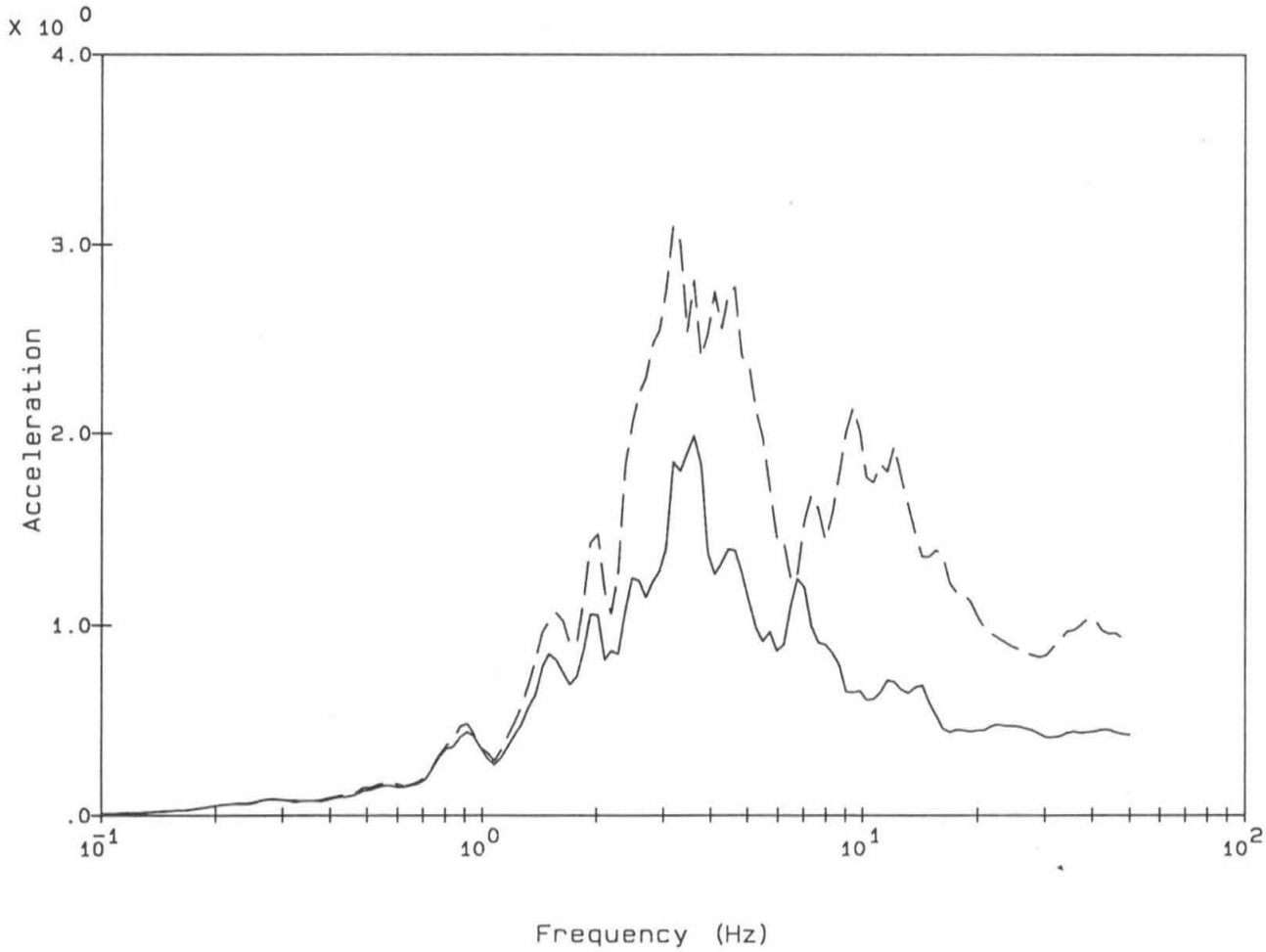

Legend:

Channel 5 Rec. ————————

Node 16 Calc. — — — — -

Notes:

Acceleration (g)

Spectra calculated at 5% damping

Figure 5-9: Comparison of Actual Recorded and Analytically Calculated 5% Floor Response Spectra Using Model 5 At Channel 5, Loma Prieta Earthquake

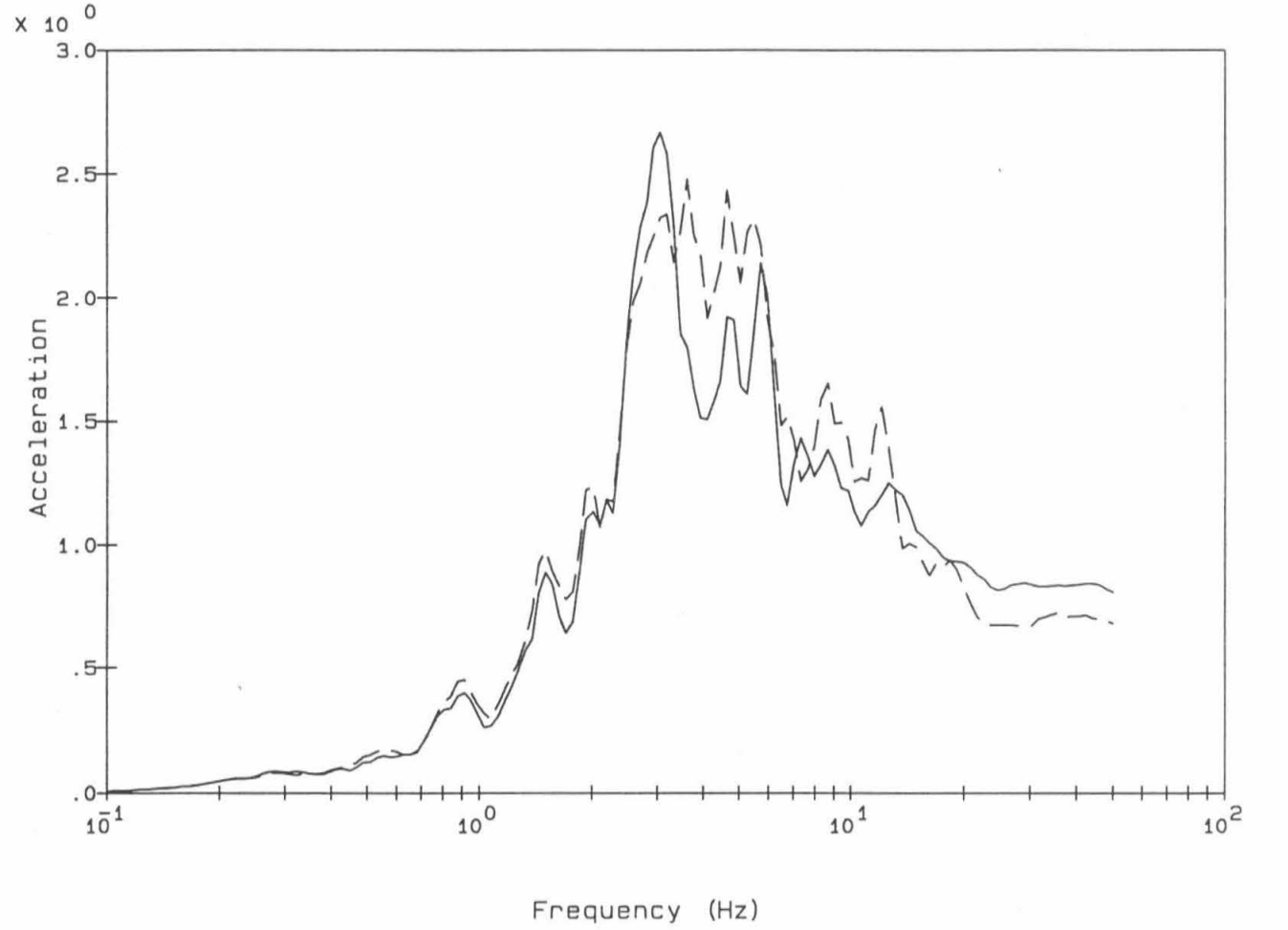

Figure 5-10: Comparison of Actual Recorded and Analytically Calculated 5% Floor Response Spectra Using Model 5 At Channel 6, Loma Prieta Earthquake

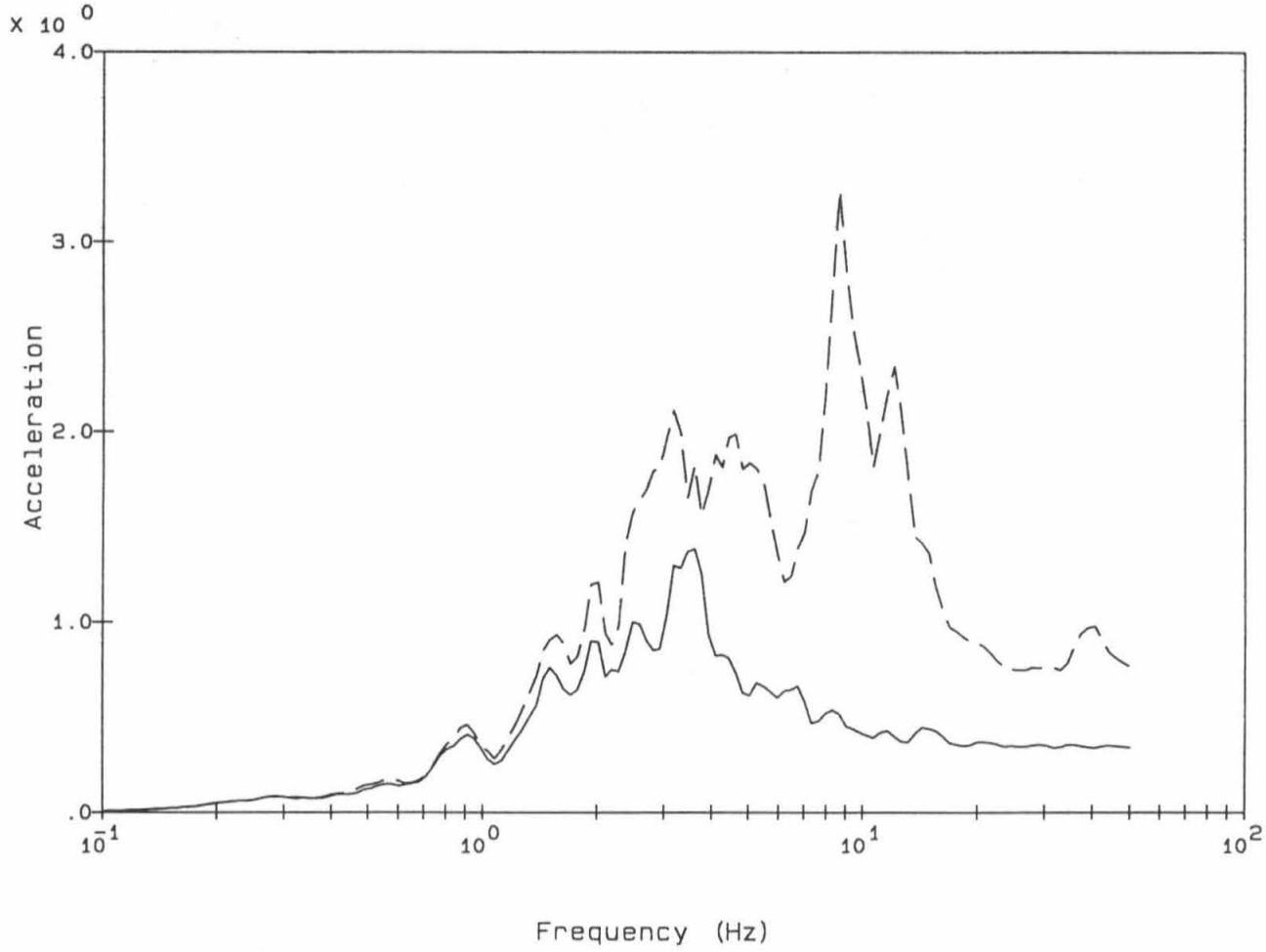

Figure 5-11: Comparison of Actual Recorded and Analytically Calculated 5% Floor Response Spectra Using Model 5 At Channel 7, Loma Prieta Earthquake

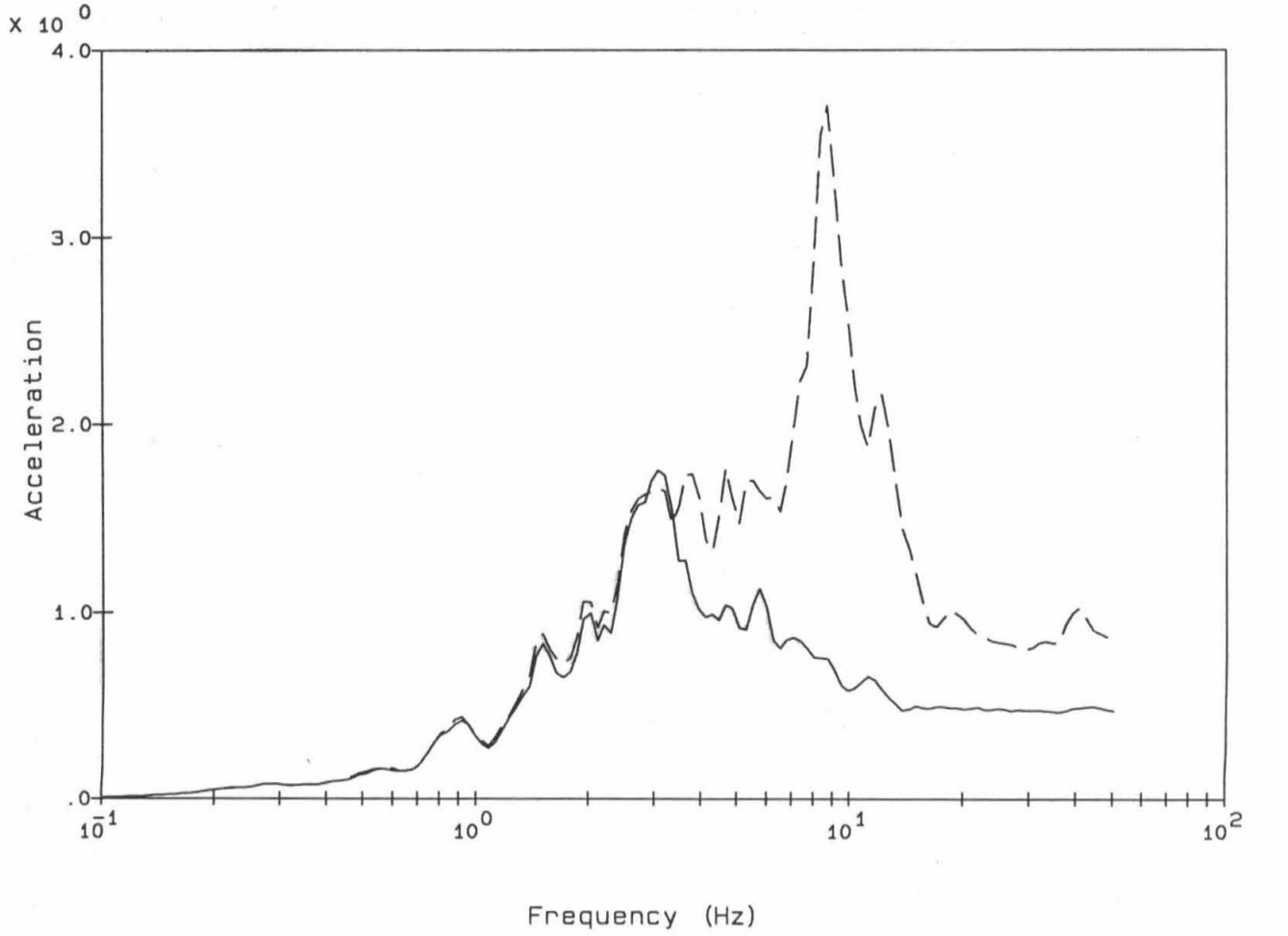

Figure 5-12: Comparison of Actual Recorded and Analytically Calculated 5% Floor Response Spectra Using Model 5 At Channel 8, Loma Prieta Earthquake

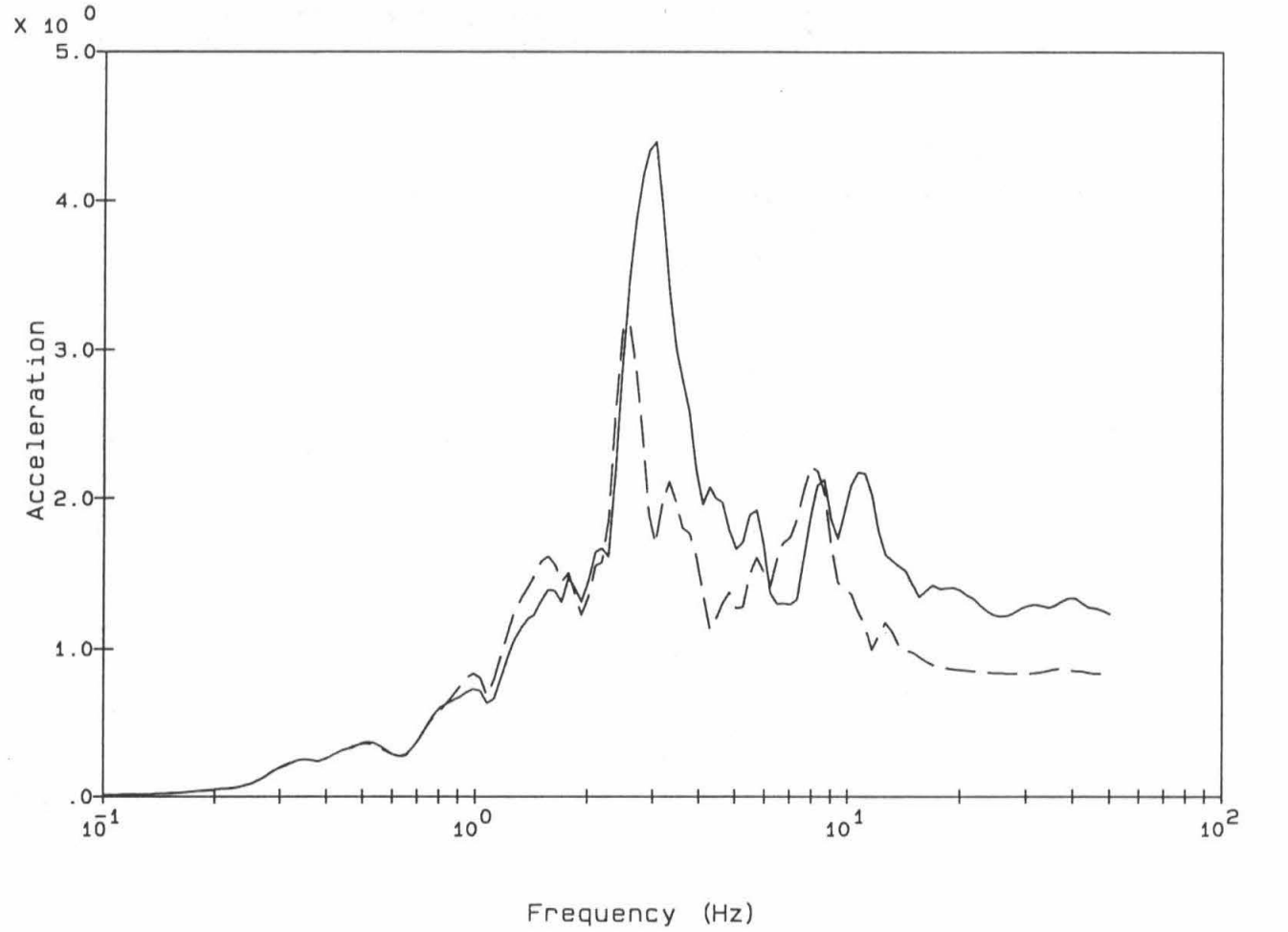

Figure 5-13: Comparison of Actual Recorded and Analytically Calculated 5% Floor Response Spectra Using Model 5X At Channel 11, Loma Prieta Earthquake

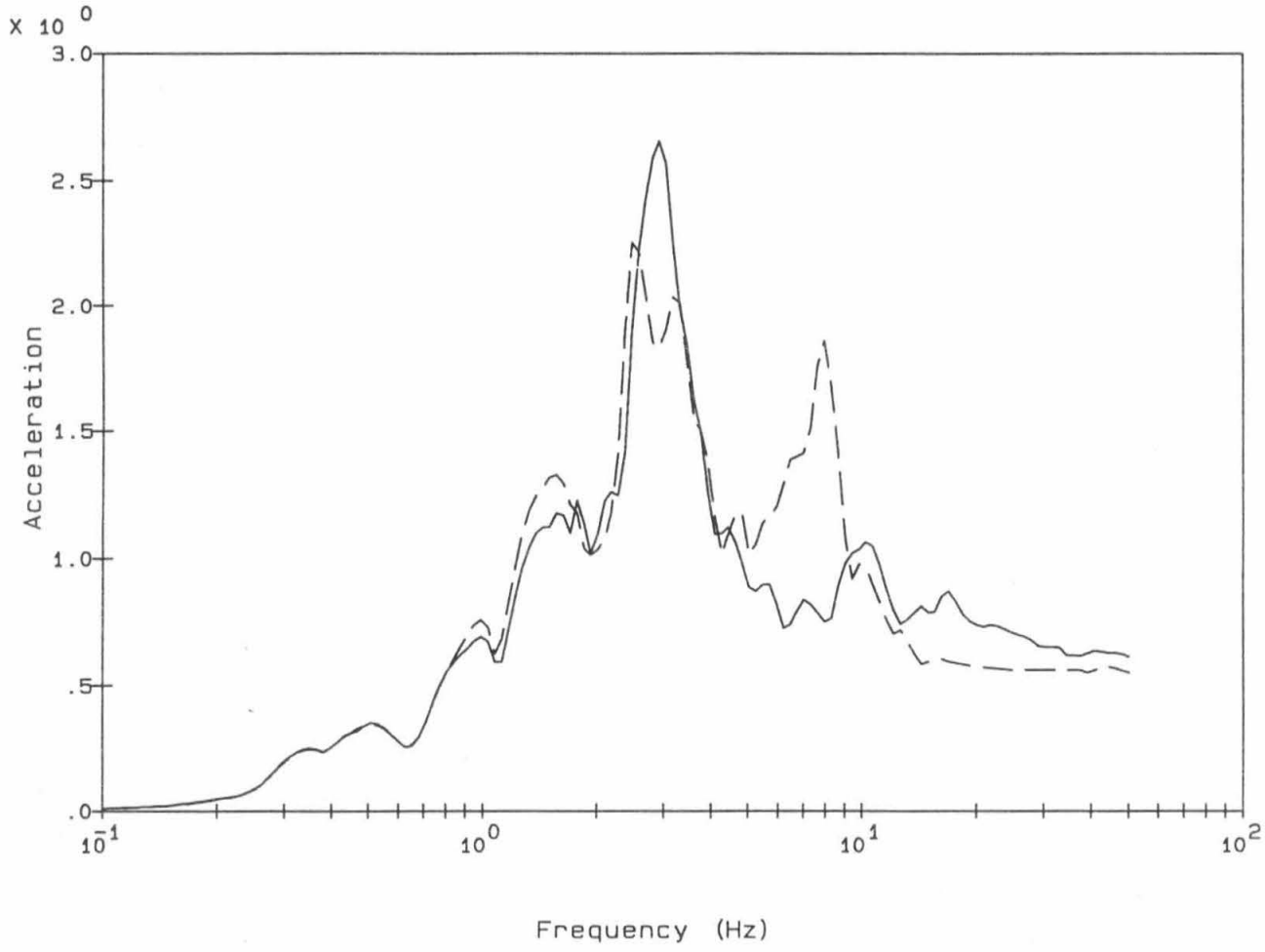

Legend:

Channel 12 Rec. ————————

Node 15 Calc. — — — — -

Notes:

Acceleration (g)

Spectra calculated at 5% damping

Figure 5-14: Comparison of Actual Recorded and Analytically Calculated 5% Floor Response Spectra Using Model 5X At Channel 12, Loma Prieta Earthquake

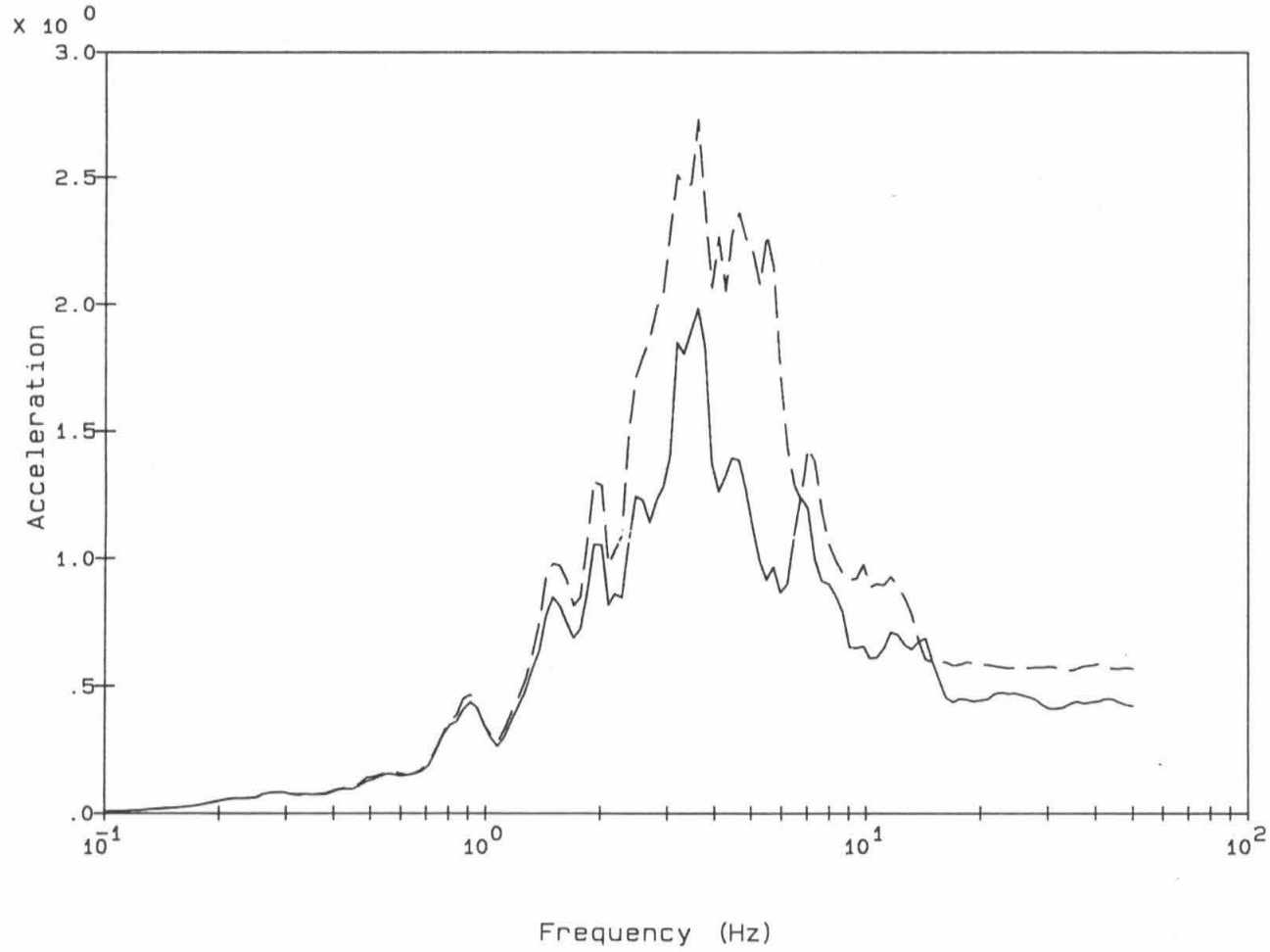

Legend:

Channel 5 Rec. ————————

Node 16 Calc. — — — — -

Notes:

Acceleration (g)

Spectra calculated at 5% damping

Figure 5-15: Comparison of Actual Recorded and Analytically Calculated 5% Floor Response Spectra Using Model 5X At Channel 5, Loma Prieta Earthquake

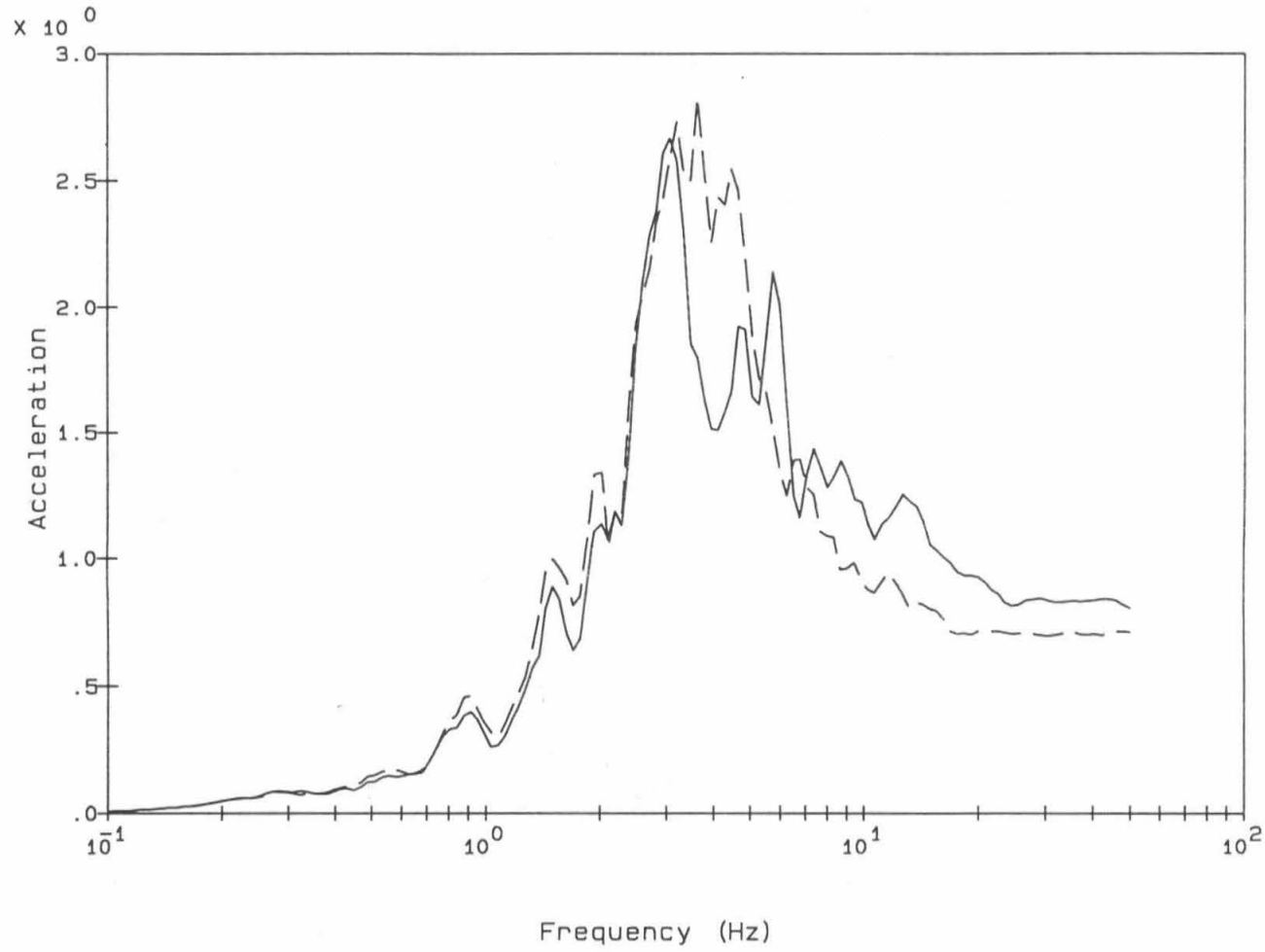

Legend:

Channel 6 Rec. ————————

Node 17 Calc. — — — — —

Notes:

Acceleration (g)

Spectra calculated at 5% damping

Figure 5-16: Comparison of Actual Recorded and Analytically Calculated 5% Floor Response Spectra Using Model 5X At Channel 6, Loma Prieta Earthquake

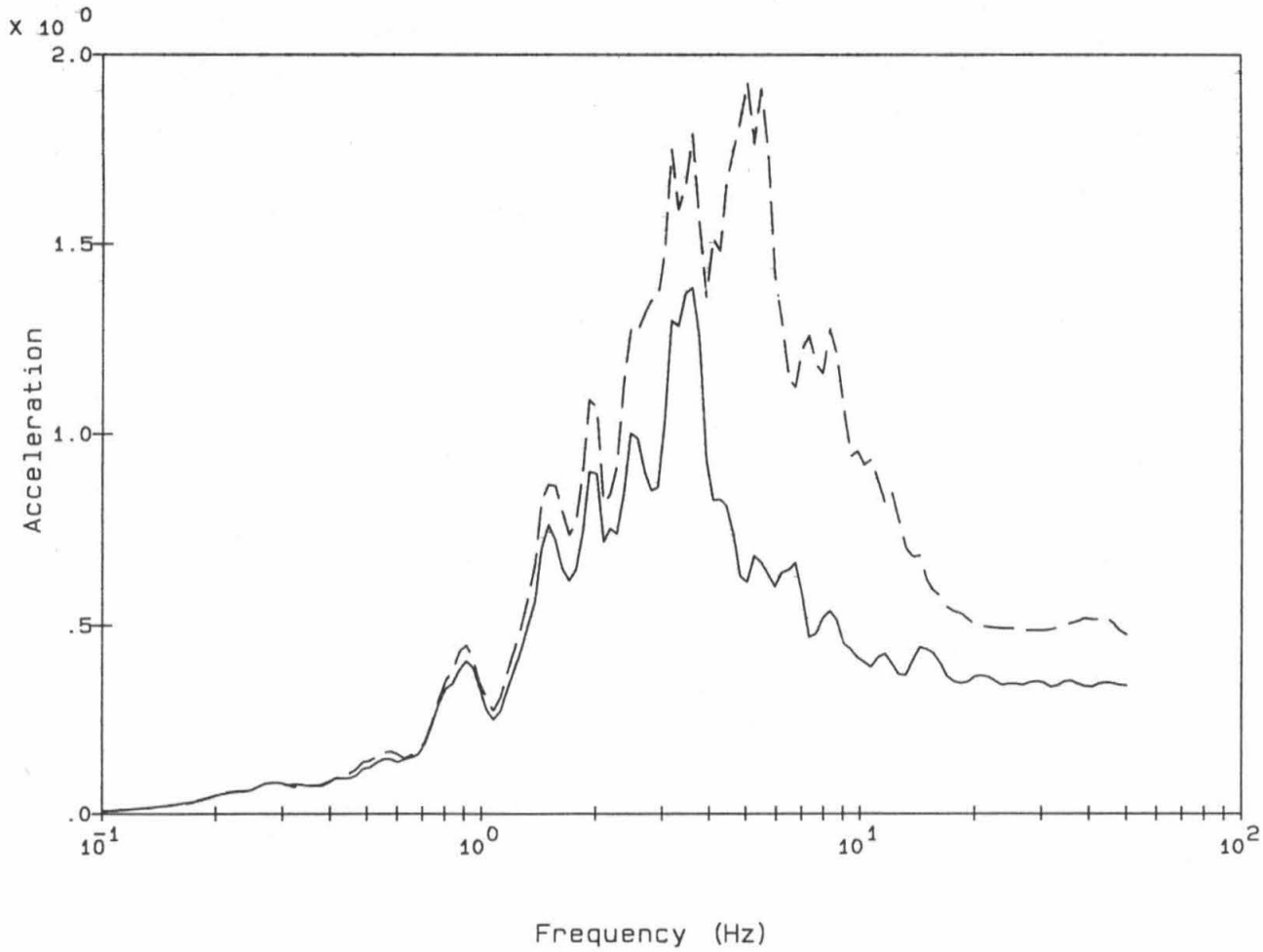

Legend:

Channel 7 Rec. ————————

Node 13 Calc. — — — — —

Notes:

Acceleration (g)

Spectra calculated at 5% damping

Figure 5-17: Comparison of Actual Recorded and Analytically Calculated 5% Floor Response Spectra Using Model 5X At Channel 7, Loma Prieta Earthquake

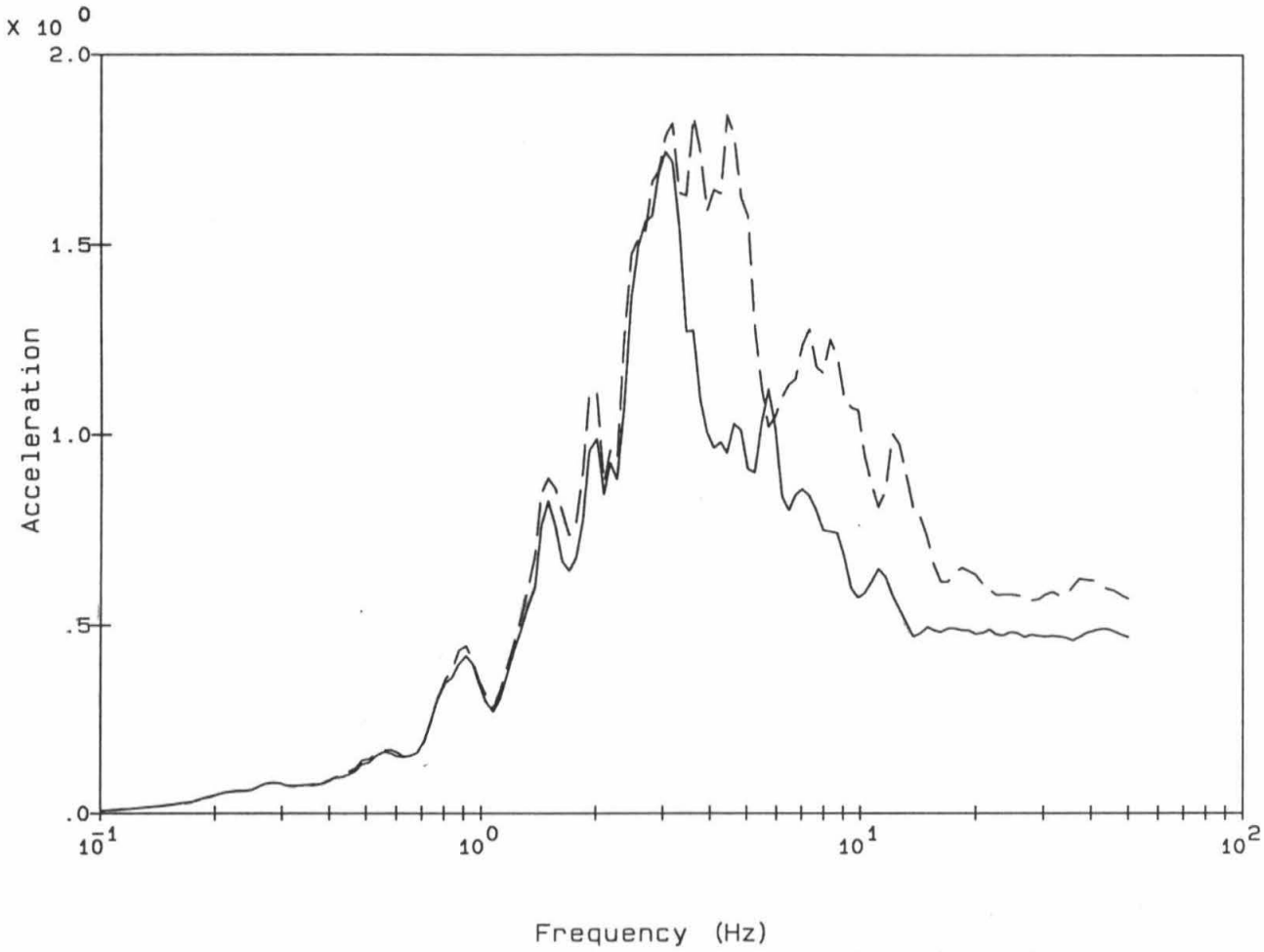

Figure 5-18: Comparison of Actual Recorded and Analytically Calculated 5% Floor Response Spectra Using Model 5X At Channel 8, Loma Prieta Earthquake

6. REVIEW OF STIFFNESS AND DAMPING DATA

Specific data on estimates of the actual structure stiffnesses and damping values have been presented in Sections 3 to 5. These data are collectively reviewed in this section. The stiffness and damping data obtained from this study are compared to laboratory tests results. Insights into the adequacy of current criteria and guidelines for the specification of nuclear plant structure stiffness and damping are also obtained.

6.1 Review of Stiffness Data

As noted in Section 1, significant quantities of data on the stiffness of low aspect ratio shear walls have been obtained in the USNRC's Seismic Category I Structures Program. In parallel, the Electric Power Research Institute has sponsored a collection and review of low aspect ratio shear wall stiffness data from other sources [Moehle, et al, 1990]. These investigations present the most current summary of test data relevant to nuclear power plant structures.

The USNRC and EPRI programs have both correlated shear wall stiffness against the average (or nominal) shear stress. This quantity is easily defined for isolated shear walls. However, for an actual structure which is composed of multiple stories and multiple walls, an average shear stress is less readily defined. This is especially true for the subject building, whose major walls are typically perforated by multiple openings.

Average shear stresses for the major walls were estimated using a simplified, approximate procedure that should provide equivalent values to the stresses reported for the laboratory specimens. The "average" wall shear stress was based on the ratio of the total wall shear force to the net wall cross-sectional area in plan, excluding any openings. Effectively, this represents the average stress in the piers of a single wall, and is appropriate since the total wall deformations are dominated by deformations of the piers. While flexibility of the spandrels also contribute to the wall deformations, the finite element models indicate that spandrel stresses are comparable to the pier stresses.

Because stiffness ratios could only be identified for the lower two and upper two stories, it was necessary to estimate average shear stresses applicable to each pair of stories. For the direction of interest (i.e., E-W or N-S), the average shear stresses of the major walls at the pair of stories (i.e., lower two or upper two) were tabulated. The maximum and minimum values were then averaged to obtain the average shear stress applicable to the pair of stories. While this process introduces further uncertainty, the calculated stresses are considered sufficiently accurate for the purposes of the following comparisons.

Stiffness ratios, defined as the ratios of the estimated actual stiffnesses to the best estimate, uncracked stiffnesses, are listed in Table 6-1 along with corresponding estimates of the average shear stresses. As shown, the stiffness ratios are in the range of 0.4 to 0.5 for average shear stresses up to about 60 psi. Varying values are obtained at average stresses of about 125 psi. A stiffness ratio of about 0.4 is obtained for the walls of the lower two stories in the E-W direction for the Morgan Hill earthquake, while a value of about 0.2 is obtained for the walls of the lower two stories in the N-S direction from the Loma Prieta earthquake.

With the exception of the stiffness ratio of 0.2, the stiffness data obtained from this building are reasonably consistent with data obtained from laboratory testing. Ratios of measured to theoretical uncracked stiffnesses obtained by Los Alamos National Laboratory in the Seismic Category I Structures Program are reproduced in Figure 6-1 (Figure 37 from Farrar, et al, 1991b). As shown, the stiffness ratios are in the range of about 0.5 to 1.1 or slightly greater for nominal base shear stresses up to about 150 psi, which is considered to be a representative value for design of a western United States nuclear plant structure to current criteria.

For EPRI, Moehle and Sozen collected and compiled stiffness data from testing of low aspect ratio shear walls, including two specimens from the Seismic Category I Structures Program. Figure 11 of Moehle, et al [1990] presents statistical results on the ratio of measured to calculated stiffness as a function of nominal shear stress. Up to nominal shear stresses of about $3(f'_c)^{1/2}$, the mean plus one standard deviation bound is about 0.8 to 0.9, and mean minus one standard deviation bound is about 0.4 to 0.5. Thus, excluding the outlier stiffness ratio of 0.2, the stiffness data are also reasonably consistent with the results obtained by Moehle and Sozen.

As noted in Section 4, based on a review of the two sources of test data described above, the ASCE Working Group has recommended a lower bound stiffness based on uncracked section properties and one-half the best estimate of the concrete modulus of elasticity. Although they are slightly lower, the estimated stiffness ratios for this building generally support this bounding value. The slight overestimation of the calculated stiffness ratios by the lower bound value recommended by the ASCE Working Group is not considered significant. There may be biases implicit in the simplified structure model used in this study, due to modeling approximations and other uncertainties, that lead to inferred stiffness ratios that underestimate the true values. Thus, these results generally support the ASCE Working Group recommendations, although further substantiation could be obtained by more refined investigation.

Moehle, Sozen, and Tang [1990] suggest that the deviation of the actual stiffnesses from the theoretical values for laboratory specimens is a consequence of cracking due to sources other than lateral load, such as handling, shrinkage, and temperature. These observations appear to be confirmed by stiffness data obtained from this building. With the exception of the single outlier, the stiffness ratios are all in the

range of 0.4 to 0.5 for average stresses ranging from 15 psi to 130 psi. These ratios are independent of earthquake, direction, and location. Although some variation in stiffness is indicated by frequency variations identified for successive time windows in the Morgan Hill earthquake, it is apparent that the stiffness ratios do not come close to 1.0, even at the start of the Morgan Hill earthquake.

Thus, except for the one outlier above, the stiffness ratios obtained from this building are within the range of values identified by these other sources, although generally at the lower end. The greater than typical reduction in stiffness associated with this building may be due to factors not represented in the laboratory data noted above. These could include more significant shrinkage cracking due to the presence of the embedded steel framing, more significant cracking due to settlement or temperature, aging effects not visible to the eye, etc.

The source of the low stiffness ratio of about 0.2 obtained from the Loma Prieta earthquake is not immediately obvious. Although the estimated demand to capacity ratios and earthquake effects for the N-S walls would suggest otherwise, some structure yielding may have occurred in this direction. It might be that the building is generally more flexible to begin with, as suggested by comparison to the test data, and that the higher stresses due to the Loma Prieta earthquake cause further stiffness reductions. Also, there might be an error in the identified frequency or mode shape, since the modal identification experienced greater difficulty in determining the modal parameters for the Loma Prieta motions.

6.2 Review of Damping Data

Damping data have been collected, compiled, and evaluated in the Structure Damping Research Program (Section 1). Figure 6-2 plots measured damping values obtained for fundamental modes of non-nuclear concrete structures against a parameter, Stress Ratio. Stress Ratio is defined as the maximum ratio of the applied dynamic load to the allowable capacity permitted by Standard Review Plan acceptance criteria, and is thus equivalent to the demand to capacity ratio used in this study. Figure 6-2 presents estimated structure damping values, with the contribution to the measured damping associated with soil-structure interaction removed by an approximate method. Figure 6-3 plots damping data obtained from testing of laboratory specimens. All data shown in these figures were obtained from structures that were essentially elastic.

Damping data obtained for this building by modal identification are summarized in Table 6-2, along with estimated demand to capacity ratios experienced by the building. The time-invariant values are listed, since these are representative of the building's energy dissipation for the entire earthquake durations. Damping values from the fixed base case, which accounts for energy dissipation within the structure alone are listed. These data are equivalent to those plotted in Figures 6-2 and 6-3.

Damping data obtained from this building will be included in the database compiled as part of the Structure Damping Research Program. Some preliminary observations can be obtained from comparison of damping values for this building to the database as a whole.

The structure damping value of 4.9% obtained for the fundamental E-W mode in the Morgan Hill earthquake is clearly consistent with other measured data. As shown in Figures 6-2 and 6-3, for Stress Ratio values between about 0.5 to 1.0, damping values range between about 3% and 8%.

The damping values identified from N-S building response appear to be higher than other measured data. The damping value of 11.6% for the fundamental N-S mode in the Morgan Hill earthquake significantly exceeds other measured damping values. For Stress Ratios in the range of about 0.25, measured damping data are generally no greater than about 5% to 6%. The damping value of 12.7% obtained for the fundamental N-S mode from the Loma Prieta earthquake is also high relative to other data. At Stress Ratios of about 1.0 or greater, measured damping values up to about 8% have been obtained.

Table 6-1

SUMMARY OF STIFFNESS RATIOS

EQ	Direction	Stories	Average Stress (psi)	Average Stress ($f'_c{}^{1/2}$) (1)	Stiffness Ratio
MH	E-W	1st and 2nd	124	2.0	0.41
MH	E-W	3rd and 4th	56	0.9	0.42
MH	N-S	1st and 2nd	34	0.5	0.41
MH	N-S	3rd and 4th	15	0.2	0.42
LP	N-S	1st and 2nd	128	2.0	0.22
LP	N-S	3rd and 4th	58	0.9	0.47

1. Based on estimated actual concrete compressive strength of 4,000 psi

Table 6-2

SUMMARY OF FIXED BASE DAMPING VALUES

Earthquake	Mode	Demand/Capacity	Damping (%)
Morgan Hill	E-W	0.75	4.9
Morgan Hill	N-S	0.25	11.6
Loma Prieta	N-S	1.2	12.7

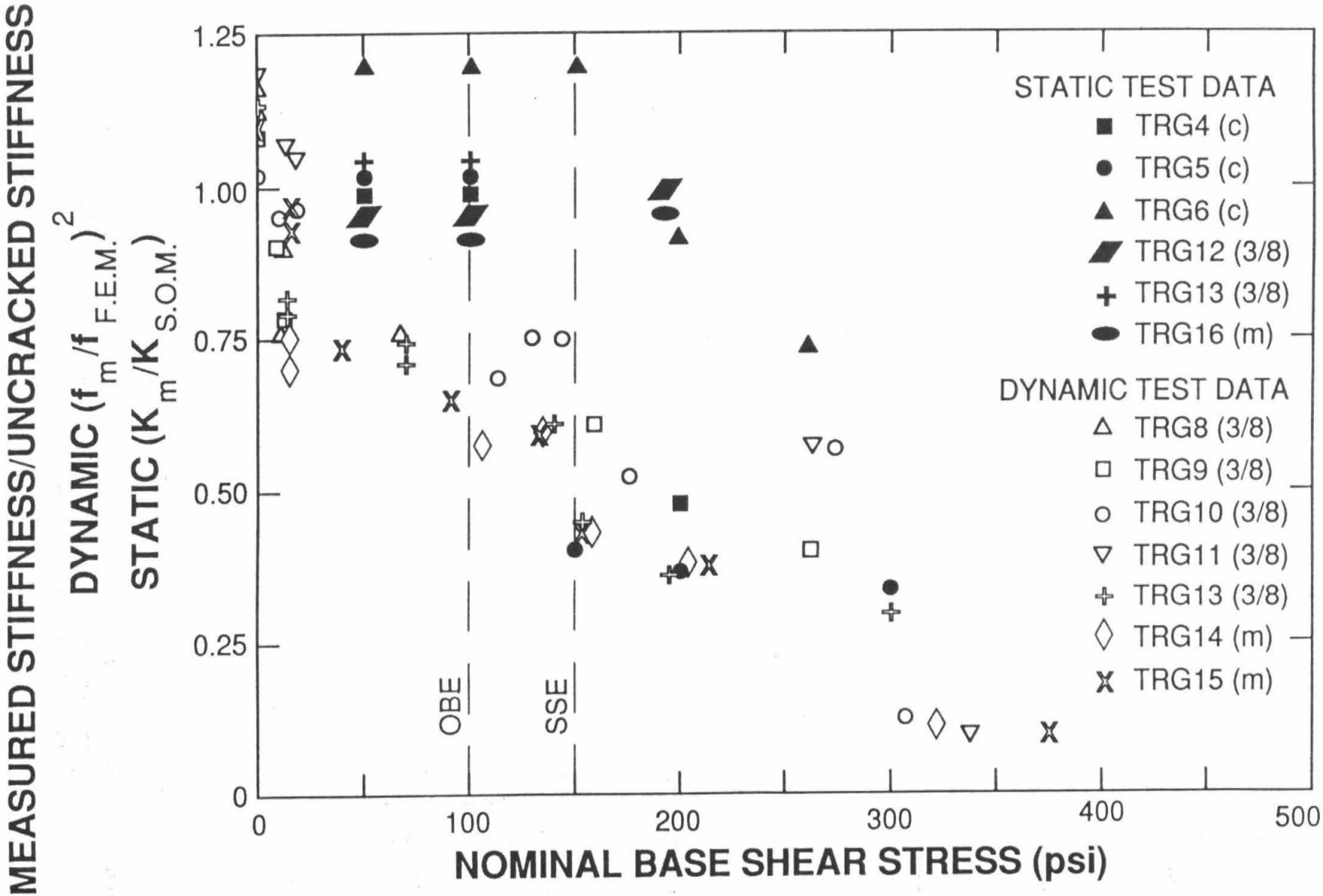

Figure 6-1: Stiffness Ratios Obtained By the Seismic Category I Structures Program (From Farrar, et al, 1991b)

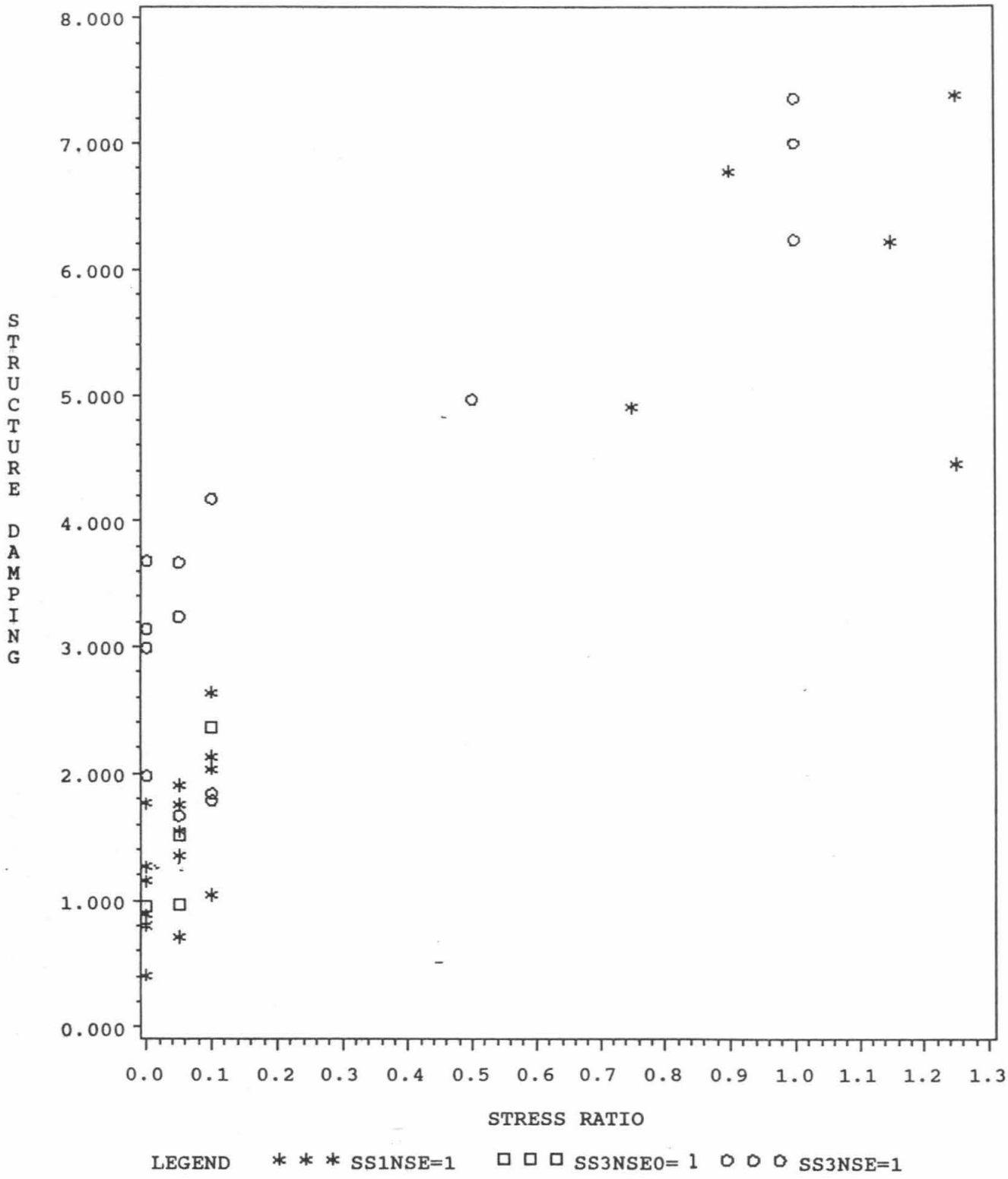

Figure 6-2: Damping Data Excluding Soil-Structure Interaction Effects From Non-Nuclear Structures Obtained By the Structure Damping Research Program

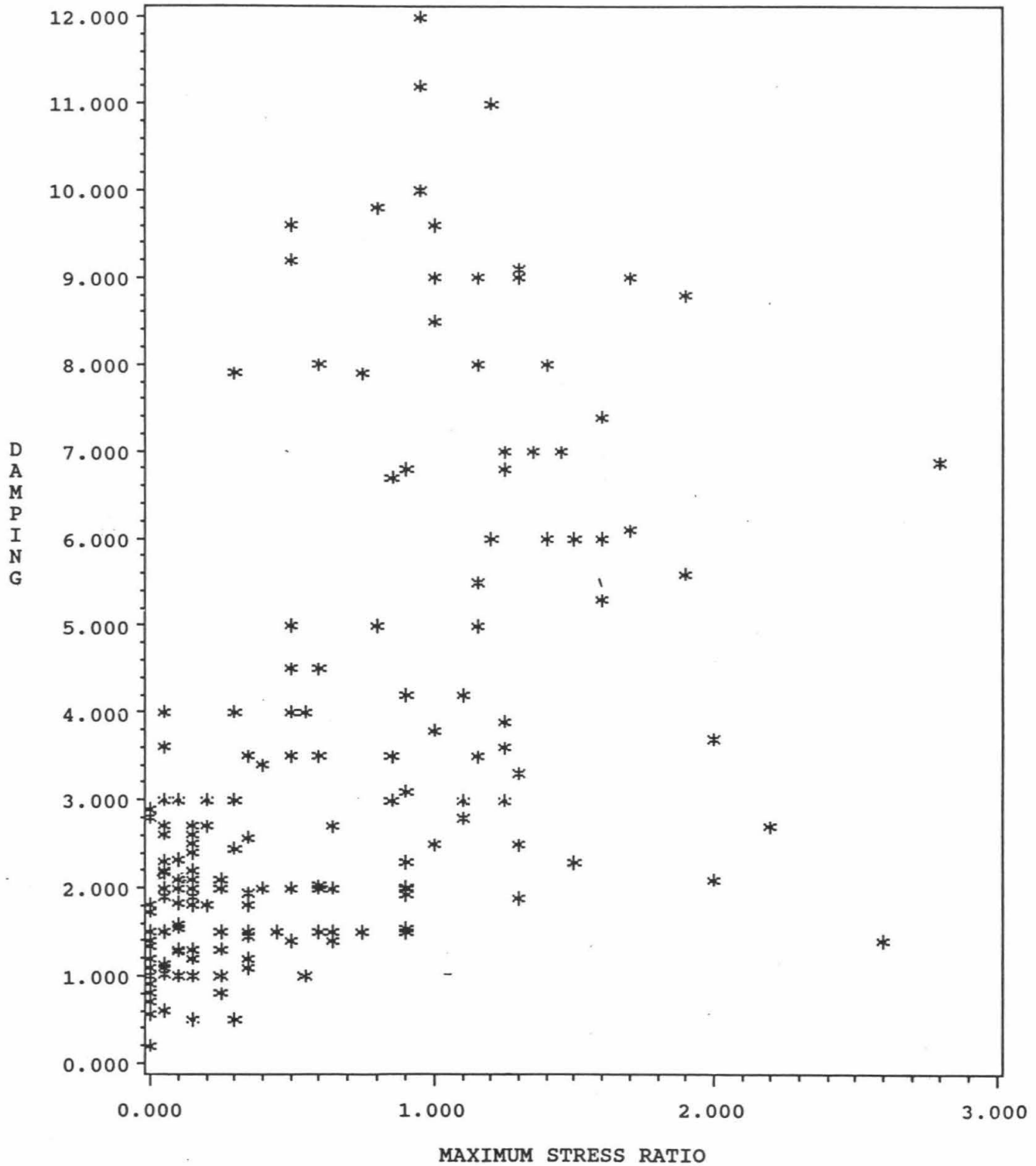

Figure 6-3: Damping Data From Test Structures Obtained By the Structure Damping Research Program

7. SUMMARY, CONCLUSIONS, AND RECOMMENDATIONS

7.1 Summary

This summary discusses structure behavior (expected and actual), modal identification (elements and results), dynamic modeling, and results.

7.1.1 Background

The Watsonville telephone building is considered similar to nuclear power plant structures in that its primary load resisting system consists of reinforced concrete shear walls with overall height-to-length ratios less than one. Its deformation under earthquake loadings is expected to be principally due to shear and its frequencies are expected to be in the frequency range of amplification for earthquake motions. The evaluations performed herein confirm these aspects of behavior.

The building is instrumented by the CDMG to obtain earthquake acceleration time history records. Thirteen instruments are located in the structure. Seven are on the ground floor with one at each corner of the building to measure vertical response (four total) and three to measure horizontal response. The third floor and roof each have three instruments measuring horizontal response. All of the instruments are recorded on a central recording system and are synchronized. Finally, the instruments on the ground floor serve to define the response of the base including all effects of soil-structure interaction (SSI), i.e., they record resultant motion of the base.

Strong motion records were recorded for two earthquakes: The Morgan Hill earthquake of April 24, 1984 and the Loma Prieta earthquake of October 17, 1989. The building experienced significant seismic response during the Loma Prieta earthquake, with peak accelerations of 1.24g (E-W) and 0.63g (N-S) on the roof, and 0.39g (E-W) and 0.28g (N-S) at the base. The building experienced less motion during the Morgan Hill event, with peak accelerations of 0.33g (E-W) and 0.15g (N-S) on the roof, and 0.11g (E-W) and 0.06g (N-S), at the base.

This study was performed in three tasks: Data collection, modal identification, and elastic analyses. Data collection entailed obtaining detailed information concerning the building (drawings and photographs), the recorded motions from the Morgan Hill and Loma Prieta earthquakes, and performing walkdowns of the facility. Modal identification was performed to estimate structure modal parameters including modal frequencies, damping values, mode shapes, and participation factors. Elastic analyses were performed for several building modeling assumptions and the results compared to the identified modal parameters and the recorded responses.

7.1.2 Building Behavior

For discussion purposes, the behavior of the building is separated into two component parts: The base and the structure. In a practical sense, the base can behave rigidly or flexibly.

The motion of a perfectly rigid base is uniquely defined by six components: Three translations and three rotations. Bases or foundations that behave essentially rigid for earthquake loading conditions are typical for structures with thick base slabs and for structures with stiff wall systems and diaphragms which, in turn, stiffen the structure/foundation system. In general, the structure can behave linearly or nonlinearly. For a rigid base, structure behavior can be depicted by linear or nonlinear models as appropriate. Lightly damped linear structure behavior is expected to be modeled well by classical normal modes. Nonlinear structure behavior is modeled by appropriate descriptions of nonlinear material and geometric effects. These linear or nonlinear models describe the contributions to response beyond the rigid body motion induced by the rigid base.

For flexible bases, linear structure behavior can be modeled by a combination of pseudostatic and dynamic response. Dynamic response can be modeled by classical normal modes which represent the contributions to response beyond the pseudostatic values. For flexible base motion and nonlinear structure behavior, a full nonlinear model must be used. Superposition concepts, i.e., the combination of pseudostatic and dynamic response, do not apply.

The building was expected to have responded in a linear or slightly nonlinear fashion for the Morgan Hill earthquake and slightly nonlinear to nonlinear for the Loma Prieta earthquake. This was verified in the study. In addition, however, the base was shown to behave flexibly which complicated the modal identification process.

Several approaches were employed to identify and assess the overall characteristics of the base and the structure. Modal identification was one such approach.

7.1.2.1 Behavior of the Base

The behavior of the base and, in particular, the validity of assuming a rigid base was assessed in several ways. Consider the base motions: E-W, N-S, vertical translations, torsion, and rocking about the E-W and N-S axes. Three components of horizontal translation were recorded at the base of the building; instrument Channels 9 and 10 in the N-S direction and Channel 13 in the E-W direction. From these components, E-W and N-S translations and torsion were defined and, in the absence of any additional information, the base of the structure was assumed to experience them as a rigid base. The four vertical instrument channels over-specify the remaining three rigid base motions; vertical translation and rocking about the E-W and N-S axes. Hence, for dynamic analysis and modal identification assuming a rigid base, a least squares fit of the time history response data to estimate vertical translation

and the two rocking components was employed. These three components were then combined at the instrument locations and compared to the four recorded motions. These comparisons suggested the rigid base assumption is reasonable, showing good agreement for both the Morgan Hill and Loma Prieta earthquakes.

In terms of dynamic response, the validity of the rigid base assumption was assessed in the following ways. First, in the modal identification procedure, one case was analyzed where all instruments on the base were included individually as input channels, rather than implicitly as rigid-base motion, and the instruments on the third floor and the roof were treated as output channels. Differences in the identified modal parameters for this case compared to the case of assuming the base to behave as a rigid body were minimal. Second, a case was analyzed assuming a rigid base but including the four vertical instrument channels on the base as output channels and used in the identification process. The result showed no change in the identified modal parameters from the case where these vertical motions were not included as output channels in the identification. In addition, mode shape values were identified for these four channels and, in an overall sense, they tended to validate rigid base motion.

While the comparisons described above suggest that the base can be modeled as rigid, more detailed investigations of the modal identification results showed that the flexibility of the base could be important to the behavior of the structure. Recall that the load-resisting system is one of external and internal shear walls with the addition of columns in the interior of the building. The major lateral load-resisting elements are the external shear walls.

Two possibilities for flexible base motion exist: (1) The bases of the interior columns and walls experience horizontal and vertical motions that differ from those of the bases of the exterior walls and (2) the motion of the base of the exterior walls is not perfectly consistent with a rigid base; i.e., a warping of the base occurs.

The columns and interior walls are more flexible than the exterior walls. If they were subjected to significantly different base motions due to wave passage effects or the soil-structure interaction process itself, their influence on the overall dynamic behavior of the structure is expected to be minimal. Their flexibility and the necessity to transfer these effects through flexible diaphragms at the various floor levels lead to this conclusion. Flexible diaphragm behavior will influence local dynamic response but should not significantly influence overall structure behavior. In addition, this local behavior would not be recorded on the in-place instruments which are all near exterior walls and, therefore, could not be verified.

The second possibility is not addressed as easily. In fact, a careful review of the recorded time histories and the identified mode shape components reveals an out-of-plane warping of the base. This warping is associated with torsion in the structure. Warping of the base and the nonlinear behavior of the structure significantly affected the modal identification procedure and the ability to match elastic models to the

response. Warping of the base and the associated torsion of the structure were more easily identified due to the location of the instruments. They reside on common shear walls and, consequently, motions recorded at the base of the shear wall are more directly transferred to and recorded at various levels in the building.

7.1.2.2 Behavior of the Structure

Observations concerning structure behavior are based on the modal identification results and field observations. The modal identification procedure was applied to two basic structure/soil configurations. First, the structure was treated as fixed base, i.e., using the six derived base motions as the input to the structure and the recorded motions on the third floor and the roof as output values. Next a rocking base case was analyzed where only the base translations are treated as input. The former case is intended to isolate the structure eliminating any SSI effects. The identified modal parameters, i.e., frequencies and damping, are associated exclusively with the structure, rather than the soil-structure system.

Significant difficulties were encountered in the modal identification process for the fixed base models for both the Morgan Hill and Loma Prieta earthquakes. Appendix C contains comparisons of total recorded motions with those attributed to rigid body motion based on the assumption of a rigid base. These comparisons allow one to qualitatively assess the amplitude and frequency content that the responses due to the identified classical normal modes need to contribute to match the total response. From these assessments, one gains insight into the difficulties in modeling the increment in response by classical normal modes. Acceleration time histories and 5% damped response spectra are compared for Channels 5, 6, 7, and 8 in the N-S direction and Channels 11 and 12 in the E-W direction. The Morgan Hill and Loma Prieta earthquakes are shown. Several of these figures are reproduced here to assist in understanding the results.

In general, two modes dominated response (one in each of the E-W and N-S directions) supplemented by a third mode with significant torsion.

Morgan Hill Earthquake

For the Morgan Hill earthquake, the E-W fixed base mode frequency was identified to be 4.0 Hz. over the duration of the event, i.e., the time-invariant value. Based upon analysis of successive time windows of the data, this E-W mode frequency varied from about 4.5 Hz. to under 4.0 Hz. indicating that the structure experienced slight degrees of nonlinearity during the excitation. This behavior would be consistent with possible loosening of non-structural elements and minor cracking not necessarily visible to the naked eye. The identified time-invariant modal damping value for this mode was 4.9% which appears reasonable compared to other data. A comparison of these modal parameters with those identified for the rocking base case shows consistency, with the rocking base frequency being less (a time-invariant value of 3.6 Hz.), and the rocking base damping value being more (a time-invariant value of 6.1%). Figure 7-1

compares response spectra on the roof for the total recorded motion with that due to rigid body motion. The response spectra contain strong and distinct frequency content at the identified frequency with obvious amplification due to modal response.

The N-S fixed base mode frequency was identified to be 5.5 Hz. over the duration of the event, varying from about 5.9 Hz. to about 5.2 Hz. Again, this is consistent with the occurrence of slight nonlinearities over the duration of the earthquake. The identified time-invariant damping value, however, is higher than expected; 11.6% over the duration of the event with variations from about 8.8% to about 12.7%. These high values lead one to question the validity of the classical normal mode assumption in conjunction with the assumption of the rigid base. Figure 7-2 compares N-S response spectra on the roof, Channel 5, for the total recorded motion with that due to rigid body motion. Obvious differences exist between the E-W and N-S directions. The N-S responses are much less distinct with overall amplification over a range of frequencies not at a single value. Also, the amplification is not as great, which obviously leads to the higher estimates of modal damping. Further evidence of the inadequacy of the normal mode assumption is the apparent difference in the identified effective modal participation factor compared to the theoretical value. Finally, the rocking base frequency and damping estimates are consistent in that the frequency is lower than the fixed base case, 4.7 Hz. vs. 5.5 Hz., and the modal damping estimate is higher, 14.7% vs. 11.6%.

An estimate of the loads induced in the structure during the Morgan Hill earthquake was made based on assumed load distributions and the measured responses. Allowable capacities were determined in accordance with ACI 349 which is currently specified for design of concrete structures by the USNRC Standard Review Plan. Ratios of induced loads to capacity (demand to capacity ratios) provide a measure of loads achieved during the event. Values greater than one suggest that the element was overstressed against the design acceptance criteria. A maximum demand to capacity ratio for structural elements resisting E-W motion was 0.75 for one of the interior walls. For N-S motion, a maximum demand to capacity ratio of about 0.25 was estimated. For the Morgan Hill earthquake, base shear coefficients were estimated to be about 0.23 and 0.10 in the E-W and N-S directions, respectively. Even though the E-W value was well in excess of the equivalent static coefficient of 0.08 considered in the original seismic design, a maximum demand to capacity ratio less than 1 was obtained. The large seismic resistance available was most likely due to the original design being intended for a larger building.

Loma Prieta Earthquake

For the Loma Prieta earthquake, the identified modal parameters are suspect due to the apparent flexibility of the base, the nonlinear behavior of the structure, and the difficulty of identifying fixed base modal parameters when the recorded response is dominated by characteristics of the combined soil-structure system. The E-W fixed base mode frequency was identified to be about 2.7 Hz. over the duration

of the event, with a very limited range from about 2.65 Hz. to 2.75 Hz. Modal damping for this mode was identified to be quite high at 17.2% for the time-invariant value and a range of about 6% to 17.3%. The rocking base frequency was approximately the same as the fixed-base value. The rocking base damping value ranged from 7% to about 8%. Figure 7-3 compares response spectra on the roof for the total recorded motion with that due to rigid body motion. It is obvious from the comparison that the total response contains strong and distinct frequency content at the identified rocking base frequency. Also, it is apparent that rigid body motion on the roof is complex in frequency content. In fact, the assumption of a rigid base may not be valid, as discussed elsewhere, and may significantly contribute to the poor performance of the modal identification process.

In the N-S direction, the fixed base mode frequency was identified to be about 4.2 Hz. for the time-invariant value with little variation over the duration. The corresponding damping value was 12.7% for the time-invariant value with, again, little variation over the event. The rocking base frequency ranged from about 3.5 Hz. to 3.9 Hz. Rocking base damping ranged from about 15% to 18%. Figure 7-4 compares response spectra on the roof, Channel 5, for the total recorded motion with that due to rigid body motion. The recorded motion shows amplification in two frequency ranges -- near 3-4 Hz. and near 7-8 Hz. The former was identified in the modal identification process with relatively high damping, which follows from the spectra. The latter is principally due to rigid body motion as, again, is evident from the figure. Hence, the complexity of the recorded motion, in conjunction with the rigid base assumption, led to the poor modal identification performance.

Loads induced in the structure during the Loma Prieta earthquake were estimated. In the E-W direction, a maximum demand to capacity ratio of about 2 was achieved in certain piers of the central E-W interior wall and the north exterior wall. A maximum demand to capacity ratio of about 1.2 was achieved in the east and west exterior walls for N-S motion. Demand to capacity ratios greater than one indicate that these walls were overstressed when compared to the conservative acceptance criteria. Only light cracking was observed in the building which demonstrates the conservatism in the current acceptance criteria.

7.1.3 Modal Identification

A well established modal identification procedure was applied to the Watsonville telephone building for the Morgan Hill and Loma Prieta earthquakes. The method estimates modal parameters by a nonlinear least squares matching of calculated and recorded response. The method can accommodate a rigid or flexible base. The effect of a flexible base is modeled by the superposition of pseudostatic and dynamic response. The effect of a rigid base is modeled by the superposition of rigid body motion and dynamic response.

In both cases, the dynamic response is modeled by classical normal modes with linear viscous damping. The method estimates all parameters necessary to solve the equations of motion in modal coordinates, i.e.,

modal frequency, damping, modal participation factors for each input degree of freedom, and mode shape components for each output degree of freedom.

Results of the modal identification procedure were discussed in Sec. 7.1.2. Behavior of the building was only understood through the interpretation of the modal identification results. Three aspects of building behavior led to difficulties, however, in identifying modal parameters -- soil-structure interaction, flexibility of the foundation, and nonlinear structure behavior.

Isolating pure structure behavior from the behavior of the soil-structure system was difficult due to the strong resonant characteristics of the coupled system. Applying the modal identification procedure to the increment in response beyond rigid body motion led to problems of numerical accuracy especially for the Loma Prieta earthquake. In essence, the precision of the recorded motions was not adequate to permit identification of the modal parameters.

Flexibility of the foundation, also, introduced some problems in the modal identification. Although it appeared that overall behavior was well modeled by the rigid base assumption, a close examination of local behavior at the base emphasized the importance of base flexibility in modeling the building. Numerous sensitivity studies were performed to better understand this aspect. In conclusion, overall behavior was modeled well by the identified modes and modal parameters. The adequacy of modeling was measured by statistical parameters and by comparing time histories and response spectra for the recorded motions with those calculated by modal analysis using the identified parameters. All measures show the fit to be reasonably good, with the fit to the Morgan Hill earthquake data better than to the Loma Prieta data. However, detailed response of the building can only be understood by taking into account the flexibility of the base.

The third aspect of building behavior which significantly affected the modal identification process was structure nonlinear behavior. It was clear from the investigation of the response of the structure that nonlinear behavior occurred during both the Morgan Hill and Loma Prieta earthquakes. It was more significant for the Loma Prieta event and significantly affected the modal identification process and the comparison of the elastic models with measured response.

7.1.4 Elastic Analysis

Two types of elastic analysis were performed differing by the dynamic models of the building. For the first, dynamic models were developed based on current criteria for shear wall structures contained in the USNRC Standard Review Plan and industry guidelines. The second type of analysis utilized dynamic models adjusted so that calculated structure frequencies and mode shapes matched those identified by modal identification.

The models were three-dimensional lumped mass models. The base was set at the ground floor. The mass characteristics of each floor were modeled by a lumped mass located at the floor center of mass. Single elements located at the story centers of horizontal rigidity modeled the horizontal, vertical, bending, and torsional stiffness between floors. Shear wall stiffnesses were treated in several ways as described in the ensuing paragraphs. In all cases, stiffness properties were based on the stiffness of the exterior and interior walls only, excluding column stiffnesses.

7.1.4.1 Current Criteria and Guidelines

Three structure models were developed based on current guidelines and industry practice for shear wall structures, i.e., the USNRC Standard Review Plan, ASCE Standard 4-86, and recent recommendations by the ASCE Dynamic Analysis Committee's (DAC) Working Group on Stiffness of Concrete Shear Wall Structures. The three models differed in their specified treatment of concrete material properties as a mechanism to incorporate reductions in stiffness observed in tests. In all cases, uncracked section properties were used and stiffness properties were generated by simple beam theory or by finite element modeling if significant openings were present in a wall. These section properties were designated best estimate.

Model 1 was the baseline model. Best estimates of concrete moduli were used for Model 1. Fixed base frequency estimates for the model were 6.29 Hz. for the lowest E-W mode, 8.55 Hz. for the lowest N-S mode, and 11.4 Hz. for the lowest torsional mode. The overall behavior was of shear and torsion in the fundamental E-W and N-S modes.

Model 2 was the upper bound stiffness model recommended by the ASCE DAC Working Group and the best estimate model recommended by ASCE Standard 4-86. It is characterized by best estimate uncracked section properties and concrete moduli based on the minimum specified concrete compressive strength. Fixed base frequency estimates were 5.72 Hz. 7.78 Hz., and 10.4 Hz. for lowest E-W, N-S, and torsional modes, respectively.

Model 3 was the lower bound stiffness model recommended by the ASCE DAC Working Group. Concrete moduli were based on one-half the best estimate values of Model 1. Fixed base frequency estimates were 4.46 Hz., 6.05 Hz., and 8.06 Hz. for lowest E-W, N-S, and torsional modes, respectively.

Differences in the three models were in frequencies only. Mode shapes were identical since the only change was a uniform change in concrete moduli. Using Model 1 as the base, the frequencies for Models 2 and 3 are approximately 0.9 and 0.7 times those of the base case.

Three measures of goodness of fit were applied to the three models: Frequencies, which are a measure of overall stiffness modeling; mode shape values which are a measure of relative stiffness modeling and structure behavior; and in-structure response, which measures the ability of the overall model (including the assumptions of the modeling

process) to estimate response. Each is discussed with respect to the two earthquakes before proceeding to a discussion of the enforced matching.

Calculated frequencies can be compared to estimated values from the modal identification procedure. For the Morgan Hill earthquake, the time invariant values were 4.0 Hz. in the E-W direction and 5.5 Hz. in the N-S direction. For the Loma Prieta earthquake, the time invariant values were 2.7 Hz. in the E-W direction and 4.2 Hz. in the N-S direction of which only the N-S mode is considered relevant.

For the Morgan Hill earthquake in the E-W and N-S directions, a comparison of model vs. identified frequencies yields the ratios of about 1.55, 1.4, and 1.1 for Models 1, 2, and 3 with respect to the identified values. All three models over-estimate the modal frequencies due to over-estimates of stiffness. Shear wall stiffnesses corresponding to the identified frequencies were, on the average, about 40%, 50%, and 80% for Models 1, 2, and 3, respectively. Recall the stress levels achieved during the Morgan Hill event -- maximum demand to capacity ratios of 0.75 in the E-W direction and 0.25 in the N-S direction. These seismic response levels are well within those for which the criteria and guidelines should apply. Coincidentally, the same frequency ratios apply to the E-W and N-S directions even though the acceleration levels in the two directions are distinctly different, with the N-S being higher. This suggests there are significant stress-independent sources of cracking, such as shrinkage and environmental effects, contributing to reductions in stiffness. Models 2 and 3 represent the ASCE DAC Working Group recommendations. Model 3 predicted frequencies about 10% higher than those identified and stiffnesses about 20% higher and is judged to be acceptably close to the identified properties, given uncertainties associated with assumptions and approximations implicit in the structure model.

The next aspect of comparison between calculated and identified modal parameters was mode shape values. The E-W mode shape values compared well, although torsion was slightly over-estimated. The N-S mode did not, with torsion opposite in direction to that obtained by modal identification. Flexibility of the foundation and some nonlinear behavior of the structure certainly affected the match.

Structure response, as measured by absolute acceleration in-structure response spectra, were also compared. These contain a component of rigid body motion and a component of dynamic response modeled by classical normal modes. Appendix C contains figures which separate these two components. The difficulties in identifying modal parameters, discussed previously, with respect to rigid body response apply here, as well.

Differences between floor response spectra corresponding to the actual recorded motions and those calculated by the analytical models vary according to the particular model, instrument location, and frequency. The calculated floor spectra generally envelope the recorded spectra at most, but not all frequencies.

7.1.4.2 Matched Models to Identified Properties

The second type of analysis was to match the identified properties to the extent possible. Adjustments were made in the models to match the identified fixed-base frequencies and mode shapes and to use the identified modal damping values in the response analysis. Mode shape values were available at the third floor and the roof only. Therefore, story stiffnesses were adjusted in pairs of stories, i.e., ground floor to the third floor, and third floor to the roof. Two revised models for each earthquake were constructed. One matched principally the overall translational response. The other attempted to match, in addition, the torsional characteristics of the response. This latter aspect, however, was not pursued beyond the model stage since a significant ingredient in the building's upper story torsion was due to flexible base behavior. Hence, this discussion focuses only on the former model.

For the Morgan Hill earthquake, based on the identified frequencies and mode shape values, a uniform change in stiffness was applied to all stories -- a reduction to 40% of the best estimate values. Mode shapes remained the same due to the uniform change in stiffness.

For the Loma Prieta earthquake, the lower two stories demonstrated a greater reduction in stiffness, i.e., to a value of approximately 20% of the best estimate value. The upper two stories experienced a stiffness reduction to 40% of the best estimate values. Hence, for this case, a change in frequency and mode shapes occurs to permit matching of the recorded data.

Before proceeding to discuss the response comparison for these matched models, the stiffness reductions should be put in perspective relative to the shear stresses induced in the walls for the two earthquakes. In general, the average story shear stresses are estimated to be in the range of 15-60 psi with the exception of the lower two stories for the Morgan Hill earthquake, E-W direction, and the Loma Prieta earthquake, N-S direction. For these latter two cases, shear stresses of approximately 125 psi were estimated. The stiffness ratios for all cases except one were in the 40-50% range. These values were consistent with published results and tend to support them. The exception is for the Loma Prieta earthquake, lower two stories , N-S direction. Identified mode shape values indicate a stiffness reduction for this case to 20% of the best estimate value. This appears to be an anomaly which may be attributed to a number of sources including the modal identification process, the method of estimating shear stress in the walls, etc. Therefore, in general, the results from this study support currently available data and criteria on shear wall stiffness reduction.

The responses to be compared are the in-structure response spectra calculated from the recorded motions. As highlighted previously when discussing model fits, these spectra are difficult to match due to the strong and somewhat erratic contributions of the rigid body motion to the total. Hence, for the present exercise, the E-W responses due to the Morgan Hill earthquake match well, whereas, the others are somewhat deficient.

7.2 Conclusions

The Watsonville telephone building was evaluated using a combination of data collection, modal identification, and elastic structural analysis. The building was evaluated for two earthquakes: The Morgan Hill earthquake of April 24, 1984 and the Loma Prieta earthquake of October 17, 1989. The building was expected to have responded in a linear or slightly nonlinear fashion for the Morgan Hill earthquake and slightly nonlinear to nonlinear for the Loma Prieta earthquake. This was verified in the study. In addition, the base of the structure was shown to behave flexibly which complicated the modal identification process.

The modal identification process was invaluable in understanding the behavior of the building. However, three aspects of the building behavior made identification of the modal parameters extremely difficult. Soil-structure system properties so dominated the overall response, especially as deformations increased, that modal frequencies and damping for the structure by itself were not always identified with confidence. Second, the flexibility of the foundation was a significant factor in understanding the behavior of the structure. Although, the modal identification process has the ability to account for this phenomenon, its application did not indicate the necessity to do so. Finally, nonlinear structure behavior had a significant impact on the results. This phenomenon is not modeled properly by the modal identification process.

The recorded building motion for the Morgan Hill earthquake were well replicated by responses calculated using the identified modal parameters. The identified parameters were reasonable and demonstrated variability during the event as emphasized below. Damping in the E-W mode is reasonable compared to other data. However, reservations persist concerning the relatively high damping value for the fundamental N-S mode and its possible connection to a relatively low modal participation factor calculated for this mode.

The high peak accelerations and structure demand to capacity ratios suggest that the building may have been loaded up to or past initial yielding during the Loma Prieta earthquake. Effective structure properties for this earthquake would be very valuable, since very little data are available at such response levels from actual low aspect ratio shear wall structures. However, significant difficulty was experienced in identifying modal parameters for the recorded Loma Prieta building motions. This difficulty stems from the flexible foundation condition and the nonlinearities expected to have occurred during the event.

Laboratory testing of low aspect ratio shear walls has generally obtained stiffnesses less than uncracked, theoretical values, even at stress levels below which cracking might be expected. This reduced stiffness has been attributed to cracking due to shrinkage, specimen handling, construction, etc. At stress levels for which representative nuclear plant structures might be designed, estimates of effective structure stiffness obtained here support the range of stiffnesses obtained by laboratory testing of low aspect ratio shear wall specimens. Thus, the stiffness data obtained in this study confirm the

applicability of test data towards the development of procedures for modeling the stiffness of nuclear plant structures. The estimated stiffnesses of the Watsonville telephone building are generally towards the lower end of ranges obtained by testing. This suggests that potential sources of greater flexibility, such as cracking due to shrinkage, temperature, settlement, etc. may be more significant to this building than laboratory specimens.

The building stiffness data generally confirm the adequacy of bounding stiffness estimates for nuclear plant structures seismic analysis recommended by the ASCE DAC Working Group on Stiffness of Concrete Shear Wall Structures. The stiffness data are slightly below the lower bound stiffness recommendations. However, this is not considered significant considering the difficulties encountered in identifying modal parameters due to the previously stated reasons.

The damping data obtained by modal identification are useful additions to the damping data base compiled for the Structure Damping Research Program.

The structure capacity evaluation obtained estimated ratios of applied loads based on elastic analysis to available capacities (demand to capacity ratios) that were significantly greater than one for the Loma Prieta earthquake. Despite the significant seismic demands, the building experienced only minor cracking in certain shear walls. These results and observations indicate that current acceptance criteria for nuclear plant structure design are appropriately conservative. These results also indicate that structure capacity evaluations for beyond design basis earthquakes should consider the additional sources of structure capacity, such as increased material and member strengths, load redistribution, etc., to obtain more realistic structure resistances against seismic loads.

In addition to the aforementioned conclusions, these data demonstrate clearly that decreases and increases in frequency occur over the duration of a single event and from event to event. These frequency shifts are a function of the excitation level and correspond to reductions in soil and structure stiffness. Linear models are, hence, valuable in an equivalent linear sense. Their parameters depend on the characteristics of the structure, including structural and non-structural features, and the load levels achieved during the event.

7.3 Recommendations

A further investigation modeling the behavior of the Watsonville telephone building is recommended. In particular, a dynamic model should be developed including, as a first step, explicit treatment of the flexible base. That is, a linear structure model that is comprised of pseudostatic modes which model the effect of the pseudostatic response due to the flexible base and normal modes that model the increase in response due to inertial effects. Dynamic response should be calculated for this case and comparisons made with recorded motions. Depending on the results, a second step is likely to be necessary and extremely valuable. This second step is to develop a model to represent

the nonlinear aspects of the response. This nonlinear model would also need to incorporate the effects of the flexible base. This additional investigation would hopefully address the differences in calculated in-structure response spectra compared to the recorded values.

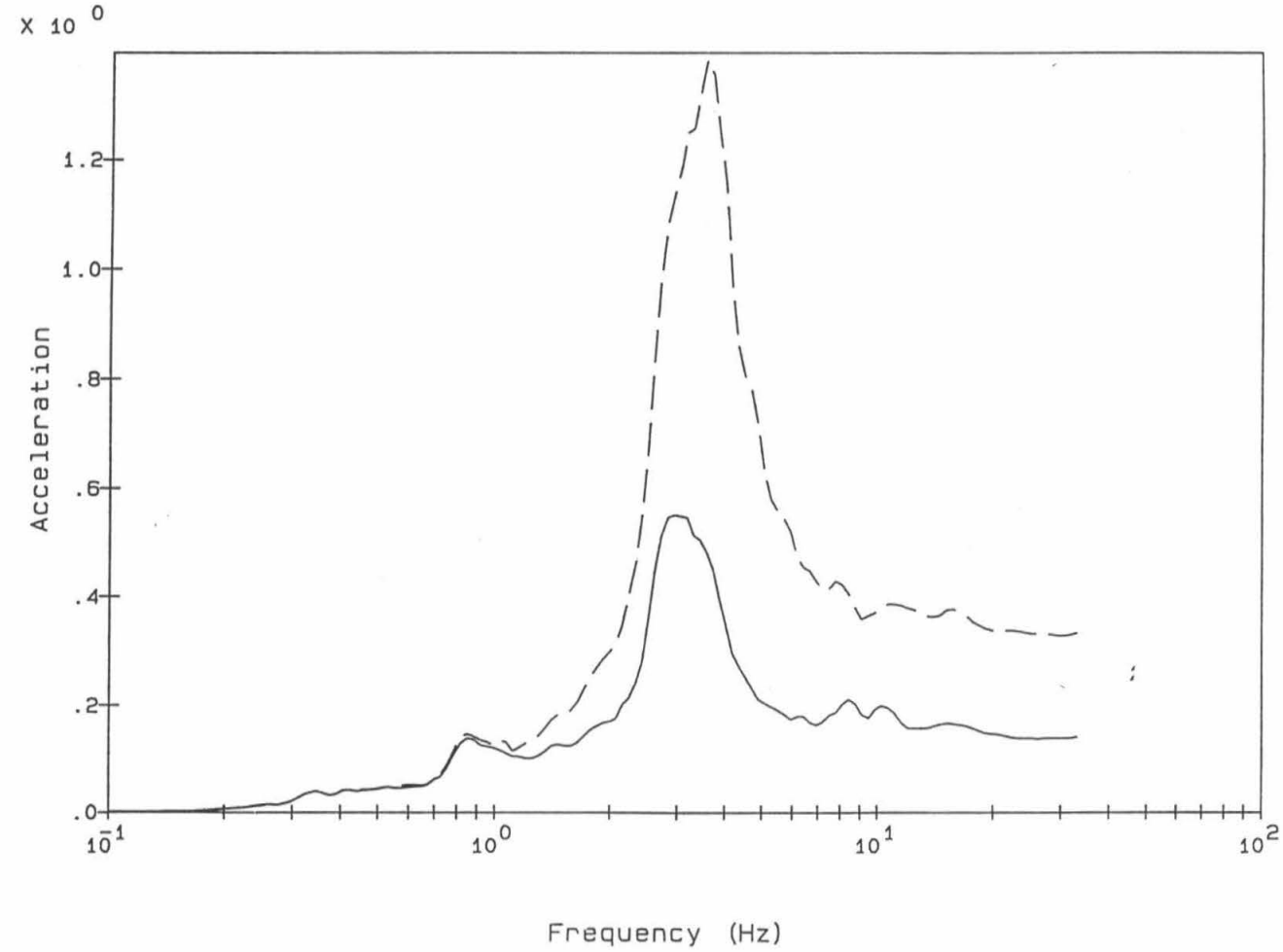

Figure 7-1: Comparison of Recorded Motion and Calculated Rigid Body Motion, Channel 11, Morgan Hill Earthquake

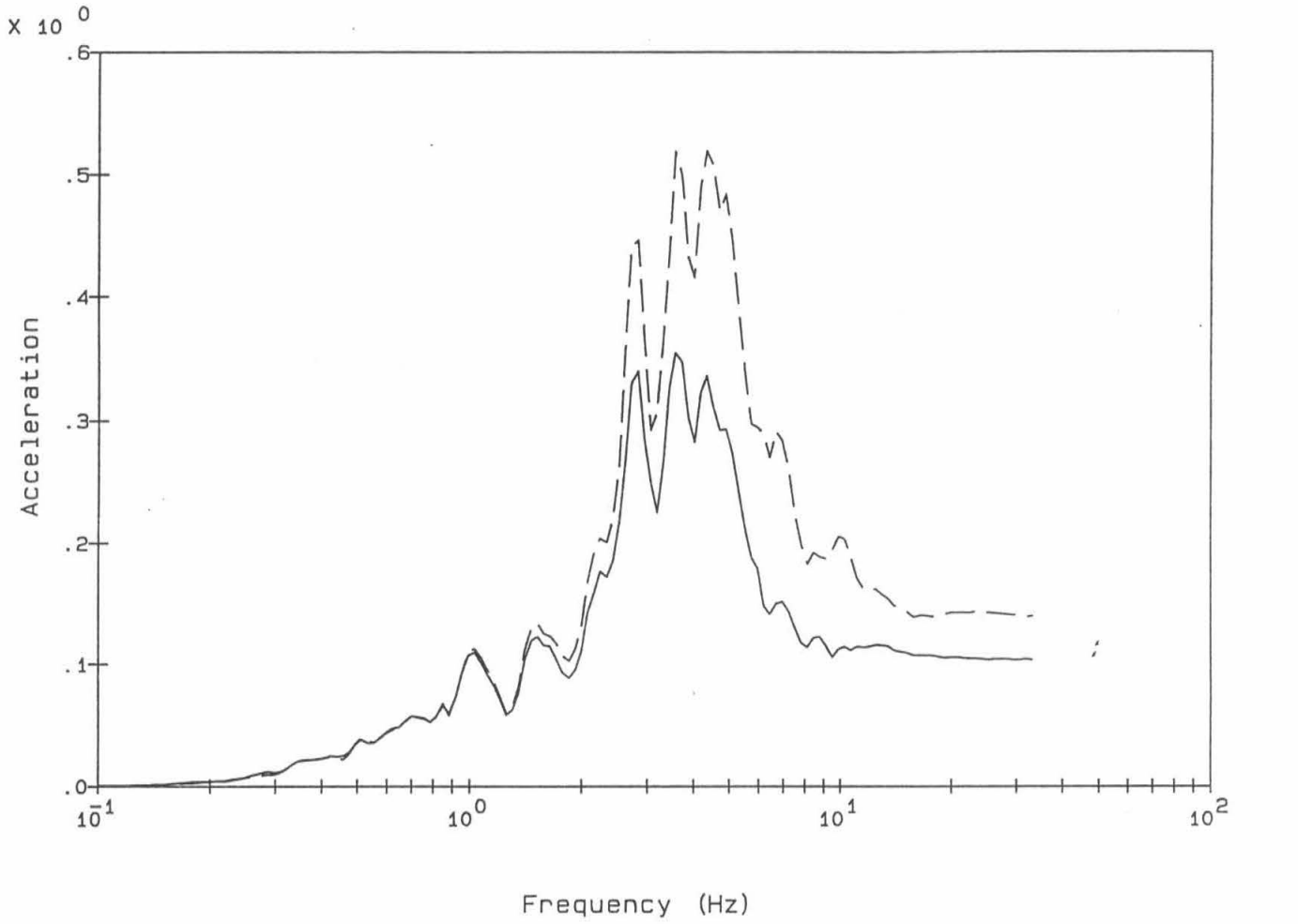

Figure 7-2: Comparison of Recorded Motion and Calculated Rigid Body Motion, Channel 5, Morgan Hill Earthquake

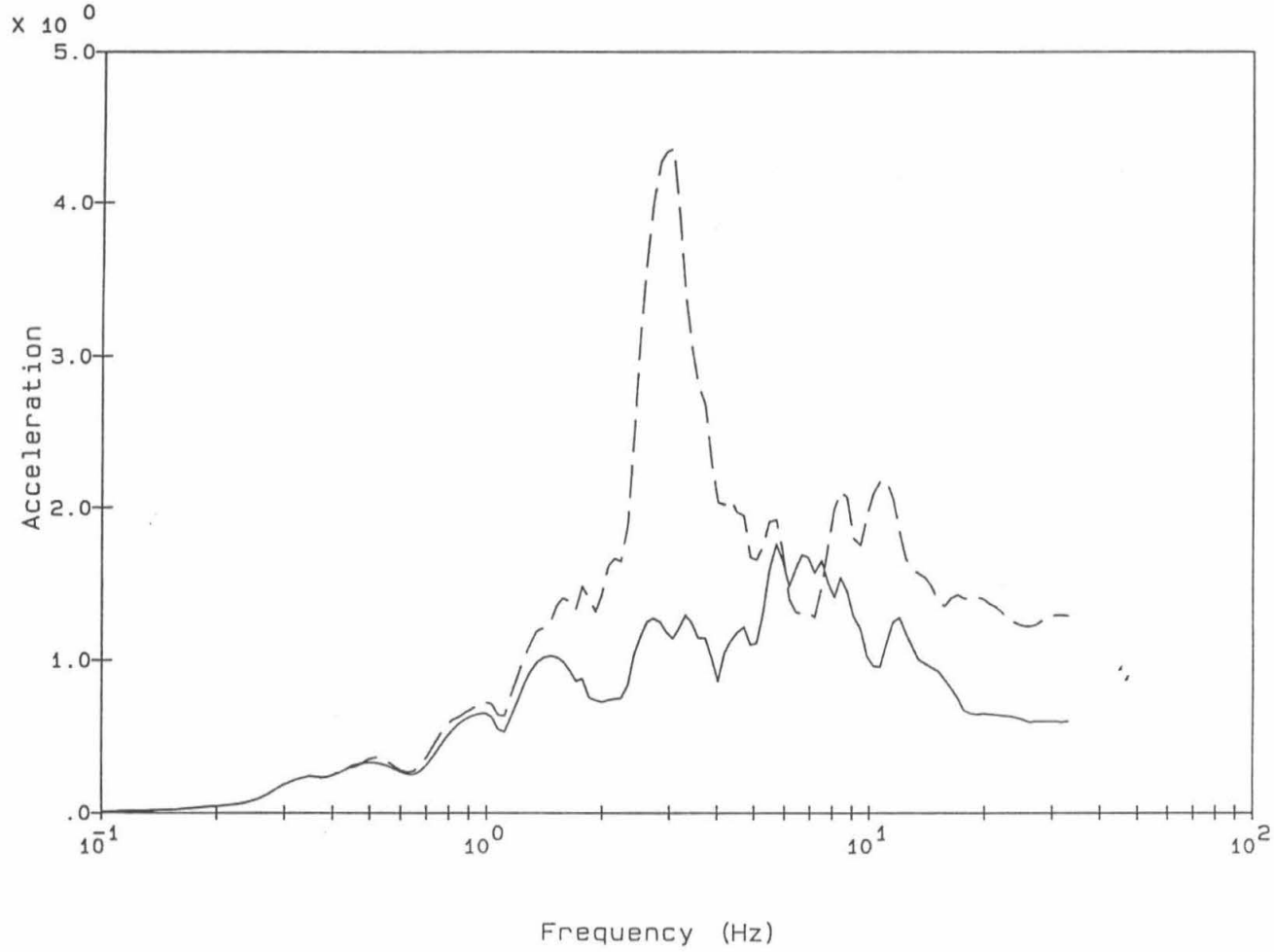

Figure 7-3: Comparison of Recorded Motion and Calculated Rigid Body Motion, Channel 11, Loma Prieta Earthquake

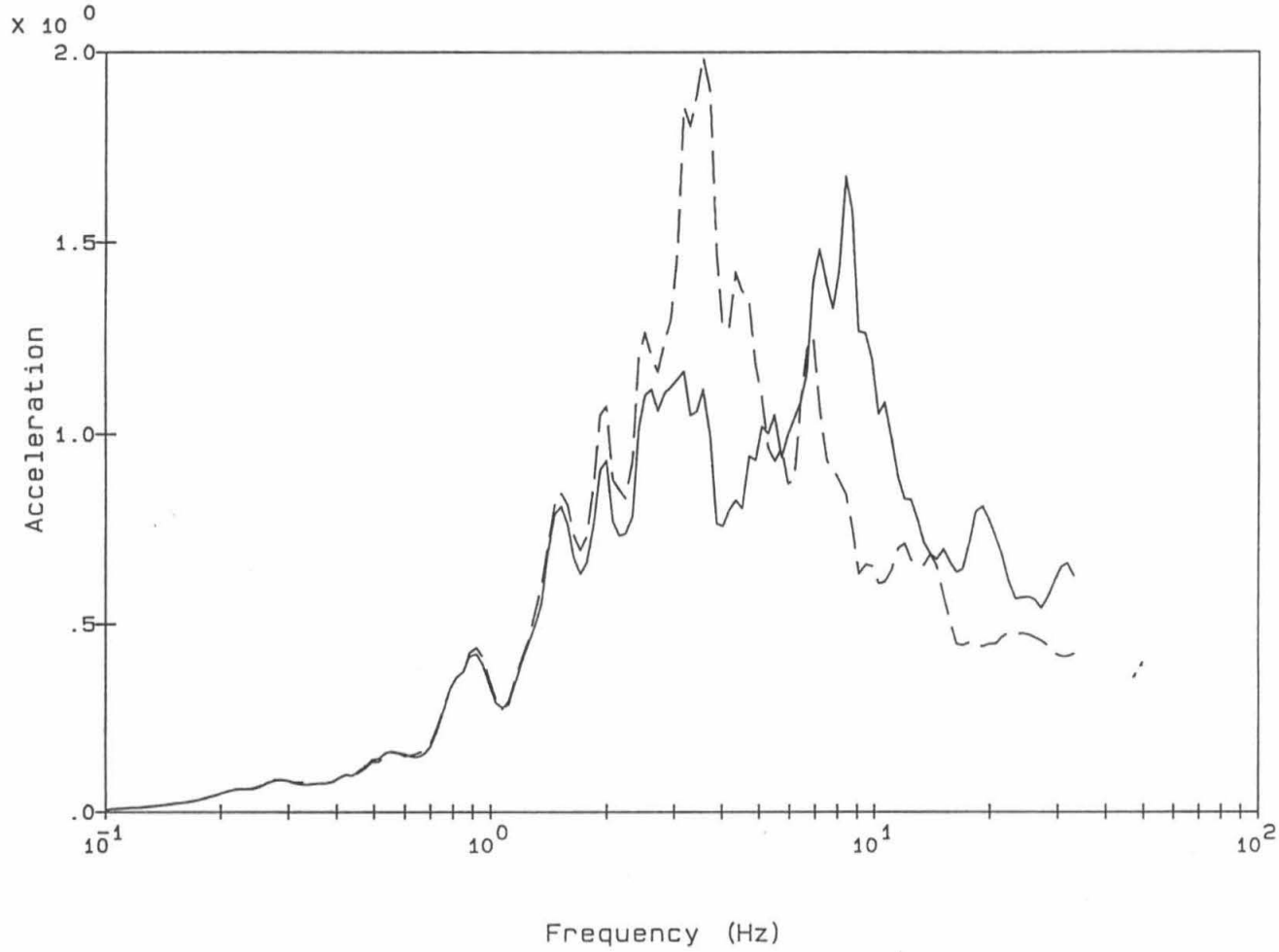

Figure 7-4: Comparison of recorded Motion and Calculated Rigid Body Motion, Channel 5, Loma Prieta Earthquake

8. REFERENCES

American Concrete Institute, "Code Requirements for Nuclear Safety Related Concrete Structures (ACI 349-85) and Commentary - ACI 349R-85," March 1986.

American Society of Civil Engineers, "Seismic Analysis of Safety-Related Nuclear Structures and Commentary on Standard for Seismic Analysis of Safety Related Nuclear Structures," ASCE Standard 4-86, September 1986.

ASCE Working Group on Stiffness of Concrete Shear Wall Structures, "Stiffness of Low Rise Reinforced Concrete Shear Walls," Draft, June, 1991.

Beck, J.L., "Determining Models of Structures From Earthquake Records," California Institute of Technology, EERL 78-01, June 1978.

Beck, J.L. and P.C. Jennings, "Structural Identification Using Linear Models and Earthquake Records," International Journal of Earthquake Engineering and Structural Dynamics, 8, pp. 145-160, April 1980.

Beck, J.L., "Statistical System Identification of Structures," Structural Safety and Reliability, American Society of Civil Engineers, pp. 1395-1402, 1990.

Beck, R.T. and J.L. Beck, "Comparison Between Transfer Function and Modal Minimization Methods for System Identification," California Institute of Technology, EERL 85-06, November 1985.

Derecho, A.T., D.M. Schultz, and M. Fintel, "Analysis and Design of Small Reinforced Concrete Buildings for Earthquake Forces," Portland Cement Association, Skokie, Illinois, 1974.

Dove, R.C., et al, "Seismic Category I Structures Program Final Report, FY 1983-84," NUREG/CR-4924, September 1987.

Electric Power Research Institute, "A Methodology for Assessment of Nuclear Power Plant Seismic Margin," EPRI NP-6041, October 1988.

Endebrock, E.G., R.C. Dove, and W.E. Dunwoody, "Analysis and Tests on Small-Scale Shear Walls, FY-82 Final Report," NUREG/CR-4274, September 1985.

Farrar, C.R. and J.G. Bennett, "An Overview of an Experimental Program for Testing Large Reinforced Concrete Shear Walls," Proceedings of the 10th Conference on Structural Mechanics in Reactor Technology, Anaheim, California, August 14-18, 1989.

Farrar, C.R. R.C. Dove and W.E. Baker, "Simulated Seismic Testing of TRG-7 Through -11," Preliminary Report, Los Alamos National Laboratory, 1991a.

Farrar, C.R. R.C. Dove and W.E. Baker, "Static and Simulated Seismic Testing of TRG-12 Through -16," Preliminary Report, Los Alamos National Laboratory, 1991b.

Farrar, C.R. and W.E. Baker, "Damping in Low Aspect Ratio Shear Wall Structures," Draft, Los Alamos National Laboratory, 1991c.

Gergely, P., "Seismic Fragility of Reinforced Concrete Structures and Components for Application to Nuclear Facilities," NUREG/CR-4123, March 1985.

Hashimoto, P.S., et al, "Review of USNRC Regulatory Guide 1.61 Structure Damping Criteria," Proceedings of the 11th Conference on Structural Mechanics in Reactor Technology, Tokyo, Japan, August, 1991.

Huang, M.J., et al, "Processed Data From the Strong-Motion Records of the Morgan Hill Earthquake of 24 April 1984, Part II. Structural-Response Records," California Department of Conservation, Division of Mines and Geology, Office of Strong Motion Studies, Report No. OSMS 85-05, December 1985.

Huang, M.J., et al, "Second Interim Set of CSMIP Processed Strong-Motion Records from the Santa Cruz Mountains (Loma Prieta) Earthquake of 17 October 1989," California Department of Conservation, Division of Mines and Geology, Office of Strong Motion Studies, Report No. OSMS 90-01, February 1990.

Kenneally, R.M. and J.J. Burns, "Experimental Investigation into the Seismic Behavior of Nuclear Power Plant Shear Wall Structures," Symposium on Current Issues Related to Nuclear Power Plant Structures, Equipment and Piping, North Carolina State University, Raleigh, North Carolina, December 1986.

Mason, A.B., J.L. Beck, J. Chen and R.R. Ullmann, "Modal Parameter Identification of an Offshore Platform From Earthquake Response Records," Proceedings of Sessions Related to Seismic Engineering at Structures Congress, American Society of Civil Engineers, pp. 271-226, May 1989.

McVerry, G.H., "Frequency Domain Identification of Structural Models from Earthquake Records," Earthquake Engineering Research Laboratory, California Institute of Technology, EERL 79-02, October 1979.

McVerry, G.H. and J.L. Beck, "Structural Identification of JPL Building 180 Using Optimally Synchoronized Earthquake Records," California Institute of Technology, EERL 83-01, August 1983.

Moehle, J.P., M.A. Sozen, and H.T. Tang, "Concrete Wall Stiffness: Calculation Vs. Measurement," Proceedings of the Third Symposium on Current Issues Related to Nuclear Power Plant Structures, Equipment and Piping, North Carolina State University, December 1990.

Murphy, L.M. (ed.), "San Fernando, California, Earthquake of February 9, 1971," U.S. Department of Commerce, National oceanic and Atmospheric Administration, 1973.

Partlow, J.G., USNRC, to All Licensees Holding Operating Licenses for Nuclear Power Reactor Facilities, Subject: Individual Plant Examination of External Events (IPEEE) for Severe Accident Vulnerabilities - 10CFR 50.54(f) (Generic Letter No. 88-20, Supplement 4), April 1, 1991.

U.S. Nuclear Regulatory Commission, Regulatory Guide 1.61, "Damping Values For Seismic Design of Nuclear Power Plants," 1973.

U.S. Nuclear Regulatory Commission, "Standard Review Plan for the Review of Safety Analysis Reports for Nuclear Power Plants - LWR Edition," USNRC Report NUREG-0800, Section 3.7.2, "Seismic System Analysis," June 1987.

U.S. Nuclear Regulatory Commission, "Procedural and Submittal Guidance for the Individual Plant Examination of External Events (IPEEE) for Severe Accident Vulnerabilities," NUREG-1407, May 1991.

Werner, S.D., J.L. Beck and M.B. Levine, "Seismic Response Evaluation of Meloland Road Overpass Using 1979 Imperial Valley Earthquake Records," International Journal of Earthquake Engineering and Structural Dynamics, 15, pp. 249-274, February 1987.

Wesley, D.A. and P.S. Hashimoto, "Seismic Structural Fragility Investigation for the Zion Nuclear Power Plant," NUREG/CR-2320, October 1981.

Wong, H.L. and J.E. Luco, "Soil-Structure Interaction: A Linear Continuum Mechanics Approach (CLASSI)," Department of Civil Engineering, University of Southern California, CE 79-03, 1980.

APPENDIX A

APPENDIX A

SUMMARY OF MODEL USED IN MODE-ID PROGRAM:

Linear modal model based on:

R modes (including pseudostatic or rigid-body "mode" if required)

N_o output degrees of freedom (displacement, velocity or acceleration)

N_i input degrees of freedom (linearly independent forces of "support" accelerations)

Response at output degrees of freedom is given by:

$$x_i(t) = \sum_{r=1}^{R} x_{ir}(t), \qquad i = 1,2,\ldots, N_o$$

where for dynamic modes, use

$$\ddot{x}_{ir} + 2\zeta_r\omega_r\dot{x}_{ir} + \omega_r^2 x_{ir} = \phi_{ir} \sum_{k=1}^{N_i} P_{rk} f_k(t)$$

with

$$x_{ir}(0) = \phi_{ir} c_r, \qquad \dot{x}_{ir}(0) = \phi_{ir} d_r, \qquad \sum_{i=1}^{N_o} \phi_{ir}^2 = 1,$$

and for pseudostatic or rigid-body "mode," use

$$\ddot{x}_{ir}(t) = \sum_{k=1}^{N_i} r_{ik} f_k(t), \qquad i = 1,2,\ldots N_o$$

Free model parameters:

For each dynamic mode:

Frequency and damping, $\{\omega r, \zeta r\}$

Modeshape components, $\{\phi_{ir}: i = 1,2,\ldots,N_o\}$

Participation factors, $\{P_{rk}: k = 1,2,\ldots,N_i\}$

Initial modal conditions, $\{c_r, d_r\}$

For pseudostatic or rigid-body "mode":

Influence matrix elements, $\{r_{ik}: i = 1,2,\ldots,N_o \; j \; k = 1,2,\ldots N_i\}$

Derived model parameters:

$\phi_{ir} \; p_{rk}: \quad r = 1,2,\ldots,R; \quad i = 1,2,\ldots,N_o; \quad k = 1,2,\ldots,N_i\}$

Effective participation factor for each mode r, each output degree of freedom i, and each input degree of freedom k.

APPENDIX B

APPENDIX B

MODAL IDENTIFICATION METHODOLOGY

The modal identification methodology implemented is described in this appendix. This material is reproduced from the following publication:

- S.D. Werner, J.L. Beck, and M.B. Levine, "Seismic Response Evaluation of Meloland Road Overpass Using 1979 Imperial Valley Earthquake Records," International Journal of Earthquake Engineering and Structural Dynamics, John Wiley & Sons, Ltd., Volume 15, pp. 249-274, February 1987.

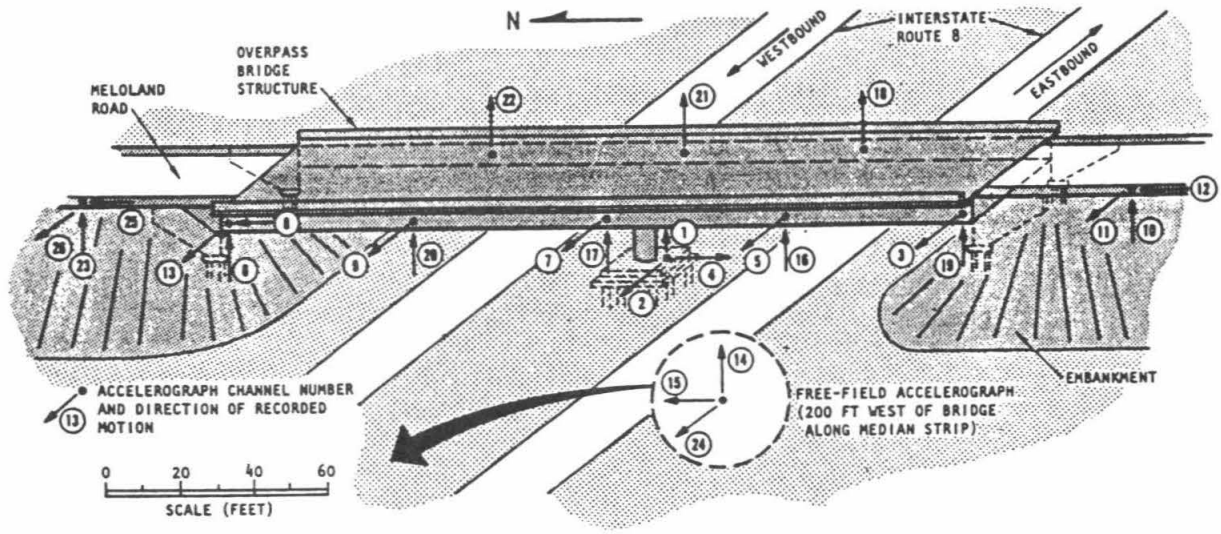

Figure 2. Meloland Road Overpass strong motion instruments

original film traces were reprocessed at the facilities of the University of Southern California. This reprocessing incorporated (1) new digitization techniques and software that were specially developed to correct the acceleration and time coordinates of the distorted traces; and (2) standard corrections for instrument frequency response and baseline adjustment.[31] The end result of this process was a set of uniformly processed time-history records, together with Fourier and response spectra from each of the 26 channels of data obtained at the MRO (e.g. Figure 4).

The recorder non-synchronization problem was identified by computing the cross correlation between several pairs of MRO acceleration records. The records that comprised each pair were typically each from a different recorder, and were measured at locations whose motions should be well correlated except for recorder-induced non-synchronization effects. Results of this assessment showed that the motion from the Channel 1-to-13 recorder consistently led the motions from the Channel 14-to-26 recorder by about 60 msec. This was corrected by an appropriate time shifting of the motions from Channels 1 to 13.

3. MODAL IDENTIFICATION METHODOLOGY

3.1. *Theoretical basis*

To evaluate the array of records measured at the MRO, a new modal identification methodology was developed. This methodology, named MODE-ID, is applicable to an elastic system with an arbitrary configuration, with classical normal modes, and with motion measurements from any number of input and system response degrees of freedom. It is also assumed that the system is initially at an at-rest position.

The MODE-ID methodology considers a system whose equations of motion are

$$[M]\{\ddot{Y}\}+[C]\{\dot{Y}\}+[K]\{Y\}=-[C_{sf}]\{\dot{Z}\}-[K_{sf}]\{Z\} \tag{1}$$

where

$[M], [C], [K]$ = mass, damping and stiffness matrices of the system
$\{Y\}$ = vector of motions at N system degrees of freedom
$\{Z\}$ = vector of input (support or 'foundation') motions at NS degrees of freedom
$[C_{sf}], [K_{sf}]$ = damping and stiffness matrices that couple the system and 'foundation' response.

Following procedures described by Clough and Penzien,[36] the acceleration of the system is expressed as

$$\{\ddot{Y}\}=\{\ddot{S}\}+\{\ddot{X}\} \tag{2}$$

where $\{\ddot{S}\}$ and $\{\ddot{X}\}$ are the pseudostatic and dynamic components of acceleration respectively. In this, the pseudostatic component represents the 'static' contributions of the individual support motions to the system response (neglecting inertial and damping effects), and can be visualized as a time-dependent 'reference' position of the structure whose deformed shape at each instant of time is dependent on the instantaneous position of the structure's supports. This pseudostatic response is expressed as

$$\{\ddot{S}\} = [\tilde{R}]\{\ddot{Z}\} \tag{3}$$

where $[\tilde{R}]$ is the pseudostatic matrix, given as

$$[\tilde{R}] = -[K]^{-1}[K_{sf}] \tag{4}$$

The dynamic component shown in equation (2) represents the contributions of the system's fixed-base modal vibrations about its pseudostatic reference position. The equations of motion for the dynamic response component are obtained by substituting equations (2) to (4) into equation (1) and neglecting the contributions of damping to the effective earthquake forces.[36] These equations take the form

$$[M]\{\ddot{X}\} + [C]\{\dot{X}\} + [K]\{X\} = -[M][\tilde{R}]\{\ddot{Z}\} \tag{5}$$

In order to get a realistic spatially discrete model for the bridge of the form described in equations (1) to (5), the total number, N, of structural degrees of freedom would normally be chosen to be much greater than the number, NR, of structural degrees of freedom at which the response is actually measured. As a consequence, it is not possible to determine uniquely the elements of the stiffness and damping matrices from the measured seismic excitation and response, even if the mass matrix is assumed known.[37] Instead, an identifiable model in which the parameters are uniquely specified by knowing the excitation and response may be derived by assuming classical modes of vibration, as presented in the following discussion.

Let s_i and x_i, $i = 1, 2, \ldots, NR$, denote the pseudostatic and dynamic components of the response at the NR degrees of freedom at which the system response is measured. The pseudostatic components s_i can be obtained from equation (3) using an $NR \times NS$ submatrix $[R]$ of the full $N \times NS$ pseudostatic matrix $[\tilde{R}]$. Also, the dynamic components x_i can be expressed as the superposition of the contributions of NM modes of vibration of the system which are significantly excited by the earthquake ($NM \ll N$). This is expressed mathematically as

$$x_i(t) = \sum_{r=1}^{NM} x_{ir}(t) \tag{6}$$

where x_{ir} is the rth mode response of the system at its ith degree of freedom. From a modal decomposition of equation (5) that incorporates orthogonality of the mode shapes, it can be shown that the modal contributions x_{ir}, $i = 1, 2, \ldots, NR$, satisfy the equation:

$$\{\ddot{x}_{ir}\} + a_r\{\dot{x}_{ir}\} + b_r\{x_{ir}\} = -[P^{(r)}]\{\ddot{Z}\} \tag{7}$$

where

$a_r = 2\zeta_r\omega_r$

$b_r = \omega_r^2$

ζ_r, ω_r = damping ratio and natural frequency respectively of the rth mode,

and $[P^{(r)}]$, the effective participation factor matrix for the rth mode, is expressed as

$$[P^{(r)}] = [p_{ij}^{(r)}] = \begin{bmatrix} \phi_{1r}\gamma_{r1} & \phi_{1r}\gamma_{r2} & \cdots & \phi_{1r}\gamma_{r,NS} \\ \phi_{2r}\gamma_{r1} & \phi_{2r}\gamma_{r2} & \cdots & \phi_{2r}\gamma_{r,NS} \\ \vdots & \vdots & & \vdots \\ \phi_{NR,r}\gamma_{r1} & \phi_{NR,r}\gamma_{r2} & \cdots & \phi_{NR,r}\gamma_{r,NS} \end{bmatrix} \tag{8}$$

In this, ϕ_{ir} is the mode shape amplitude of the rth mode at the ith degree of freedom ($i = 1,2, \ldots, NR$), and γ_{rj} is the conventional participation factor of the rth mode for the jth support degree of freedom ($j = 1,2, \ldots, NS$).

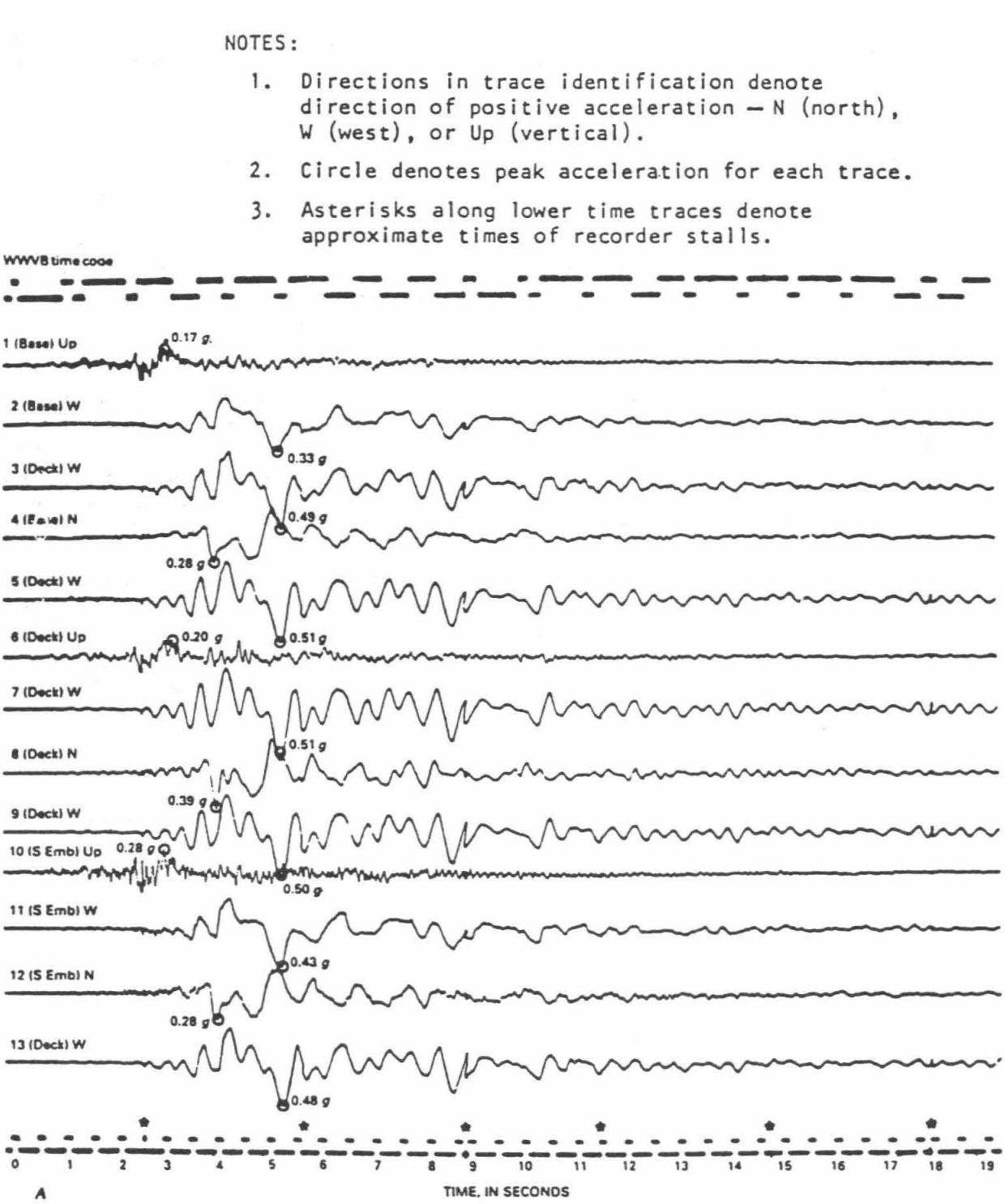

Figure 3 (a). Accelerograms from Channels 1 to 13 obtained at MRO during 1979 Imperial Valley earthquake.

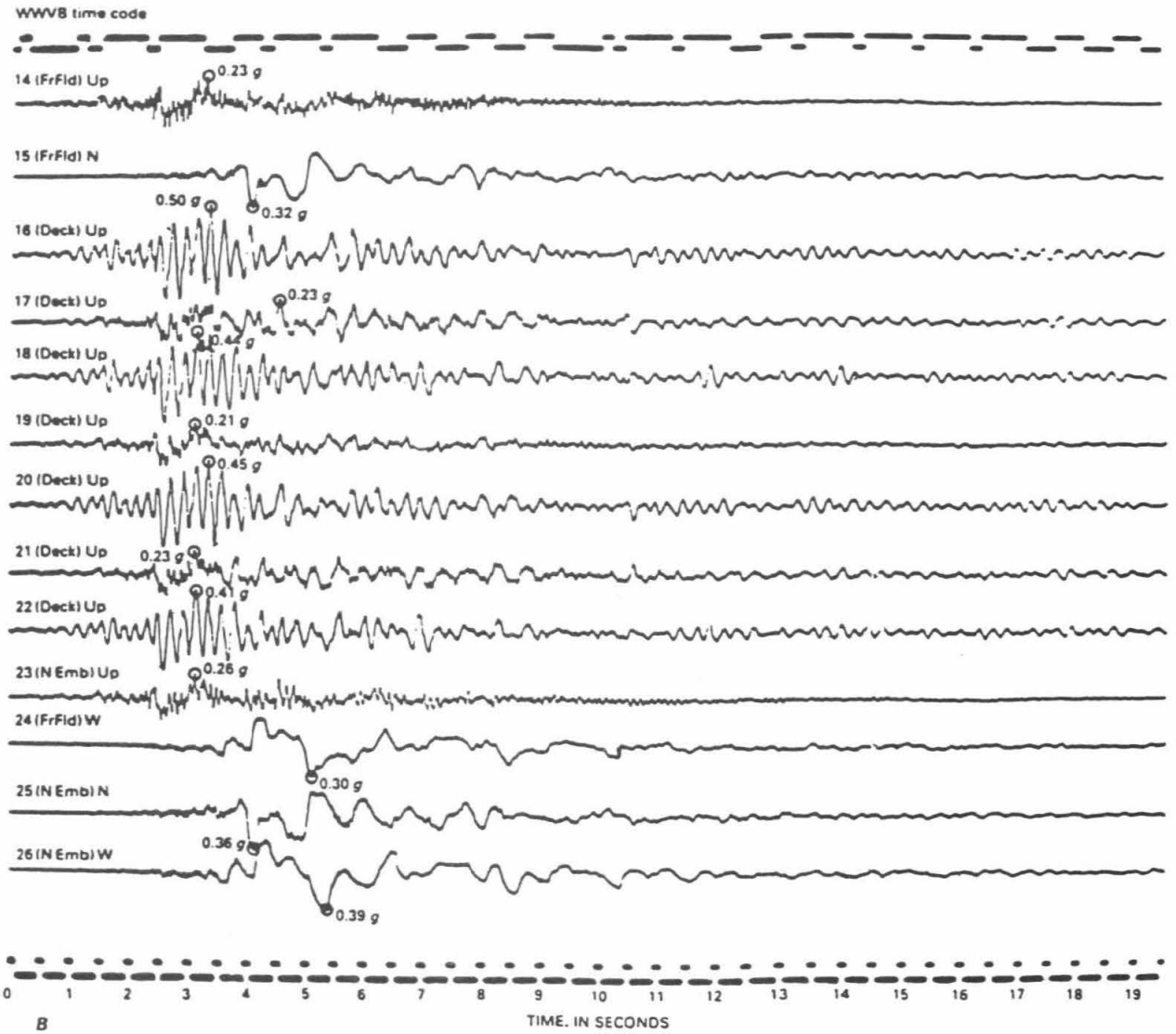

Figure 3 (b). Accelerograms from Channels 14 to 26 obtained at MRO during 1979 Imperial Valley earthquake.

The γ_{rj} are elements of the matrix.

$$[\Gamma] = [\gamma_{rj}] = [\phi]^{\mathrm{T}}[M][\tilde{R}] \tag{9}$$

where $[\phi] = [\phi_{ir}]$ is the mode shape matrix. It is seen from equation (8) that the jth column of $[P^{(r)}]$ contains the common factor γ_{rj}. Therefore, once $[P^{(r)}]$ is obtained, the mode shape for the rth mode can in theory be readily calculated as the ratio of the elements in each row of any of the columns of $[P^{(r)}]$. However, these calculations are ill-conditioned when the various support motions are nearly identical, which is the case for the MRO.[31] Therefore, for such conditions, it is more desirable to obtain the mode shape from the ratios of sums of the rows of $[P^{(r)}]$. This ill-conditioning is discussed further in Section 3.3.

3.2. *Identification procedure*

The above discussion shows that the pseudostatic matrix $[R]$, and the normal mode parameters a_r, b_r and $[P^{(r)}]$, $(r = 1, 2, \ldots, NM)$ represent the complete set of parameters needed to fully characterize the system's response as its measured degrees of freedom when it is subjected to the measured input motions. In MODE-ID, an optimization procedure is applied to estimate these parameters, in which the following error function is

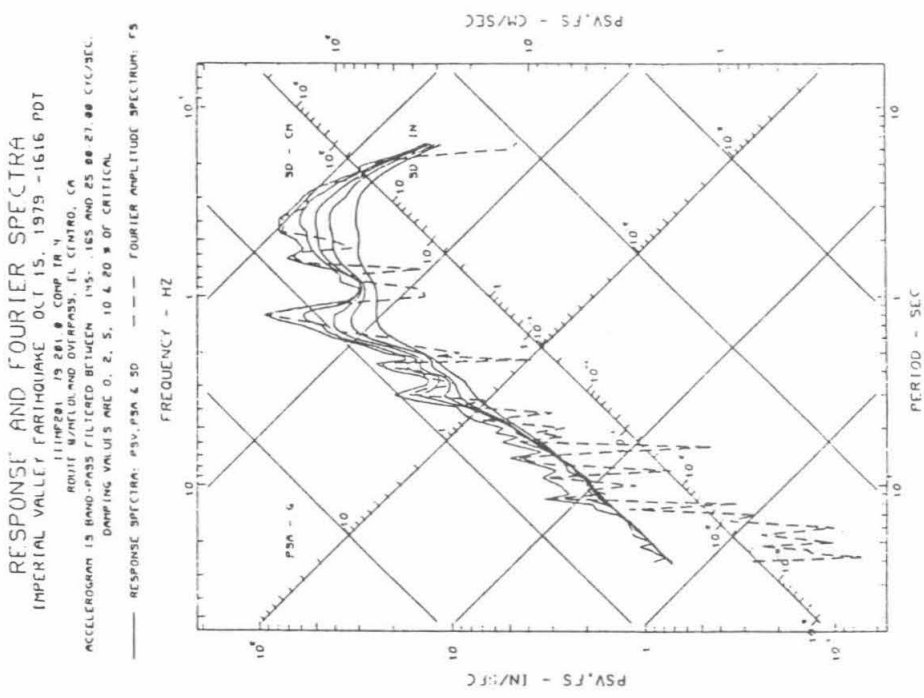

(b) Fourier and response spectra

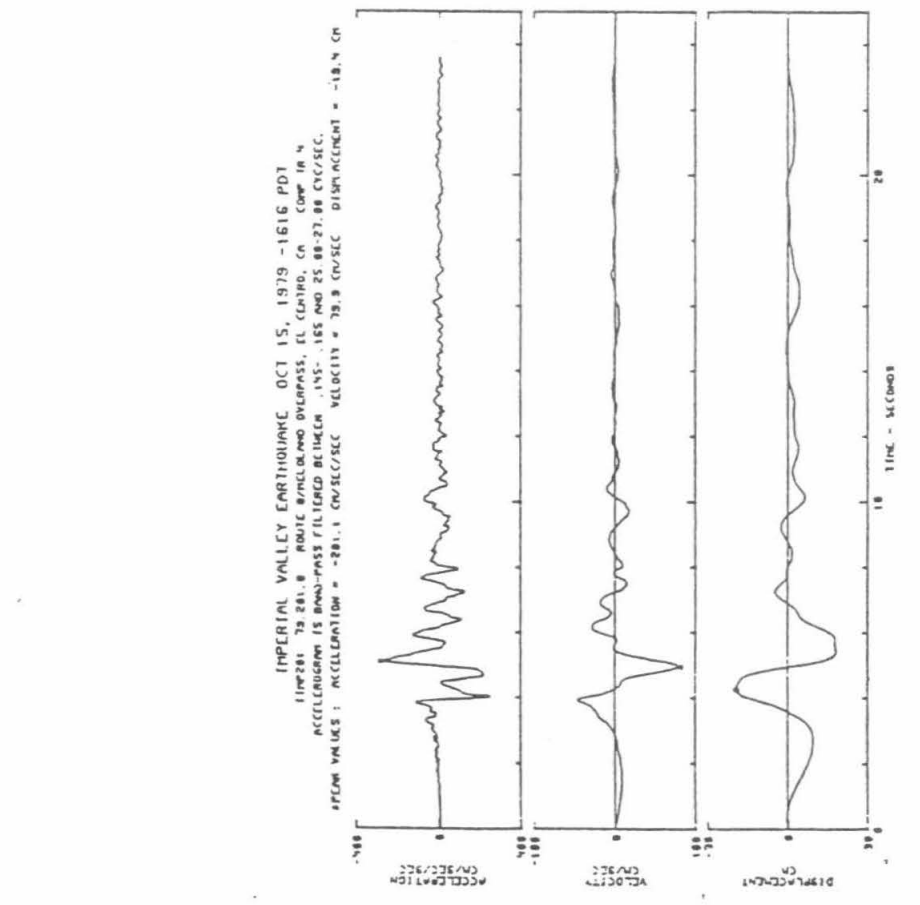

(a) Corrected time histories

Figure 4. Example of reprocessed data incorporating corrections for recorder stall effects (for Channel 4)

minimized:

$$J(\theta) = \frac{1}{V} \sum_{i=1}^{NR} \sum_{n=0}^{NT} [\ddot{w}_i(n\Delta t) - \ddot{y}_i(n\Delta t; \theta)]^2 \tag{10}$$

where

$\ddot{w}_i, \ddot{y}_i$ = measured acceleration and model acceleration at the ith measured response degree of freedom
Δt = sample interval of the digitized accelerograms
NT = total number of time samples (at interval Δt)
θ = modal parameters to be estimated
$= \{[R]; a_r, b_r, [P^{(r)}]: r = 1, 2, \ldots, NM\}$

and V is a normalizing factor given by

$$V = \sum_{i=1}^{NR} \sum_{n=0}^{NT} \ddot{w}_i^2(n\Delta t) \tag{11}$$

Therefore, J may be interpreted as the ratio of the mean-square error in the model acceleration to the mean-square of the measured acceleration.

The minimization of J with respect to the model parameters is implemented in MODE-ID using an iterative algorithm that is an adaptation of the modal-minimization method developed by Beck.[37] This algorithm consists of a series of modal sweeps in which, during each sweep, the estimates of the elements of the pseudostatic matrix $[R]$ are first updated by minimizing J with respect to these elements only. Then, the estimates of the parameters of each mode $(a_r, b_r, [P^{(r)}])$ are successively updated by a series of single-mode minimizations of J. This minimization for each mode actually corresponds to least-squares matching of a modified measured response in which the contributions of the pseudostatic response and the other modes are subtracted out; these contributions are computed from the new parameter estimates for those modes already treated in the sweep, and from the prior parameter estimates for those modes not yet treated. A single sweep is completed when the pseudostatic response and all significant modes have been treated in this manner. Successive modal sweeps are performed until the fractional decrease in J is less than a prescribed value, or until a prescribed maximum number of modal sweeps has been completed.

Usually only the first one or two of the strongest excited modes selected from the Fourier amplitude spectra of the records are initially included in the optimization process. Additional modes are then added, one at a time, by choosing appropriate initial estimates for the natural frequency and the damping ratio. Successive optimizations are performed until it is judged that all modes that significantly affect the response have been included. The modes are added successively in this manner so that it is easier to observe whether or not a mode has a significant effect on the match of the measured response.

In performing the minimization of J for each mode, the effective participation factors $p_{ij}^{(r)}$ ($i = 1, 2, \ldots, NR$; $j = 1, 2, \ldots, NS$) are treated as being independent. This is not strictly correct since certain auxiliary conditions must be satisfied.[31] For example, the mode shapes derived from the effective participation factor matrices should satisfy the orthogonality conditions. These auxiliary conditions on the $p_{ij}^{(r)}$ are not enforced since they involve the complete mode shape and pseudostatic matrices, whereas only those submatrices corresponding to the measured response degrees of freedom are actually estimated from the data. Therefore, the model used in the identification process may be viewed as being more general than the classical normal mode model described above. However, if the assumptions inherent in a classical normal mode model are sufficiently accurate, then the auxiliary conditions should be satisfied automatically by the estimated $p_{ij}^{(r)}$.

3.3. *Effects of nearly identical support motions*

The development provided in Sections 3.1 and 3.2 applies to the general case of any arbitrary input motions measured at each of the NS support degrees of freedom of the system. However, inspection of Figure 3 shows that the recorded 'support' motions of the MRO at the abutments, embankments and pier base in a given direction are nearly the same. Therefore, it is appropriate to consider the equations of motion for the limiting case where the support motions in a given direction are identical.

The vector of support accelerations may be expressed in this 'rigid-base' case as

$$\{\ddot{Z}(t)\} = \ddot{z}_T(t)\{I_T\} + \ddot{z}_V(t)\{I_V\} \tag{12}$$

where $\ddot{z}_T$ and $\ddot{z}_V$ are the common accelerations of the transverse and vertical support degrees of freedom respectively; $\{I_T\}$ is an $NS \times 1$ vector whose elements are unity and zero corresponding respectively to transverse and vertical support degrees of freedom; and $\{I_V\}$ is an $NS \times 1$ vector whose elements are unity and zero corresponding respectively to vertical and transverse support degrees of freedom.

Using equation (12), equation (3) becomes

$$\{\ddot{S}(t)\} = [\tilde{R}]\{I_T\}\ddot{z}_T(t) + [\tilde{R}]\{I_V\}\ddot{z}_V(t) \tag{13}$$

showing that the pseudostatic response is controlled by the two $N \times 1$ vectors

$$\{s_T\} = [\tilde{R}]\{I_T\}$$

$$\text{and} \qquad \{s_V\} = [\tilde{R}]\{I_V\} \tag{14}$$

and not by the values of the individual elements of the pseudostatic matrix $[\tilde{R}]$. From equation (14), each element of the vectors $\{s_T\}$ and $\{s_V\}$ is equal to the sum of the elements in the corresponding row of $[\tilde{R}]$, summed over the transverse and vertical support degrees of freedom respectively. Furthermore, because $\{s_T\}$ represents the system's static response to unit rigid-body translation in the transverse direction, its elements are unity and zero, corresponding respectively to transverse and vertical response degrees of freedom. Similarly, since $\{s_V\}$ represents the system's static response to unit vertical rigid-body translation, its elements are unity and zero, corresponding respectively to vertical and transverse response degrees of freedom.

In a similar manner, substituting equation (12) into the right-hand side of equation (7) leads to

$$-[P^{(r)}]\{\ddot{Z}\} = -[P^{(r)}]\{I_T\}\ddot{z}_T - [P^{(r)}]\{I_V\}\ddot{z}_V \tag{15}$$

showing that the excitation of the rth mode contribution to the system's dynamic response is controlled by the two $NR \times 1$ vectors

$$\{p_T^{(r)}\} = [P^{(r)}]\{I_T\}$$

$$\text{and} \qquad \{p_V^{(r)}\} = [P^{(r)}]\{I_V\} \tag{16}$$

and not by the values of the individual elements of the effective participation factor matrix $[P^{(r)}]$. From equation (16), each element of the vectors $\{p_T^{(r)}\}$ and $\{p_V^{(r)}\}$ is equal to the sum of the elements in the corresponding row of $[P^{(r)}]$, summed over the transverse and vertical support degrees of freedom respectively. From this, it can be shown that

$$\{p_T^{(r)}\} = \gamma_T^{(r)}\{\phi^{(r)}\}$$

$$\text{and} \qquad \{p_V^{(r)}\} = \gamma_V^{(r)}\{\phi^{(r)}\} \tag{17}$$

where $\{\phi^{(r)}\}$ is the $NR \times 1$ mode shape vector of the rth mode for the measured response degrees of freedom, and the scalars $\gamma_T^{(r)}$ and $\gamma_V^{(r)}$ are the conventional rigid-base participation factor for the rth mode in the transverse and vertical directions respectively.

The above discussion shows that the parameters controlling the response of the model when the support motions in a given direction are identical are $\{s_T\}$, $\{s_V\}$ and the parameters $\{p_T^{(r)}\}$, $\{p_V^{(r)}\}$, ω_r and ζ_r for each mode. It follows that it is only these parameters which can be determined uniquely during the application of system identification, using the measured common support motions $\ddot{z}_T$ and $\ddot{z}_V$ together with the measured response. The individual elements of the matrices $[R]$ and $[P^{(r)}]$ are not identifiable. If the support motions in each direction are nearly identical, as in the MRO, then the elements of these matrices might be identifiable in theory, but in practice the estimation process is ill-conditioned because of the presence of measurement noise and model error. The aforementioned parameters controlling the model response should, however, still be reliably estimated.

In view of this ill-conditioning, the mode shapes for MRO were evaluated using equations (16) and (17), that is, the elements in each row of the identified effective participation factor matrix were summed over the transverse and vertical support degrees of freedom separately. This gave the transverse and vertical components respectively of the scaled mode shape vector. Also, the elements in each row of the identified pseudostatic matrix were summed over the transverse and vertical support degrees of freedom separately to compute the vectors $\{s_T\}$ and $\{s_V\}$ in equations (14). These vectors were then checked to assure that their elements were close to the theoretical values of zero or unity.

As a final remark, if MODE-ID were applied to a long bridge with markedly different support motions because of travelling wave effects, then the above ill-conditioning would not occur. In this case, the individual elements of $[R]$ and $[P^{(r)}]$ should be estimated reliably by MODE-ID.

4. OVERVIEW OF SEISMIC EVALUATION PROCESS

The evaluation of the MRO's seismic response was comprised of two main steps which involved (1) initial assessment of the MRO's modal and seismic response characteristics; and (2) application of MODE-ID to arrays of the MRO's measured strong-motion records. In performing these steps, sound judgment is an essential element in the proper application of the system identification methodology. The steps are described more fully by Werner *et al.*[31].

4.1. *Initial assessment process*

An initial assessment of the MRO's seismic response characteristics is essential for initializing the MODE-ID applications and for aiding in the interpretation of their results. This process involved the steps outlined below.

Evaluation of earthquake records. A detailed examination of each of the measured time-history records and Fourier amplitude spectra at the MRO was an important first step in this process. A comparison of the peak amplitudes, time variations and Fourier amplitude spectra of the motions recorded at the various instrument locations indicated such basic response characteristics as (1) the extent of any soil/structure interaction at the bridge abutments and at the base of the central pier; (2) the effects of the embankments on the motions transmitted to the bridge abutments during the earthquake; (3) the degree of amplification of the deck motions relative to the abutment motions, and the frequency range over which these amplifications took place; and (4) likely values of natural frequencies of significant modes of vibration.

Transfer functions from Fourier spectra. Another initialization process involved computation of 'transfer functions' derived as ratios of Fourier spectra of various sets of single response channels and input channels. This provided initial estimates of bridge modes by identifying those frequencies where, for several different combinations of input and response channels, the amplitudes of the transfer functions consistently exhibited a prominent peak and their phase angles consistently exhibited a 180° phase shift.

Sensitivity studies from analytical models. Bounds on modal characteristics of the MRO were obtained from the use of simple analytical models of the bridge to compute mode shapes and frequencies. These computations were carried out as sensitivity studies in which reasonable variations of the model stiffness and mass parameters were considered, and mode shapes and frequencies were computed for each set of parameters.

Single-input/single-output modal identification. A single-input/single-output version of MODE-ID, named IDSISO, was also employed to estimate modes of the MRO. Since only a single input motion was used, IDSISO is strictly applicable only if all support motions are identical (i.e. if 'rigid base' conditions apply). Nevertheless, IDSISO represented a numerically efficient means of obtaining approximate estimates of the natural frequencies of the various normal modes of the MRO. This was particularly true because of the relatively short length and the geometric symmetry of the MRO, which resulted in the motions at its various supports being reasonably similar.

REFERENCES

1. T. Iwasaki and R. Hagiwara, 'Dynamic response analysis of Shizunai bridge, damaged by the Urakawa-Oki earthquake', *Proc. 15th joint meet. US–Japan panel wind seismic eff.* Tsukuba, Japan, (1983).
2. P. C. Jennings (Ed.), 'Earthquake engineering and hazards reduction in China', *SCSPRC Report No. 8*, National Academy of Sciences, Washington, D.C., 1980.
3. P. C. Jennings and J. H. Wood, 'Earthquake damage to freeway structures', Engineering Features of the San Fernando earthquake, February 9, 1971, *Report No. EERL 71–02*, California Institute of Technology, Pasadena, CA, 1971. Chapter 6. pp. 366–433.
4. R. K. Miller and S. F. Felszeghy, 'Engineering features of the Santa Barbara earthquake of August 13, 1978', *Report No. UCSB-ME-78-2*, University of California, Santa Barbara, CA, 1978.
5. G. C. Sturman, 'The Alaska railroad', *The Great Alaska Earthquake of 1964, Engineering*, National Academy of Sciences, Washington, D.C., 1973. pp. 958–986.
6. G. C. Sturman, 'The Alaska highway system', *The Great Alaska Earthquake of 1964, Engineering*, National Academy of Sciences, Washington, D.C., 1973, pp. 987–1009.
7. P. I. Yanev (Ed.), 'Miyagi-Ken-Oki, Japan earthquake, June 12, 1978', Earthquake Engindering Research Institute, Berkeley, CA, 1978.
8. J. H. Gates, 'California's seismic design criteria for bridges', *J. struct. div. ASCE* **102**, 2301–2314 (1976).
9. J. H. Gates, 'Factors considered in the development of the California seismic design criteria for bridges', *Proc. workshop earthquake resist. highway bridges* San Diego, Applied Technology Council, 141–162 (1979).
10. Applied Technology Council, 'Seismic design guidelines for highway bridges', *Report No. FHWA/RD-81/081*, Palo Alto, CA, 1981.
11. Applied Technology Council, 'Seismic retrofitting guidelines for highway bridges', *Report No. FHWA/RD-83/007*, Palo Alto, CA, 1983.
12. American Association of State Highway and Transportation Officials (AASHTO), 'Guide specifications for seismic design of highway bridges', Washington, D.C., 1983.
13. T. Iwasaki, J. Penzien and R. W. Clough, 'Literature survey—seismic effects on highway bridges', *Report No. EERC 72-11*, Earthquake Engineering Research Center, University of California, Berkeley, CA, 1972.
14. Public Works Research Institute, 'A case history of bridge performance during earthquakes in Japan', *Proc. int. conf. case hist. geotech. eng.* St. Louis, MO, (1984).
15. O. H. Degenkolb and P. Jurach, 'Highway and bridge damage, Imperial Valley earthquake of October 15, 1979', *Reconnaissance Report, Imperial County, California Earthquake, October 15, 1979* (Ed. D. J. Leeds), Earthquake Engineering Research Institute, Berkeley, CA, 1980.
16. S. D. Werner *et al.*, 'Effects of traveling seismic waves on the response of bridges', *Proc. workshop earthquake resist. highway bridges*, San Diego, Applied Technology Council, (1979).
17. R. A. Imbsen, 'Implementation of the analytical capabilities required for the aseismic design of bridges', *Proc. US–Japan bridge workshop* Tsukuba, Japan. (1984).
18. W. S. Tseng and J. Penzien, 'Analytical investigations of the seismic response of long multiple span highway bridges', *Report No. EERC 73-12*, Earthquake Engineering Research Center, University of California, Berkeley, CA, 1973.
19. M. Chen and J. Penzien, 'Soil/structure interaction of short highway bridges', *Proc. workshop earthquake resist. highway bridges*, San Diego, Applied Technology Council, (1979).
20. L. G. Selna, 'Box girder bridge hinge restrainer program', *Proc. US–Japan bridge workshop* Tsukuba, Japan (1984).
21. H. S. Lew 'NBS large scale seismic testing program', *Proc. US–Japan bridge workshop* Tsukuba, Japan (1984).
22. R. J. T. Park *et al.*, 'The seismic performance of steel-encased reinforced concrete bridge piles', *Proc. 8th world conf. earthquake eng.* San Francisco **VI**, 897–904, (1984).
23. W. C. Godden, 'Seismic model studies of long-span curved bridges', *Proc. workshop earthquake resist. highway bridges* San Diego, Applied Technology Council (1979).
24. A. M. Abdel-Ghaffar *et al.*, 'Analysis of the dynamic characteristics of the Golden Gate Bridge by ambient vibration measurements', *Report No. SM-83-8*, Princeton University, Princeton, NJ, 1983.
25. J. H. Gates and M. J. Smith, 'Verification of dynamic modeling methods by prototype excitation', *Report No. FHWA/CA/SD-82/07*, California Department of Transportation, Office of Structures Design, Sacramento, CA, 1982.
26. B. M. Douglas and G. M. Norris, 'Bridge dynamic test implications for seismic design', *J. tech. topics civil eng. ASCE* **109**, 1–22 (1983).
27. B. M. Douglas and W. H. Reid, 'Dynamic tests and system identification of bridges', *J. struct. div. ASCE* **108**, 2295–2312 (1982).
28. J. C. Wilson, 'Analysis of the observed earthquake response of a multiple span bridge', *Report No. EERL 84-01*, Earthquake Engineering Research Laboratory, California Institute of Technology, Pasadena, CA, 1984.
29. J. D. Raggett and C. Rojahn, 'Use and interpretation of strong motion records from highway bridges', *Report No. FHWA-RD-78-158*, U.S. Geological Survey, Menlo Park, CA, 1978.
30. C. Rojahn and J. D. Raggett, 'Guidelines for strong-motion instrumentation of highway bridges', *Report No. FHWA-RD-78-158*, U.S. Geological Survey, Menlo Park, CA, 1981.
31. S. D. Werner *et al.*, 'Seismic response characteristics of Meloland Road Overpass during 1979 Imperial Valley earthquake', *Report No. R-8222-5603*, Agbabian Associates, El Segundo, CA, 1985.
32. J. N. Brune *et al.*, 'Strong motion data recorded in Mexico during the main shock', *The Imperial Valley California Earthquake of October 15, 1979, Geological Survey Professional Paper 1254*, Washington, D.C., 1982, pp. 319–350.
33. R. D. McJunkin and J. T. Ragsdale, 'Compilation of strong-motion records and preliminary data from the Imperial Valley earthquake of October 15, 1979', *Preliminary Report 26*, California Division of Mines and Geology, Office and Strong-Motion Studies, Sacramento, CA, 1980.
34. R. L. Porcella *et al.*, 'Strong-motion data recorded in the United States', *The Imperial Valley California Earthquake of October 15, 1979, Geological Survey Professional Paper 1254*, Washington, D.C., 1982, pp. 289–318.

35. C. Rojahn *et al.*, 'Main-shock strong motion records from Meloland Road–Interstate 8 highway overcrossing', *The Imperial Valley California Earthquake of October 15, 1979, Geological Survey Professional Paper 1254*, Washington, D.C., 1982, pp. 377–384.
36. R. W. Clough and J. Penzien, *Dynamics of Structures*, McGraw-Hill, New York, 1975.
37. J. L. Beck, 'Determining models of structures from earthquake records', *Report No. EERL 78-01*, Earthquake Engineering Research Laboratory, California Institute of Technology, Pasadena, CA, 1978.
38. M. B. Levine and R. F. Scott, 'Verification of a simple bridge/foundation dynamic model', to be submitted to *J. geotech. eng. div. ASCE* (1986).

APPENDIX C

RECORDED MOTIONS:

TOTAL VS. RIGID BODY CONTRIBUTIONS

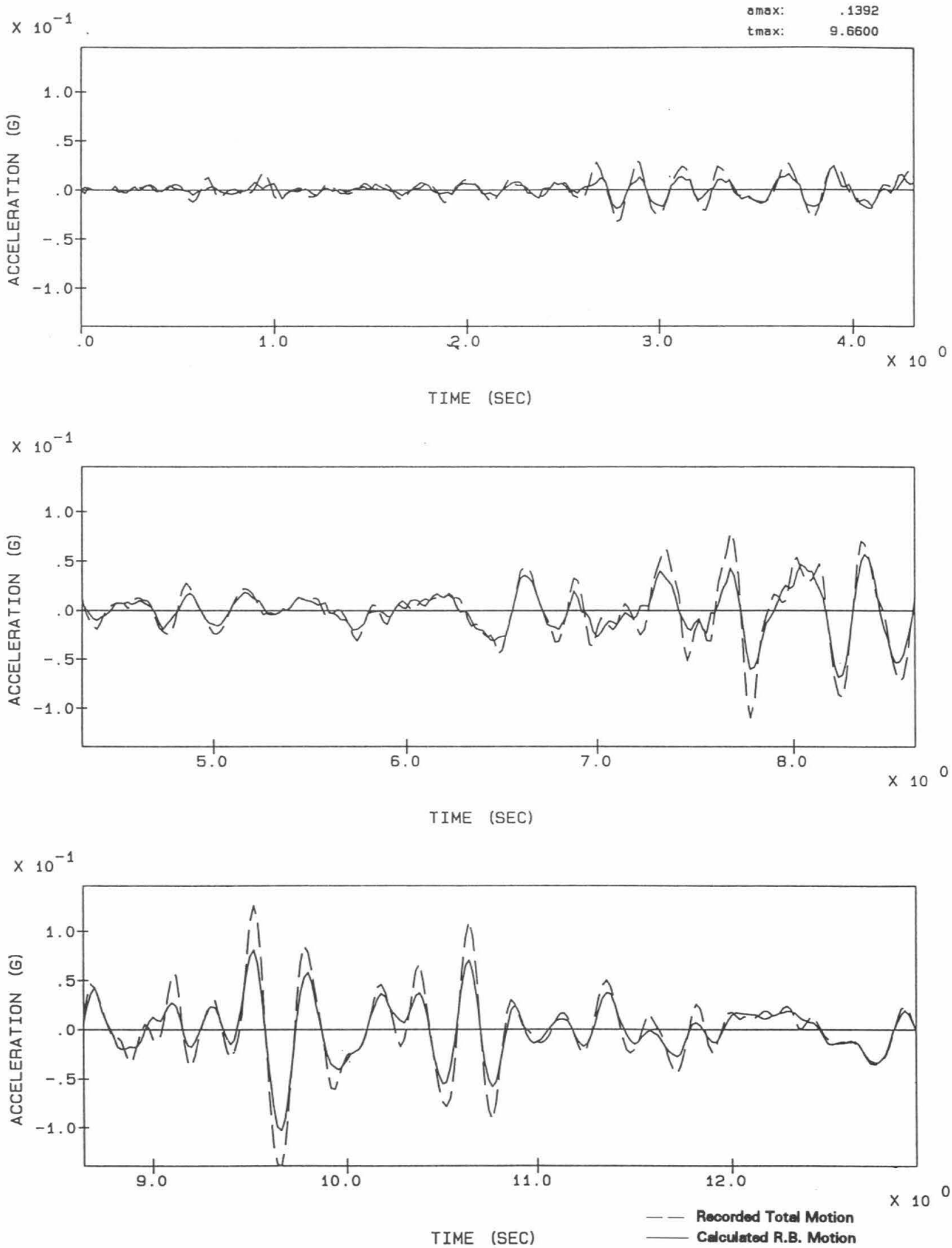

Figure C-1: Comparison of Acceleration Time-Histories For Recorded Total Motion and Calculated Rigid Body Motion, Channel 5, Morgan Hill Earthquake

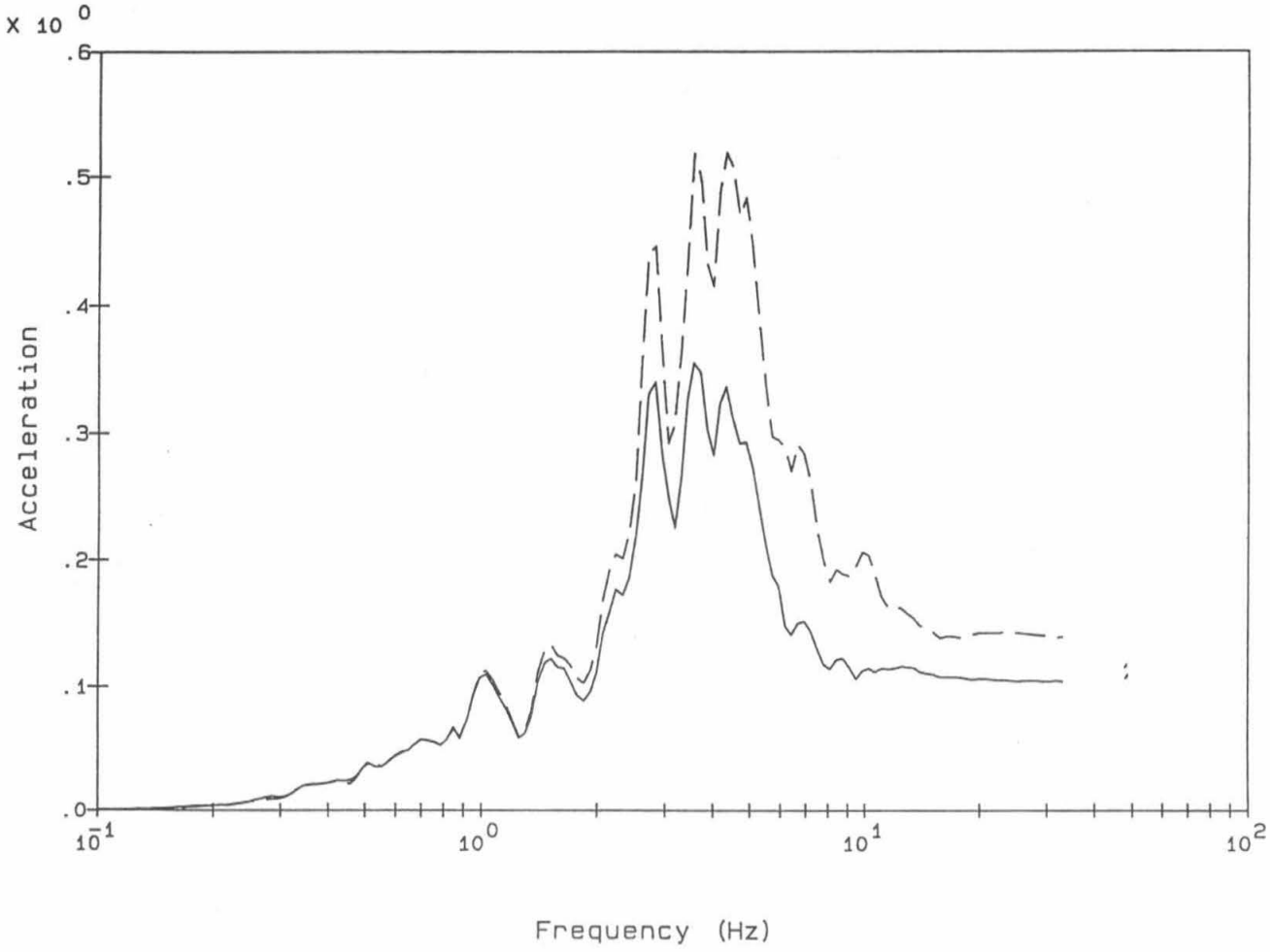

Legend:

Calc RB motion ————————

Recorded motion — — — — -

Notes:

Acceleration in g's

Spectra calculated for 5% damping

Figure C-2: Comparison of Floor Response Spectra For Recorded Total Motion and Calculated Rigid Body Motion, Channel 5, Morgan Hill Earthquake

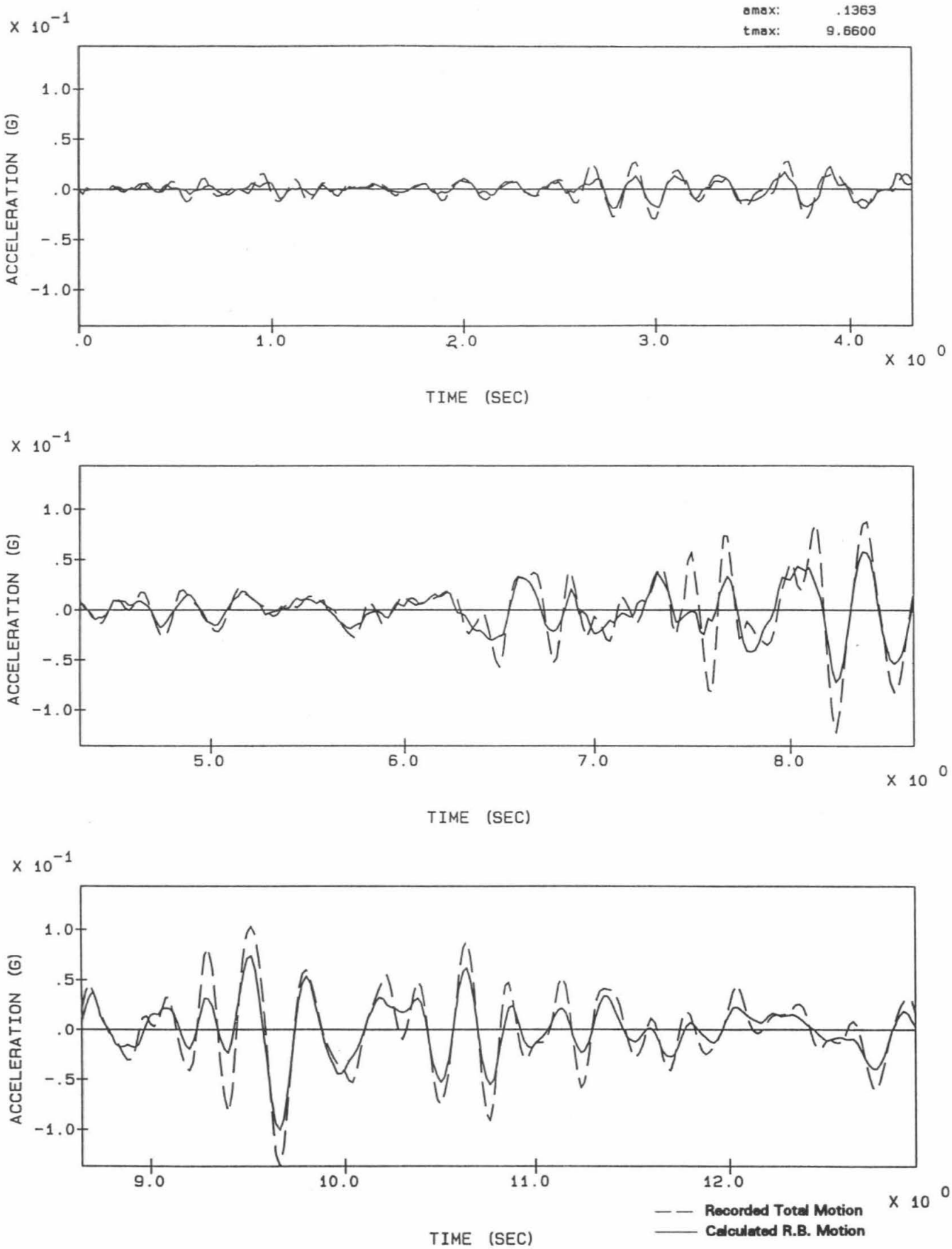

Figure C-3: Comparison of Acceleration Time-Histories For Recorded Total Motion and Calculated Rigid Body Motion, Channel 6, Morgan Hill Earthquake

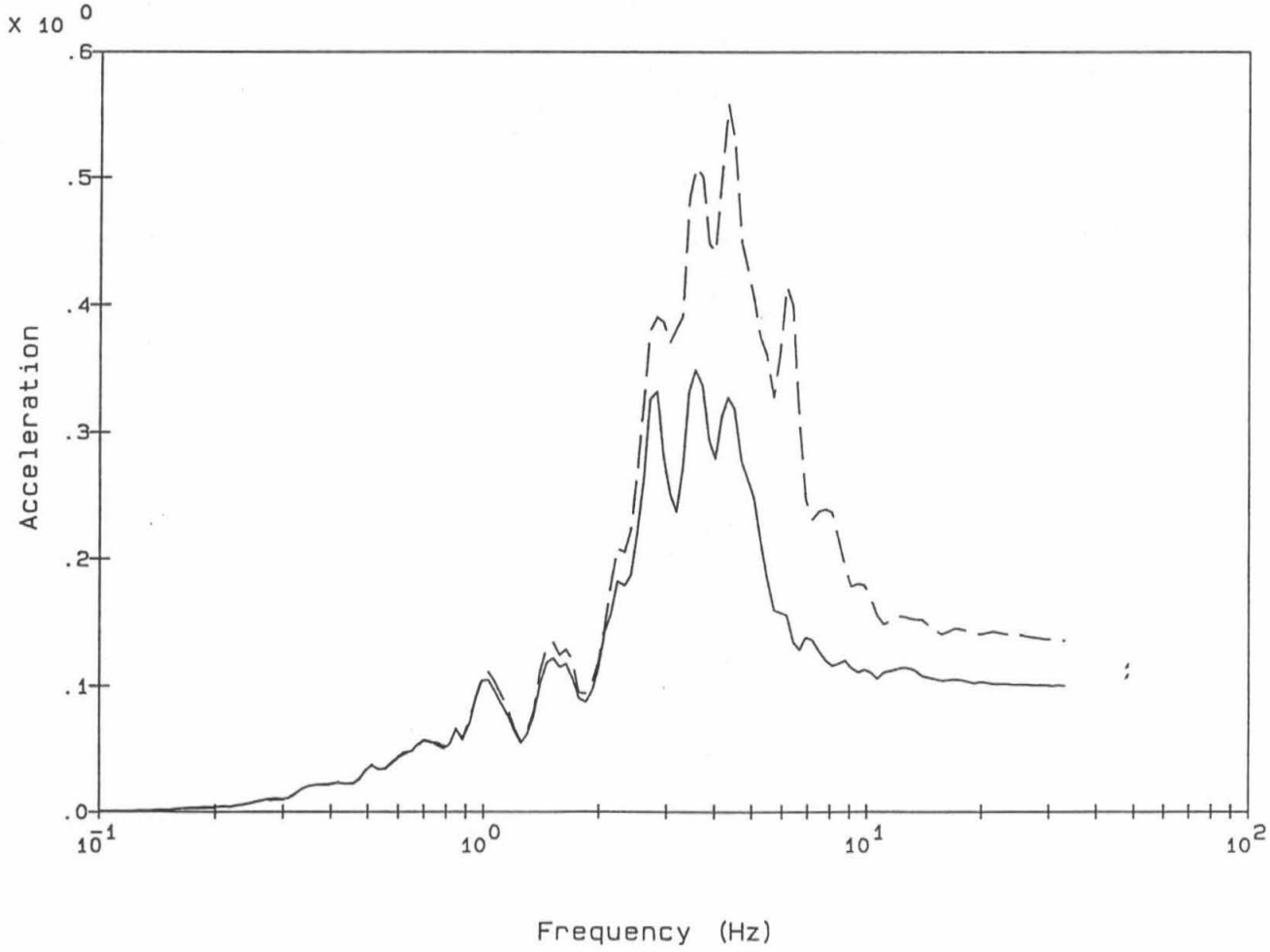

Figure C-4: Comparison of Floor Response Spectra For Recorded Total Motion and Calculated Rigid Body Motion, Channel 6, Morgan Hill Earthquake

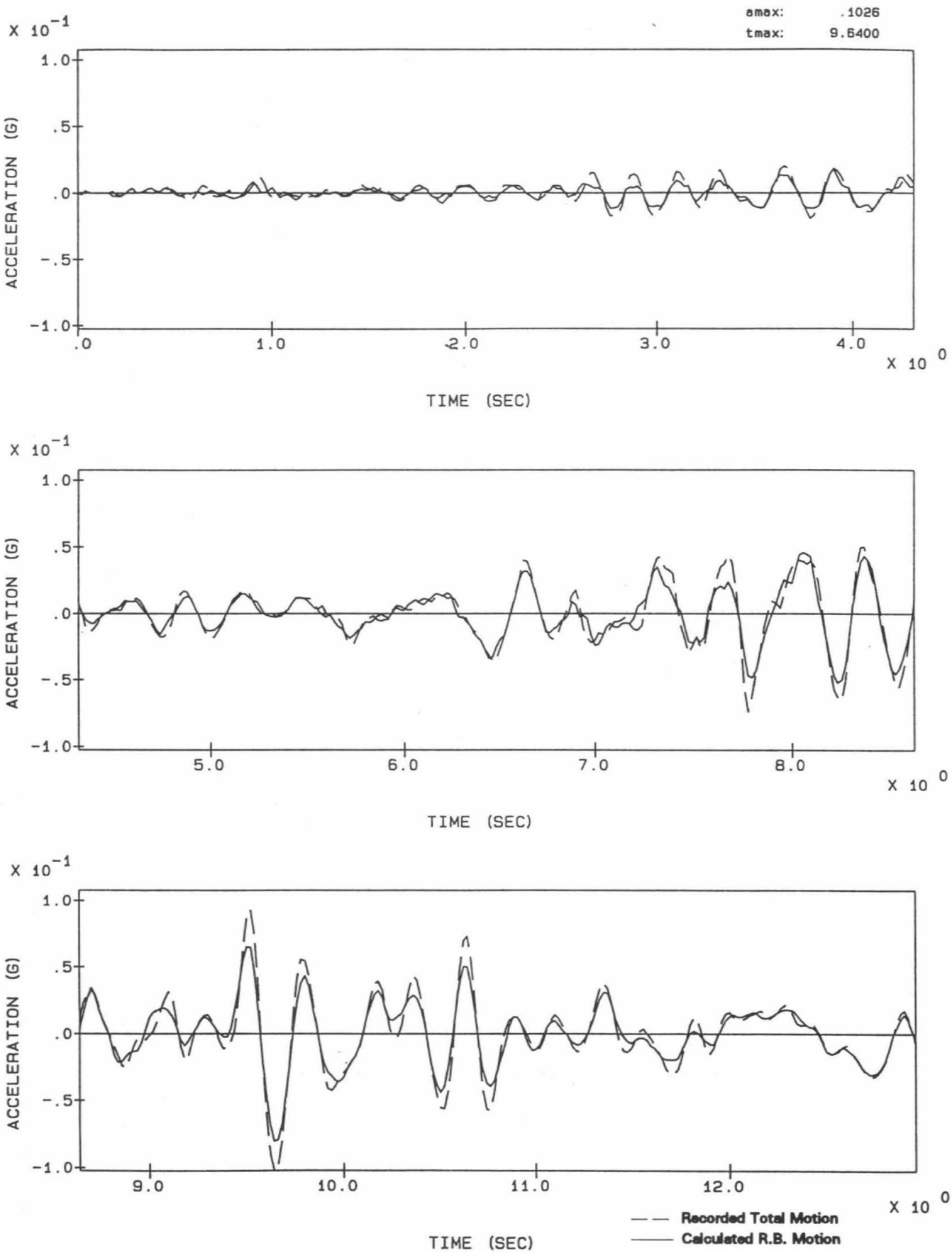

Figure C-5: Comparison of Acceleration Time-Histories For Recorded Total Motion and Calculated Rigid Body Motion, Channel 7, Morgan Hill Earthquake

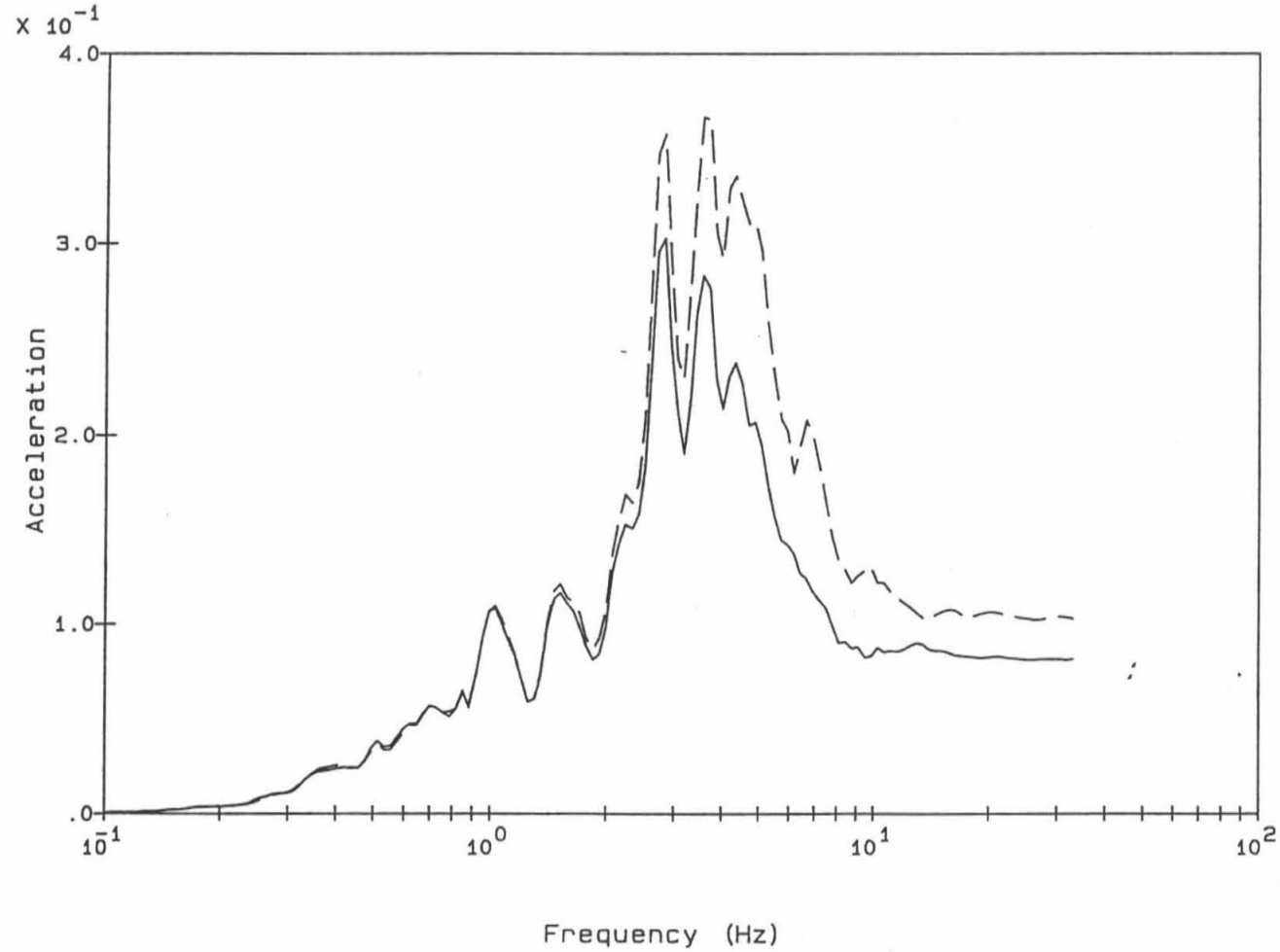

Figure C-6: Comparison of Floor Response Spectra For Recorded Total Motion and Calculated Rigid Body Motion, Channel 7, Morgan Hill Earthquake

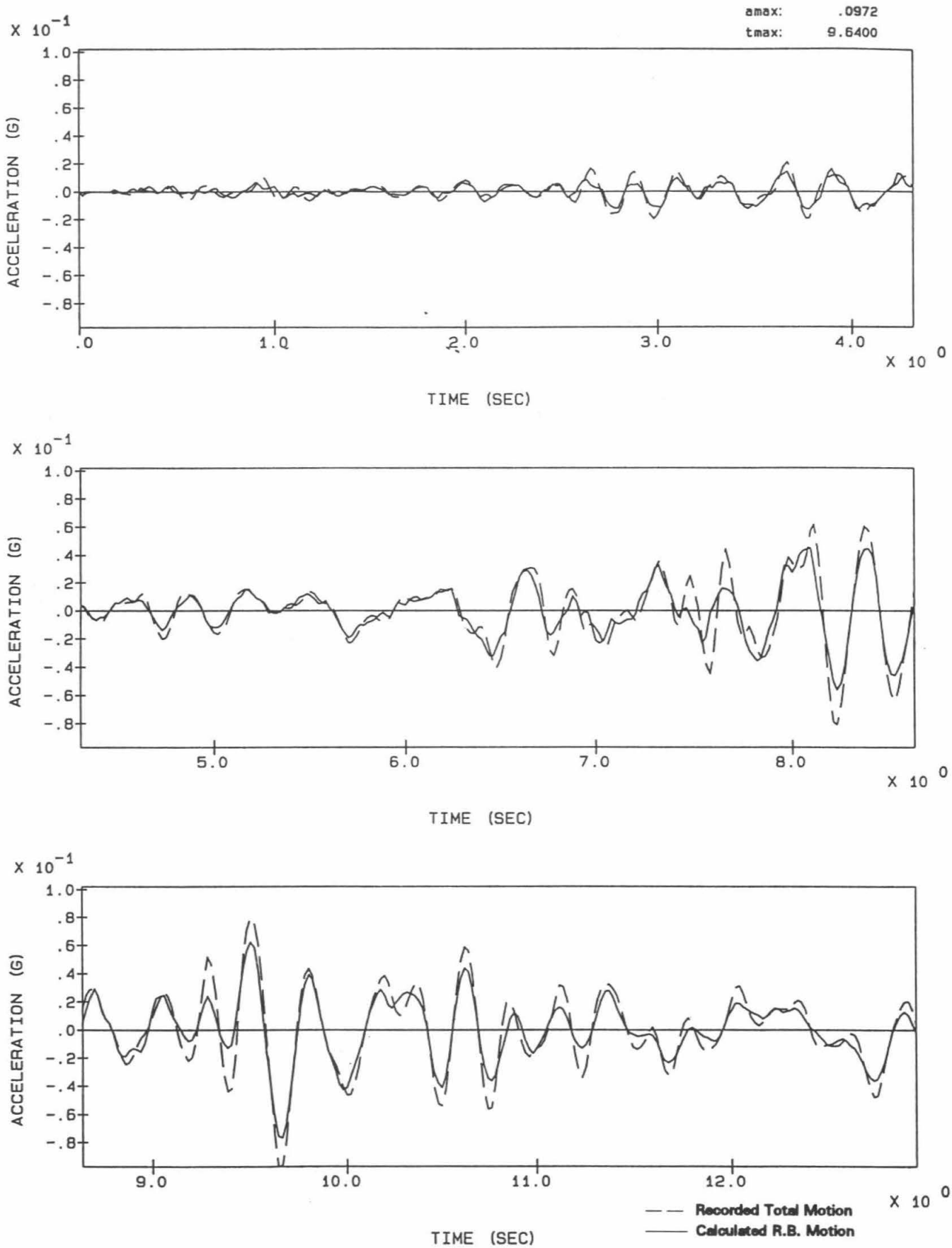

Figure C-7: Comparison of Acceleration Time-Histories For Recorded Total Motion and Calculated Rigid Body Motion, Channel 8, Morgan Hill Earthquake

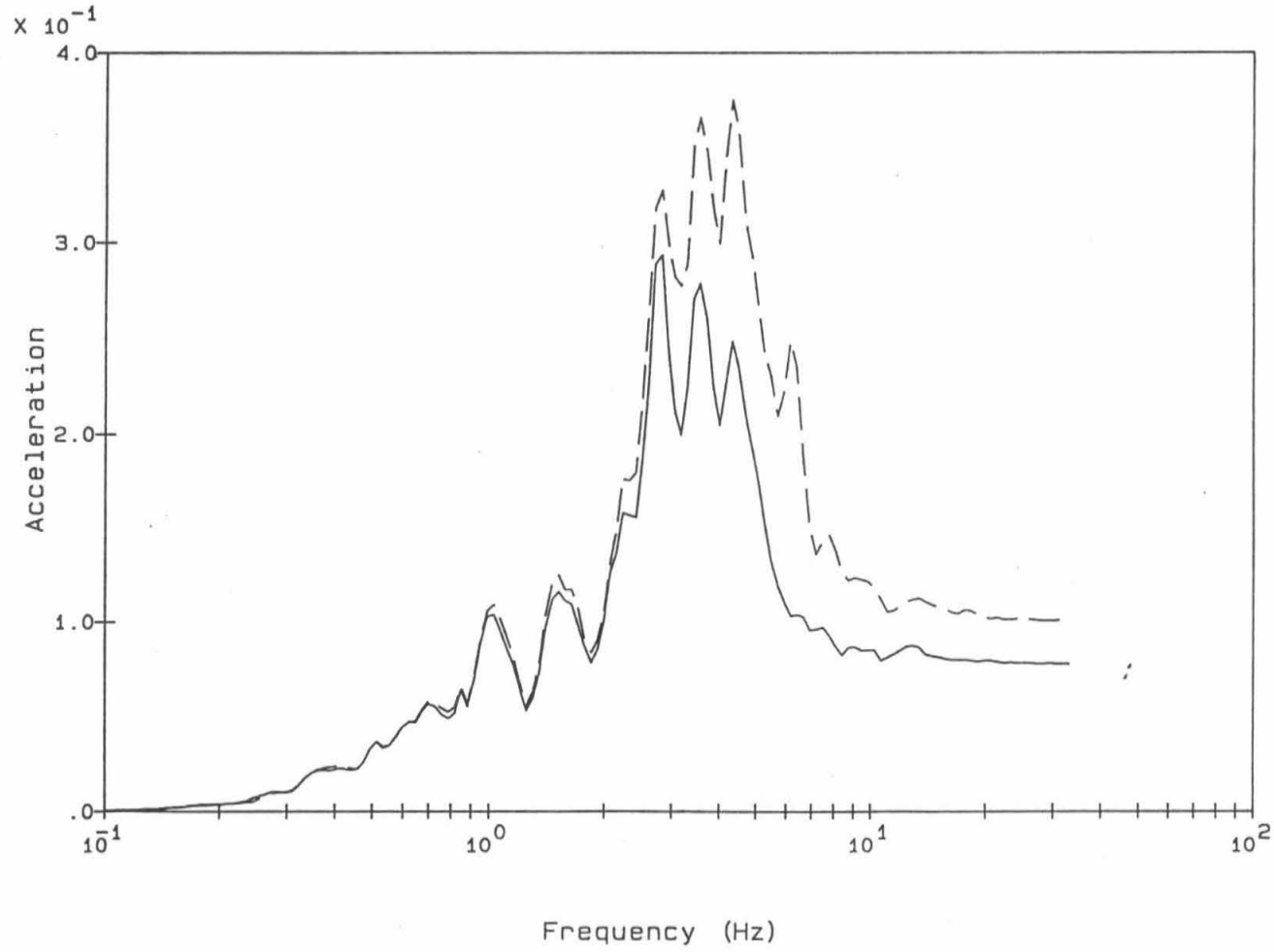

Figure C-8: Comparison of Floor Response Spectra For Recorded Total Motion and Calculated Rigid Body Motion, Channel 8, Morgan Hill Earthquake

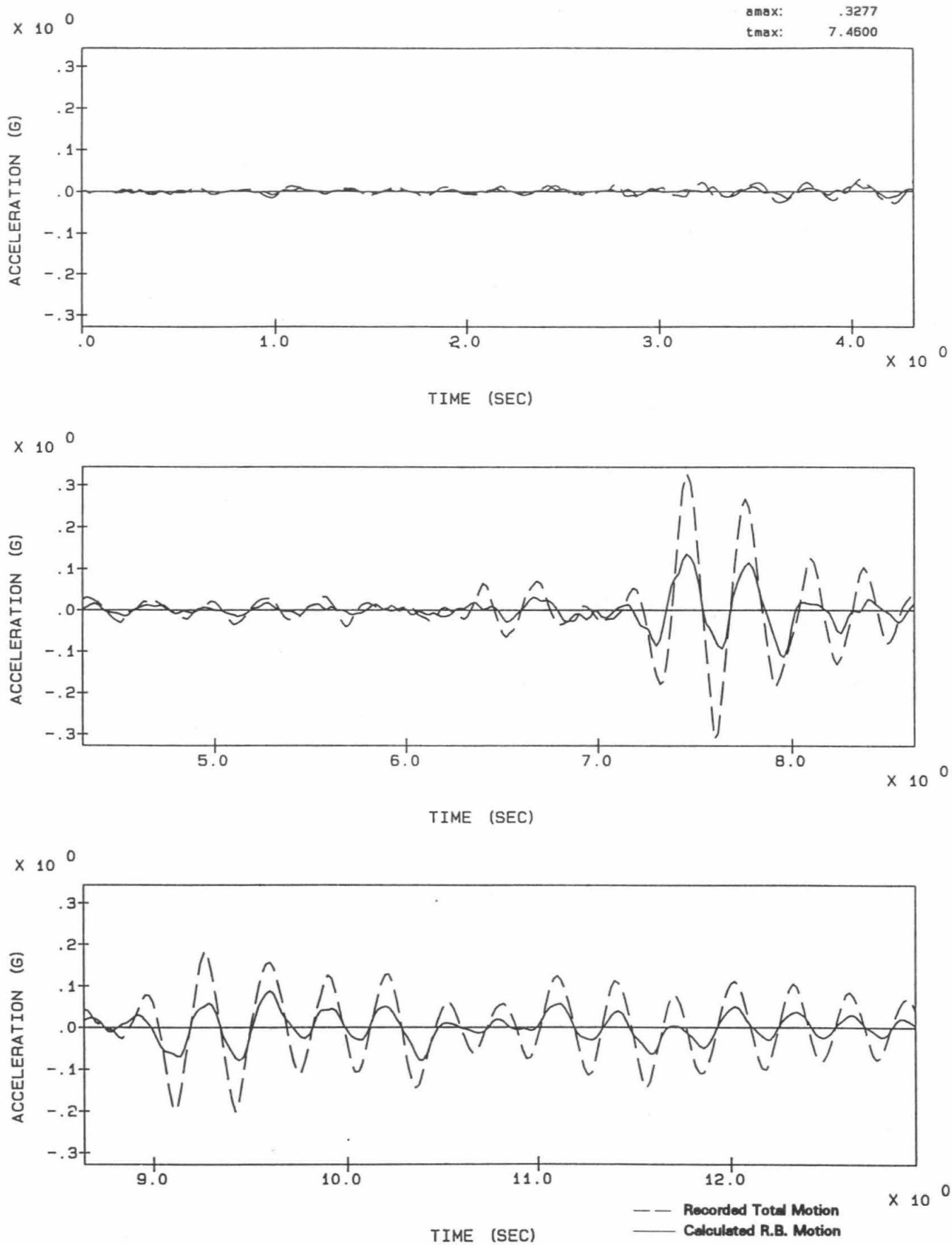

Figure C-9: Comparison of Acceleration Time-Histories For Recorded Total Motion and Calculated Rigid Body Motion, Channel 11, Morgan Hill Earthquake

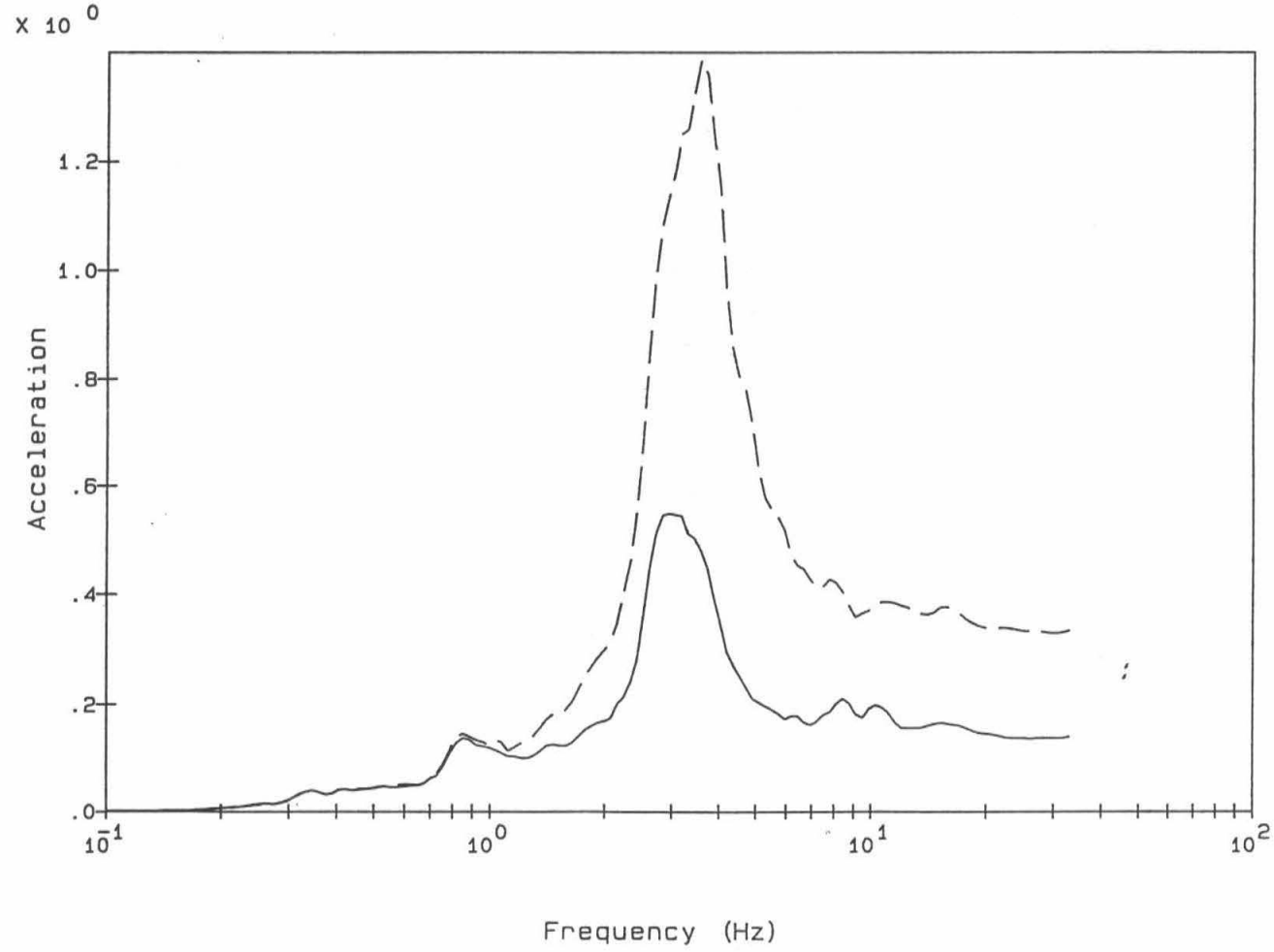

Legend:

Calc RB motion ————————

Recorded motion — — — — -

Notes:

Acceleration in g's

Spectra calculated for 5% damping

Figure C-10: Comparison of Floor Response Spectra For Recorded Total Motion and Calculated Rigid Body Motion, Channel 11, Morgan Hill Earthquake

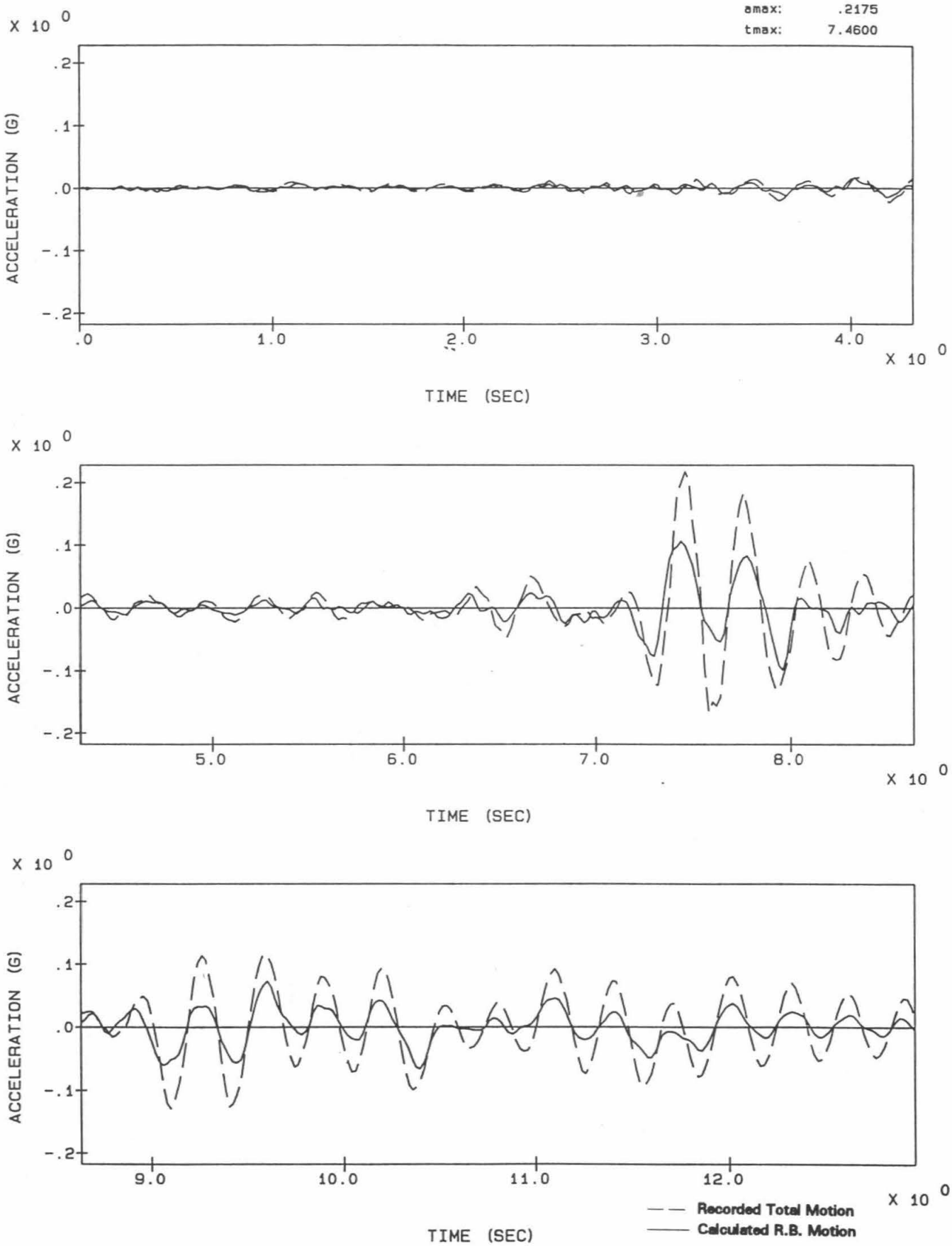

Figure C-11: Comparison of Acceleration Time-Histories For Recorded Total Motion and Calculated Rigid Body Motion, Channel 12, Morgan Hill Earthquake

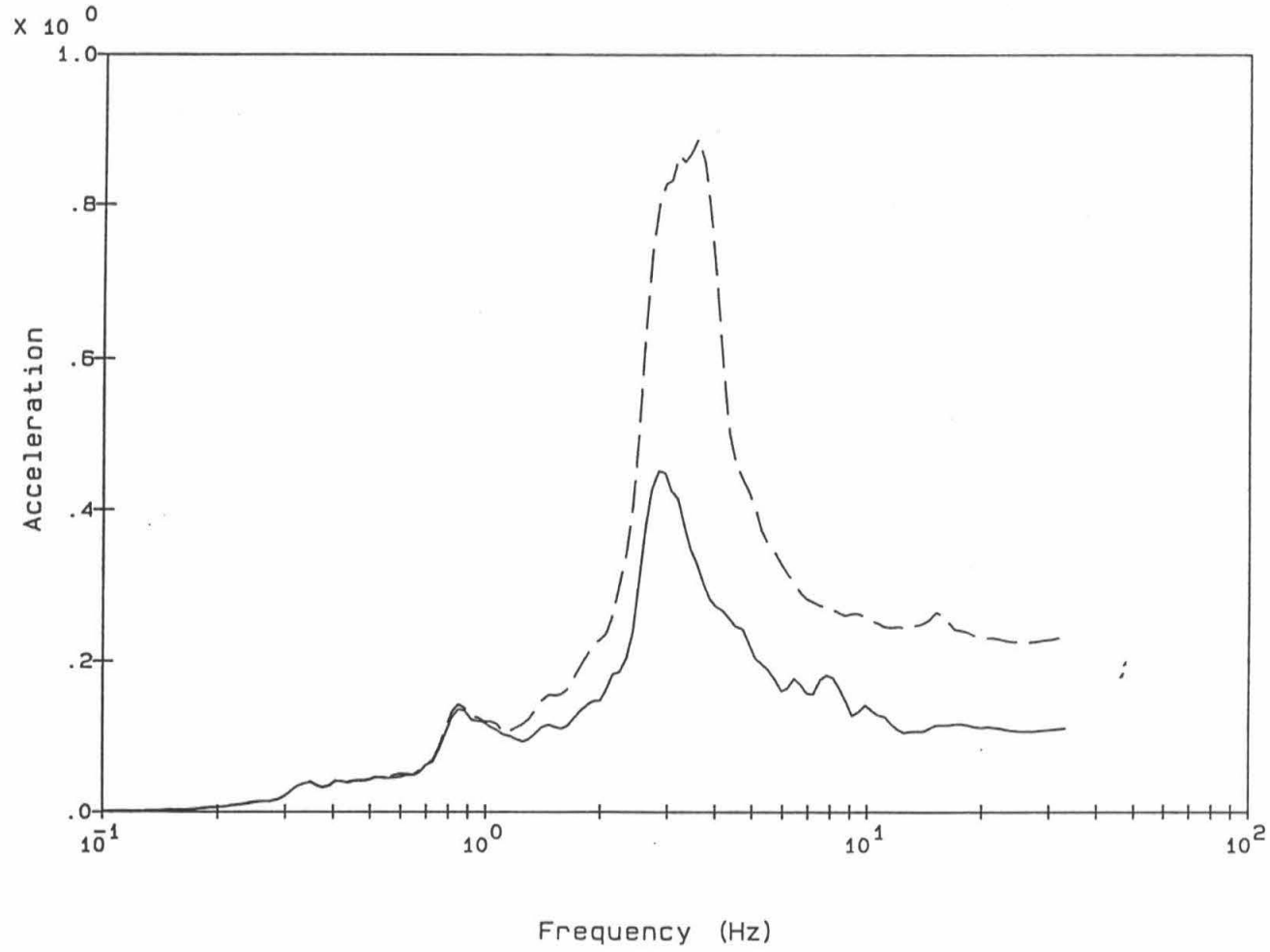

Figure C-12: Comparison of Floor Response Spectra For Recorded Total Motion and Calculated Rigid Body Motion, Channel 12, Morgan Hill Earthquake

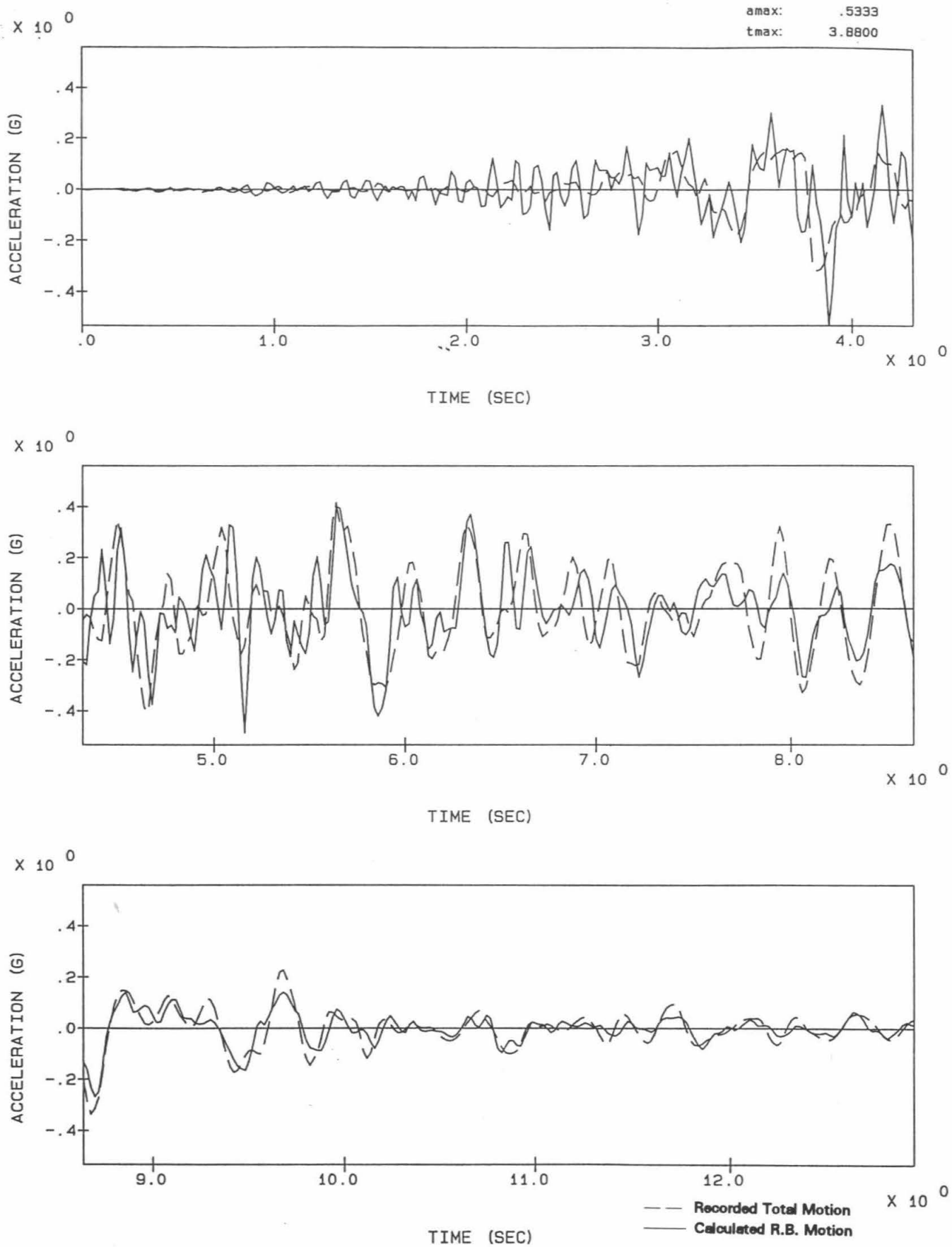

Figure C-13: Comparison of Acceleration Time-Histories For Recorded Total Motion and Calculated Rigid Body Motion, Channel 5, Loma Prieta Earthquake

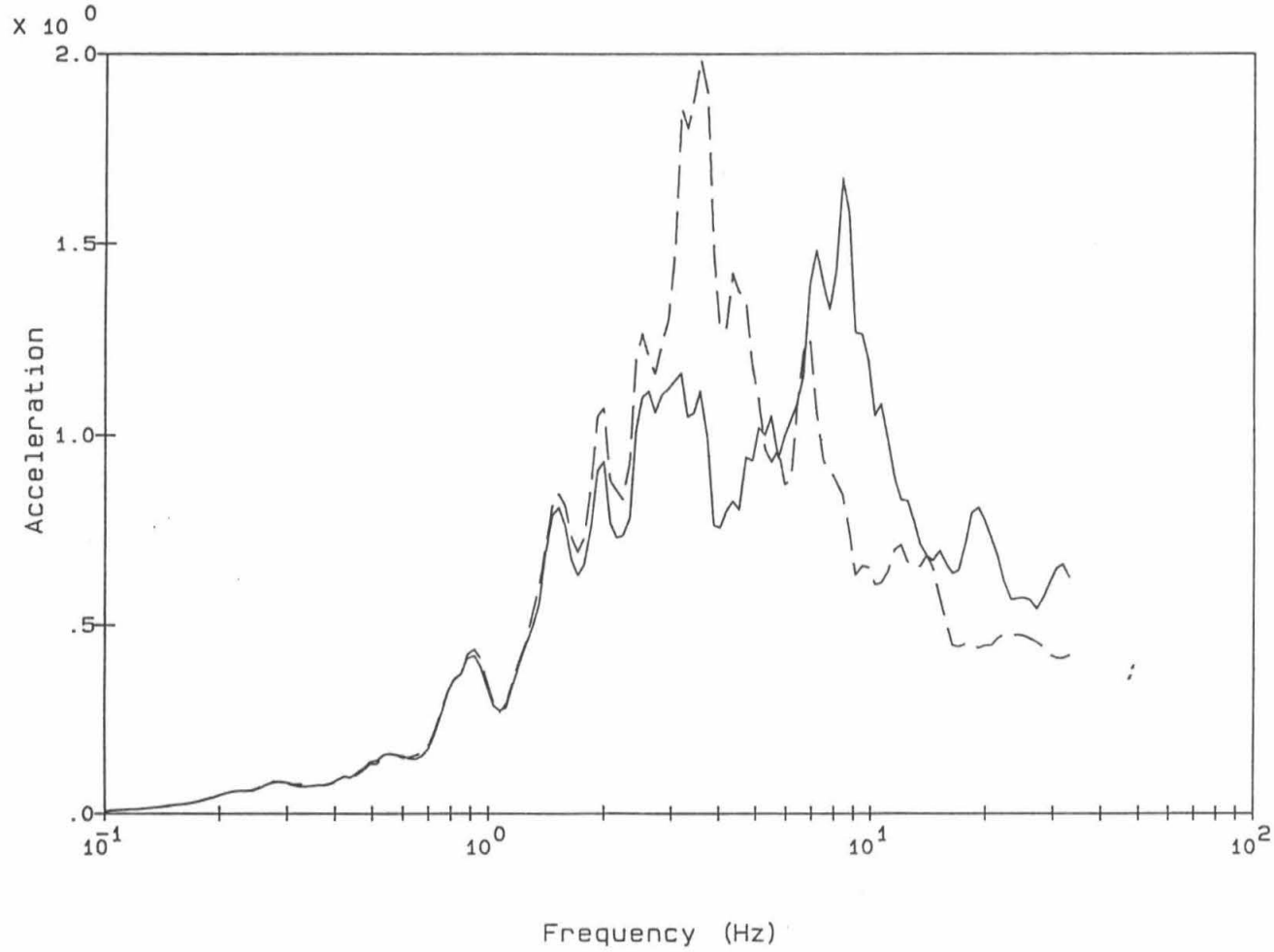

Figure C-14: Comparison of Floor Response Spectra For Recorded Total Motion and Calculated Rigid Body Motion, Channel 5, Loma Prieta Earthquake

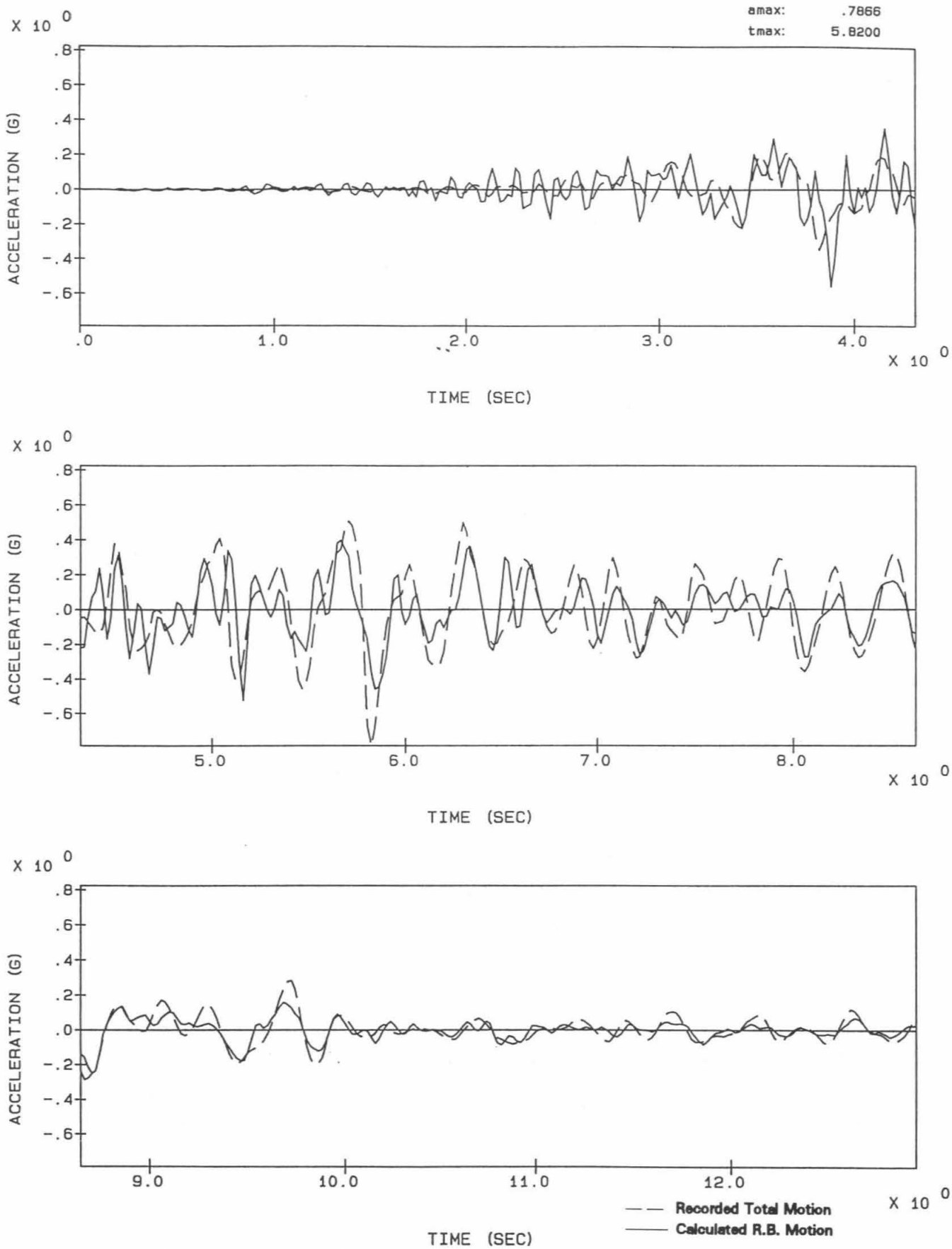

Figure C-15: Comparison of Acceleration Time-Histories For Recorded Total Motion and Calculated Rigid Body Motion, Channel 6, Loma Prieta Earthquake

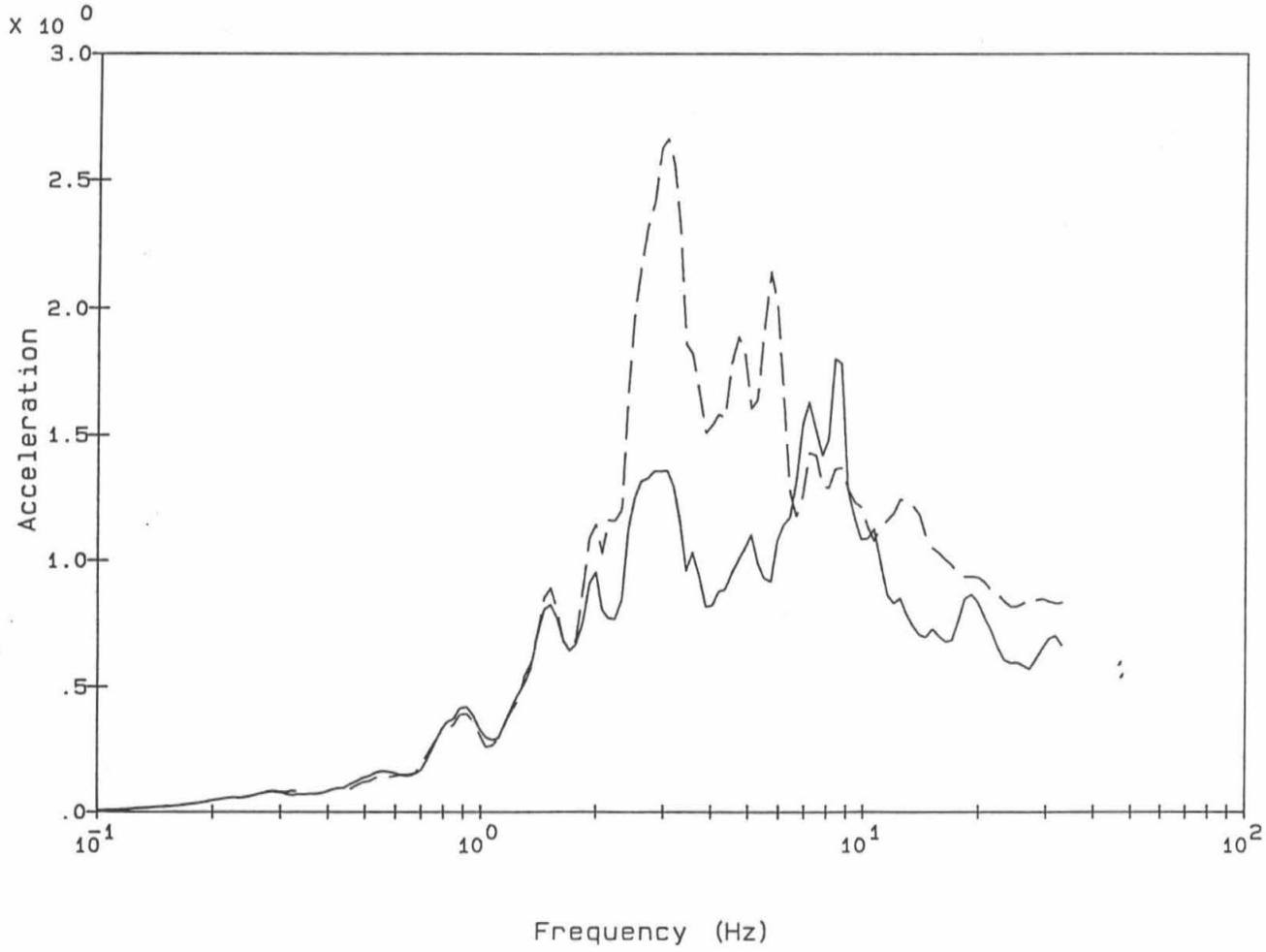

Legend:

Calc RB motion ————————

Recorded motion — — — — -

Notes:

Acceleration in g's

Spectra calculated for 5% damping

Figure C-16: Comparison of Floor Response Spectra For Recorded Total Motion and Calculated Rigid Body Motion, Channel 6, Loma Prieta Earthquake

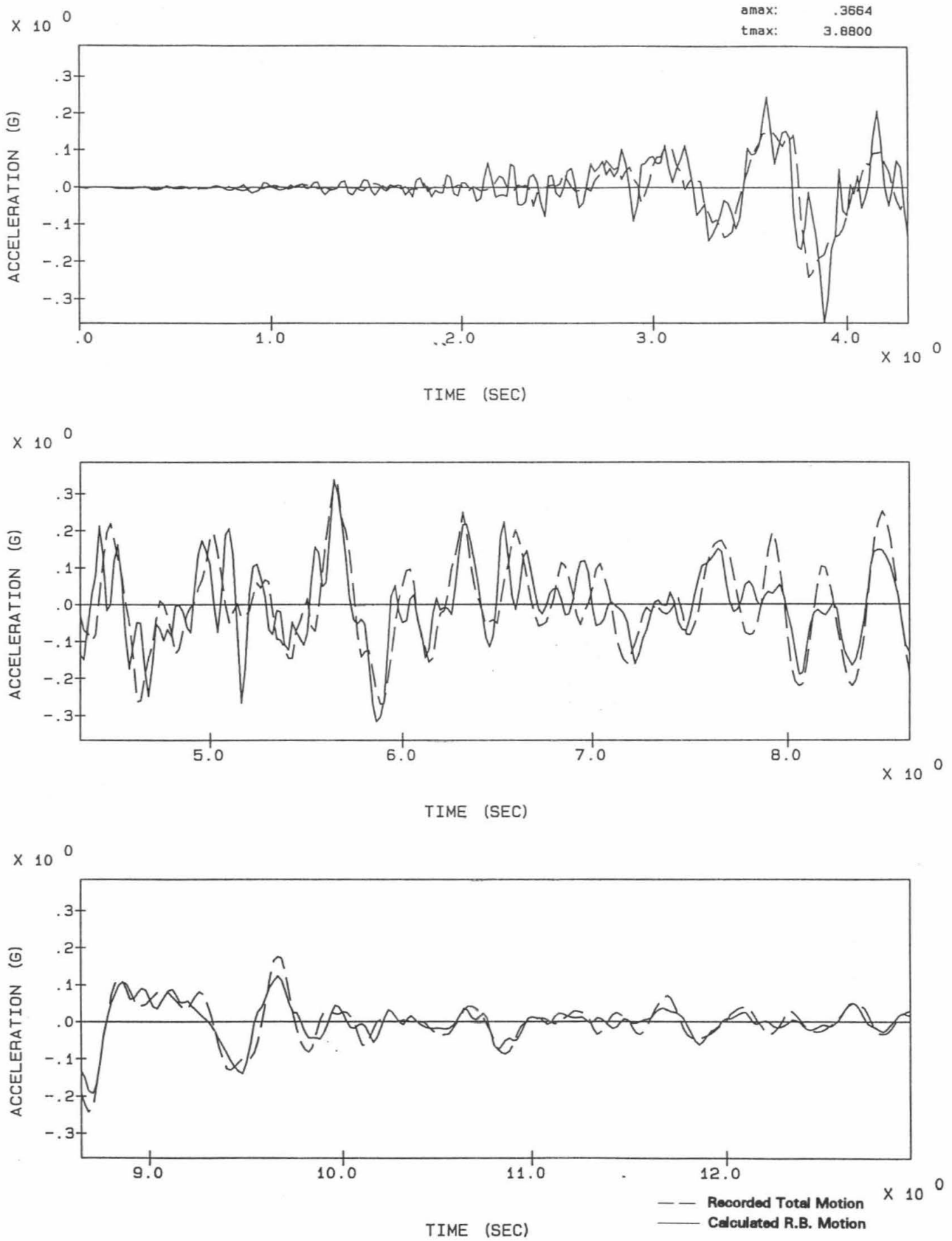

Figure C-17: Comparison of Acceleration Time-Histories For Recorded Total Motion and Calculated Rigid Body Motion, Channel 7, Loma Prieta Earthquake

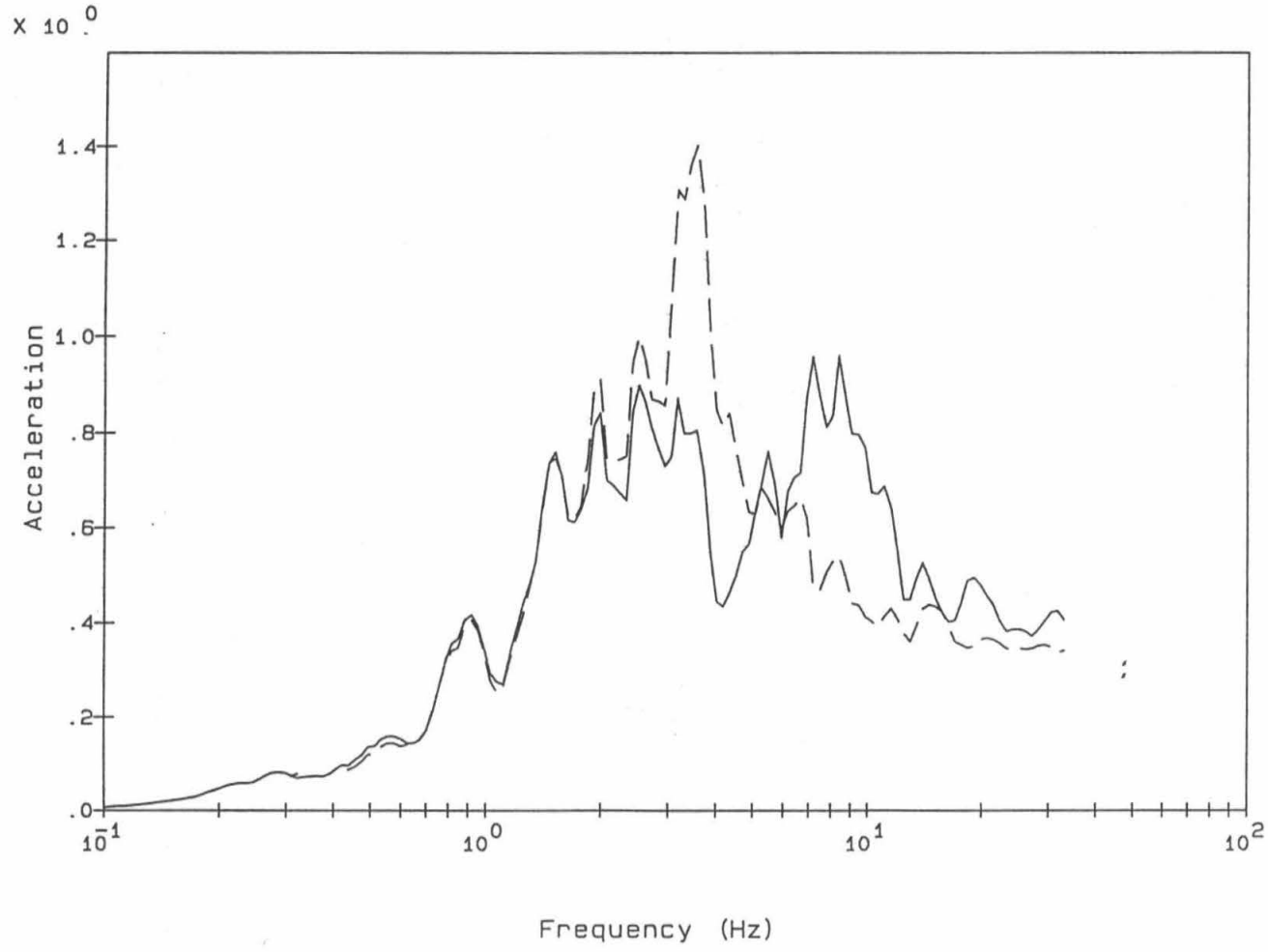

Figure C-18: Comparison of Floor Response Spectra For Recorded Total Motion and Calculated Rigid Body Motion, Channel 7, Loma Prieta Earthquake

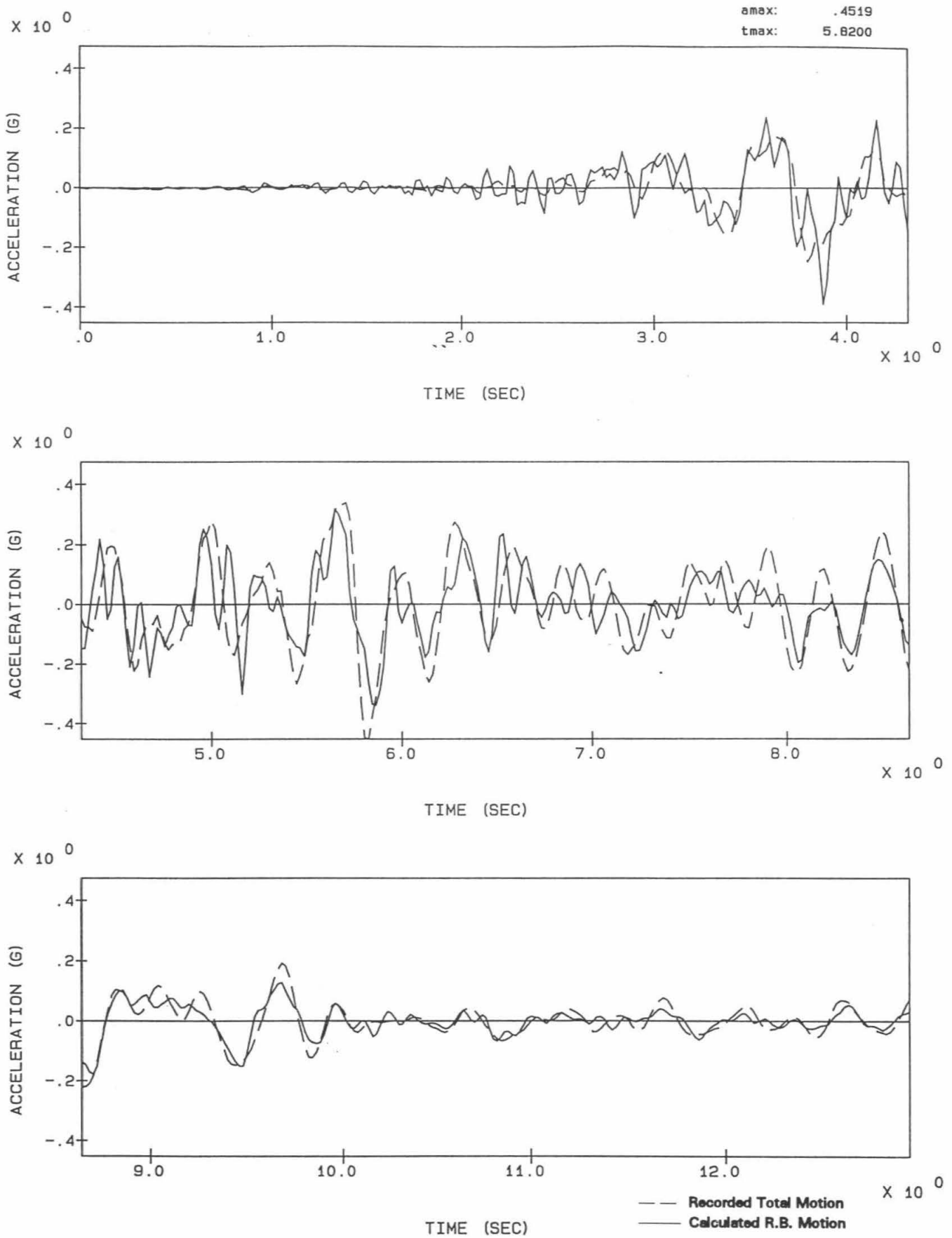

Figure C-19: Comparison of Acceleration Time-Histories For Recorded Total Motion and Calculated Rigid Body Motion, Channel 8, Loma Prieta Earthquake

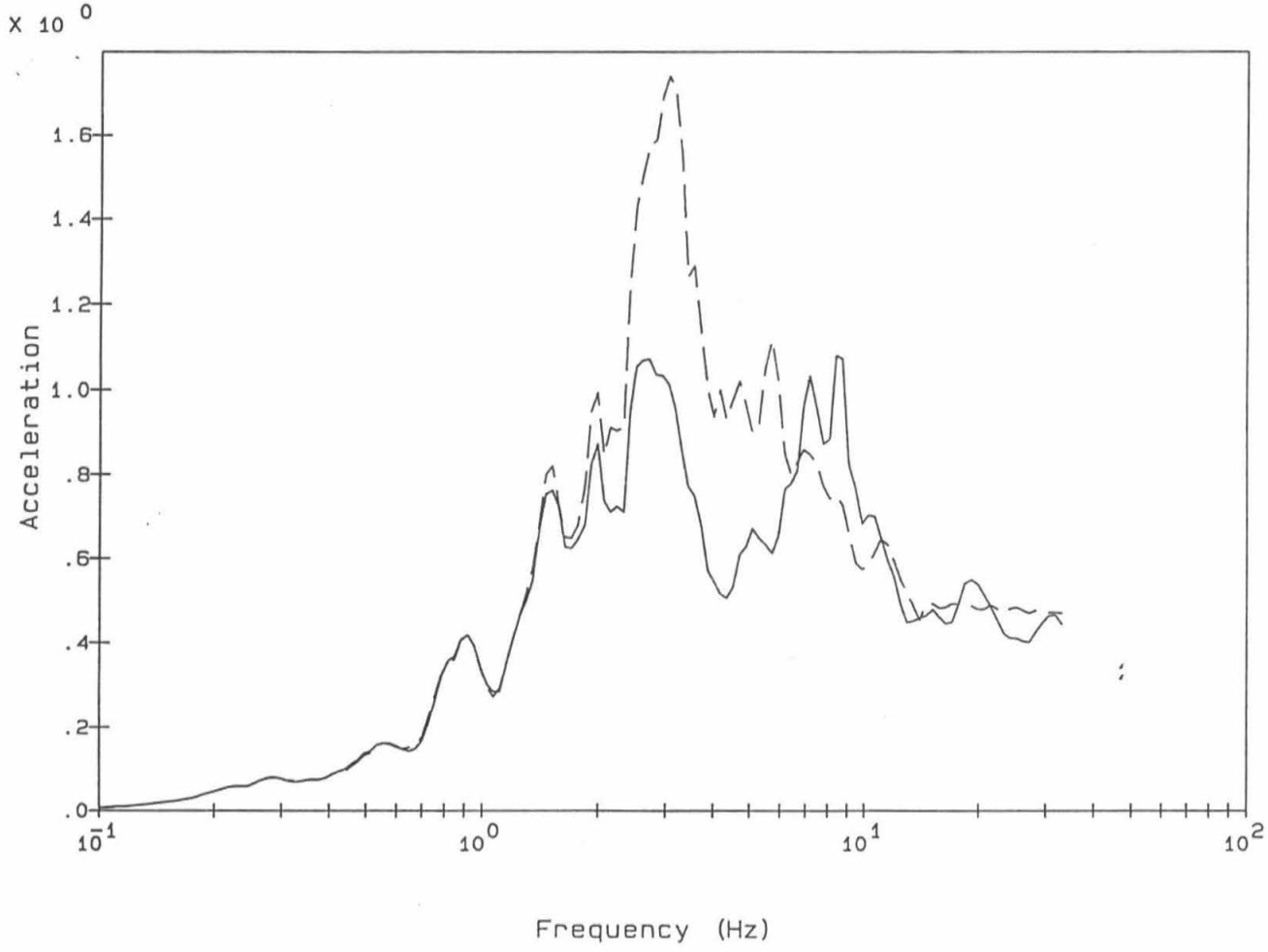

Figure C-20: Comparison of Floor Response Spectra For Recorded Total Motion and Calculated Rigid Body Motion, Channel 8, Loma Prieta Earthquake

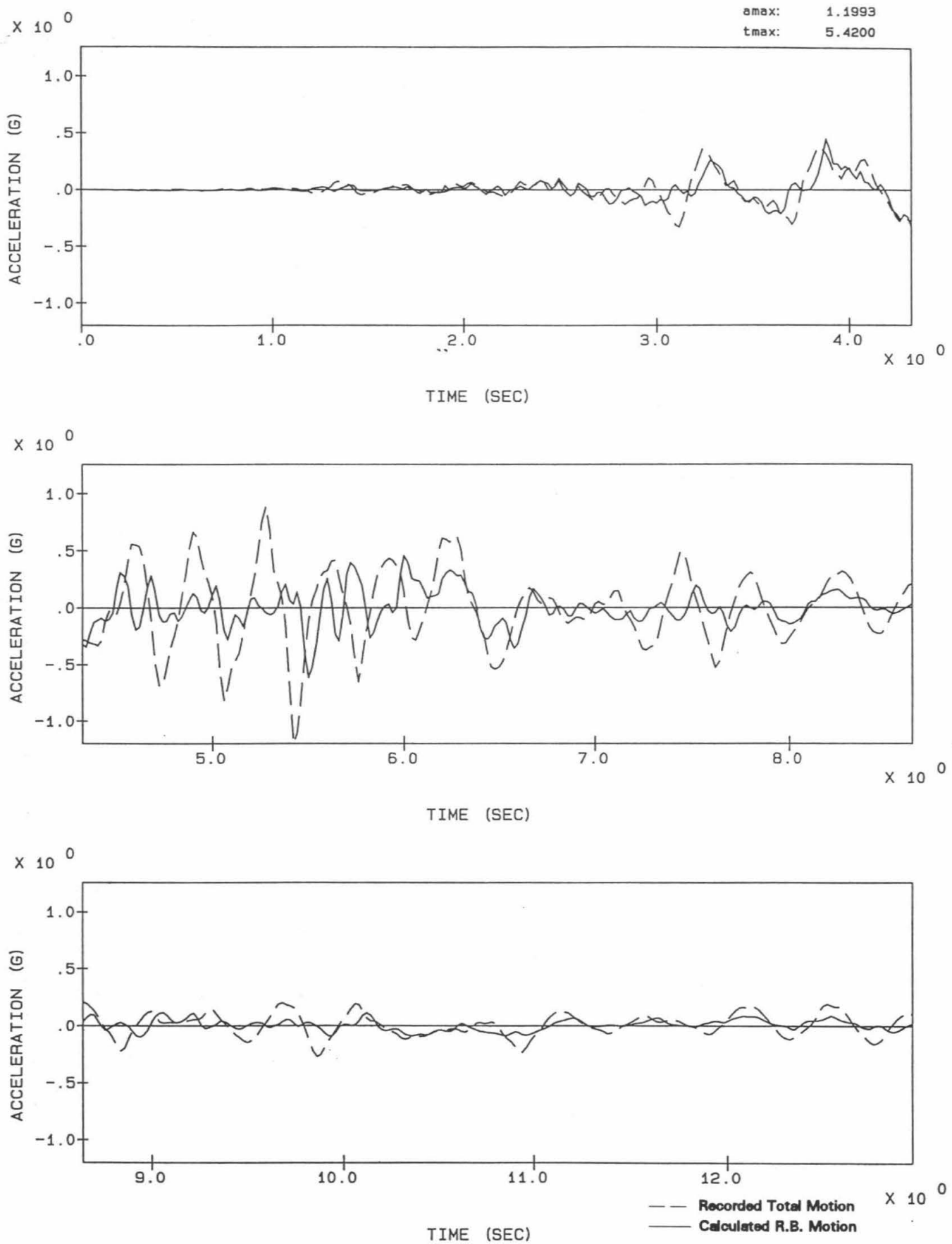

Figure C-21: Comparison of Acceleration Time-Histories For Recorded Total Motion and Calculated Rigid Body Motion, Channel 11, Loma Prieta Earthquake

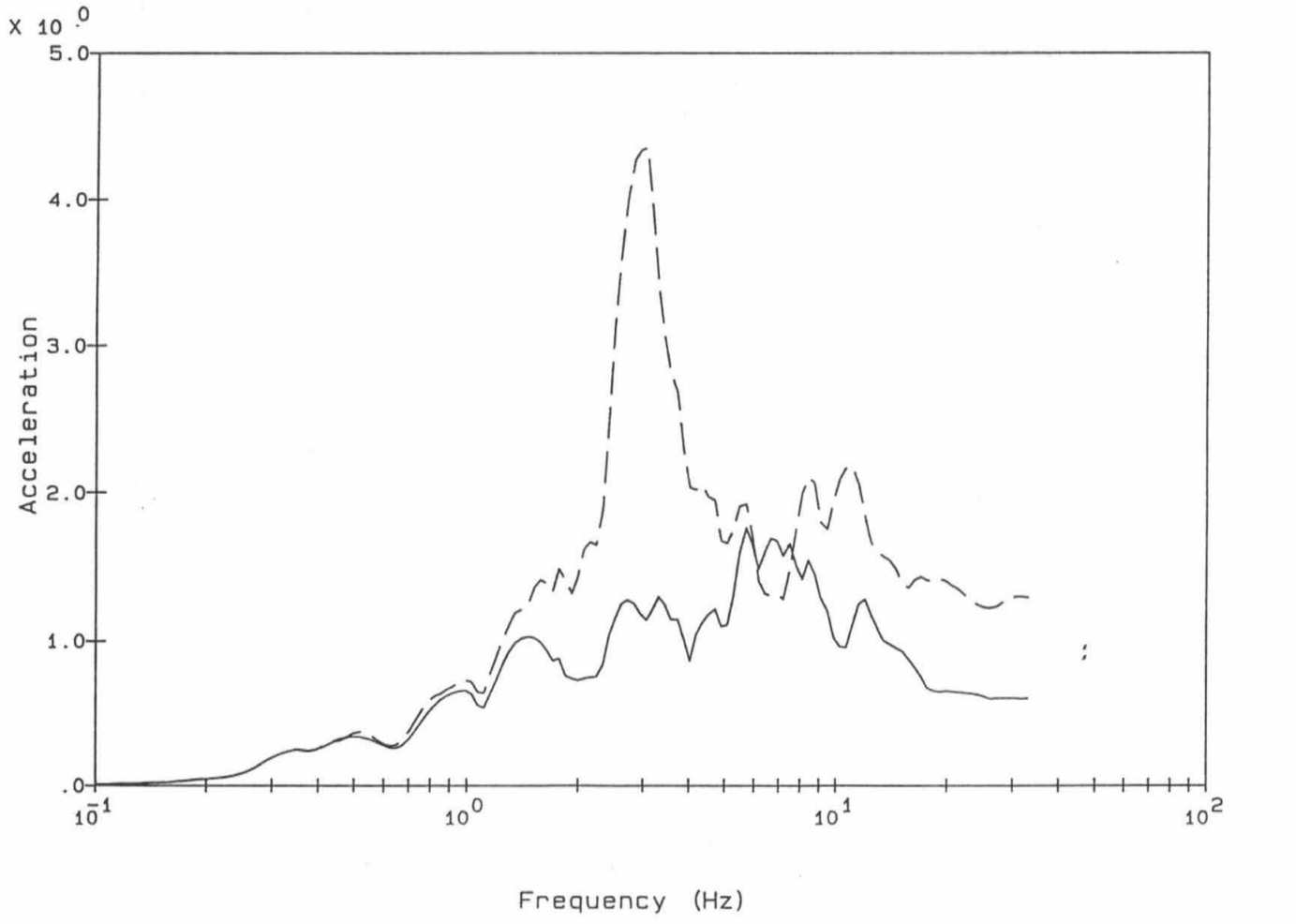

Figure C-22: Comparison of Floor Response Spectra For Recorded Total Motion and Calculated Rigid Body Motion, Channel 11, Loma Prieta Earthquake

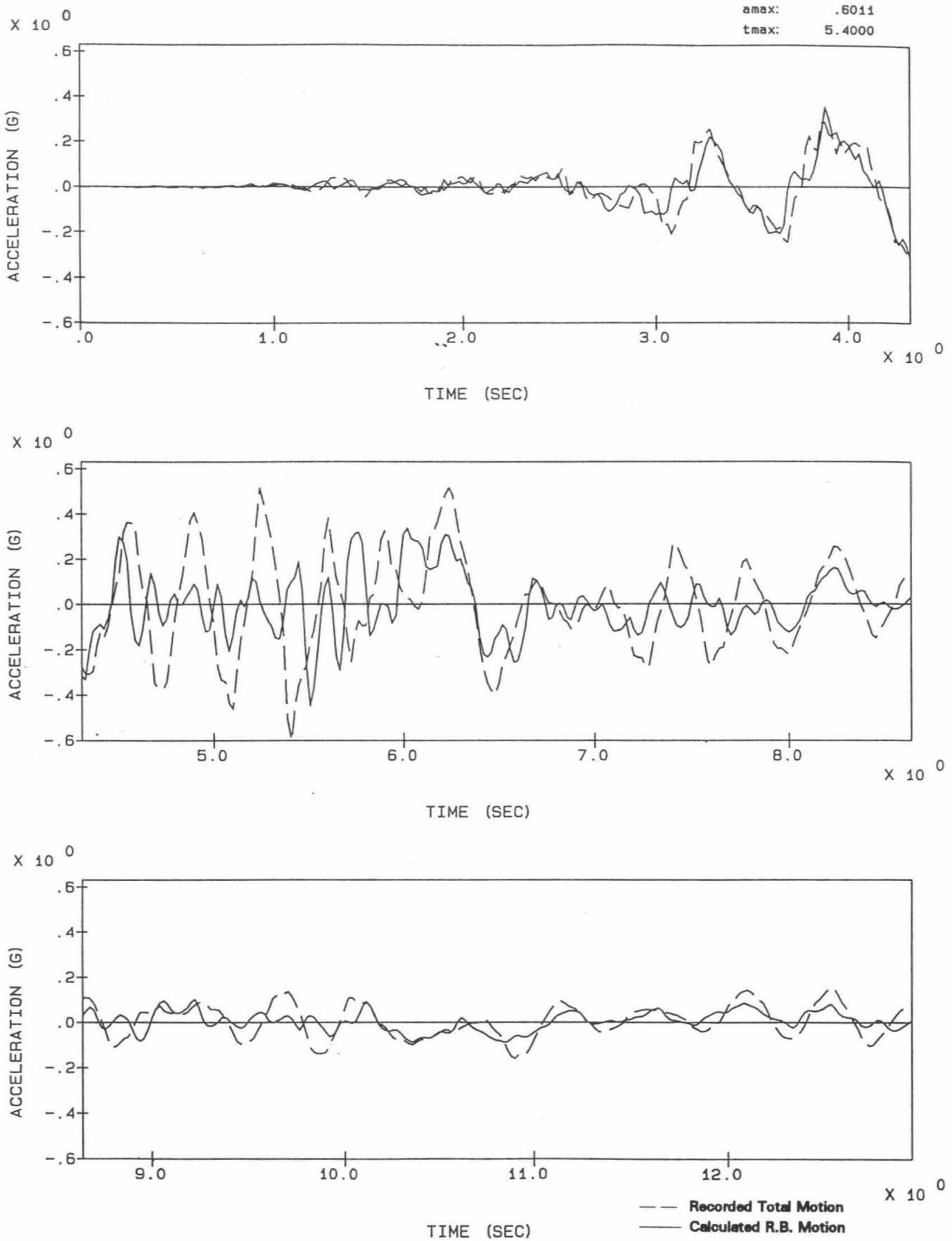

Figure C-23: Comparison of Acceleration Time-Histories For Recorded Total Motion and Calculated Rigid Body Motion, Channel 12, Loma Prieta Earthquake

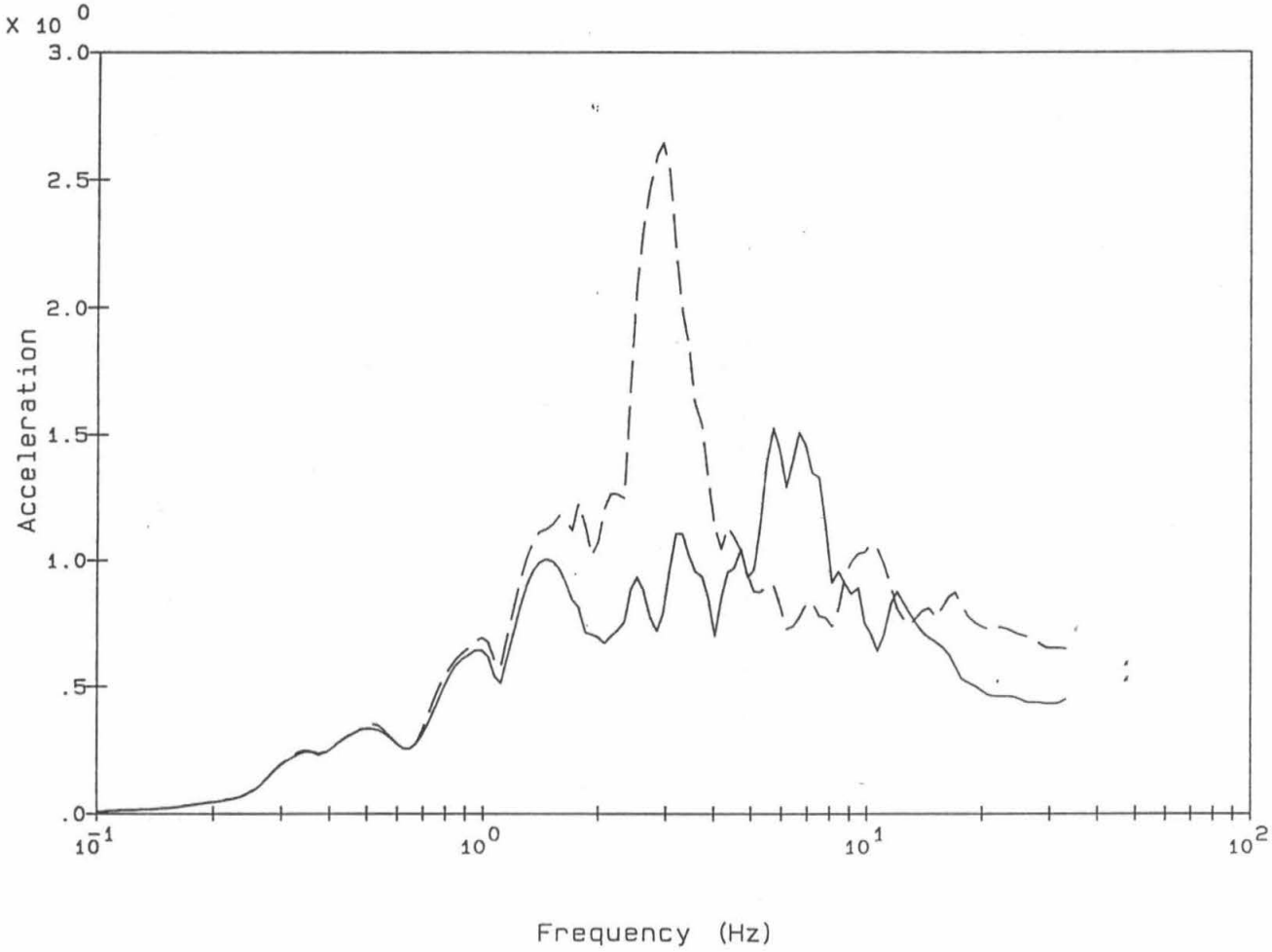

Figure C-24: Comparison of Floor Response Spectra For Recorded Total Motion and Calculated Rigid Body Motion, Channel 12, Loma Prieta Earthquake

NRC FORM 335 (2-89) NRCM 1102, 3201, 3202

U.S. NUCLEAR REGULATORY COMMISSION

BIBLIOGRAPHIC DATA SHEET

(See instructions on the reverse)

1. REPORT NUMBER (Assigned by NRC. Add Vol., Supp., Rev., and Addendum Numbers, if any.)

NUREG/CR-6012

2. TITLE AND SUBTITLE

Stiffness and Damping Properties of a Low Aspect Ratio Shear Wall Building Based on Recorded Earthquake Responses

3. DATE REPORT PUBLISHED

MONTH	YEAR
March	1993

4. FIN OR GRANT NUMBER

D1730

5. AUTHOR(S)

P. S. Hashimoto, L. W. Tiong, L. K. Steele, J. J. Johnson, EQE Engineering Consultants
J. L. Beck, California Institute of Technology

6. TYPE OF REPORT

Technical

7. PERIOD COVERED *(Inclusive Dates)*

8. PERFORMING ORGANIZATION – NAME AND ADDRESS *(If NRC, provide Division, Office or Region, U.S. Nuclear Regulatory Commission, and mailing address; if contractor, provide name and mailing address.)*

EQE Engineering Consultants
18101 Von Karman Ave., Suite 400
Irvine, CA 92715

Subcontractor:
California Institute of Technology
Pasadena, CA 91125

9. SPONSORING ORGANIZATION – NAME AND ADDRESS *(If NRC, type "Same as above"; if contractor, provide NRC Division, Office or Region, U.S. Nuclear Regulatory Commission, and mailing address.)*

Division of Engineering
Office of Nuclear Regulatory Research
U.S. Nuclear Regulatory Commission
Washington, DC 20555

10. SUPPLEMENTARY NOTES

11. ABSTRACT *(200 words or less)*

An investigation into the structural properties and seismic responses of a low aspect ratio shear wall building, which has construction similarity to typical nuclear plant structures, has been performed using actual recorded earthquake motions. This effort used a combination of modal identification to obtain structure modal parameters directly from the recorded motions, and elastic structural analysis using methods and criteria frequently employed by the nuclear industry. Modal parameters determined by modal identification provide excellent fits to the building motions recorded during the 1984 Morgan Hill earthquake. Modal parameters identified for the 1989 Loma Prieta earthquake are more uncertain. Investigation of building stiffnesses generally confirms the adequacy of bounding estimates currently recommended for nuclear plant structure seismic analysis. Damping values identified for this building supplement the database being compiled to investigate current nuclear plant structure damping criteria.

12. KEY WORDS/DESCRIPTORS *(List words or phrases that will assist researchers in locating the report.)*

Structure stiffness, structure damping, seismic analysis, nuclear power plant structures, earthquake response, modal identification, shear wall buildings

13. AVAILABILITY STATEMENT

Unlimited

14. SECURITY CLASSIFICATION

(This Page) Unclassified

(This Report) Unclassified

15. NUMBER OF PAGES

16. PRICE